ISSN 0368-0797
eISSN 2410-2091

МИСИС
УНИВЕРСИТЕТ НАУКИ И ТЕХНОЛОГИЙ

СибГИУ
Сибирский государственный индустриальный университет

ИЗВЕСТИЯ ВЫСШИХ УЧЕБНЫХ ЗАВЕДЕНИЙ ЧЕРНАЯ МЕТАЛЛУРГИЯ

IZVESTIYA. FERROUS METALLURGY

fermet.misis.ru

2025 Том Vol. 68 № No. 4

МАТЕРИАЛОВЕДЕНИЕ

Перспективы создания быстрорежущих высокоэнтропийных сталей

ЭКОЛОГИЯ И РАЦИОНАЛЬНОЕ ПРИРОДОПОЛЬЗОВАНИЕ

Перспективные конструкции газоанализаторов для металлургии

ИННОВАЦИИ В МЕТАЛЛУРГИЧЕСКОМ ПРОМЫШЛЕННОМ И ЛАБОРАТОРНОМОБОРУДОВАНИИ, ТЕХНОЛОГИЯХ И МАТЕРИАЛАХ

Металлизация рудноугольных брикетов в кольцевой печи, отапливаемой генераторным газом

МИСИС УНИВЕРСИТЕТ
СибГИУ Сибирский государственный индустриальный университет

ISSN 0368-0797
eISSN 2410-2091

ИЗВЕСТИЯ ВЫСШИХ УЧЕБНЫХ ЗАВЕДЕНИЙ ЧЕРНАЯ МЕТАЛЛУРГИЯ

Научно-технический журнал

Издается с января 1958 г. Выпускается 6 раз в год

2025 Том Vol. 68 № No. 4

IZVESTIYA FERROUS METALLURGY

Scientific and Technical Journal

Published since January 1958. Issued 6 times a year

IZVESTIYA FERROUS METALLURGY

www.fermet.misis.ru

ISSN 0368-0797 *(Print)* ISSN 2410-2091 *(Online)*

Alternative title:

Izvestiya vuzov. Chernaya metallurgiya

Founders:

MISIS
UNIVERSITY OF SCIENCE AND TECHNOLOGY

SibSIU
Siberian State Industrial University

Publisher:

National University of Science and Technology "MISIS"

Editorial Office Address:

in Moscow
4 Leninskii Ave., Moscow 119049, Russian Federation
National University of Science and Technology "MISIS"
Tel.: +7 (495) 638-44-11 *E-mail*: ferrous@misis.ru

in Novokuznetsk
42 Kirova Str., Novokuznetsk, Kemerovo Region – Kuzbass
654007, Russian Federation
Siberian State Industrial University
Tel.: +7 (3843) 74-86-28 *E-mail*: redjizvz@sibsiu.ru

In accordance with paragraph 5 of the Rules for the formation of the Higher Attestation Comission list journal "Izvestiya. Ferrous metallurgy" is included in the list of leading peer-reviewed scientific journals, publication in which is taken into account in the defense of candidate and doctoral dissertations, as indexed in internatonal data bases.

Indexed: Scopus, Russian Science Citation Index (RSCI), Research Bible, Chemical Abstracts, OCLC and Google Scholar

Registered in Federal Service for Supervision in the Sphere of Mass Communications **PI number FS77-35456**.

ИЗВЕСТИЯ
ВЫСШИХ УЧЕБНЫХ ЗАВЕДЕНИЙ
ЧЕРНАЯ МЕТАЛЛУРГИЯ

www.fermet.misis.ru

ISSN 0368-0797 *(Print)* ISSN 2410-2091 *(Online)*

Варианты названия:

Известия вузов. Черная металлургия

Izvestiya. Ferrous Metallurgy

Учредители:

МИСИС
УНИВЕРСИТЕТ НАУКИ И ТЕХНОЛОГИЙ

СибГИУ
Сибирский государственный индустриальный университет

Издатель:

Национальный исследовательский технологический университет «МИСИС»

Адреса подразделений редакции:

в Москве
Россия, 119049, Москва, Ленинский просп., д. 4, стр. 1
Национальный исследовательский технологический университет «МИСИС»
Тел.: +7 (495) 638-44-11 *E-mail*: ferrous@misis.ru

в Новокузнецке
Россия, 654007, Новокузнецк,
Кемеровская обл. – Кузбасс, ул. Кирова, зд. 42
Сибирский государственный индустриальный университет
Тел.: +7 (3843) 74-86-28 *E-mail:* redjizvz@sibsiu.ru

В соответствии п. 5 Правил формирования перечня ВАК журнал «Известия вузов. Черная металлургия» входит в перечень ведущих рецензируемых научных журналов и изданий, публикация в которых учитывается при защитах кандидатских и докторских диссертаций как индексируемый в МБД.

Индексирование: Scopus, Russian Science Citation Index (RSCI), Research Bible, Chemical Abstracts, OCLC и Google Scholar

Зарегистрирован Федеральной службой по надзору в сфере связи и массовых коммуникаций **ПИ № ФС77-35456**.

Izvestiya. Ferrous Metallurgy.
2025;68(4)

Известия вузов. Черная металлургия.
2025;68(4)

CONTENTS / СОДЕРЖАНИЕ

METALLURGICAL TECHNOLOGIES

ECOLOGY AND RATIONAL USE OF NATURAL RESOURCES

MATERIALS SCIENCE

INNOVATIONS IN METALLURGICAL INDUSTRIAL AND LABORATORY EQUIPMENT, TECHNOLOGIES AND MATERIALS

МЕТАЛЛУРГИЧЕСКИЕ ТЕХНОЛОГИИ

ЭКОЛОГИЯ И РАЦИОНАЛЬНОЕ ПРИРОДОПОЛЬЗОВАНИЕ

МАТЕРИАЛОВЕДЕНИЕ

ИННОВАЦИИ В МЕТАЛЛУРГИЧЕСКОМ ПРОМЫШЛЕННОМ И ЛАБОРАТОРНОМОБОРУДОВАНИИ, ТЕХНОЛОГИЯХ И МАТЕРИАЛАХ

CONTENTS *(Continuation)*

СОДЕРЖАНИЕ *(продолжение)*

INFORMATION TECHNOLOGIES AND AUTOMATIC CONTROL IN FERROUS METALLURGY

IN THE ORDER OF DISCUSSION

ИНФОРМАЦИОННЫЕ ТЕХНОЛОГИИ И АВТОМАТИЗАЦИЯ В ЧЕРНОЙ МЕТАЛЛУРГИИ

В ПОРЯДКЕ ДИСКУССИИ

UDC 669.162.1
DOI 10.17073/0368-0797-2025-4-332-338

Original article
Оригинальная статья

Modeling the distribution of components emitted from oiled scale between water, gas, and dust media in blast furnace dedusting plant

A. S. Kharchenko, V. I. Sysoev, S. K. Sibagatullin, A. V. Dzyuba, A. S. Savinov, E. O. Kharchenko

Nosov Magnitogorsk State Technical University (38 Lenina Ave., Magnitogorsk, Chelyabinsk Region 455000, Russian Federation)

as.mgtu@mail.ru

Abstract. Distribution of oil from oiled scale between various types of waste from blast furnace dedusting plant: dust, sludge, and slime water was estimated by physical modeling using a vertical tubular electric furnace. According to the mathematical modeling of thermal state of a metal container with oiled scale, intensive evaporation of oil in a blast furnace begins after it is loaded and lowered along the shaft to a depth approximately corresponding to three feeds. The oil was passed through a layer of sinter and pellets of the Mikhailovsky GOK heated to 500 °C with a mass of 0.6 kg and a particle size of 10 – 12 mm. Together with oil vapors, finely ground material was injected into the layer of iron ore raw materials (IORM), which imitated in component and fractional composition a mixture of blast furnace dust and sludge from a vacuum filtration plant (VFC) of blast furnace shop, taken in a ratio of 36:64. The physical modeling ensured compliance with the actual gas-dynamic mode in the area of blast furnace ore ridge, based on equality of the Reynolds criterion. The value of this criterion, equal to 215, was achieved in the laboratory model when argon was supplied with a flow rate of 70 L/min. According to the experimental results, distribution of oil was, % of the initial amount: 74.8 % decomposed on the IORM layer corresponding to three feeds; 9.1 % turned into blast furnace dust; 15.9 % turned into VFC sludge; there was no oil in the wet gas purification water; 0.2 % (30 mg) of the oil underwent wet dedusting in the form of an aerosol; a small amount of soot was observed on the pipeline walls. Gas phase of oil decomposition contained: 70 – 90 % H_2; 1.5 % CO; 0.5 – 7.0 % CO_2; 3.2 – 22.2 % CH_4; 0.1 – 2.5 % Σ(C_2H_4, C_2H_6, C_3H_6, C_3H_8). The content of benzo(a)pyrene controlled in Russia in oil vapor did not exceed 0.00058 %.

Keywords: technogenic waste disposal, oiled scale, recycling methods, oil evaporation, blast furnace

For citation: Kharchenko A.S., Sysoev V.I., Sibagatullin S.K., Dzyuba A.V., Savinov A.S., Kharchenko E.O. Modeling the distribution of components emitted from oiled scale between water, gas, and dust media in blast furnace dedusting plant. *Izvestiya. Ferrous Metallurgy*. 2025;68(4):332–338. https://doi.org/10.17073/0368-0797-2025-4-332-338

Моделирование распределения компонентов, выделившихся из замасленной окалины, между водо-газо-пылевыми средами системы газоочистки доменной печи

А. С. Харченко, В. И. Сысоев, С. К. Сибагатуллин, А. В. Дзюба, А. С. Савинов, Е. О. Харченко

Магнитогорский государственный технический университет им. Г.И. Носова (Россия, 455000, Челябинская обл., Магнитогорск, пр. Ленина, 38)

as.mgtu@mail.ru

Аннотация. Физическим моделированием с использованием вертикальной трубчатой электропечи оценили распределение масла из замасленной окалины между различными видами отходов газоочистки доменного производства: пылью, шламом и шламовой водой. Согласно математическому моделированию теплового состояния металлического контейнера с замасленной окалиной интенсивное испарение масла в доменной печи начинается после его загрузки и опускания вдоль шахты на глубину, примерно соответствующую трем подачам. Масло пропускали через нагретый до 500 °С слой агломерата и окатышей Михайловского ГОК массой 0,6 кг и крупностью частиц 10 – 12 мм. Вместе с парами масла в слой железорудного сырья (ЖРС) подавали (вдували) тонко измельченный материал, имитиро-

вавший по компонентному и фракционному составам смесь колошниковой пыли и шламов вакуумной фильтровальной установки (ВФУ) доменного производства, взятых в соотношении 36:64. Физическое моделирование обеспечивало соответствие фактическому газодинамическому режиму в зоне рудного гребня доменной печи, исходя из равенства критерия Рейнольдса. Значение этого критерия, равное 215, было достигнуто в лабораторной модели при подаче аргона с расходом 70 л/мин. По результатам эксперимента распределение масла составило, % от исходного количества: 74,8 % разложилось на слое ЖРС, соответствующем трем подачам; 9,1 % перешло в колошниковую пыль; 15,9 % перешло в шлам ВФУ; в воде мокрой газоочистки масло отсутствовало; 0,2 % (30 мг) масла проходило мокрую газоочистку в форме аэрозоля; на стенках трубопровода наблюдалось незначительное количество сажи. Газовая фаза процессов разложения масла содержала: 70 – 90 % H_2; 1 – 5 % CO; 0,5 – 7,0 % CO_2; 3,2 – 22,2 % CH_4; 0,1 – 2,5 % Σ(C_2H_4, C_2H_6, C_3H_6, C_3H_8). Содержание контролируемого в России бензо(а)пирена в парах масла не превышало 0,00058 %.

Ключевые слова: утилизация техногенных отходов, замасленная окалина, методы переработки, испарение масла, доменная печь

Для цитирования: Харченко А.С., Сысоев В.И., Сибагатуллин С.К., Дзюба А.В., Савинов А.С., Харченко Е.О. Моделирование распределения компонентов, выделившихся из замасленной окалины, между водо-газо-пылевыми средами системы газоочистки доменной печи. *Известия вузов. Черная металлургия*. 2025;68(4):332–338. https://doi.org/10.17073/0368-0797-2025-4-332-338

Introduction

Improving the environmental performance of ferrous metals production and processing increasingly rely on recycling technogenic waste back into production [1; 2]. Among the most valuable iron bearing waste products generated at ferrous metallurgy plants is oiled scale from rolling mills [3 – 5]. This material consists almost entirely of iron oxides (with an iron content of 69 – 72 %) and contains virtually no gangue [6; 7]. Two main types of rolling scale are distinguished, differing in particle size and oil content. The coarse fraction (+2 mm), which accounts for up to 70 – 80 % of the total scale, contains less than 3 % oil and can be effectively used in the sinter burden. The fine fraction (particles smaller than 100 μm) contains a much higher oil content (up to 20 – 30 %), which makes its use in sintering more problematic. During sintering of a burden with elevated oil content, unburned oil residues evaporate, forming explosive mixtures in the oxidizing zones of the sinter machine gas tract. After condensation, the oil contaminates the exhauster blades, reducing their service life [8].

Alternative utilization methods for oiled rolling scale include preliminary chemical treatment (washing with alkali and surfactant solutions) [9; 10] or preliminary thermal treatment (rotary kilns, thermostats, mixers) [11; 12]. The de oiled product is then processed through sintering [14; 15] or briquetting [16]. However, these approaches have not been implemented on an industrial scale due to techno economic constraints, and the problem remains unresolved.

A more recent alternative to the multistage and costly preparation of oiled scale for blast furnace smelting – via sintering or briquetting with prior de oiling – is the direct charging of oiled scale into the blast furnace [17; 18]. According to a patented method [17], instead of using low strength briquettes, oiled scale can be placed in a metallic container designed to melt at temperatures of at least 1500 °C. This approach requires minimal additional equipment, shortens preparation time, eliminates the need for separate storage and disposal of extracted organic compounds, and avoids the purification of contaminated circulating water. However, when granulated oiled scale is charged into the blast furnace, incomplete decomposition of oil vapors passing through the burden may complicate the operation of the furnace dedusting system [19]. Therefore, it is important to evaluate how the oil contained in oiled scale affects the composition of blast furnace dust, VFC sludge, slime water, and the formation of the gas phase in blast furnace off takes.

Materials and methods

In this study, the distribution of oil among various types of blast furnace dedusting wastes (dust, sludge, and slime water) was investigated by physical modeling in a vertical tubular electric furnace. A heated layer of sinter and pellets from the Mikhailovsky GOK, with a particle size of 10 – 12 mm and a mass of 0.6 kg, was successively charged together with a mixture that reproduced, in component and fractional composition, blast furnace dust and sludge from the vacuum filtration plant (VFC) in a ratio of 36:64.

The iron ore raw materials (IORM) were placed in the isothermal zone of the furnace. Their mass was determined from calculations of the amount of material located above the horizon of intensive oil evaporation in the furnace. According to mathematical modeling of the thermal state of a metal container with oiled scale, intensive oil evaporation in the blast furnace begins after the container is charged and lowered along the shaft to a depth corresponding to approximately three feeds. Consequently, the oil vapors pass through a layer of IORM roughly equal in height to three feeds [20 – 22].

To generate a gas flow in which mixing of dust and oil occurred, high grade argon (99.987 %) in accordance with GOST 10157–2016 was supplied at a rate of 70 L/min. This provided a Reynolds criterion value corresponding to the actual gas dynamic mode in the burden ridge zone of the blast furnace. At the furnace outlet, a bottle for “dry” dust collection was installed to simulate the cyclone dedusting unit, followed by a bottle with water for “wet” sludge collection, representing wet gas purification in scrubbers (see Figure).

The parameters of gas and material movement in the laboratory installation were modeled to reflect the following blast furnace operating conditions:

– average daily IORM consumption – 6278 t;

– pellet share in IORM – 36 %;

– average daily consumption of oiled scale (1 % of IORM mass) – 63 t;

– average daily pig iron production – 3798 t;

– average daily top gas generation – 7,139,563 nm^3;

– oil content in oiled scale – 15 %;

– oil mass in oiled scale – 9.4 t;

– water content in oiled scale – 10 %;

– water mass in oiled scale – 6.3 t;

– IORM mass per feed – 39 t;

– blast furnace dust yield – 4.6 kg/t hot metal;

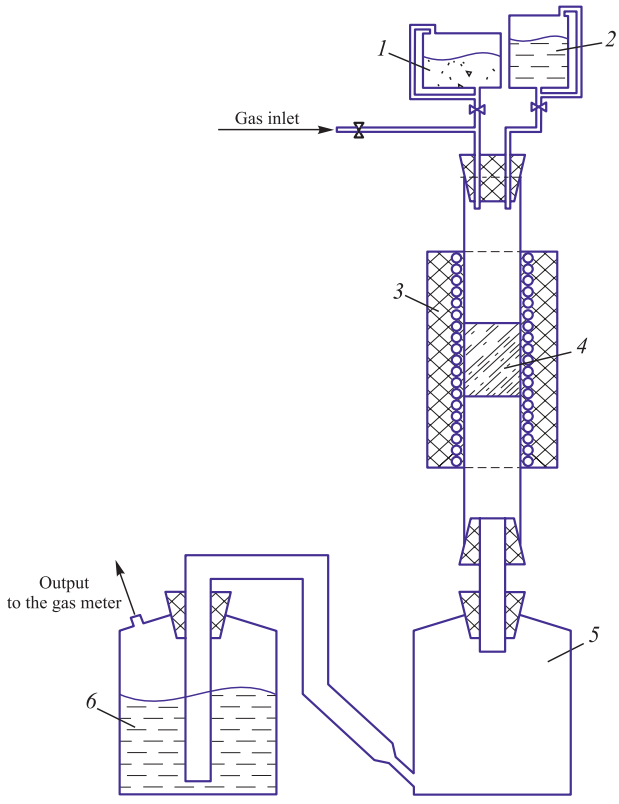

Scheme of experimental installation for physical modeling of the effect of oil on composition of blast furnace dust, sludge and water:
1 – dust bunker; *2* – oil bunker; *3* – laboratory electric tubular furnace; *4* – layer of iron ore raw materials; *5* – bottle for "dry" dust collection; *6* – bottle for "wet" sludge collection

Схема экспериментальной установки для физического моделирования влияния масла на состав колошниковой пыли, шлама и воды:
1 – резервуар с пылью; *2* – резервуар с маслом; *3* – лабораторная электрическая трубчатая печь; *4* – слой железорудного сырья; *5* – емкость для «сухого» улавливания пыли; *6* – емкость с водой для «мокрого» улавливания шлама

– VFC sludge yield – 8.1 kg/t hot metal.

The component composition of dust used in the laboratory experiments was as follows:

1. Blast furnace dust (36 % of total mass):

– fractional composition: 10 % of class 1 – 3 mm and 90 % of class 0 – 1 mm;

– component composition:

– 75 % IORM mixture (64 % sinter and 36 % pellets);

– 25 % coke dust.

2. Sludge fraction (64 % of total mass):

– fractional composition: 100 % of class 0 – 0.2 mm;

– component composition:

– 75 % IORM mixture (64 % sinter and 36 % pellets);

– 25 % coke dust.

During the study, gas samples were taken and analyzed for the content of monoatomic, diatomic, and triatomic gases, as well as light hydrocarbons, using a Chromatec Crystal 5000 gas chromatograph system. For analysis, a packed column HayeSep Q (3 m) and a packed column NaX (3 m) with a Carboxen precolumn (0.5 m) were employed.

Oil samples were also taken to determine the content of seven polynuclear aromatic hydrocarbons (PAHs) – fluorene, phenanthrene, anthracene, fluoranthene, pyrene, chrysene, and benzo[a]pyrene – included in the list of 16 PAHs classified by the US Environmental Protection Agency (US EPA) as priority pollutants. Chromatographic analysis of the oil was carried out using a capillary column CR-5ms (5 % diphenyl/95 % dimethyl (polysiloxane)), 30 m × 0.32 mm × 0.25 μm.

Results

Calculated parameters of the laboratory study:

Oil mass for simulating vapor filtration through the IORM layer, corresponding to one feed, g	0.3
Gas volume required for one feed, based on the oil vapor fraction in blast furnace top gas, L	228
Duration of oil injection corresponding to one feed, min	3
Dust mass loaded into the laboratory installation corresponding to one feed, g	1.5
Reynolds number, Re	215
Number of feeds in the laboratory installation	50

To determine the oil content, thermogravimetric analysis was performed on the collected dust and sludge samples by heating them in an argon atmosphere. Weight losses were 5.2 % for dust and 4.9 % for sludge. With

a dust-to-sludge ratio of 36:64, the overall oil content in the samples after testing was 5.0 %.

Water evaporation from bottle 6 after the experiment showed no significant oil in the aqueous phase. The oil aerosol concentration after wet scrubbing was determined from a vapor–gas sample collected with an NP ZM sampling pump in accordance with GOST R 51945–2002, using indicator tubes for oil aerosols.

Based on the laboratory experiments, the oil distribution was as follows (percent of the initial oil content):

– 74.8 – decomposed in the IORM layer equivalent to three batches;

– 9.1 – transferred to blast furnace dust;

– 15.9 – incorporated into vacuum filtration sludge;

– 0.2 (30 mg) – passed through wet gas cleaning as aerosol.

A small amount of soot was observed on the inner walls of the pipeline during the experiments. No oil was detected in the wet gas purification water, indicating that nearly all of it was adsorbed by suspended fine coke dust particles, which were subsequently filtered, dried, and incorporated into the vacuum filtration sludge. Under industrial conditions, this process would simplify the treatment of recirculating water.

The chemical composition of the gas phase containing oil decomposition products was also analyzed. Across different gas samples, the concentrations of the main components were within the following ranges: 70 – 90 % H_2; 1 – 5 % CO; 0.5 – 7.0 % CO_2; 3.2 – 22.2 % CH_4; 0.1 – 2.5 % Σ (C_2H_4, C_2H_6, C_3H_6, C_3H_8). The formation of these gas components is associated with three main oil decomposition pathways:

1 – (catalytic) dehydrogenation of oil hydrocarbons with cleavage of C–H bonds, producing hydrogen gas and unsaturated compounds prone to polymerization and oxidation. This process is promoted by calcium, iron, and manganese oxides;

2 – (catalytic) cracking of oil hydrocarbons with cleavage of C–C bonds, producing lower molecular weight hydrocarbons, including gaseous hydrocarbons such as methane, ethane, propane, and butane. This process is strongly promoted by complex silicates and aluminosilicates in the agglomerate binder, such as pyroxenes and olivines.

3 – reduction of iron oxides with the formation of CO and CO_2, which is intensified at higher temperatures and when using iron ore raw materials with higher reducibility.

Analysis of oil samples for polynuclear aromatic hydrocarbons (PAHs) showed that the concentration of benzo[a]pyrene, which is regulated in Russia, did not exceed 0.00058 % in oil vapors.

Conclusions

An experimental assessment was conducted to evaluate the distribution of oil from oiled scale among different types of blast furnace dedusting plant – dust, sludge, and slime water – through physical modeling in a vertical tubular electric furnace. A mixture of sinter and pellets of the Mikhailovsky GOK (particle size 10 – 12 mm, mass 0.6 kg) was used to simulate, in terms of component and particle-size composition, blast furnace dust and vacuum filter sludge in a 36:64 ratio. When passing through a layer of iron ore raw materials (IORM) heated to 500 °C, 74.8 % of the oil decomposed within the IORM layer corresponding to three feeds; 9.1 % was transferred to blast furnace dust; and 15.9 % entered the vacuum filter sludge. Only 0.2 % of the oil underwent wet dedusting in the form of an aerosol, while no oil was detected in the wet gas purification water.

The gas phase of oil decomposition contained 70 – 90 % H_2; 1 – 5 % CO; 0.5 – 7.0 % CO_2; 3.2 – 22.2 % CH_4; 0.1 – 2.5 % Σ (C_2H_4, C_2H_6, C_3H_6, C_3H_8). A small amount of soot was observed on the pipeline walls, suggesting the possibility of soot deposition in blast furnace off-gas ducts.

Characteristics and content of polynuclear aromatic hydrocarbons in the oil vapor condensate sample

Характеристики и содержание полиядерных ароматических углеводородов в пробе конденсата паров масла

Substance	Fluorene	Phenanthrene	Anthracene	Fluoranthene	Pyrene	Chrysene	Benzo[a]pyrene
Molecular formula	$C_{13}H_{10}$	$C_{14}H_{10}$	$C_{14}H_{10}$	$C_{16}H_{10}$	$C_{16}H_{10}$	$C_{18}H_{12}$	$C_{20}H_{12}$
Molecular weight, a.u.	166	178	178	202	202	228	252
Boiling point, °C	294	340	340	382	402	448	495
IARC carcinogenicity classification*)	3	3	3	3	3	2B	1
Content in sample, %	$8.0 \cdot 10^{-5}$	$5.6 \cdot 10^{-2}$	–	$7.9 \cdot 10^{-5}$	$7.2 \cdot 10^{-5}$	$3.0 \cdot 10^{-4}$	$5.8 \cdot 10^{-4}$
*IARC – International Agency for Research on Cancer.							

References / Список литературы

1. Rovin S.L., Rovin L.E. New concept of recycling of dispersed iron-containing waste. In: *Proceedings of the X Int. Sci. and Pract. Conf. "Progressive Casting Technologies", Moscow, November 9–13, 2020*. Moscow: Maska; 2020;238–243. (In Russ.).

   Ровин С.Л., Ровин Л.Е. Новая концепция рециклинга дисперсных железосодержащих отходов. В кн.: *Труды X Международной научно-практической конференции «Прогрессивные литейные технологии», Москва, 9–13 ноября 2020 г*. Москва: Маска; 2020;238–243.
2. Bulatov K.V., Gazaleeva G.I. Prospects for development of the technologies for recycling of ferrous metallurgy waste. In: *Fundamental Research and Applied Developments of Processes of Processing and Utilization of Technogenic Formations: Proceedings of the V Congress with Int. Participation and the Conf. of Young Scientists "TECHNOGEN-2021"*. Yekaterinburg: UB RAS; 2021:21–33. (In Russ.). https://doi.org/10.34923/technogen-ural.2021.60.16.003

   Булатов К.В., Газалеева Г.И. Перспективы развития технологий переработки отходов черной металлургии. В кн.: *Фундаментальные исследования и прикладные разработки процессов переработки и утилизации техногенных образований: труды V Конгресса с международным участием и Конференции молодых ученых «ТЕХНОГЕН-2021»*. Екатеринбург: УрО РАН; 2021:21–33. https://doi.org/10.34923/technogen-ural.2021.60.16.003
3. Leont'ev L., Ponomarev V., Sheshukov O. Recycling and disposal of industrial waste from metallurgical production. *Ecology and Industry of Russia*. 2016;20(3):24–27. (In Russ.). https://doi.org/10.18412/1816-0395-2016-3-24-27

   Леонтьев Л., Пономарев В., Шешуков О. Переработка и утилизация техногенных отходов металлургического производства. *Экология и промышленность России*. 2016;20(3):24–27. https://doi.org/10.18412/1816-0395-2016-3-24-27
4. Remus M., Monsonet M.A.A., Roudier S., Sancho L.D. Best Available Techniques (BAT) Reference Document for Iron and Steel Production. Luxemburg: Publications office of the European Union; 2013:627.
5. Yessengaliev D., Mukhametkhan M., Mukhametkhan Ye., Zhabalova G., Kelamanov B., Kolesnikova O., Shyngysbayev B., Aikozova L., Kaskataeva K., Kuatbay Y. Studies of the possibility of improving the quality of iron ores and processing of technogenic composite iron-containing waste of metallurgical production. *Journal of Composites Science*. 2023;7(12):501. https://doi.org/10.3390/jcs7120501
6. Furmanski L.M., Muller T.G., Nuernberg J.B., Martins M.A., Arnt Â.B.C., da Rocha M.R., Zaccaron A., Peterson M. Efficient production of ferrous sulfate from steel mill scale waste. *Journal of Sustainable Metallurgy*. 2024;10(3):1783–1794. https://doi.org/10.1007/s40831-024-00900-8
7. Hryhoriev S., Petryshchev A., Sinyaeva N., Yurchenko A., Sklyar O., Kvitka S., Borysov V., Vlasiuk V., Tsymbal B., Borysova S. Studying the physicalchemical properties of alloyed metallurgical waste as secondary resourcesaving raw materials. *Eastern-European Journal of Enterprise Technologies*. 2018;4(12(94)):43–48. https://doi.org/10.15587/1729-4061.2018.140924
8. Shatokha V.I., Gogenko O.O., Kripak S.M. Utilising of the oiled rolling mills scale in iron ore sintering process. *Resources, Conservation and Recycling*. 2011;55(4):435–440. https://doi.org/10.1016/j.resconrec.2010.11.006
9. Tanutrov I., Sviridova M. Directions to improve the processing methods of anthropogenic waste of the Ural Region. *Ecology and Industry of Russia*. 2015;19(8):31–35. (In Russ.). https://doi.org/10.18412/1816-0395-2015-8-31-35

   Танутров И., Свиридова М. Направления совершенствования способов переработки техногенных отходов Уральского региона. *Экология и промышленность России*. 2015;19(8):31–35. https://doi.org/10.18412/1816-0395-2015-8-31-35
10. Tanutrov I.N., Sviridova M.N., Chesnokov Yu.A., Marshuk L.A. Technological modeling of joint leaching of oily rolling scale and red mud. *Izvestiya. Ferrous Metallurgy*. 2020;63(11-12):891–898. (In Russ.). https://doi.org/10.17073/0368-0797-2020-11-12-891-898

    Танутров И.Н., Свиридова М.Н., Чесноков Ю.А., Маршук Л.А. Технологическое моделирование совместного выщелачивания замасленной прокатной окалины и красного шлама. *Известия вузов. Черная металлургия*. 2020;63(11-12):891–898. https://doi.org/10.17073/0368-0797-2020-11-12-891-898
11. Nemenov A.M. Events in figures and facts. *Metallurg*. 2016;(9):108–112. (In Russ.).

    Неменов А.М. События в цифрах и фактах. *Металлург*. 2016;(9):108–112.
12. Chesnokov Yu.A., Marshuk L.A., Tanutrov I.N., Sviridova M.N. Pyro-metallurgical scheme of joint recycling of red sludge and rolled scale. In: *Fundamental Research and Applied Developments of Processes of Processing and Utilization of Technogenic Formations: Proceedings of the V Congress with Int. Participation and the Conf. of Young Scientists "TECHNOGEN-2021"*. Yekaterinburg: UB RAS; 2021:415–419. (In Russ.).

    Чесноков Ю.А., Маршук Л.А., Танутров И.Н., Свиридова М.Н. Пирометаллургическая схема совместной переработки красных шламов и прокатной окалины. В кн.: *Фундаментальные исследования и прикладные разработки процессов переработки и утилизации техногенных образований: труды V Конгресса с международным участием и Конференции молодых ученых «ТЕХНОГЕН-2021»*. Екатеринбург: УрО РАН; 2021;415–419.
13. Rostovskii V.I., Pliskanovskii S.T., Ivanov A.I., Ispolov V.B., Gladush V.D., Ruchkin I.I., Zhunev A.G., Golubov A.F., Korop N.A. Certificate of authorship USSR no. 1086024 A1, MPC C22B 1/16. Method of agglomeration of iron ore materials. *Bulleten' izobretenii*. 1984;14. (In Russ.).

    А.с. 1086024 А1 СССР, МПК С22В 1/16. Способ агломерации железорудных материалов / В.И. Ростовский, С.Т. Плискановский, А.И. Иванов, В.Б. Исполатов, В.Д. Гладуш, И.И. Ручкин, А.Г. Жунев, А.Ф. Голубов, Н.А. Короп; заявл. 17.12.1981; опубл. 15.04.1984. Бюл. 14.
14. Gurkin M.A., Tabakov M.S., Loginov V.N., Kashkarov E.A., Nevraev V.P., Nesterov A.S., Kuchin V.Yu., Detkova T.V., Yakushev V.S. Patent RF no. 2418079 C2, IPC C22B 1/16. Method of sinter production for blast furnace smelting. *Bulleten' izobretenii*. 2011;13. (In Russ.).

Пат. 2418079 С2 РФ, МПК С22В 1/16. Способ производства агломерата для доменной плавки / М.А. Гуркин, М.С. Табаков, В.Н. Логинов, Е.А. Кашкаров, В.П. Невраев, А.С. Нестеров, В.Ю. Кучин, Т.В. Деткова, В.С. Якушев; заявл. 06.07.2009; опубл. 10.05.2011. Бюл. 13.

15. Gotovtsev A.A., Efimenko Yu.G., Kabanov A.V., Koval Yu.I., Salnikov I.M., Stolberg E.Ya., Khvatov Yu.A.; Certificate of authorship USSR no. 1407979 A1, MPC C22B 1.14. Charge for disposal of oiled scale during agglomeration. *Bulleten' izobretenii*. 1988;25. (In Russ.).

А.с. 1407979 А1 СССР, МПК С22В 1/14. Шихта для утилизации замасленной окалины при агломерации / А.А. Готовцев, Ю.Г. Ефименко, А.В. Кабанов, Ю.И. Коваль, И.М. Сальников, Е.Я. Стольберг, Ю.А. Хватов; заявл. 13.05.1986: опубл. 07.07.1988. Бюл. 25.

16. Salekh A.I.Sh., Gritsishin A.M. Patent RF no. 2321647 C1, IPC C22B 1.242, C22B 1.245. Method of briquetting iron-containing waste in the form of scale for smelting. *Bulleten' izobretenii*. 2006;10. (In Russ.).

Пат. 2321647 С1 РФ, МПК С22В 1/242, С22В 1/245. Способ брикетирования железосодержащих отходов в виде окалины для плавки / А.И.Ш. Салех, А.М. Грицишин; заявл. 06.07.2006; опубл. 10.04.2008. Бюл. 10.

17. Gubanov V.I., Seifulov R.V., Selivanov V.N., Chernousov P.I., Yusfin Yu.S. Patent RF no. 2131929 C1, IPC C21B 5/00. Method for producing pig iron using blast furnace production at a metallurgical enterprise. *Bulleten' izobretenii*. 1999. (In Russ.).

Пат. RU 2131929 С1 РФ, МПК С21В 5/00. Способ получения чугуна с использованием доменного производства на металлургическом предприятии / В.И. Губанов, Р.В. Сейфулов, В.Н. Селиванов, П.И. Черноусов, Ю.С. Юсфин; заявл. 26.06.1998; опубл. 20.06.1999.

18. Khusnutdinov I.Sh., Khusnutdinov S.I., Alekseeva A.A., Bazhin V.Yu., Dubovikov O.A., Johann L.Sh. Patent RF no. 2730304 C1, IPC F23G 7/05, F23G 5/027. Method of disposal of oil- and oil-containing waste, oiled scale, waste from coke production. *Bulleten' izobretenii*. 2020;24. (In Russ.).

Пат. 2730304 С1 РФ, МПК F23G 7/05, F23G 5/027. Способ утилизации масло-нефтесодержащих отходов, замасленной окалины, отходов коксохимического производства / И.Ш. Хуснутдинов, С.И. Хуснутдинов, А.А. Алексеева, В.Ю. Бажин, О.А. Дубовиков, Л.Ш. Иоганн; заявл. 19.03.2019; опубл. 21.08.2020. Бюл. 24.

19. Somova Yu.V., Sviridova T.V., Alekseeva P.A., Nekerov E.A., Schwabecher D. Analysis of methods for processing oily mill scale and oily sludge for iron and steel production. *IOP Conference Series: Earth and Environmental Science*. 2021;839:042046. https://doi.org/10.1088/1755-1315/839/4/042046

20. Savinov A.S., Kharchenko A.S., Sibagatullin S.K., Dzyuba A.V., Sysoev V.I., Kharchenko E.O., Pavlov A.V. Forecasting the temperature of oiled scale packed in a metal container when moving in a blast furnace from the blast-furnace mouth to the iron receiver. *Theory and technology of metallurgical production*. 2024;(4(51)):24–29. (In Russ.).

Савинов А.С., Харченко А.С., Сибагатуллин С.К., Дзюба А.В., Сысоев В.И., Харченко Е.О., Павлов А.В. Прогнозирование температуры замасленной окалины, упакованной в металлический контейнер, при движении в доменной печи от колошника к горну. *Теория и технология металлургического производства*. 2024;(4(51)):24–29.

21. Molgaard J., Smeltzer W.W. Thermal conductivity of magnetite and hematite. *Journal of Applied Physics*. 1971; 42(9):3644–3647. https://doi.org/10.1063/1.1660785

22. Dzyuba A.V., Savinov A.S., Kharchenko A.S., Sibagatullin S.K., Sysoev V.I., Kharchenko M.V. Strength characteristics of containers with oiled scale made approximately to the size of coke. In: *Heat Engineering and Computer Science in Education, Science and Production: Proceedings of the XII All-Rus. Sci. and Pract. Conf. of Students, Postgraduates and Young Scientists (TIM'2024) with International Participation. Yekaterinburg, May 16–17, 2024*. Yekaterinburg: UrFU; 2024:37–41. (In Russ.).

Дзюба А.В., Савинов А.С., Харченко А.С., Сибагатуллин С.К., Сысоев В.И., Харченко М.В. Прочностные характеристики контейнеров с замасленной окалиной, изготовленных приближенно к крупности кокса. В кн.: *Теплотехника и информатика в образовании, науке и производстве: сборник докладов XII Всероссийской научно-практической конференции студентов, аспирантов и молодых ученых (ТИМ'2024) с международным участием. Екатеринбург, 16–17 мая 2024 г.* Екатеринбург: УрФУ; 2024:37–41.

Information about the Authors / Сведения об авторах

Aleksandr S. Kharchenko, *Dr. Sci. (Eng.), Assist. Prof., Head of the Chair of Metallurgy and Chemical Technologies,* Nosov Magnitogorsk State Technical University
ORCID: 0000-0002-0454-6399
E-mail: as.mgtu@mail.ru

Victor I. Sysoev, *Cand. Sci. (Eng.), Head of the Laboratory of the Chair of Metallurgy and Chemical Technologies,* Nosov Magnitogorsk State Technical University
ORCID: 0000-0003-3537-7695
E-mail: v.sysoev@magtu.ru

Salavat K. Sibagatullin, *Dr. Sci. (Eng.), Prof. of the Chair of Metallurgy and Chemical Technologies,* Nosov Magnitogorsk State Technical University
ORCID: 0009-0004-0220-0126
E-mail: 10tks@mail.ru

Александр Сергеевич Харченко, *д.т.н., доцент, заведующий кафедрой металлургии и химических технологий,* Магнитогорский государственный технический университет им. Г.И. Носова
ORCID: 0000-0002-0454-6399
E-mail: as.mgtu@mail.ru

Виктор Иванович Сысоев, *к.т.н, заведующий лабораторией кафедры металлургии и химических технологий,* Магнитогорский государственный технический университет им. Г.И. Носова
ORCID: 0000-0003-3537-7695
E-mail: v.sysoev@magtu.ru

Салават Камилович Сибагатуллин, *д.т.н., профессор кафедры металлургии и химических технологий,* Магнитогорский государственный технический университет им. Г.И. Носова
ORCID: 0009-0004-0220-0126
E-mail: 10tks@mail.ru

Andrei V. Dzyuba, *Postgraduate of the Chair of Metallurgy and Chemical Technologies*, Nosov Magnitogorsk State Technical University
ORCID: 0000-0002-7303-8208
E-mail: dzyuba.98@bk.ru

Aleksandr S. Savinov, *Dr. Sci. (Eng.), Assist. Prof., Head of the Chair of Mechanics*, Nosov Magnitogorsk State Technical University
ORCID: 0000-0001-7440-5404
E-mail: savinov_nis@mail.ru

Elena O. Kharchenko, *Cand. Sci. (Eng.), Senior Lecturer of the Chair of Metallurgy and Chemical Technologies*, Nosov Magnitogorsk State Technical University
E-mail: eo.mgtu@mail.ru

Андрей Викторович Дзюба, *аспирант кафедры металлургии и химических технологий*, Магнитогорский государственный технический университет им. Г.И. Носова
ORCID: 0000-0002-7303-8208
E-mail: dzyuba.98@bk.ru

Александр Сергеевич Савинов, *д.т.н., доцент, заведующий кафедрой механики*, Магнитогорский государственный технический университет им. Г.И. Носова
ORCID: 0000-0001-7440-5404
E-mail: savinov_nis@mail.ru

Елена Олеговна Харченко, *к.т.н, старший преподаватель кафедры металлургии и химических технологий*, Магнитогорский государственный технический университет им. Г.И. Носова
E-mail: eo.mgtu@mail.ru

Contribution of the Authors / Вклад авторов

A. S. Kharchenko – problem statement, analysis of research results, formulation of conclusions.
V. I. Sysoev – testing of samples on the gas chromatographic complex "Chromatec Crystal 5000".
S. K. Sibagatullin – carrying out calculations, obtaining results, obtaining drawings and graphs.
A. V. Dzyuba – description of results, formulation of conclusions, critical analysis of literature.

A. S. Savinov – problem statement, analysis of research results, formulation of conclusions.
E. O. Kharchenko – establishing the rational composition of water, gas, and dust media of blast furnace gas dedusting plant, analysis of research results.

А. С. Харченко – постановка задачи, анализ результатов исследований, формулирование выводов.
В. И. Сысоев – испытания образцов на газохроматографическом комплексе «Хроматэк Кристалл 5000».
С. К. Сибагатуллин – проведение расчетов, получение результатов, создание рисунков и графиков.
А. В. Дзюба – описание результатов, испытания образцов в вертикальной трубчатой электропечи, критический анализ литературы.
А. С. Савинов – постановка задачи, анализ результатов исследований, формулирование выводов.
Е. О. Харченко – установление рациональной водо-газо-пылевой среды системы газоочистки доменной печи, анализ результатов исследований.

Received 20.05.2025
Revised 09.06.2025
Accepted 16.06.2025

Поступила в редакцию 20.05.2025
После доработки 09.06.2025
Принята к публикации 16.06.2025

Metallurgical technologies / Металлургические технологии

UDC 669.168.3:621.365.2
DOI 10.17073/0368-0797-2025-4-339-341

Short Report
Краткое сообщение

Modeling the operation of ferroalloy furnace with increased power and electrode diameters

A. P. Shkirmontov

Financial University under the Government of the Russian Federation (49/2 Leningradskii Ave., Moscow 125167, Russian Federation)

aps-panor@yandex.ru

Abstract. Using an electrolytic model, the authors investigated the operation of a ferroalloy furnace with increased electrode diameters and power. A traditional aqueous solution with a concentration of 0.2 % NaCl was used as the working fluid. Diameter of the electrodes was increased from 30 to 150 mm. The parameters of furnaces with a capacity from 7.5 – 10.5 to 81 MV·A during ferrosilicon smelting correspond to the results of simulation experiments, which were confirmed during the smelting of 45 % ferrosilicon in industrial furnaces with similar relative technological parameters. The type of dependence of the decrease in bath resistance on the increase in electrode diameter for industrial ferroalloy furnaces is similar to the dependence obtained as a result of modeling experiments. The factor of a significant decrease in the bath resistance due to an increase in electrode diameter for ferroalloy furnaces of different capacities during the smelting of a single alloy is very significant. With an increase in current strength of the electrode, electrical efficiency, the furnace power factor and the share of active power in the bath decrease. Analysis of the furnace parameters during smelting of 45 % ferrosilicon confirms the conclusions of electrolytic modeling of ferroalloy furnaces about the significant role of increasing the diameter of furnace electrodes in reducing the bath active resistance.

Keywords: ferroalloy furnace, electric furnace models, electrode diameter, electrode decay, active bath resistance, power factor

For citation: Shkirmontov A.P. Modeling the operation of ferroalloy furnace with increased power and electrode diameters. *Izvestiya. Ferrous Metallurgy*. 2025;68(4):339–341. https://doi.org/10.17073/0368-0797-2025-4-339-341

Моделирование работы ферросплавной печи при увеличении мощности и диаметра электродов

А. П. Шкирмонтов

Финансовый университет при Правительстве Российской Федерации (Россия, 125167, Москва, Ленинградский пр., 49/2)

aps-panor@yandex.ru

Аннотация. На электролитической модели авторы исследовали работу ферросплавной печи при увеличении диаметра электродов и повышении мощности. В качестве рабочего тела использовали традиционный водный раствор с концентрацией 0,2 % NaCl. Диаметр электродов увеличивали от 30 до 150 мм. Параметры печей мощностью от 7,5 – 10,5 до 81 МВ·А при выплавке ферросилиция соответствуют результатам опытов моделирования, которые были подтверждены при выплавке 45 %-ного ферросилиция в промышленных печах с аналогичными относительными технологическими параметрами. Вид зависимости снижения сопротивления ванны от увеличения диаметра электродов для промышленных ферросплавных печей аналогичен зависимости, полученной в результате опытов по моделированию. Фактор значительного снижения сопротивления ванны от увеличения диаметра электрода для ферросплавных печей различной мощности при выплавке одного сплава имеет весьма существенное значение. При увеличении силы тока электрода снижаются электрический КПД, коэффициент мощности печи и доля активной мощности в ванне технологического процесса. Проведенный анализ параметров печей при выплавке 45 %-ного ферросилиция подтверждает выводы электролитического моделирования ферросплавных печей о значительной роли увеличения диаметра электродов печей в снижении активного сопротивления ванны.

Ключевые слова: ферросплавная печь, модель электропечи, диаметр электрода, распад электродов, активное сопротивление ванны, коэффициент мощности

Для цитирования: Шкирмонтов А.П. Моделирование работы ферросплавной печи при увеличении мощности и диаметров электродов. *Известия вузов. Черная металлургия*. 2025;68(4):339–341. https://doi.org/10.17073/0368-0797-2025-4-339-341

Introduction

Studies of ferroalloy electric furnace models have a long history and continue in a number of research works aimed at improving the arc model in three-phase furnaces [1] and achieving effective heat distribution in closed-arc baths [2]. In [3], comprehensive modeling of furnace operation during ferronickel smelting was carried out. Several domestic studies have investigated: charge melting models in six-electrode furnaces [4]; furnace control models with maintenance of slag bath resistance [5]; and favorable current distribution in multi-electrode furnaces [6]. A number of these models adequately reproduce real processes, making it possible to obtain reliable information on the parameters of furnace operation and their interaction. Various simulation models of furnaces are widely used, including electrolytic modeling of ferroalloy furnace baths.

Increasing the power of ferroalloy furnaces is accompanied by larger electrode diameters, which results in higher capital and operating costs, greater consumption of non-ferrous and ferrous metals, and technological challenges. For example, when furnace power increases from 7.5 – 10.5 to 10^5 MV·A, the diameter of self-baking electrodes grows significantly – from 900 to 1800 – 2000 mm (a 2.0 – 2.2-fold increase). The electrode current rises from 32 – 37 to 160 kA and above (a 4.3 – 5.0-fold increase). By contrast, the operating voltage increases far less significantly – from 130 to 230 – 300 V (a 1.8 – 2.3-fold increase) [7]. This only indirectly indicates a decrease in the active bath resistance of the furnace and the power factor, leading to higher power losses in the short network.

On an electrolytic furnace model, studies were carried out to determine and evaluate changes in active bath resistance (in the electrode–hearth section) as electrode diameters increased. For comparison, an analysis of the operating parameters of industrial ferroalloy furnaces with different capacities and electrode diameters was also performed.

Experimental procedure

A traditional aqueous solution with a concentration of 0.2 % NaCl was used as the working fluid in the model. The experiments followed a method similar to that described in [7]. The diameter of the graphitized electrodes was varied from 30 to 150 mm. The diameter of the conducting hearth of the model was calculated using the expression $D_{\text{hearth}} = d_e + 2a$, where d_e is the electrode diameter, mm and a is the distance from the electrode to the bath wall, mm. Typically, the electrode-to-wall distance in furnaces is $(0.8 \div 1.0)d_e$, with an average value of $0.9d_e$. For all experiments, it was assumed that $D_{\text{hearth}} = 2.8d_e$. For ferroalloy smelting, the electrode–hearth distance corresponds to the range of $(0.6 \div 0.8)d_e$ [8] (expressed in electrode diameters). The relative sub-electrode gap (h/d_e) was set at 0.7 of the electrode diameter. The electrode immersion depth Δh in the electrolyte was taken as equal to the electrode diameter.

Installation description

Alternating current at 50 Hz was supplied through an autotransformer and an isolation transformer to a vertically positioned electrode and the conducting hearth of the furnace model. Bath resistance for each electrode diameter was determined from current and voltage measurements.

Conditions for modeling electrical parameters: $\rho = \text{const}$ – specific electrical resistivity of the model bath, Ω·cm; $h/d_e = \text{const}$ – sub-electrode gap, expressed in electrode diameters; $\Delta h/d_e = \text{const}$ – electrode immersion depth, in electrode diameters; $t = \text{const} = 23$ °C – electrolyte temperature during the experiments. The variation in bath resistance of the model with increasing electrode diameter is shown in Fig. *a*.

For comparison, parameters of 43 furnaces used for ferrosilicon smelting (operating voltage, electrode current, and power factor) were analyzed. The active bath resistance of the furnace, R_{act} (mΩ), was determined according to the relation

$$R_{\text{act}} = \frac{U_{\text{oper}} \cos\varphi}{1.73 I_e},$$

where U_{oper} is the operating voltage at the transformer stage, V, $\cos\varphi$ is the furnace power factor, and I_e is the electrode current, kA.

The processed data for industrial ferrosilicon furnaces, showing the change in active bath resistance with increasing electrode diameter, are presented in Fig. *b*.

Discussion of the results

Increasing the electrode diameter in the ferroalloy furnace model results in a marked decrease in bath resistance. To validate this dependence, the parameters of 43 furnaces were analyzed. The power of the furnace transformers ranged from 7.5 – 10.5 to 81 MV·A, while the diameter of self-baking electrodes increased from 750 – 900 to 1900 – 2000 mm.

Notably, in industrial ferroalloy furnaces, the reduction in bath resistance with increasing electrode diameter follows the same trend as observed in the modeling experiments.

The findings can be applied as a methodological basis for laboratory training in ferroalloy production, particu-

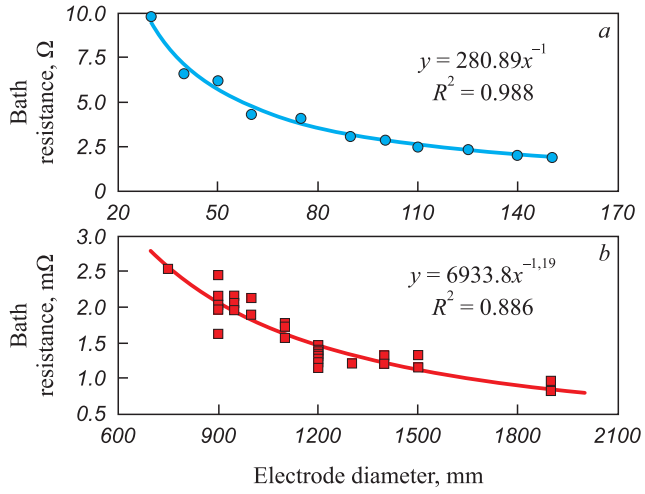

Change in the bath active resistance with an increase in the electrode diameters on electrolytic model of a ferroalloy furnace (*a*) and on 43 industrial furnaces (*b*) with a capacity of 7.5 – 81.0 MV·A during smelting of 45 % ferrosilicon

Изменение активного сопротивления ванны при увеличении диаметра электродов на электролитической модели ферросплавной печи (*a*) и на 43 промышленных печах (*b*) мощностью 7,5 – 81,0 МВ·А при выплавке 45 %-ного ферросилиция

larly for studying the relationship between furnace power and self-baking electrode diameter.

The significant reduction in bath resistance with increasing electrode diameter across ferroalloy furnaces of different capacities, when smelting the same alloy, is of considerable importance. However, as electrode current rises substantially, energy performance indicators deteriorate: electrical efficiency, furnace power factor, and the proportion of active power in the bath all decrease.

Conclusions

Analysis of furnace parameters during the smelting of 45 % ferrosilicon confirmed the results of electrolytic modeling of ferroalloy furnace operation, highlighting the significant role of increasing electrode diameter in lowering active bath resistance. In this case, the use of carbonaceous reducers with higher specific electrical resistivity, along with additional reactive power compensation, becomes necessary.

References / Список литературы

1. Saevarsdottir G., Larsen H.L., Bakken J.A. Modelling of AC arcs in three-phase submerged arc furnaces. In: *Proceedings of the VII Int. Ferroalloys Congress: INFACON VII. Beijing, China. 7 – 10 June 1998*. Beijing; 1998:317–322.
2. Li J. Discussion of ideal smelting model of submerged-arc furnace. In: *Proceedings of the IX Int. Ferroalloys Congress: INFACON IX. Quebec City, Canada. 3 – 6 June 2001*. Quebec City; 2001:121–130.
3. Oterdoom H., Degel R. Building a FeNi smelter simulator. In: *Proceedings of the XII Int. Ferroalloys Congress: INFACON XII. Helsinki, Finland. 6 – 9 June 2010*. Helsinki; 2010:215–227.
4. Lastochkina M.A. Model of charge melting in the bath of an ore-thermal furnace. *Zapiski Gornogo instituta*. 2002;150:119–123. (In Russ.).

   Ласточкина М.А. Модель плавления шихты в ванне руднотермической печи. *Записки Горного института*. 2002;150:119–123.
5. Ryabov V.P., Khomyakov I.V., Chursin A.Yu. The model of an electric ore smelting furnace control system with maintaining the slag bath resistance. *Bulletin of MPEI*. 2020;(1): 82–88. (In Russ.). https://doi.org/10.24160/1993-6982-2020-1-82-88

   Рябов В.П., Хомяков И.В., Чурсин А.Ю. Разработка модели системы управления руднотермической печью с поддержанием сопротивления шлаковой ванны. *Вестник Московского энергетического института*. 2020;(1): 82–88. https://doi.org/10.24160/1993-6982-2020-1-82-88
6. Il'gachev A.N., Mikhadarov D.G. Study of the current in the multielectrode plant bath. *Vestnik Chuvashskogo universiteta*. 2023;(4):99–108. (In Russ.). https://doi.org/10.47026/1810-1909-2023-4-99-108

   Ильгачёв А.Н., Михадаров Д.Г. Токи в ванне многоэлектродной установки. *Вестник Чувашского университета*. 2023;(4):99–108. https://doi.org/10.47026/1810-1909-2023-4-99-108
7. Shkirmontov A.P. Establishing the theoretical foundations and energy parameters for the production of ferroalloys with a larger-than-normal gap under the electrode. *Metallurgist*. 2009;53(5-6):300–308.
8. Shkirmontov A.P. Energy-Technological Parameters of Ferroalloy Smelting in Electric Furnaces. Moscow: NITU MISiS; 2018:216. (In Russ.).

   Шкирмонтов А.П. Энерготехнологические параметры выплавки ферросплавов в электропечах. Москва: ИД МИСиС; 2018:216.

Information about the Author / Сведения об авторе

Aleksandr P. Shkirmontov, *Dr. Sci. (Eng.), Director of the Editorial Center of Scientific Journals,* Financial University under the Government of the Russian Federation
E-mail: aps-panor@yandex.ru

Александр Прокопьевич Шкирмонтов, *д.т.н., директор Центра Редакции научных журналов,* Финансовый университет при Правительстве Российской Федерации
E-mail: aps-panor@yandex.ru

Received 03.12.2024
Revised 27.12.2024
Accepted 05.05.2025

Поступила в редакцию 03.12.2024
После доработки 27.12.2024
Принята к публикации 05.05.2025

ECOLOGY AND RATIONAL USE OF NATURAL RESOURCES / **ЭКОЛОГИЯ И РАЦИОНАЛЬНОЕ ПРИРОДОПОЛЬЗОВАНИЕ**

UDC 504.064.38+54-165+544.014
DOI 10.17073/0368-0797-2025-4-342-348

Original article
Оригинальная статья

Promising designs of gas analyzers for metallurgy

M. V. Vasina[1], L. P. Bashchenko[2]

[1] **Omsk State Technical University** (11 Mira Str., Omsk 644050, Russian Federation)
[2] **Siberian State Industrial University** (42 Kirova Str., Novokuznetsk, Kemerovo Region – Kuzbass 654007, Russian Federation)

89609949132@mail.ru

Abstract. Gas analysis is one of the key methods for assessing the quality of atmospheric air in populated areas, as well as in the work area of production facilities. Atmospheric air monitoring is especially necessary at facilities that have a significant negative impact on the environment, in particular, at ferrous metallurgy enterprises. The peculiarities of the gas analyzers used for air quality monitoring system are their sensitivity and selectivity. To achieve these indicators, a properly selected sensing element is needed: a gas analyzer converter. Synthesized solid solutions of semiconductor binary components, which proved themselves to be good adsorbents, are proposed as materials for the manufacture of converters. In this paper, the authors examined semiconductor systems consisting of ZnTe and CdSe, conditions for synthesis of the solid solutions based on them, and methods for their identification, which allowed the obtained materials to be certified as solid substitution solutions with cubic sphalerite and hexagonal wurtzite structures (depending on the composition). *X*-ray, micro-, electron-microscopic, and IR spectroscopic studies of solid solutions made it possible to understand the surface structure of adsorbents. Results of the studies of the surface chemical composition, acid-base properties of solid solutions and binary components of the system allow us to conclude that the Lewis and Brønsted acid centers responsible for CO adsorption on the surface are present on the surface. In the ZnTe–CdSe systems, there is a tendency to move from a slightly acidic region to a relative increase in the surface basicity with an increase in ZnTe content. When materials are placed in a CO atmosphere, gas adsorption on the surface of solid solutions occurs in the same dependence, which was confirmed by the direct catalytic studies. The established patterns of changes with the composition of bulk and surface properties allow us to recommend new obtained materials as primary converters of sensors.

Keywords: gas analyzer, carbon monoxide, semiconductor, new materials, solid solution, chemical composition, surface and bulk properties, regularities

For citation: Vasina M.V., Bashchenko L.P. Promising designs of gas analyzers for metallurgy. *Izvestiya. Ferrous Metallurgy*. 2025;68(4):342–348. https://doi.org/10.17073/0368-0797-2025-4-342-348

Перспективные конструкции газоанализаторов для металлургии

М. В. Васина[1], Л. П. Бащенко[2]

[1] **Омский государственный технический университет** (Россия, 644050, Омск, пр. Мира, 11)
[2] **Сибирский государственный индустриальный университет** (Россия, 654007, Кемеровская обл. – Кузбасс, Новокузнецк, ул. Кирова, 42)

89609949132@mail.ru

Аннотация. Газовый анализ – один из ключевых методов оценки качества атмосферного воздуха в населенных пунктах, а также в рабочей зоне производств. Особенно необходим мониторинг атмосферного воздуха на объектах, оказывающих значительное негативное воздействие на окружающую среду, в частности, на предприятиях черной металлургии. Особенность газоанализаторов, используемых для системы наблюдения за качеством воздуха, заключается в их чувствительности и селективности. Для достижения данных показателей необходим правильно подобранный чувствительный элемент: преобразователь газоанализатора. В качестве материалов для изготовления преобразователей предлагаются синтезированные твердые растворы полупроводниковых бинарных компонентов, которые зарекомендовали себя как хорошие адсорбенты. В настоящей работе авторы рассмотрели полупроводниковые системы, состоящие из ZnTe и CdSe, условия синтеза твердых растворов на их основе, способы их идентификации, которые позволили аттестовать полученные материалы как твердые растворы замещения с кубической структурой (сфалерита) и гексагональной структурой (вюрцита) (в зависимости от состава). Выполненные рентгенографические, микро-, электронно-микроскопические, ИК-спектроскопические исследования твердых растворов позволили понять структуру поверхности адсорбентов. Результаты исследований химического состава поверхности, кислотно-основных свойств твердых растворов и бинарных компонентов систем позволяют сделать вывод о присутствии на поверхности льисовских и бренстедовских кислотных центров, отвечающих за адсорбцию CO на поверхности. В системах ZnTe–CdSe наблюдается тенденция перехода от слабокислой области к относительному повышению основности поверхности с увеличением содержания ZnTe. При помещении мате-

риалов в атмосферу CO в такой же зависимости происходит адсорбция газа на поверхности твердых растворов, что подтвердили прямые каталитические исследования. Установленные закономерности изменений с составом объемных и поверхностных свойств позволяют рекомендовать новые полученные материалы в качестве первичных преобразователей сенсоров-датчиков.

Ключевые слова: газоанализатор, угарный газ, полупроводник, новые материалы, твердые растворы, химический состав, поверхностные и объемные свойства, закономерности

Для цитирования: Васина М.В., Бащенко Л.П. Перспективные конструкции газоанализаторов для металлургии. *Известия вузов. Черная металлургия*. 2025;68(4):342–348. https://doi.org/10.17073/0368-0797-2025-4-342-348

Introduction

In industrial zones of metallurgical enterprises, the concentration of carbon monoxide in the ambient air often exceeds permissible limits, posing serious risks to both employee health and the environment. To monitor air quality, gas analyzers are utilized; these devices rely on the bulk and surface properties of their sensing elements, which ensure high sensitivity, rapid response, and selectivity. Timely detection of carbon monoxide in the workplace is critical for preventing accidents, minimizing environmental damage, and safeguarding personnel health.

Semiconductor materials are commonly used as sensing elements in gas analyzers due to their excellent adsorption properties [1]. Their sensitivity is primarily based on gas molecule adsorption at the surface, the formation of space-charge regions, and changes in the concentration of charge carriers in the near-surface layer. The efficiency of adsorption depends on the semiconductor's structural type, the nature and concentration of active surface centers, and its specific surface area [2]. Gas detection occurs through changes in the electrical conductivity of the sensing element (sensor signal) upon exposure to the target gas [3]. Therefore, the choice of sensing material is a key factor in analyzer performance. One promising approach to enhancing the adsorption capacity of binary materials involves the synthesis of diamond-like semiconductors to produce novel multicomponent materials in the form of solid solutions.

There is growing scientific and practical interest in investigating the previously unexplored physicochemical properties of ZnTe–CdSe solid solutions. These materials demonstrate favorable performance characteristics combined with low production costs, making them promising candidates for sensor applications [4]. Varying the component ratio in the ZnTe–CdSe system allows for the synthesis of solid solutions with tailored properties, enabling their use in a wide range of applications.

The aim of this study is to synthesize and characterize ZnTe–CdSe solid solutions and to determine potential areas of practical application based on their physicochemical properties.

To achieve this, the following objectives were set:

– to synthesize and characterize ZnTe–CdSe solid solutions;

– to investigate the physicochemical surface properties of the system components;

– to evaluate the application potential of the resulting materials in sensor technology as a cost-effective alternative.

Materials and methods

The study investigated fine powders of the binary compounds ZnTe and CdSe, along with their solid solutions $(ZnTe)_x(CdSe)_{1-x}$, synthesized using a method specifically developed for this material system [5]. The powders had specific surface areas ranging from 0.3 to 0.91 m^2/g. Confirmation of successful synthesis, formation of solid solutions, and structural characteristics was carried out through *X*-ray diffraction (XRD), optical and electron microscopy, and infrared (IR) spectroscopy. The molar compositions of the synthesized solid solutions were verified against elemental compositions derived from scanning electron microscopy (SEM) images.

XRD analysis was performed using a D8 Advance Powder *X*-ray diffractometer (Bruker AXS, Germany) with CuK_α radiation ($\lambda = 0.15406$ nm) at $T = 293$ K. Measurements followed a wide-angle scanning protocol [6; 7], using a Lynxeye position-sensitive detector. Data interpretation and refinement of the crystal lattice parameters were conducted using the ICDD PDF-2 powder diffraction database and TOPAS 3.0 software (Bruker) [8].

Microscopic examinations were carried out using a KN 8700 microscope (Hilox, Japan) and a Micromed POLAR 3 optical microscope with a resolution capacity of up to 7000× [9]. SEM analysis was performed on a JCM–5700 scanning electron microscope equipped with a JED-2300 energy-dispersive spectroscopy (EDS) attachment [10].

Surface acid–base properties were analyzed using hydrolytic adsorption (to determine the isoelectric point) and non-aqueous conductometric titration [11]. Catalytic properties were evaluated using a non-gradient flow-circulation method, under conditions that minimized the influence of mass and heat transfer. Tests were conducted at temperatures ranging from 298 to 423 K and a pressure of 101.3 kPa. The carrier gas (argon) was circulated at a rate of 22 mL/min, and the pulse volume was

set to 5 mL. Gas composition after reaction was assessed by chromatographic analysis.

In the hydrolytic adsorption method, the pH value was determined at which the amphoteric adsorbents (ZnTe, CdSe, and their solid solutions $(ZnTe)_x(CdSe)_{1-x}$) released equal and minimal amounts of H^+ and OH^- ions. These materials exhibited distinct isoelectric points corresponding to their minimum solubility. The pH_{iso} values were used to assess the average strength and the ratio of acidic to basic surface centers.

Reproducibility and measurement accuracy were evaluated through parallel experiments, with data analyzed using standard methods of mathematical statistics and quantitative analysis. Numerical processing, error estimation, and the construction and analysis of graphical data were performed using Stat-2, Microsoft Excel, and Origin software.

Results and discussion

Synthesis of the solid solutions was performed in two stages: heating of sealed ampoules from 573 to 1273 K, followed by controlled cooling to 725 K [12; 13]. The synthesis parameters are presented in Table 1.

XRD analysis confirmed the formation of substitutional solid solutions in the ZnTe–CdSe system. In the diffraction patterns of the solid solutions, characteristic peaks were shifted relative to those of the binary compounds, indicating changes in the crystal structure [14]. Zinc telluride and solid solutions with excess ZnTe exhibited a cubic sphalerite-type structure, while cadmium selenide and solid solutions with excess CdSe demonstrated a hexagonal wurtzite-type structure [15].

Lattice parameters (a, c), unit cell volume (V_p), interplanar spacing (d_{hkl}), and X-ray density (ρ_r) varied smoothly or linearly with composition [16]. The size of the coherent scattering region was estimated using the Scherrer equation.

The elemental distribution within the solid solutions was assessed using scanning electron microscopy (SEM) on a JCM-5700 microscope equipped with a nitrogen-free energy-dispersive X-ray spectrometer.

SEM images of the powders of the binary compounds and solid solutions of the studied system are shown in Fig. 1.

In the phase-contrast SEM images of ZnTe–CdSe solid solutions, bright CdSe inclusions smaller than 5 μm were observed on the homogeneous background of ZnTe grains. ZnTe binary compound is characterized by coarser grains, a feature that persists in the solid solutions with higher ZnTe content (Table 2).

The specific geometric surface area, surface-area mean diameter, number-average diameter, volume-weighted diameter, and polydispersity index of the systems (Table 3) were calculated using the following formulas:

Table 1. **Mode of obtaining solid solutions based on the ZnTe–CdSe system components**

Таблица 1. **Режим получения твердых растворов на основе компонентов системы ZnTe–CdSe**

Mode	Holding temperature, °C	Holding time, h
Heating	300	21.0
	500	19.0
	600	10.0
	700	37.0
	800	29.0
	900	20.5
	1000	29.0
Cooling	900	50.0
	700	25.0
	500	111.0
Total		**351.5**

$$S = \frac{6\sum n_i d_i^2}{\rho \sum n_i d_i} = \frac{6}{\rho d_s};$$

$$K = \frac{d_n}{d_q},$$

where S is the specific geometric surface area, m^2/kg; d_i is the mean diameter of particles in each fraction; n is the number of particles in the system; ρ is the X-ray density of the particles; d_s, d_n, d_q represent the surface-area, number-average, and volume-weighted mean diameters, respectively; K is the polydispersity index.

The chemical nature of the acid centers responsible for gas adsorption was determined using conductometric titration [17], which also allowed quantification of their concentration on the surface of the ZnTe–CdSe system components. The acid centers responsible for gas adsorption on the surface are as follows: surface atoms with varying degrees of coordination unsaturation – namely, Cd and Zn atoms (Lewis acid centers), as well as adsorbed water molecules and hydroxyl groups OH^- (Brønsted acid centers) [18]. These conclusions were supported by measurements of the isoelectric point (pH) and IR spectra of the surface [19].

The total concentration of acid centers exhibits an extremal dependence on composition, with maxima observed for $(ZnTe)_{0.26}(CdSe)_{0.74}$ and $(ZnTe)_{0.68}(CdSe)_{0.32}$ (Fig. 2). These compositions therefore demonstrate the highest surface acidity, indicating a strong adsorption

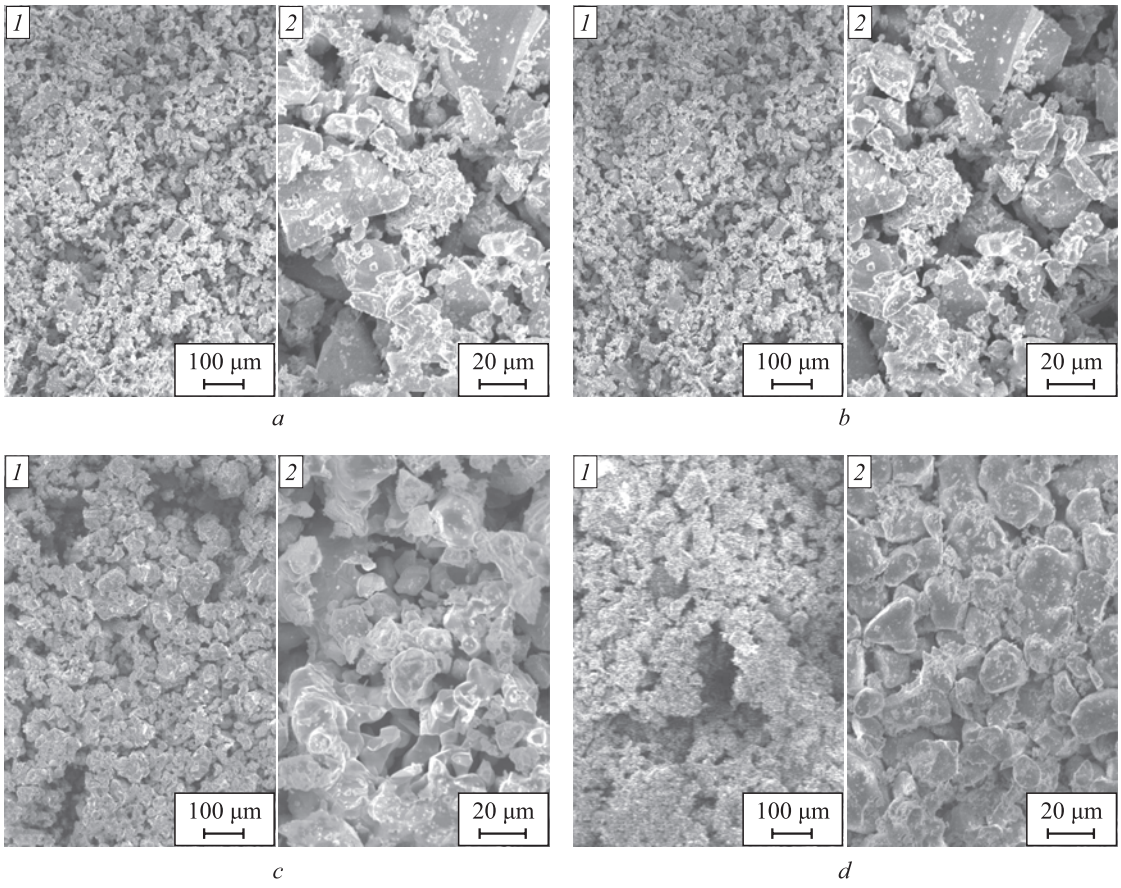

Fig. 1. SEM images of powders CdSe (*a*), $(ZnTe)_{0.26}(CdSe)_{0.74}$ (*b*), $(ZnTe)_{0.68}(CdSe)_{0.32}$ (*c*) and ZnTe (*d*) obtained at different magnifications (*1 – 2*)

Рис. 1. SEM изображения порошков CdSe (*a*), $(ZnTe)_{0,26}(CdSe)_{0,74}$ (*b*), $(ZnTe)_{0,68}(CdSe)_{0,32}$ (*c*) и ZnTe (*d*), полученных при разном увеличении (*1 – 2*)

capacity of $(ZnTe)_{0.26}(CdSe)_{0.74}$ and $(ZnTe)_{0.68}(CdSe)_{0.32}$ toward basic gases.

The increased surface activity $(ZnTe)_{0.68}(CdSe)_{0.32}$ and $(ZnTe)_{0.26}(CdSe)_{0.74}$ solid solutions is further supported by the results of acid–base property analysis. The pH_{iso} values of the studied semiconductors (Table 4), measured after air exposure, increase steadily with rising ZnTe content. Upon exposure to CO, extrema appear in the ZnTe – CdSe system corresponding to the compositions $(ZnTe)_{0.68}(CdSe)_{0.32}$ and $(ZnTe)_{0.26}(CdSe)_{0.74}$, and overall, a shift in *p*H values toward the alkaline region is observed. This behavior is attributed to the high electron density of the carbon and oxygen atoms and the strong double bond between them. The lone electron pairs of CO and its vacant orbitals partially neutralize the coordinatively unsaturated surface atoms (Zn, Cd), thereby enabling the interaction. These findings support the donor–acceptor interaction mechanism [20].

Table 2. **Results of particle counting by microscopic analysis**

Таблица 2. **Результаты подсчета частиц микроскопическим анализом**

Composition	Number of particles by size range, μm										
	5 – 7	10 – 14,5	15 – 17,5	18 – 20	21 – 24	25 – 31	32 – 35	37 – 40	41 – 43	50 – 53	57 – 60
CdSe	2	2	4	3	2	5	–	–	–	–	–
$(ZnTe)_{0.12}(CdSe)_{0.88}$	–	5	2	5	3	6	1	–	–	–	–
$(ZnTe)_{0.26}(CdSe)_{0.74}$	–	4	9	6	4	3	–	–	–	–	–
$(ZnTe)_{0.68}(CdSe)_{0.32}$	–	5	4	2	4	4	–	–	–	–	–
$(ZnTe)_{0.75}(CdSe)_{0.25}$	–	3	2	4	6	4	2	–	–	–	–
ZnTe	–	1	–	–	2	4	–	4	3	1	3

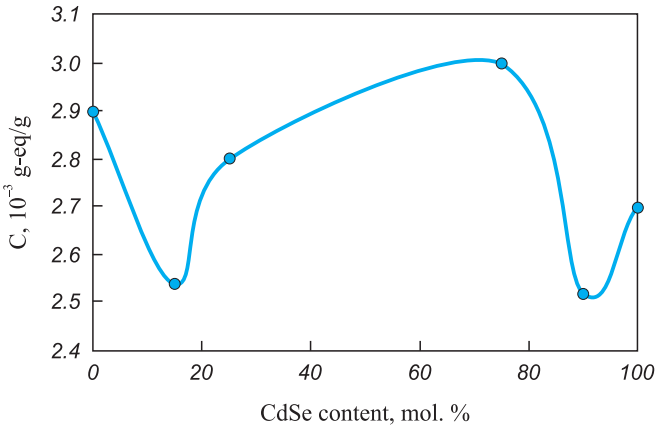

Fig. 2. Dependence of the total concentration of acidic centers of the ZnTe–CdSe system components exposed to air

Рис. 2. Зависимость общей концентрации кислотных центров компонентов системы ZnTe–CdSe, экспонированных на воздухе

The most pronounced difference in pH_{iso} values was observed between CdSe and the solid solutions containing 26 and 68 % ZnTe in CdSe, respectively. These two compositions were selected as candidate sensing materials for carbon monoxide gas analyzers.

The pH_{iso} behavior in a CO atmosphere, along with IR spectroscopic data indicating enhanced CO adsorption in $CO + O_2$ mixtures [19], allows for a preliminary (pre-adsorption testing) prediction of high catalytic activity in $(ZnTe)_{0.26}(CdSe)_{0.74}$ and $(ZnTe)_{0.68}(CdSe)_{0.32}$. This prediction was subsequently confirmed through direct catalytic testing under identical conditions (Fig. 3).

Analysis of the experimental data indicates a significant degree of catalytic CO conversion (χ_{CO}) even at room temperature. For the $(ZnTe)_{0.26}(CdSe)_{0.74}$ composition, the CO conversion rate reaches 79 %. As the temperature increases, χ_{CO} values generally rise, with maximum conversion observed at 373 K.

A comparison of the CO oxidation efficiency and CO adsorption capacity shows that CdSe and the solid solution $(ZnTe)_{0.26}(CdSe)_{0.74}$ demonstrate higher catalytic activity, which is consistent with their surface acid–base characteristics. In contrast, ZnTe exhibits lower catalytic activity and adsorption capacity.

In summary, substitutional solid solutions were successfully synthesized from the binary components ZnTe and CdSe. The solid solutions obtained exhibit a cubic structure when zinc telluride is in excess and a hexagonal structure when cadmium selenide predominates. Electron microscopy confirmed the molar and elemental composition of the samples.

Among the synthesized materials the $(ZnTe)_{0.26}(CdSe)_{0.74}$ and $(ZnTe)_{0.68}(CdSe)_{0.32}$ compositions demonstrated the largest specific surface area. A similar trend was observed in these samples when analyzing the nature of active surface centers after exposure to air and carbon monoxide, using hydrolytic adsorption and non-aqueous conductometric titration. These results indicate that the surfaces of these solid solutions are highly active

Table 3. **Results of variance analysis**

Таблица 3. **Результаты дисперсионного анализа**

Composition	d_n, μm	S, m^2/kg	K
CdSe	19.0	47.3	0.76
$(ZnTe)_{0.12}(CdSe)_{0.88}$	14.3	44.4	0.56
$(ZnTe)_{0.26}(CdSe)_{0.74}$	18.3	50.6	0.82
$(ZnTe)_{0.68}(CdSe)_{0.32}$	19.4	46.6	0.81
$(ZnTe)_{0.75}(CdSe)_{0.25}$	17.5	42.6	0.66
ZnTe	38.5	22.9	0.78

Table 4. **pH values of isoelectric state of the surface of the ZnTe–CdSe solid solutions (x – ZnTe mole fraction) exposed to air (*I*) and in the CO atmosphere (*II*)**

Таблица 4. **Значения pH изоэлектрического состояния поверхности твердых растворов ZnTe–CdSe (x – мол. доли ZnTe) при экспонировании на воздухе (*I*) и в атмосфере CO (*II*)**

Exposure conditions	Surface isoelectric point (pH) of ZnTe–CdSe solid solutions at x					
	0	12	26	68	75	100
I	7.87	7.21	7.15	7.12	7.01	6.84
II	8.35	7.37	7.82	7.75	7.32	7.80

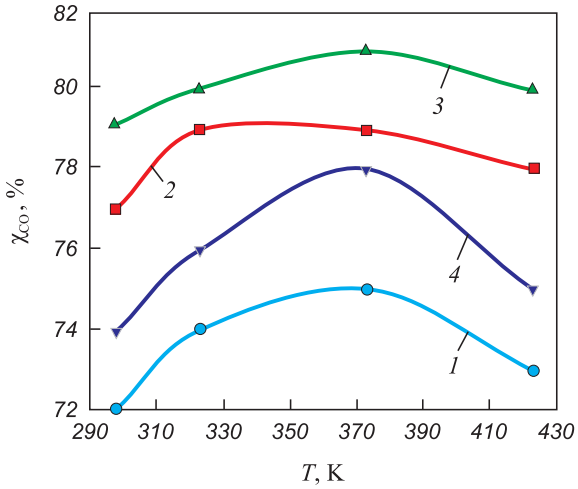

Fig. 3. Dependence of transformation degree (χ_{CO}) on temperature (T) of the ZnTe–CdSe system components: ZnTe (*1*), $(ZnTe)_{0.68}(CdSe)_{0.32}$ (*2*), $(ZnTe)_{0.26}(CdSe)_{0.74}$ (*3*), CdSe (*4*)

Рис. 3. Зависимости степени превращения (χ_{CO}) от температуры (T) компонентов системы ZnTe–CdSe: ZnTe (*1*), $(ZnTe)_{0.68}(CdSe)_{0.32}$ (*2*), $(ZnTe)_{0.26}(CdSe)_{0.74}$ (*3*), CdSe (*4*)

toward carbon monoxide. Their enhanced adsorption capacity in both CO and CO + O_2 atmospheres was further confirmed by IR spectroscopy.

Conclusions

The study of catalytic CO oxidation over samples of the ZnTe – CdSe system made it possible to preliminarily determine the temperature ranges at which CO oxidation occurs, as well as the most catalytically active compositions. Catalytic tests confirmed the activity of the solid solutions $(ZnTe)_{0.26}(CdSe)_{0.74}$ and $(ZnTe)_{0.68}(CdSe)_{0.32}$, making them suitable for use in environmental diagnostics to detect carbon monoxide in the workplace air of metallurgical enterprises.

References / Список литературы

1. Fang X., Zhai T., Gautam U.K., Li L., Wu L., Bando Y., Golberg D. ZnS nanostructures: From synthesis to applications. *Progress in Materials Science*. 2011;56(2):175–287. https://doi.org/10.1016/j.pmatsci.2010.10.001
2. Kirovskaya I.A., Nor P.E., Ekkert A.O., Ekkert R.V., Chernous N.V. New materials based on the systems InP–CdTe and CdS–CdTe; Their comparative properties. *Inorganic Materials: Applied Research*. 2023;14(4):1075–1081. https://doi.org/10.1134/s2075113323040214
3. Peter Y.Yu., Cardona M. Fundamentals of Semiconductors. Physics and Material Properties. Springer; 2010:775. https://doi.org/10.1007/978-3-642-00710-1
4. Kirovskaya I.A., Nor P.E., Bukashkina T.L., Mironova E.V. Surface properties of semiconductor analogs of CdB^{VI} and their solid substitution solutions. *Russian Journal of Physical Chemistry A*. 2016;90(3):522–529. https://doi.org/10.1134/S0036024416030213
5. Kirovskaya I.A. Physico-Chemical Properties of Binary and Multicomponent Diamond-Like Semiconductors. Novosibirsk: SB RAS; 2015:368. (In Russ.).

   Кировская И.А. Физико-химические свойства бинарных и многокомпонентных алмазоподобных полупроводников. Новосибирск: Изд-во СО РАН; 2015:368.
6. Smyslov E.F. Express *X*-ray method for determining the lattice period of nanocrystalline materials. *Industrial laboratory. Diagnostics of materials*. 2006;72(5):33–34. (In Russ.).

   Смыслов Е.Ф. Экспрессный рентгеновский метод определения периода решетки нанокристаллических материалов. *Заводская лаборатория. Диагностика материалов*. 2006;72(5):33–34.
7. Gorelik S.S., Rastorguev L.N., Skakov Yu.A. Radiographic and Electron-Optical Analysis. Moscow: Metallurgiya; 1970:366. (In Russ.).

   Горелик С.С., Расторгуев Л.Н., Скаков Ю.А. Рентгенографический и электроннооптический анализ. Москва: Металлургия; 1970:366.
8. Fedyaeva O.A., Vasina M.V., Poshelyuzhnaya E.G. *X*-ray powder diffraction and electron microscopic studies of the ZnTe–CdSe system. *Russian Journal of Inorganic Chemistry*. 2014;59(2):172–175. (In Russ.). https://doi.org/10.7868/S0044457X14020068

   Федяева О.А., Васина М.В., Пошелюжная Е.Г. Рентгеновские и электронно-микроскопические исследования системы ZnTe–CdSe. *Журнал неорганической химии*. 2014;59(2):172–175. https://doi.org/10.7868/S0044457X14020068
9. Clarke A.R., Eberhardt C.N. Microscopy Techniques for Materials Science. Elsevier; 2002:456.

   Кларк Э.Р., Эберхардт К.Н. Микроскопические методы исследования материалов. Москва: Техносфера; 2007:375.
10. Krishtal M.M., Yasnikov I.S., Polunin V.I. Scanning Electron Microscopy and X-ray Spectral Microanalysis in Practical Applications. Moscow: Technosfera; 2009:206. (In Russ.).

    Сканирующая электронная микроскопия и рентгеноспектральный микроанализ в примерах практического применения / М.М. Криштал, И.С. Ясников, В.И. Полунин. Москва: Техносфера; 2009:206.
11. Kirovskaya I.A. Catalysis. Semiconductor Catalysts. Omsk: OmSTU; 2004:272. (In Russ.).

    Кировская И.А. Катализ. Полупроводниковые катализаторы. Омск: Изд-во ОмГТУ; 2004:272.
12. Charbonnier M., Murat M. Sur la détermination des diagrammes de phases à température ambiante des sulfures mixtes appartenant aux systèmes Zn-Cd-S, Zn-Hg-S, Cd-Hg-S. *Comptes Rendus de l'Académie des Sciences*. 1974;278(4):259–261. (In French).
13. Cherin P., Lind E.L., Davis E.A. The preparation and crystallography of cadmium zinc sulfide solid solutions. *Journal of the Electrochemical Society*. 1970;117(2):233–236.
14. Kirovskaya I.A., Vasina M.V. Structure and acid-base properties of the surface of semiconductors of the ZnTe–CdSe system. *Zhurnal fizicheskoi khimii*. 2014;88(10):1569–1576. (In Russ.). https://doi.org/10.7868/S0044453714100227

    Кировская И.А., Васина М.В. Структура и кислотно-основные свойства поверхности полупроводников системы ZnTe–CdSe. *Журнал физической химии*. 2014;88(10):1569–1576. https://doi.org/10.7868/S0044453714100227
15. Čapek R.K., Moreels I., Lambert K., De Muynck D., Zhao Q., Tomme A.V., Vanhaecke F., Hens Z. Optical properties of zincblende cadmium selenide quantum dots. *Journal of Physical Chemistry C*. 2010;114(14):6371–6376. https://doi.org/10.1021/jp1001989
16. Goldstein J.I., Newbury D.E., Echlin P., Joy D.C., Lyman C.E., Lifshin E., Sawyer L., Michael J.R. Scanning Electron Microscopy and *X*-ray Microanalysis. New York: Plenum Press; 2003:708. https://doi.org/10.1007/978-1-4615-0215-9
17. Kirovskaya I.A., Ekkert R.V., Umansky I.Yu., Ekkert A.O., Kropotin O.V. Comparison of the bulk and surface properties of InB^{V}–ZnS semiconductor solid solutions. *Semiconductors*. 2020;54(11):1459–1466. https://doi.org/10.1134/S1063782620110147
18. Kirovskaya I.A., Vasina M.V., Mironova E.V., Brueva O.Yu., Ekkert A.O., Zhigarova O.Yu. Relative influence of binary components on the bulk and surface properties of GaAs–CdSe and ZnTe–CdSe solid solutions. *Journal of Surface Investigation. X-ray, Synchrotron and Neutron Techniques*. 2021;15(2): 321–326. (In Russ.). https://doi.org/10.1134/S1027451021020233

Кировская И.А., Васина М.В., Миронова Е.В., Бруева О.Ю., Эккерт А.О., Жигарова О.Ю. Относительное влияние бинарных компонентов на объемные и поверхностные свойства твердых растворов систем GaAs–CdSe и ZnTe–CdSe. *Поверхность. Рентгеновские, синхротронные и нейтронные исследования*. 2021;(4):12–18. https://doi.org/10.31857/S1028096021040051

19. Kirovskaya I.A., Vasina M.V., Yuryeva A.V., Shalaeva M.E., Eremin E.N., Matyash Yu.I., Korneev S.A. Chemical composition and acid-base surface properties of solid solutions $(ZnTe)_x(CdSe)_{1-x}$. *Omsk Scientific Bulletin*. 2014;(1(127)):32–37. (In Russ.).

Кировская И.А., Васина М.В., Юрьева А.В., Шалаева М.Е., Еремин Е.Н., Матяш Ю.И., Корнеев С.А. Химический состав и кислотно-основные свойства поверхности твердых растворов $(ZnTe)_x(CdSe)_{1-x}$. *Омский научный вестник*. 2014;(1(127)):32–37.

20. Aven M. Mobility of holes and interaction between acceptor defects in ZnTe. *Journal of Applied Physics*. 1967; 38(11):4421–4430. https://doi.org/10.1063/1.1709141

Information about the Authors

Marina V. Vasina, *Cand. Sci. (Chem.), Assist. Prof. of the Chair of Industrial Ecology and Safety*, Omsk State Technical University
ORCID: 0000-0003-0236-8151
E-mail: 896099949132@mail.ru

Lyudmila P. Bashchenko, *Cand. Sci. (Eng.), Assist. Prof. of the Chair "Thermal Power and Ecology"*, Siberian State Industrial University
ORCID: 0000-0003-1878-909X
E-mail: luda.baschenko@gmail.com

Сведения об авторах

Марина Владимировна Васина, *к.х.н., доцент кафедры «Промышленная экология и безопасность»*, Омский государственный технический университет
ORCID: 0000-0003-0236-8151
E-mail: 896099949132@mail.ru

Людмила Петровна Бащенко, *к.т.н., доцент кафедры теплоэнергетики и экологии*, Сибирский государственный индустриальный университет
ORCID: 0000-0003-1878-909X
E-mail: luda.baschenko@gmail.com

Received 18.04.2025
Revised 16.05.2025
Accepted 21.05.2025

Поступила в редакцию 18.04.2025
После доработки 16.05.2025
Принята к публикации 21.05.2025

MATERIALS SCIENCE / МАТЕРИАЛОВЕДЕНИЕ

UDC 669.017.15
DOI 10.17073/0368-0797-2025-4-349-356

Original article
Оригинальная статья

Prospects for creation of high-speed high-entropy steels

V. E. Gromov, S. S. Minenko, A. S. Chapaikin, A. P. Semin, Yu. A. Shlyarova

Siberian State Industrial University (42 Kirova Str., Novokuznetsk, Kemerovo Region – Kuzbass 654007, Russian Federation)

gromov@physics.sibsiu.ru

Abstract. A new class of materials created at the beginning of the 21st century – high–entropy alloys – attracts the attention of researchers in the field of physical materials science. Based on the analysis of recent literature data, the current state of the problem of creating and researching medium- and high-entropy high-speed steels is considered. Due to solid-solution hardening and nano-precipitation hardening based on medium- and high-entropy alloys of complex composition, it is possible to create high-speed steels with high hardness, thermal resistance and impact strength. The presented results of studies of tribological characteristics and microhardness of high-speed steels indicate the dependence of these characteristics on entropy. The lowest values of cutting forces and contact temperatures are typical for cutting tools made of high-speed steel with a high level of entropy. Thus, when developing new high-speed grades, preference should be given to the compositions with a high level of entropy, since they provide better tribological characteristics and higher wear resistance. The structural and phase state of surfacing of high-entropy high-speed molybdenum steel of non-equiatomic composition on medium-carbon steel in a nitrogen medium was studied by the methods of modern physical materials science. *X*-ray spectral analysis methods determined the elemental composition of surfacing outer layer, and *X*-ray phase analysis revealed that solid solutions based on α-iron (88 wt. %) and γ-iron (12 wt. %) are the main phases of the deposited layer material. The calculation of the configuration entropy of this high-speed high-entropy steel gives a value of 1.93*R* (where *R* is the universal gas constant). The conclusion is made about the relevance and prospects of the development and research of high-energy alloys.

Keywords: high-entropy high-speed steel, tribological properties, structure, phase composition, carbide phase, hardening mechanisms

Acknowledgements: The work was supported by the Russian Science Foundation, grant No. 23-19-00186, https://rscf.ru/project/23-19-00186.

For citation: Gromov V.E., Minenko S.S., Chapaikin A.S., Semin A.P., Shlyarova Yu.A. Prospects for creation of high-speed high-entropy steels. *Izvestiya. Ferrous Metallurgy*. 2025;68(4):349–356. https://doi.org/10.17073/0368-0797-2025-4-349-356

Перспективы создания быстрорежущих высокоэнтропийных сталей

В. Е. Громов, С. С. Миненко, А. С. Чапайкин, А. П. Семин, Ю. А. Шлярова

Сибирский государственный индустриальный университет (Россия, 654007, Кемеровская обл. – Кузбасс, Новокузнецк, ул. Кирова, 42)

gromov@physics.sibsiu.ru

Аннотация. Созданный в начале XXI века новый класс материалов – высокоэнтропийные сплавы – привлекает внимание исследователей в области физического материаловедения. На основе анализа литературных данных последних лет рассмотрено современное состояние проблемы создания и исследования средне- и высокоэнтропийных быстрорежущих сталей. Благодаря твердорастворному упрочнению и упрочнению нановыделениями на основе средне- и высокоэнтропийных сплавов сложного состава возможно создание быстрорежущих сталей с высокими твердостью, термической стойкостью и ударной вязкостью. Приведенные результаты исследований трибологических характеристик и микротвердости быстрорежущих сталей свидетельствуют о зависимости этих характеристик от энтропии. Наименьшие значения сил резания и контактных температур характерны для режущего инструмента из быстрорежущей стали с высоким уровнем энтропии. Таким образом, при разработке новых быстрорежущих марок предпочтение следует отдавать составам с высоким уровнем энтропии, поскольку они обеспечивают лучшие трибологические характеристики и более высокую износостойкость. Методами современного физического материаловедения изучено структурно-фазовое состояние наплавки в среде азота высокоэнтропийной быстрорежущей молибденовой стали неэквиатомного состава на среднеуглеродистую сталь. Методами рентгеноспектрального анализа определен

элементный состав поверхностного слоя наплавки, а рентгенофазным анализом установлено, что твердые растворы на основе α-железа (88 мас. %) и γ-железа (12 мас. %) являются основными фазами материала наплавленного слоя. Проведенный расчет конфигурационной энтропии данной быстрорежущей высокоэнтропийной стали дает значение 1,93*R* (где *R* – универсальная газовая постоянная). Сделан вывод об актуальности и перспективах разработки и исследования высокоэнтропийных сплавов.

Ключевые слова: высокоэнтропийная быстрорежущая сталь, трибологические свойства, структура, фазовый состав, карбидная фаза, механизмы упрочнения

Благодарности: Работа выполнена при поддержке гранта Российского научного фонда № 23-19-00186, https://rscf.ru/project/23-19-00186.

Для цитирования: Громов В.Е., Миненко С.С., Чапайкин А.С., Семин А.П., Шлярова Ю.А. Перспективы создания быстрорежущих высокоэнтропийных сталей. *Известия вузов. Черная металлургия*. 2025;68(4):349–356. https://doi.org/10.17073/0368-0797-2025-4-349-356

Introduction

The emergence of a new class of materials – high-entropy alloys (HEAs) and compounds – at the beginning of the 21st century marked a significant milestone in the development of metallic materials [1; 2]. The original findings from research into the structural–phase states and properties of a broad range of HEAs have been summarized in several studies [3; 4], as well as in analytical reviews and monographs [5 – 8]. Subsequent reports have described high-entropy carbides, borides, nitrides, silicides, and thin films and coatings produced via magnetron sputtering. The number of HEAs and related compounds synthesized to date is vast and continues to grow steadily. The composition and properties of HEAs can be predicted using thermodynamic calculations, particularly through the CALPHAD software package [9]. However, regardless of the design method used, it is ultimately the data on the structural–phase states and resulting material properties that determine potential areas of application. For example, several HEAs demonstrate high strength and ductility at low and even cryogenic temperatures, making them promising candidates for use in Arctic and Antarctic environments [9 – 11]. A review of recent publications in materials science, condensed matter physics, metallurgy, and heat treatment shows that all major types of HEAs with practical relevance are currently under development and investigation. These include structural, cryogenic-, and heat-resistant alloys, as well as corrosion-, radiation-, and wear-resistant materials, and those with specific magnetic or electrical properties. Particularly noteworthy are medium- and high-entropy high-speed steels [12; 13]. However, the number of publications dedicated to this topic remains limited.

High-speed steels are a subgroup of high-carbon martensitic steels that contain strong carbide-forming elements – primarily tungsten, molybdenum, vanadium, and others. Over the past century, since the development of the R18 high-speed steel grade, a range of tungsten–molybdenum steel grades – including R6M5, R7M4K5, and others – have been developed to meet the specific needs of the metalworking, mechanical engineering, and metallurgical industries. A major direction in the further development of high-speed steels involves replacing tungsten, which is both scarce and expensive, with molybdenum. This substitution is well justified, as molybdenum and tungsten are located in the same group and in adjacent periods of the Periodic Table of Elements developed by D.I. Mendeleev, and thus have comparable effects on the structure and properties of high-speed steels.

In recent years, researchers and practitioners alike have shown increasing interest in the development of HSSs based on high-entropy (HEAs) and medium-entropy alloys (MEAs) with complex compositions. These materials exhibit high hardness, thermal stability, and impact toughness as a result of solid-solution strengthening and nano-precipitation hardening [4; 14; 15]. An innovative HEA design strategy was proposed in [15], which involves introducing ductile, multicomponent intermetallic nanoparticles with high density. This approach has been shown to yield strength levels up to 1.5 GPa and ductility of up to 50 %. The addition of alloying elements such as aluminum, copper, cobalt, and nickel in equiatomic ratios increases the alloy's configuration entropy, thereby improving its performance characteristics [16]. A comparative analysis was conducted on the properties of a newly developed MEA-based high-speed steel with the composition $Fe_x(Al, Co, Cr, Cu, Ni)_{88.05}Mo_5N_6C_{0.95}$. The results demonstrated that this alloy shows superior hardness after quenching and tempering compared to the conventional R6M5 high-speed steel. This improvement is attributed to the alloy's high degree of alloying, which enhances both solid-solution hardening within the martensitic matrix and dispersion strengthening. Additionally, the transformation of Me_2C-type carbides contributes to compensating for the loss of hardness typically associated with a reduced total volume of carbides.

Ongoing research into the use of HEAs and MEAs for high-speed steel developing also offers economic advantages, particularly due to the use of low-cost base elements such as iron. When an alloy contains three or more elements in equiatomic proportions, its configuration entropy increases. For MEAs, the configuration entropy is typically around 1.0*R* to 1.5*R* (where *R* is the universal gas constant) [17 – 24]. In [25], laser surfacing was employed to produce a coating of medium-entropy high-speed steels with the composition $Fe_{68}(Al, Co, Cr, Cu, Mo, Ni, V, W)_{32}$. The resulting coating exhibited a hard martensitic matrix

with secondary hardening and a network of coherent nanoscale Me_2C carbides. The high concentration of alloying elements provided excellent wear and oxidation resistance, with no formation of undesirable precipitates or coarse carbides. The addition of aluminum and cobalt was shown to improve strength and enhance secondary hardening [26; 27], while copper contributed to the formation of nanoscale carbide particles, helping to achieve an optimal balance of strength and impact strength [28]. Notably, the incorporation of chromium, cobalt, aluminum, and other antioxidant elements led to significantly lower thermal wear compared to laser-deposited coatings based on conventional high-speed steel grade R6M5. At the same time, the microstructure of the MEA-based coating remained similar to that of traditional high-speed steel and consists of a martensitic matrix with a finely dispersed carbide phase [25].

The optimized carbide distribution achieved through alloying and heat treatment, along with high hardness, makes MEA- and HEA-based high-speed steels promising for industrial applications. First, in conventional high-speed steel, increasing hardness typically requires raising the carbon content, which leads to the formation of a continuous network of primary carbides, thereby reducing impact toughness. Second, the high hardness and brittleness of conventional high-speed steels after quenching often impair machinability. In contrast, MEA- and HEA-based high-speed steels experience significant strengthening during tempering, allowing for lower hardness in the as-quenched state – an advantage that enhances their suitability for machining.

The CALPHAD (*Calculation Phase Diagram*) thermodynamic modeling approach enables the prediction of phase compositions in HEAs, as shown in studies [29 – 32]. However, this task remains challenging, largely due to incomplete thermodynamic descriptions – particularly for ternary systems [29].

A quantitative relationship between the entropy of high-speed steels and their tribological properties under dry sliding against structural and stainless steels was established in studies [12; 13; 33]. Focusing on the practical outcomes of these investigations, the authors interpret entropy primarily in terms of "thermal entropy," which likely reflects the vibrational contribution – in addition to configurational and electronic components – to the total mixing entropy [34]. As shown in [34], mixing entropy is a key thermodynamic parameter for predicting the phase stability of HEAs. Using density functional theory (DFT) calculations, the authors quantified the individual contributions of vibrational, configurational, and electronic entropy. Accounting for all entropy components is crucial for developing a robust theoretical framework for the computational design of stable high-entropy alloys.

The ability to predict certain performance characteristics of experimental cutting tool materials in advance is supported by the study of thermodynamic aspects of wear processes under friction and cutting conditions. Wear resistance, a key factor determining tool life, is largely governed by the material's tribological properties. Significant reductions in wear rate during friction and cutting can be achieved by creating a thermodynamic state characterized by a low density of accumulated thermal entropy. This effect can be achieved by using materials with inherently high entropy. High-entropy high-speed steels used in cutting applications are characterized by low absolute and relative thermoelectromotive force (thermo-EMF), which improves their resistance to gas corrosion. Both thermal entropy and thermo-EMF depend on the chemical composition of the material and can serve as integrated indicators of its structure. Thermal entropy (S), like other thermodynamic potentials, can be calculated using the additivity rule, provided the chemical composition is known (see Table 1). In [12], a correlation between the entropy of high-speed steel and its tribological properties as well as its elastic–strength characteristics in surface layers was confirmed experimentally.

Studies on structural steel 30KhGSA have shown that increasing the entropy of high-speed steel leads to a rise in the microhardness and microelastic modulus of surface layers, while the coefficient of friction decreases at a sliding speed of 1 m/s.

Table 1. **Composition and thermal entropy of high-speed steels [12; 13]**

Таблица 1. **Состав и термическая энтропия быстрорежущих сталей [12; 13]**

Steel	S, J/(mol·K)	Composition
R6M3	26.86	W (6 %) + Mo (3 %) + Fe
R6M5	27.26	W (6 %) + Mo (5 %) + Fe
R6M4F4	27.46	W (6 %) + Mo (4 %) + V (4 %) + Fe
R8M3F4	27.53	W (8 %) + Mo (3 %) + V (4 %) + Fe
R18	28.04	W (18 %) + Fe
EP658	30.60	W (6 %) + V (2 %) + Co (8 %) + Mo (5 %) + Fe
EP657	30.78	W (12 %) + V (2 %) + Co (8 %) + Mo (3 %) + Fe

Analysis of the steady-state friction force indicates a reduction in the adhesive component of friction in high-entropy high-speed steels. This effect is attributed to the lower tendency to form adhesive junctions and the reduced shear strength of those junctions, resulting in a lower friction coefficient.

The tendency of materials to form adhesive bonds (weld bridges) is influenced by the surface properties of low-entropy high-speed steels, such as R6M3 and R6M5 grades (Fig. 1). In these materials, lower hardness and higher ductility promote faster degradation of the protective surface film and more rapid formation of adhesive junctions.

The most favorable friction characteristics have been observed in steels with high entropy, which appears to be linked to the formation behavior and composition of the third body (transfer layer). In high-entropy high-speed steel, the growth rate of the third body exceeds its rate of breakdown, and the resulting third-body layer thickness promotes separation of the contacting surfaces, thereby reducing both the strength of adhesive bonds and the coefficient of friction. These effects manifest under conditions of sufficiently high thermomechanical activation in the friction zone. It has been established that deposited layers on samples of high-entropy high-speed steel exhibit greater stability due to the high hardness and low ductility of their surface layers. In [12], the authors examined third-body formation during friction in high-speed steels with different entropy levels. In the first approximation, this process is characterized by two parameters: the maximum attainable thickness of the transfer layer under given conditions and its relative growth rate. The study demonstrates that entropy, as a structure-sensitive parameter, can be used to predict the tribological behavior of both existing and newly developed high-speed steel grades.

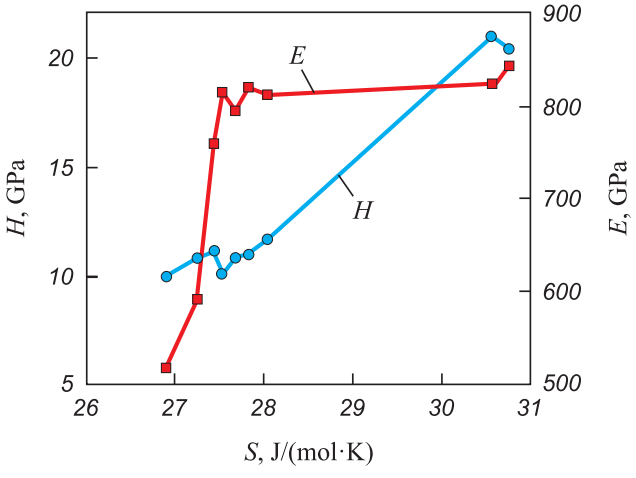

Fig. 1. Dependence of microhardness (H) and microelastic modulus (E) of surface layers on entropy of high-speed steel [12; 13]

Рис. 1. Зависимость микротвердости (H) и модуля микроупругости (E) поверхностных слоев от энтропии быстрорежущей стали [12; 13]

Tribological tests of standard high-speed steel grades under dry sliding against 12Kh18N9T stainless steel have shown that frictional interaction in high-entropy high-speed steels is accompanied by a gradual thickening of the layer composed of dissipative structures over time [13]. This intermediate layer serves a shielding function, protecting the surfaces of the contacting bodies from damage. However, it also exhibits high shear resistance, resulting in elevated coefficients of friction. In contrast, the friction process in high-speed steels with low thermal entropy is characterized by a gradual convergence of the contacting bodies over time. This group of steels demonstrated lower friction coefficients, along with significant changes in surface microrelief compared to the initial condition.

Study [33] addresses the pressing issue of how cutting temperature and cutting forces relate to the entropy of high-speed steels. While tool wear resistance is known to be closely linked to the entropy of the material, the specific relationship between entropy – particularly as a structure-sensitive property – and cutting forces or temperatures during machining remains poorly understood. In machining, heat dissipation is the dominant energy loss mechanism in the cutting zone, and its intensity can be evaluated by monitoring temperature. Cutting temperature is primarily influenced by process parameters such as cutting speed, depth of cut, and feed rate – with cutting speed being the most critical. Elevated temperatures, driven by increased cutting forces, accelerate tool wear and limit the maximum usable cutting speed due to the heat resistance of the tool material.

Experimental studies of the same high-entropy high-speed steels (Table 1) demonstrated that, across all cutting speeds within the tested range, tools made from high-speed steel with higher thermal entropy consistently exhibited lower cutting forces and contact temperatures. These findings suggest that in the development of advanced high-speed steels, preference should be given to compositions with high thermal entropy, as they offer better tribological performance, greater wear resistance, and support higher cutting speeds and productivity compared to low-entropy alternatives.

In recent years, there has been growing interest in developing resource-efficient and energy-saving technologies for plasma and electric arc surfacing using high-hardness high-speed steels [35; 36]. The incorporation of nitrogen as an alloying element in these processes significantly improves wear resistance, strength, corrosion resistance, and impact strength. These enhancements are primarily attributed to increased microhardness of the coating's structural components, resulting from the formation of carbonitrides. Electric arc surfac-

ing in a nitrogen-rich shielding and alloying atmosphere using a current-carrying flux-cored wire offers significant advantages over alternative surfacing methods [35; 36].

However, there remains a notable lack of studies – particularly those employing modern physical materials science techniques – focused on elucidating the mechanisms responsible for the enhanced functional properties of M10-type high-speed steel surfacing. This knowledge gap limits their broader industrial application.

The objective of the present study is to investigate the structure, elemental composition, and phase composition of a non-equiatomic high-entropy M10-type high-speed steel surfacing using methods of modern physical materials science.

Materials and methods

The samples for investigation were fabricated by plasma surfacing using a current-carrying flux-cored wire in a nitrogen atmosphere on 30KhGSA structural steel. The chemical composition of 30KhGSA steel (wt. %): C 0.3; Cr 0.9; Mn 0.8; Si 0.9; balance – Fe. The chemical composition of the M10 surcacing alloy (wt. %): Mo 11.87; Cr 4.24; Co 3.48; V 1.77; Si 0.94; Mn 0.50. Technical-grade nitrogen (GOST 9293–74) was used as the shielding gas at a flow rate of 20–22 L/min. The surfacing was performed on a UD-417 unit under the following parameters: welding current 140 – 160 A, arc voltage 50 – 55 V, surfacing speed 15 – 18 m/h, and arc length 20 mm. The coating was deposited in four layers, with a total thickness of 9 mm.

The microstructure and elemental composition of the deposited layer were examined using a KYKY-EM6900 scanning electron microscope equipped with a thermionic tungsten cathode and an energy-dispersive *X*-ray spectrometer (EDS) for elemental microanalysis. Phase composition and structural parameters were analyzed using an XRD-6000 diffractometer with CuK_α radiation. Phase identification was carried out using the PDF-4+ database in combination with full-pattern refinement via POWDER CELL 2.4 software.

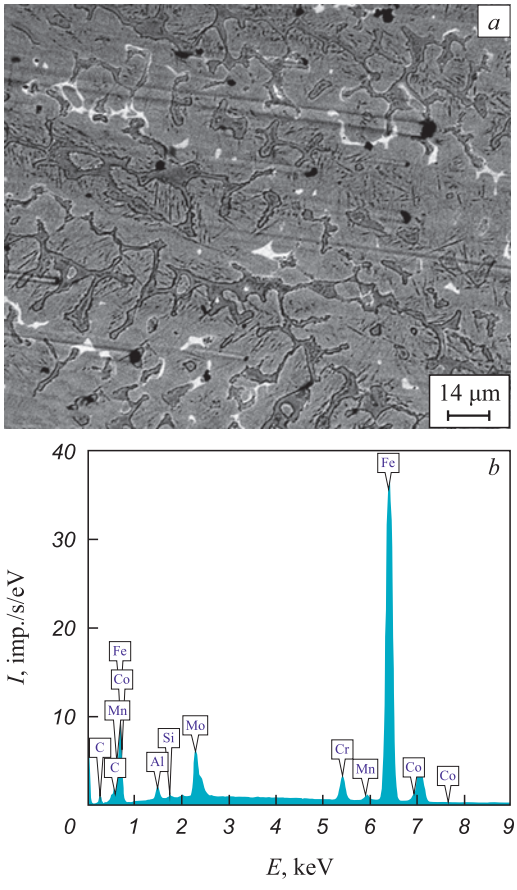

Fig. 2. Electron microscopic image of structure of the deposited layer after polishing and etching (*a*) and energy spectra (*b*) obtained from the surfacing section shown in *a*

Рис. 2. Электронно-микроскопическое изображение структуры наплавленного слоя после полирования и травления (*a*) и энергетические спектры (*b*), полученные с участка наплавки, изображенного на поз. *a*

Results and discussion

The etched cross-section of the layer formed by surfacing 30KhGSA steel with M9Yu flux-cored wire in a nitrogen atmosphere revealed a polycrystalline dendritic structure, as shown in Fig. 2.

Energy-dispersive *X*-ray spectroscopy (EDS) analysis of the deposited surface (Fig. 2, Table 2) confirmed the presence of chemical elements matching the nominal composition of the alloy.

Elemental mapping revealed localized enrichment of several alloying elements – namely molybdenum,

Table 2. **Results of micro-*X*-ray spectral analysis of elemental composition of a section of the deposited layer, electron microscopic image of which is presented in Fig. 1, *a***

Таблица 2. **Результаты микрорентгеноспектрального анализа элементного состава участка наплавленного слоя, электронно-микроскопическое изображение которого представлено на рис. 1, *a***

Element	Content	
	wt. %	at. %
C (*K*)	7.09	26.44
Al (*K*)	1.28	2.13
Si (*K*)	0.19	0.30
Cr (*K*)	3.26	2.81
Mn (*K*)	0.51	0.41
Fe (*K*)	79.46	63.75
Co (*K*)	1.09	0.83
Mo (*L*)	7.12	3.32

chromium, and aluminum – within the surface layer of the deposited material, indicating a non-uniform distribution of elements.

X-ray phase analysis identified the dominant phases in the surfaced layer as solid solutions based on α-iron (88 wt. %) and γ-iron (12 wt. %). The formation of these solid solutions is corroborated by notable deviations of the measured lattice parameters – 0.28803 nm for α-Fe and 0.36050 nm for γ-Fe – from their standard reference values [37]. In addition, the XRD patterns exhibited low-intensity diffraction peaks attributed to carbide phases present in the surfaced layer.

The configuration entropy of the high-entropy high-speed steel investigated in this study, calculated following the methodology outlined in [38], was found to be 1.93*R*.

This analysis of recent advances in the development and characterization of medium- and high-entropy high-speed steels, combined with the authors' experimental findings on the structural and phase composition of arc-surfaced layers produced in a nitrogen atmosphere using a non-equiatomic molybdenum-based high-entropy alloy, underscores the scientific and practical relevance of this research direction.

Conclusion

The article provides an overview of recent domestic and international studies on medium- and high-entropy high-speed steels. These steels exhibit superior hardness after quenching and tempering compared to conventional high-speed steel grade R6M5. The underlying strengthening mechanisms are examined, and correlations between configuration entropy and tribological performance under dry sliding conditions are discussed. The study presents experimental data on the structure, chemical composition, and phase constituents of a surfaced layer deposited onto medium-carbon steel using a high-entropy molybdenum-based high-speed steel. The findings support the conclusion that the development of next-generation high-entropy high-speed steels represents a promising direction in advanced tool material design.

References / Список литературы

1. Yeh J.-W., Chen Y.-L., Lin S.-J., Chen S.-K. High-entropy alloys – A new era of exploration. *Materials Science Forum*. 2007;560:1–9. https://doi.org/10.4028/www.scientific.net/MSF.560.1
2. Chapaikin A.S., Gromov V.E., Zhang P., Ivanov Yu.F., Kryukov R.E., Shlyarov V.V., Semin A.P. Structural-phase states and properties of plasma surfacing with high-speed steel in a nitrogen enviroment. *Bulletin of the Siberian State Industrial University*. 2024;(1(47)):35–46. (In Russ.). https://doi.org/10.57070/2304-4497-2024-1(47)-35-47

Чапайкин А.С., Громов В.Е., Чжан П., Иванов Ю.Ф., Крюков Р.Е., Шляров В.В., Семин А.П. Структурно-фазовые состояния и свойства плазменной наплавки быстрорежущей сталью в среде азота. *Вестник Сибирского государственного индустриального университета*. 2024;(1(47)):35–46. https://doi.org/10.57070/2304-4497-2024-1(47)-35-47
3. Pochetukha V.V., Bashchenko L.P., Gostevskaya A.N., Budovskikh E.A., Gromov V.E., Chapaikin A.S. Structure and properties of plasma coatings from high-speed steel after high-temperature tempering. *Bulletin of the Siberian State Industrial University*. 2023;(3(45)):30–38. (In Russ.). https://doi.org/10.57070/2304-4497-2023-3(45)-30-38

Почетуха В.В., Бащенко Л.П., Гостевская А.Н., Будовских Е.А., Громов В.Е., Чапайкин А.С. Структура и свойства плазменных покрытий из быстрорежущей стали после высокотемпературного отпуска. *Вестник Сибирского государственного индустриального университета*. 2023;(3(45)):30–38. https://doi.org/10.57070/2304-4497-2023-3(45)-30-38
4. Liu H., Gu C., Zhai K., Wang C. Strengthening and toughening the FeNiCrMn medium entropy alloy by novel ultrafine precipitate networks. *Vacuum*. 2020;184:109995. https://doi.org/10.1016/j.vacuum.2020.109995
5. Miracle D.B., Senkov O.N. A critical review of high entropy alloys and related concepts. *Acta Materialia*. 2017;122:448–511. https://doi.org/10.1016/j.actamat.2016.08.081
6. Zhang W., Liaw P.K., Zhang Y. Science and technology in high-entropy alloys. *Science China Materials*. 2018;61(1):2–22. https://doi.org/10.1007/s40843-017-9195-8
7. Gromov V.E., Konovalov S.V., Ivanov Yu.F., Osintsev K.A. Structure and Properties of High-Entropy Alloys. Springer, Advanced Structured Materials: 2021;107:110. https://doi.org/10.1007/978-3-030-78364-8
8. Gromov V.E., Ivanov Yu.F., Osintsev K.A., Shlyarova Yu.A., Panchenko I.A. High Entropy Alloys: Structure and Properties. Moscow: Ru Science; 2022:204.
9. Rogachev A.S. Structure, stability, and properties of high-entropy alloys. *Physics of Metals and Metallography*. 2020;121:733–864. https://doi.org/10.1134/S0031918X20080098

Рогачев А.С. Структура, стабильность и свойства высокоэнтропийных сплавов. *Физика металлов и металловедение*. 2020;121(8):807–841. https://doi.org/10.31857/S0015323020080094
10. Murty B.S., Yeh J.-W., Ranganathan S., Bhattacharjee P.P. High-Entropy Alloys. 2nd ed. Amsterdam: Elsevier; 2019:374.
11. Zhang Y. High-Entropy Materials: A Brief Introduction. Singapore: Springer Nature; 2019:159. https://doi.org/10.1007/978-981-13-8526-1
12. Ryzhkin A.A., Fominoff E.V., Shuchev C.G. Study on tribological characteristics of high entropy high-speed steels in conditions of dry friction on structural steel. In: *Proceedings of the 4th Int. Conf. on Industrial Engineering*. 2018:1819–1827. https://doi.org/10.1007/978-3-319-95630-5_195
13. Fominov E., Shuchev C., Cherednichenko O., Metelkova N., Filonenko L. Tribological properties of high-entropy high-speed steels under conditions of friction on stainless steel 12H18N9T. In: *XI Int. Sci. and Pract. Conf. Innovative Technologies in Environmental Science and Education (ITSE-2023)*. 2023;431:06013. https://doi.org/10.1051/e3sconf/202343106013

14. He J.Y., Wang H., Huang H.L, Xu X.D., Chen M.W., Wu Y., Liu X.J., Nieh T.G., An K., Lu Z.P. A precipitation-hardened high-entropy alloy with outstanding tensile properties. *Acta Materialia*. 2016;102:187–196. https://doi.org/10.1016/j.actamat.2015.08.076

15. Yang T., Zhao Y.L., Tong Y., Jiao Z.B., Wei J., Cai J.X., Han X.D., Chen D., Hu A., Kai J.J., Lu K., Liu Y., Liu C.T. Multicomponent intermetallic nanoparticles and superb mechanical behaviors of complex alloys. *Science*. 2018; 362(6427):933–937. https://doi.org/10.1126/science.aas8815

16 Dou B., Zhang H., Tao Y., Ma Q., Guo S. Effect of Fe on type and distribution of carbides in medium-entropy high-speed steels. *Tungsten*. 2023;5(1):189–197. https://doi.org/10.1007/s42864-022-00138-5

17. Gludovatz B., Hohenwarter A., Thurston K.V.S., Bei H., Wu Z., George E.P., Ritchie R.O. Exceptional damage-tolerance of a medium-entropy alloy CrCoNi at cryogenic temperatures. *Nature Communications*. 2016;7:10602. https://doi.org/10.1038/ncomms10602

18. Huang H., Wang J., Yang H., Ji S., Liu Z. Strengthening CoCrNi medium-entropy alloy by tuning lattice defects. *Scripta Materialia*. 2020;188:216–221. https://doi.org/10.1016/j.scriptamat.2020.07.027

19. Zhang H., Pan Y., He Y.Z., Jiao H.S. Microstructure and properties of 6FeNiCoSiCrAlTi high-entropy alloy coating prepared by laser cladding. *Applied Surface Science*. 2011;257(6):2259–2263. https://doi.org/10.1016/j.apsusc.2010.09.084

20. Yao M.J., Pradeep K.G., Tasan C.C., Raabe D. A novel, single phase, non-equiatomic FeMnNiCoCr high-entropy alloy with exceptional phase stability and tensile ductility. *Scripta Materialia*. 2014;72-73:5–8. https://doi.org/10.1016/j.scriptamat.2013.09.030

21. Zhuang Y.X., Liu W.J., Chen Z.Y., Xue H.D., He J.C. Efect of elemental interaction on microstructure and mechanical properties of FeCoNiCuAl alloys. *Materials Science and Engineering: A*. 2012;556:395–399. https://doi.org/10.1016/j.msea.2012.07.003

22. Aguilar-Hurtado J.Y., Vargas-Uscategui A., Zambrano-Mera D., Palma-Hillerns R. The effect of boron content on the microstructure and mechanical properties of $Fe_{50-X}Mn_{30}Co_{10}Cr_{10}B_X$ (X = 0, 0.3, 0.6 and 17 wt.%) multicomponent alloys prepared by arc-melting. *Material Science and Engineering: A*. 2019;748:244–252. https://doi.org/10.1016/j.msea.2019.01.088

23. Choi M., Ondicho I., Park N., Tsuji N. Strength–ductility balance in an ultrafne-grained non-equiatomic $Fe_{50}(CoCrMnNi)_{50}$ mediumentropy alloy with a fully recrystallized microstructure. *Journal of Alloys Compounds*. 2019;780:959–966. https://doi.org/10.1016/j.jallcom.2018.11.265

24. Li R., Wang Z., Guo Z., Liaw P., Tao Z., Li L., Zhang Y. Graded microstructures of Al-Li-Mg-Zn-Cu entropic alloys under supergravity. *Science China Materials*. 2019;62(5): 736–744. https://doi.org/10.1007/s40843-018-9365-8

25. Zhang H., Dou B., Tang H., He Y., Guo S. Secondary hardening in laser rapidly solidified $Fe_{68}(MoWCrVCoNiAlCu)_{32}$ medium-entropy high-speed steel coatings. *Materials and Design*. 2018;159:224–231. https://doi.org/10.1016/j.matdes.2018.08.050

26. Ma S., Pan W., Xing J., Guo S., Fu H., Lyu P. Microstructure and hardening behavior of Al-modified Fe–1.5 wt%B–0.4 wt%C highspeed steel during heat treatment. *Materials Characterization*. 2017;132:1–9. https://doi.org/10.1016/j.matchar.2017.08.001

27. Moon H.K., Lee K.B., Kwon H. Influences of Co addition and austenitizing temperature on secondary hardening and impact fracture behavior in P/M high speed steels of W–Mo–Cr–V(–Co) system. *Material Science and Engineering: A*. 2008;474(1-2):328–334. https://doi.org/10.1016/j.msea.2007.04.014

28. Long B.Z., Zhang Y., Guo C.H., Cui Y., Sun L.X., Chen D., Jiang F.C., Zhao T., Zhao G., Zhang Z.W. Enhanced dynamic mechanical properties and resistance to the formation of adiabatic shear band by Cu-rich nano-precipitates in high-strength steels. *International Journal of Plasticity*. 2020;138:102924. https://doi.org/10.1016/j.ijplas.2020.102924

29. Do H.-S., Choi W.-M., Lee B.-J. A thermodynamic description for the Co-Cr-Fe-Mn-Ni system. *Journal of Materials Science*. 2022;57:1373–1389. https://doi.org/10.1007/s10853-021-06604-8

30. Otto F., Dlouhý A., Pradeep K.G., Kuběnová M., Raabe D., Eggeler G., George E.P. Decomposition of the single-phase high-entropy alloy CrMnFeCoNi after prolonged anneals at intermediate temperatures. *Acta Materialia*. 2016;112:40–52. https://doi.org/10.1016/j.actamat.2016.04.005

31. Stepanov N.D., Shaysultanov D.G., Ozerov M.S., Zherebtsov S.V., Salishchev G.A. Second phase formation in the CoCrFeNiMn high entropy alloy after recrystallization annealing. *Materials Letters*. 2016;185:1–4. https://doi.org/10.1016/j.matlet.2016.08.088

32. Shafiei A. Design of eutectic high entropy alloys. *Metallurgical and Materials Transactions A*. 2022;53:4329–4361. https://doi.org/10.1007/s11661-022-06831-x

33. Beskopylny A.N., Fominov E.V., Shuchev C.G., Egorov M.S. The influence of thermodynamical characteristics of high speed steels on temperature and forces values when turning construction steel. *IOP Conference Series: Materials Science and Engineering*. 2020;996:012003. https://doi.org/10.1088/1757-899X/996/1/012003

34. Mauzoor A., Pandey S., Chokraborty D., Phillpot S.R., Aidhy D.S. Entropy contributions to phase stability in binary random solid solutions. *Computational Materials*. 2018;4(1):47. https://doi.org/10.1038/s41524-018-0102-y

35. Gromov V.E., Chapaikin A.S., Nevskii S.A. Structure, Properties and Models of High-Speed Steel after Tempering and Electron Beam Treatment. Novokuznetsk: Polygraphist; 2024:171. (In Russ.).

Громов В.Е., Чапайкин А.С., Невский С.А. Структура, свойства и модели быстрорежущей стали после отпуска и электронно-пучковой обработки. Новокузнецк: Полиграфист; 2024:171.

36. Ivanov Yu.F., Gromov V.E., Potekaev A.I., Guseva T.P., Chapaikin A.S., Vashchuk E.S., Romanov D.A. Structure and properties of R18U surfacing of high-speed steel after its high tempering. *Russian Physics Journal*. 2023:66(7): 731–739. https://doi.org/10.1007/s11182-023-02999-w

37. Kurdyumov V.G., Utevskii L.M., Entin R.I. Transformations in Iron and Steel. Moscow: Nauka; 1977:238. (In Russ.).

Курдюмов В.Г., Утевский Л.М., Энтин Р.И. Превращения в железе и стали. Москва: Наука; 1977:238.

38. Osintsev K.A., Panchenko I.A., Konovalov S.V. Prediction of the phase composition of Co-Cr-Zr-Mn-Ni high-entropy alloy by calculating phenomenological criteria. *Fundamental'nye problemy sovremennogo materialovedeniya*. 2021;18(4):441–449. (In Russ.).
https://doi.org/10.25712/ASTU.1811-1416.2021.04.006

Осинцев К.А., Панченко И.А., Коновалов С.В. Прогнозирование фазового состава высокоэнтропийного сплава CoCr-Zr-Mn-Ni с помощью расчета феноменологических критериев. *Фундаментальные проблемы современного материаловедения*. 2021;18(4):441–449.
https://doi.org/10.25712/ASTU.1811-1416.2021.04.006

Information about the Authors / Сведения об авторах

Viktor E. Gromov, *Dr. Sci. (Phys.-Math.), Prof., Head of the Chair of Science named after V.M. Finkel'*, Siberian State Industrial University
ORCID: 0000-0002-5147-5343
E-mail: gromov@physics.sibsiu.ru

Sergei S. Minenko, *Candidates for a degree of Cand. Sci. (Eng.) of the Chair of Science named after V.M. Finkel'*, Siberian State Industrial University
ORCID: 0009-0003-6592-2276
E-mail: mss121278@mail.ru

Aleksandr S. Chapaikin, *Postgraduate of the Chair of Science named after V.M. Finkel'*, Siberian State Industrial University
E-mail: thapajkin.as@yandex.ru

Aleksandr P. Semin, *Cand. Sci. (Eng.), Senior Researcher of the Department of Scientific Research, Assist. Prof. of the Chair of Engineering Structures, Building Technologies and Materials*, Siberian State Industrial University
ORCID: 0000-0002-3989-7420
E-mail: syomin53@gmail.com

Yuliya A. Shlyarova, *Research Associate of Department of Scientific Researches*, Siberian State Industrial University
ORCID: 0000-0001-5677-1427
E-mail: rubannikova96@mail.ru

Виктор Евгеньевич Громов, *д.ф.-м.н., профессор, заведующий кафедрой естественнонаучных дисциплин им. профессора В.М. Финкеля*, Сибирский государственный индустриальный университет
ORCID: 0000-0002-5147-5343
E-mail: gromov@physics.sibsiu.ru

Сергей Сергеевич Миненко, *соискатель степени к.т.н. кафедры естественнонаучных дисциплин им. профессора В.М. Финкеля*, Сибирский государственный индустриальный университет
ORCID: 0009-0003-6592-2276
E-mail: mss121278@mail.ru

Александр Сергеевич Чапайкин, *аспирант кафедры естественнонаучных дисциплин им. профессора В.М. Финкеля*, Сибирский государственный индустриальный университет
E-mail: thapajkin.as@yandex.ru

Александр Петрович Семин, *к.т.н., старший научный сотрудник управления научных исследований, доцент кафедры инженерных конструкций, строительных технологий и материалов*, Сибирский государственный индустриальный университет
ORCID: 0000-0002-3989-7420
E-mail: syomin53@gmail.com

Юлия Андреевна Шлярова, *научный сотрудник управления научных исследований*, Сибирский государственный индустриальный университет
ORCID: 0000-0001-5677-1427
E-mail: rubannikova96@mail.ru

Contribution of the Authors / Вклад авторов

V. E. Gromov – conceptualization, scientific guidance, writing the text.

S. S. Minenko – literature review, preparation of the samples for SEM.
A. S. Chapaikin – conducting research using scanning electron microscopy methods, interpreting the results.
A. P. Semin – analyzing the results of electron microscopic studies.

Yu. A. Shlyarova – discussing the results, editing the text.

В. Е. Громов – концепция работы, научное руководство, написание текста.
С. С. Миненко – обзор литературы, подготовка образцов для СЭМ.
А. С. Чапайкин – проведение исследований методами сканирующей электронной микроскопии, интерпретация результатов.
А. П. Семин – анализ результатов электронно-микроскопических исследований.
Ю. А. Шлярова – обсуждение результатов, редактирование текста.

Received 03.06.2024
Revised 10.10.2024
Accepted 12.12.2024

Поступила в редакцию 03.06.2024
После доработки 10.10.2024
Принята к публикации 12.12.2024

MATERIALS SCIENCE / МАТЕРИАЛОВЕДЕНИЕ

UDC 669.018.25+621.373.8:621.78
DOI 10.17073/0368-0797-2025-4-357-365

Original article
Оригинальная статья

Limiting energy characteristics during laser pulse treatment of tungsten-cobalt hard alloys

S. I. Yaresko[1], S. N. Balakirov[1], T. N. Oskolkova[2]

[1] **Samara Branch of the Lebedev Institute of Physics, Russian Academy of Sciences** (221 Novo-Sadovaya Str., Samara 443011, Russian Federation)
[2] **Siberian State Industrial University** (42 Kirova Str., Novokuznetsk, Kemerovo Region – Kuzbass 654007, Russian Federation)

serg19541959@mail.ru

Abstract. The considered analytical method for determining the optimal mode of hardening pulsed laser treatment (LT) of tungsten-cobalt hard alloys is based on the study of the patterns of temperature field formation during hardening of hard alloys, determination of thermal stresses occurring in the laser exposure zone (LEZ) during laser pulse treatment, and their comparison with the stresses of fracture of the alloy individual structural elements. The optimal modes of hardening LT of the alloys of WC group are considered to be modes that meet two criteria. First, the temperature on the LEZ surface should be in the range of 1290 °C < T < 1400 °C, when the alloy does not contain weakening it phases of the η-Co_3W_3C, θ-Co_3W_2C, or χ-$Co_3W_9C_4$ types, and increase in grain size of the carbide phase is insignificant. Secondly, cracks of an arbitrary scale are unacceptable in the LEZ, that is, the thermal stresses resulting from the fracture should not exceed the stresses of fracture of the alloy structural elements. The calculation of thermal stresses occurring in a hard alloy during LT within a single carbide grain was carried out in accordance with the Hooke's law. Calculations performed for both single and multiple treatments allow us to establish that for all the studied modes, with variations in the laser energy density from 0.9 to 1.8 J/mm^2 and treatment multiplicity from 1 to 10, when the surface temperature is in the range of 1290 – 1400 °C, the thermal stresses in the carbide phase are lower than minimum fracture stresses and do not exceed 80 MPa. The proposed analytical method for determining the limiting energy characteristics makes it possible to establish pulsed LT modes that provide dispersion hardening of hard alloys of the WC group in the absence of destructive changes in the material. The data obtained on defect-free LT modes are in good agreement with the earlier results of measurements of acoustic emission signals during treatment of hard alloys (VK8 alloy).

Keywords: laser pulse treatment, tungsten-cobalt hard alloy, crack resistance, temperature field, thermal stresses, temperature gradient, carbide phase

For citation: Yaresko S.I., Balakirov S.N., Oskolkova T.N. Limiting energy characteristics during laser pulse treatment of tungsten-cobalt hard alloys. *Izvestiya. Ferrous Metallurgy*. 2025;68(4):357–365. https://doi.org/10.17073/0368-0797-2025-4-357-365

Предельные энергетические характеристики при лазерной импульсной обработке вольфрамокобальтовых твердых сплавов

С. И. Яресько[1], С. Н. Балакиров[1], Т. Н. Осколкова[2]

[1] **Самарский филиал Физического института им. П.Н. Лебедева РАН** (Россия, 443011, Самара, ул. Ново-Садовая, 221)
[2] **Сибирский государственный индустриальный университет** (Россия, 654007, Кемеровская обл. – Кузбасс, Новокузнецк, ул. Кирова, 42)

serg19541959@mail.ru

Аннотация. Рассматриваемый аналитический метод определения оптимального режима упрочняющей импульсной лазерной обработки (ЛО) вольфрамокобальтовых твердых сплавов основан на исследовании закономерностей формирования температурного поля при упрочнении твердых сплавов, определении термических напряжений, возникающих в зоне лазерного воздействия (ЗЛВ) при лазерной импульсной обработке, и сравнении их с напряжениями разрушения отдельных структурных элементов сплава. Оптимальными режимами упрочняющей ЛО сплавов группы ВК считаются режимы, удовлетворяющие двум критериям. Во-первых, температура на поверхности ЗЛВ должна находиться в интервале 1290 °C < T < 1400 °C, когда в ЗЛВ не присутствуют разупрочняющие сплав фазы типов η-Co_3W_3C, θ-Co_3W_2C, χ-$Co_3W_9C_4$, а укрупнение зерен карбидной фазы незначительно. Во-вторых, в ЗЛВ недопустимо появление трещин произвольного масштаба, то есть термические напряжения, возникающие в результате ЛО, не должны превышать напряжений разрушения струк-

турных элементов сплава. Расчет термических напряжений, возникающих в твердом сплаве при лазерной обработке в пределах одного карбидного зерна, выполняется в соответствии с законом Гука. Расчеты, выполненные как для однократной, так и для многократной обработки, позволяют установить, что для всех исследованных режимов при вариации плотности энергии лазерного излучения от 0,9 до 1,8 Дж/мм^2 и кратности обработки от 1 до 10, когда температура на поверхности находится в диапазоне 1290 – 1400 °С, термические напряжения в карбидной фазе меньше минимальных напряжений разрушения и не превосходят 80 МПа. Предложенный аналитический метод определения предельных энергетических характеристик позволяет установить режимы импульсной ЛО, которые обеспечивают дисперсионное упрочнение твердых сплавов вольфрамокобальтовой группы при отсутствии деструктивных изменений в ЗЛВ. Полученные данные о режимах бездефектной лазерной обработки хорошо согласуются с более ранними результатами измерений сигнала акустической эмиссии при обработке твердых сплавов (сплава ВК8).

Ключевые слова: лазерная импульсная обработка, вольфрамокобальтовый твердый сплав, трещиностойкость, температурное поле, термические напряжения, градиент температуры, карбидная фаза

Для цитирования: Яресько С.И., Балакиров С.Н., Осколкова Т.Н. Предельные энергетические характеристики при лазерной импульсной обработке вольфрамокобальтовых твердых сплавов. *Известия вузов. Черная металлургия*. 2025;68(4):357–365.
https://doi.org/10.17073/0368-0797-2025-4-357-365

Introduction

In mechanical engineering production, the primary tool materials are hard alloys, specifically WC–Co system alloys with a cobalt content of 6 – 8 wt. %. Modern industrial demands require enhanced wear resistance of hard-alloy cutting tools (CT), primarily due to the expanding range of workpiece materials – from heat-resistant and high-temperature alloys to composite materials. Various approaches have been proposed to address this issue by modifying the composition and structure of hard alloys, both in the bulk and at the surface. One such method is hardening laser treatment (LT) of the rake face of the cutting edge. This method has been shown to significantly increase the service life of hard-alloy tools – by several times [1 – 3]. Nevertheless, in mechanical engineering practice, laser hardening of CTs is used much less frequently than other methods, such as the application of wear-resistant coatings [4; 5]. Wear-resistant coatings, like the modified structures formed in the surface layer of the laser treatment zone, act as effective barriers against diffusion interaction between the workpiece and tool materials under high cutting speeds. After LT, increased resistance to fracture of the cobalt binder phase – manifested as reduced embrittlement of the surface layer during tool operation – is attributed to the presence of excess tungsten dissolved in cobalt, which inhibits iron diffusion into cobalt and the formation of iron – tungsten carbides during cutting [6].

Despite the advantages of laser hardening of hard alloys, one of the key challenges in improving the performance of CTs lies in determining the optimal LT modes. This is due to the complex stress state formed in the laser treatment zone, which arises from the differing thermophysical properties of the alloy phases and the limited size of the heated area. The optimal LT mode must ensure hardening of the alloy while preserving the continuity of the surface layer. When selecting parameters for hardening LT of hard alloys, it is essential to develop a prompt, reliable, and well-substantiated methodology.

The aim of this study is to develop a method for determining the optimal pulsed laser treatment mode for hardening tungsten – cobalt hard alloys.

Problem statement

A major advantage of pulsed laser treatment of hard alloys – when wear-resistant structures form in the laser exposure zone (LEZ) – is that it can be performed without compromising the integrity of the surface layer. In such cases, no additional modification of the cutting edge geometry is required, which significantly expands the range of applications. In particular, this makes it possible to process replaceable polyhedral hard-alloy inserts alongside brazed inserts.

However, the process of laser thermal treatment of tungsten–cobalt hard alloys is highly specific due to the material's inherent heterogeneity and the characteristics of its manufacturing process. As a result, treatment often leads to destructive changes in the LEZ, including carbide grain coarsening, porosity, crack formation, and the development of complex (double) carbides [2; 7 – 13].

The requirements for laser irradiation (LI) parameters that ensure defect-free processing of hard alloys have only been established for a limited number of specific cases. For instance, reference [2] describes single-pass irradiation using a Gaussian intensity distribution. To obtain a compact, fine-grained remelted layer at the surface, the use of a CO_2 laser operating in pulsed mode is recommended [11]. However, for the most effective approach – repeated laser irradiation [2] – the issue of selecting processing parameters that ensure defect-free laser exposure and achieve actual hardening of the alloy remains unresolved.

Determining the appropriate parameters for LT of hard alloys is challenging. At insufficient laser energy densities, alloy hardening does not occur, while excessively high energy densities result in crack formation within the laser treatment zone (Fig. 1).

Cracks – regardless of their origin, location, or depth – are the primary destructive factor during LT and play a critical role in determining the performance of hard alloys [7; 11 – 14]. Several causes of crack formation in the LEZ can be identified. One major cause is the non-uniform energy distribution across the laser beam cross-section, which leads to cracks spanning the entire treated area. This issue can be addressed, for example, by using a focusing prismatic raster [2; 6; 15], which ensures that the intensity variation in the LEZ does not exceed 5 %. The limited heating depth also causes cracks, resulting in a fine-meshed pattern on the surface (Fig. 1) that penetrates to a depth comparable to the thickness of the modified layer. Another type of cracking affects the alloy microstructure itself, with cracks propagating through primary α-WC grains or along WC – WC grain boundaries. The main contributing factors are the mismatch between the thermal expansion coefficients of WC and the cobalt binder phase ($\alpha_{WC} = 4.4 \cdot 10^{-6}$ °C^{-1}; $\alpha_{Co} = 14.2 \cdot 10^{-6}$ °C^{-1} [1]), strain hardening, and phase transformations during LT – particularly the formation of brittle complex carbides along grain boundaries, which deplete cobalt content in the alloy [2; 6; 15].

These mechanisms of crack formation result from the redistribution of micro- and macro-stresses within the LEZ. Under rapid heating during laser processing, the thermal stresses induced in the LEZ at certain irradiation doses may exceed the fracture stresses of individual structural elements of the alloy [1]. This phenomenon forms the basis for a method to determine the optimal LT parameters for WC–Co group alloys.

Given these considerations, it is appropriate to define the limiting energy characteristics of pulsed LT for tungsten – cobalt hard alloys based on the onset of microcrack formation on the LEZ surface. LT parameters should be selected to provide maximum surface temperature and depth of the hardened zone while reliably preventing the appearance of microcracks in the LEZ. This can be achieved by optimizing both the energy density and the number of laser pulses.

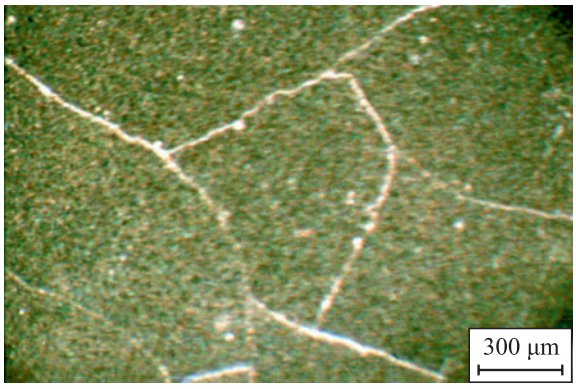

Fig. 1. Cracks on the surface of laser treatment zone (VK8 alloy) at energy density 2.0 J/mm^2, treatment multiplicity 10

Рис. 1. Трещины на поверхности зоны лазерной обработки (сплав ВК8) при плотности энергии 2,0 Дж/мм^2, кратности обработки 10

The laser treatment modes that lead to the onset of crack formation can be experimentally determined by gradually increasing the laser energy density and monitoring the integrity of the LEZ surface – either through visual inspection at (50 – 60)$^\times$ magnification or by detecting acoustic emission (AE) signals [2]. However, this method is labor-intensive and suitable only under laboratory conditions.

Therefore, there is a growing need to develop a method for rapidly determining the limiting energy parameters of pulsed LT that ensure effective hardening of WC – Co group alloys without crack formation. In this study, an analytical method is proposed based on modeling the temperature field during LT, calculating the resulting thermal stresses in the LEZ, and comparing them with the fracture thresholds of the alloy's structural components.

Materials and equipment

The study focused on a two-phase hard alloy VK6 (WC – 6 % Co), which, according to GOST 3882–74, is primarily intended for use in cutting and drilling tools. A methodology was developed and validated for calculating thermal stresses in the LEZ during pulsed laser treatment of this alloy. The same approach can also be applied to other alloys within the WC – Co group.

Irradiation was carried out using a laser system based on a pulsed solid-state glass laser doped with neodymium. The laser energy density (ε) ranged from 0.8 to 1.8 J/mm^2, with a pulse duration of $\tau = (5 – 11) \cdot 10^{-3}$ s and a pulse repetition rate of 1 Hz. A focusing prismatic raster was used to create a uniform distribution of energy density in the LT zone at a area of 4×4 mm [2; 6; 15]. Several LT schemes and irradiation modes were tested in this study – both with and without the raster – and at different number of laser pulses (N).

The alloy microstructure after LT was examined on cross-sectional specimens using a Neophot-30 optical microscope and a Jeol JSM 6390A scanning electron microscope.

Temperature field distributions and temperature gradients in the LEZ were calculated using the Mathcad software package.

Calculation method

According to a structural model commonly used to describe the microstructure of tungsten–cobalt hard

alloys [1; 16], the key structural elements in sintered hard alloys include WC grains, the cobalt binder, WC–WC grain boundaries, and WC–Co interfaces (Fig. 2). WC–Co group alloys are composite tool materials whose performance under contact loading – such as during cutting – is governed by the strength of each individual structural component [17]. The fracture stresses (σ_f) of the structural elements in the VK8 alloy are as follows: cobalt binder layer (1.5 μm thick): $\sigma_f = 5000$ MPa, WC grain (2 μm): $\sigma_f = 180$ MPa, WC–WC boundary: $\sigma_f = 80$ MPa, WC–Co boundary: $\sigma_f = 100$ MPa [18]. These values indicate that fracture in the alloy most often initiates at the WC grain contacts, making the intergranular boundaries the weakest structural elements. In contrast, the cobalt binder phase is the most mechanically robust.

Finite element modeling of the stress state in VK8 alloy confirms [19] that the junctions of WC grains act as stress concentrators under both thermal stresses and mechanical loads, with local stress intensities several times higher than the applied stress. These findings are supported by [20], which showed that microcracks primarily initiate at WC/WC grain contacts and WC/Co phase boundaries. The sequence of weak links during the propagation of a main crack typically follows the path: WC/WC → WC → WC/Co → Co.

To model and calculate the thermal stresses induced during laser treatment, a representative structure containing all the alloy's key elements was analyzed (Fig. 2). Within this structure, an individual tungsten carbide grain interacting with neighboring grains and the cobalt interlayer was isolated. It is assumed that the WC grain does not undergo plastic deformation, although slip along basal planes under external loading is possible [21]. The thermal stress that develops within a single WC grain, in accordance with Hooke's law, can be calculated as:

$$\sigma = \Delta T \alpha E, \quad (1)$$

where ΔT is the temperature difference within the grain depth during LT; $\alpha = 4.9 \cdot 10^{-6}$ °C^{-1} is the coefficient of linear thermal expansion [2]; $E = 628$ GPa is Young's modulus [2].

The grain size of the carbide phase in hard alloys ranges from 0.5 to 6.0 μm [18]. For the purposes of validating the calculation methodology, an average carbide grain size of 4 μm was used in the modeling. This corresponds to the typical WC grain size in coarse-grained VK6-V and VK8-V hard alloys [2; 22].

The temperature field during pulsed laser treatment not only governs the structural and phase transformations in the LEZ [2; 6; 15] – which enhance interphase bonding – but also plays a critical role in determining the magnitude and distribution of residual stresses in the LEZ and, ultimately, the crack resistance of the alloy during processing. The selection of limiting energy parameters for pulsed LT of WC–Co group alloys must ensure dispersion hardening of the material without compromising the surface integrity of the LEZ.

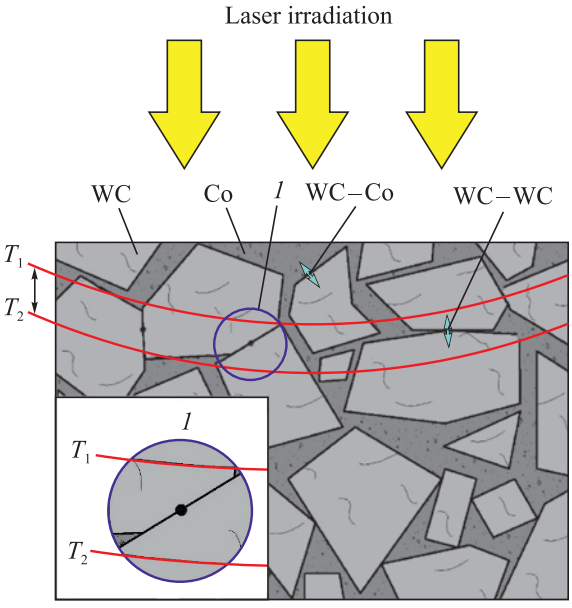

Fig. 2. Structural elements of a tungsten-cobalt alloy and the scheme of its laser treatment

Рис. 2. Структурные элементы вольфрамокобальтового сплава и схема его лазерной обработки

Results and discussion

The temperature distribution in the LEZ during pulsed laser treatment was obtained using a one-dimensional linear heat conduction model for a semi-infinite homogeneous body exposed to a uniform planar surface heat source [2]. Fig. 3 presents the calculated temperature (T_m) profiles of the carbide phase (WC) as a function of depth (z) within the LEZ, under various values of laser energy density (ε) and number of laser pulses (N).

Table 1 provides calculated surface temperature values in the LEZ, which were used to estimate the thermal stresses in those structural elements of the alloy most susceptible to fracture.

Microstructural and compositional analysis of the LEZ indicates that the most favorable conditions for pulsed LT of WC–Co hard alloys occur when the local temperature approaches the eutectic melting range of 1298 – 1357 °C or lies slightly outside it – specifically within the range of 1290 – 1400 °C – while the exposure time is maximized [2]. Under these conditions, grain coarsening in the carbide phase remains minimal, and the solubility of tungsten carbide in cobalt increases significantly compared to its solid-state solubility.

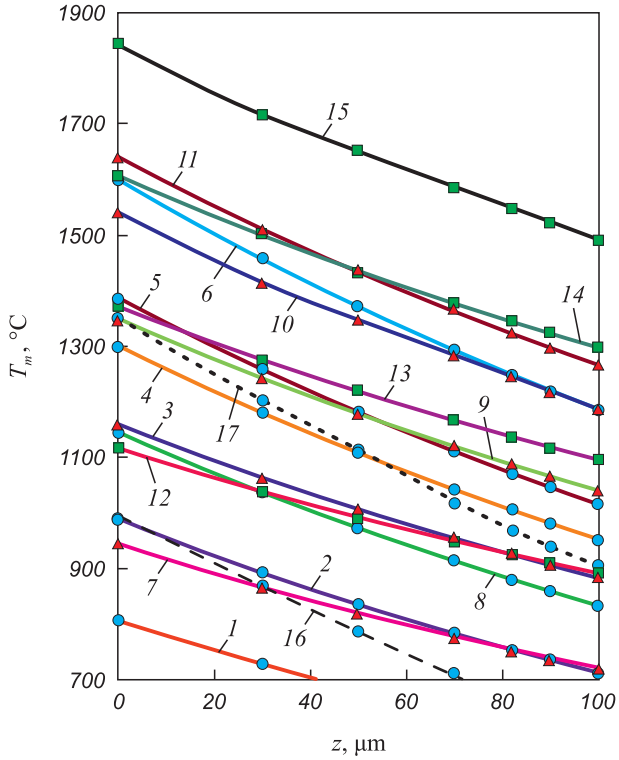

Fig. 3. Temperature of VK6 alloy carbide phase as a function of LEZ depth under various irradiation conditions using a raster:
● – N = 1; ▲ – N = 5; ■ – N = 10;
1, *7*, *12* – ε = 0.8 J/mm²; *2*, *3*, *13* – ε = 1.0 J/mm²; *8*, *9*, *14* – ε = 1.2 J/mm²; *4*, *10*, *15* – ε = 1.4 J/mm²;
5, *11* – ε = 1.5 J/mm²; *6* – ε = 1.8 J/mm²; *16*, *17* – without raster at N = 1 and ε 0.8 and 1.2 J/mm²

Рис. 3. Температура карбидной фазы сплава ВК6 в зависимости от глубины ЗЛВ при различных условиях облучения с использованием растра:
● – N = 1; ▲ – N = 5; ■ – N = 10;
1, *7*, *12* – ε = 0,8 Дж/мм²; *2*, *3*, *13* – ε = 1,0 Дж/мм²; *8*, *9*, *14* – ε = 1,2 Дж/мм²; *4*, *10*, *15* – ε = 1,4 Дж/мм²;
5, *11* – ε = 1,5 Дж/мм²; *6* – ε = 1,8 Дж/мм²; *16*, *17* – без применения растра при N = 1 и ε 0,8 и 1,2 Дж/мм²

According to the simulation results, this optimal temperature range corresponds to LT modes *4* (ε = 1.4 J/mm², N = 1), *5* (ε = 1.5 J/mm², N = 1), *9* (ε = 1.2 J/mm², N = 5), and *13* (ε = 1.0 J/mm², N = 10) (Table 1), which align well with durability test data for laser-irradiated hard-alloy cutting tools [2; 6; 15]. Under these modes, the coarsening of carbide grains is negligible, and no formation of strength-degrading complex carbides such as η-Co_3W_3C, θ-Co_3W_2C, or χ-$Co_3W_9C_4$ is observed. These phases reduce the content of metallic cobalt in the binder by chemically bonding with it, weakening the retention of the carbide framework, and ultimately leading to alloy fracture.

The temperature rise dynamics on the LEZ surface under repeated laser irradiation at ε = 0.9 J/mm² are shown in Fig. 4 (the optimal temperature range

Table 1. **Calculated values of LEZ surface temperature (z = 0) under various heating conditions of LT**

Таблица 1. **Расчетные значения температуры на поверхности ЗЛВ (z = 0) при различных режимах ЛО**

Parameter	Value									
ε, J/mm²	0.8			1.0			1.1	1.2		
N	1	5	10	1	5	10	10	1	5	10
T, °C	806 (*1*)	945 (*5*)	1117 (*12*)	987 (*2*)	1159 (*3*)	1371 (*10*)	1486 (*10*)	1145 (*8*)	1349 (*9*)	1606 (*14*)
ε, J/mm²	1.4			1.5		1.8	0.8		1.2	
N	1	5	10	1	5	1	without raster N = 1			
T, °C	1300 (*4*)	1542 (*10*)	1844 (*15*)	1385 (*5*)	1641 (*11*)	1600 (*6*)	990 (*16*)	1350 (*17*)		
N o t e. The numbers in parentheses indicate the curve (mode) number in Fig. 3.										

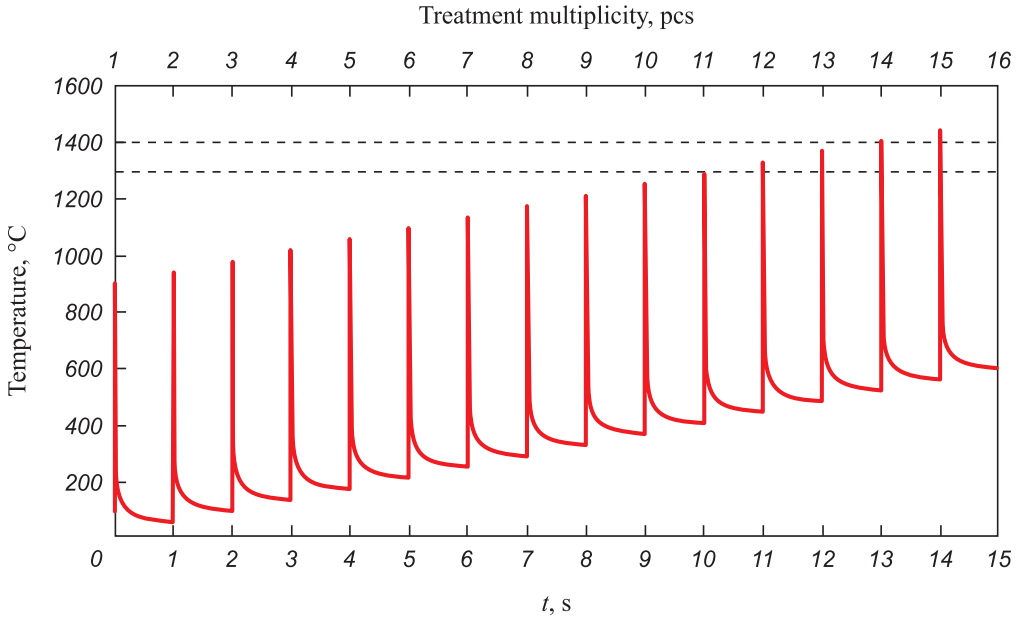

Fig. 4. Change in temperature of VK6 alloy surface under repeated irradiation (ε = 0.9 J/mm²)

Рис. 4. Изменение температуры на поверхности сплава ВК6 при многократном облучении (ε = 0,9 Дж/мм²)

of 1290 – 1400 °C is indicated by dashed lines). The LEZ surface temperature exceeds 1290 °C only after the twelfth pulse. Further increases in the number of laser pulses lead to destructive changes in the LEZ.

The LT modes and corresponding surface temperature ranges in the LEZ are summarized in Fig. 5. When the energy density exceeds 0.9 J/mm², the target temperature range is reached with fewer pulses. For example, at ε = 1.1 J/mm², it is achieved by the 7th or 8th pulse, and at ε = 1.4 J/mm² – by the 1st or 2nd pulse.

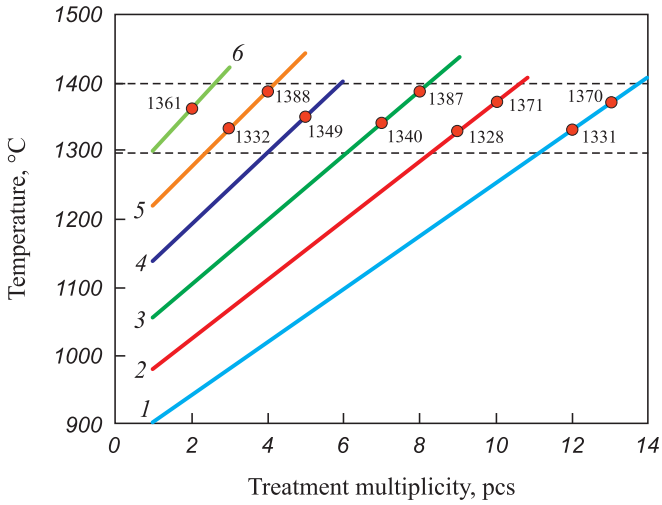

Fig. 5. Temperature range of hardening of VK6 alloy under repeated irradiation at J/mm²:
1 – 0.9; *2* – 1.0; *3* – 1.1; *4* – 1.2; *5* – 1.3; *6* – 1.4

Рис. 5. Диапазон температур упрочнения сплава ВК6 при многократном облучении, Дж/мм²:
1 – 0,9; *2* – 1,0; *3* – 1,1; *4* – 1,2; *5* – 1,3; *6* – 1,4

The temperature distribution in the LEZ not only governs the structural and phase transformations during LT but also determines the thermal stress field, thereby directly influencing the mechanical strength of the material.

Assuming that the temperature gradient reaches its maximum at time $t = 0{,}5\tau_p$ (i.e., at the midpoint of the laser pulse duration), the temperature difference ΔT required for calculating thermal stresses using equation (1) was obtained from the analytical temperature distribution $T(z, t)$ described in [2]. Thermal stresses in the carbide phase – one of the structural elements most prone to fracture under load – were calculated for each LT mode by differentiating the $T(z, t)$ function and adjusting the result to the typical WC grain size.

The optimal pulsed laser treatment modes for hardening WC–Co group alloys are those that meet two criteria. First, the surface temperature in the LEZ must lie within the range of 1290 °C < T < 1400 °C, where no strength-degrading phases are formed and grain coarsening of the carbide phase remains minimal. Second, no cracking of any scale should occur in the LEZ – that is, the thermal stresses induced by LT must not exceed the fracture strength of the alloy's structural elements. It was established that for all investigated modes where the surface temperature remains within 1290 – 1400 °C (Fig. 5), the calculated thermal stresses in the carbide phase remain below the critical fracture stresses. The values of these stresses, calculated using equation (1), are presented in Table 2.

Exceeding the upper limit of the specified temperature range does not necessarily cause grain fracture, but it typically promotes excessive grain growth and the forma-

Table 2. **Stresses in VK6 alloy carbide phase under various heating conditions of LT**

Таблица 2. **Напряжения в карбидной фазе сплава ВК6 при различных режимах ЛО**

ε, J/mm^2	*N*	Maximum temperature, °C	σ, MPa
0.9	12	1331	58.2
1.0	10	1371	62.6
1.1	8	1387	66.7
1.2	5	1349	70.6
1.3	4	1388	74.2
1.4	2	1361	78.4

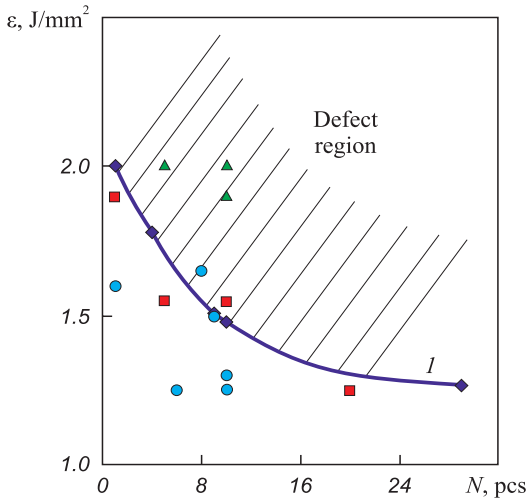

Fig. 6. Limiting values of ε corresponding to appearance of surface visually fixed cracks depending on the number of laser pulses during VK6 alloy treatment with a raster (curve *1*), and data obtained by the acoustic emission method: ● – $N_\Sigma = 0$; ■ – $N_\Sigma \le 4 \div 6$; ▲ – $N_\Sigma > 4 \div 6$

Рис. 6. Предельные значения ε, соответствующие появлению поверхностных визуально фиксируемых трещин, в зависимости от кратности облучения при обработке сплава ВК6 с растром (кривая *1*), и данные, полученные методом АЭ: ● – $N_\Sigma = 0$; ■ – $N_\Sigma \le 4 \div 6$; ▲ – $N_\Sigma > 4 \div 6$

tion of complex carbides along grain boundaries, which compromises the performance of the material as a cutting tool.

The results correlate well with acoustic emission (AE) signal measurements obtained during treatment of VK8 alloy (Fig. 6) [2]. As the total number of recorded AE pulses increases, crack resistance decreases. According to the experimental data, the defect-free processing region ($N_\Sigma = 0$) lies below the curve in Fig. 6 and corresponds to the following LT conditions: $N = 10$ at ε = 1.25 and 1.30 J/mm^2; $N = 9$ at ε = 1.5 J/mm^2; $N = 6$ at ε = 1.25 J/mm^2; $N = 1$ at ε = 1.6 J/mm^2. Assuming that VK6 and VK8 alloys are comparable in terms of thermophysical properties [23], the data presented in Fig. 6 can be aligned with the calculated LT modes in Table 2. All LT modes listed in Table 2 fall within the defect-free processing region, where the stresses in the carbide phase remain below the fracture stresses.

The proposed analytical method for determining limiting energy parameters allows for identifying pulsed LT modes that achieve dispersion hardening of the alloy without introducing destructive changes in the LEZ.

Conclusions

A methodology has been developed and validated for determining the limiting energy parameters of pulsed laser hardening of tungsten – cobalt hard alloys. It has been shown that the optimal LT modes must satisfy two conditions: first of all, the surface temperature in the LEZ should remain within 1290 – 1400 °C, where no strength-degrading phases are present and grain coarsening is minimal; secondly, the thermal stresses induced by LT must not exceed the fracture stress of the alloy's structural components.

For all studied LT modes where the surface temperature lies within 1290 – 1400 °C, the calculated thermal stresses in the carbide phase remain below the fracture limit.

The identified defect-free laser treatment conditions correspond well with acoustic emission data obtained during processing of VK8 alloy.

References / Список литературы

1. Loshak M.G. Strength and Durability of Hard Alloys. Kiev: Naukova dumka; 1984:328. (In Russ.).
Лошак М.Г. Прочность и долговечность твердых сплавов. Киев: Наукова думка; 1984:328.
2. Yaresko S.I., Oskolkova T.N., Balakirov S.N. Modification of Structure and Properties of Tungsten-Cobalt Hard Alloys. Moscow; Vologda: Infra-Inzheneriya; 2023:400. (In Russ.).
Яресько С.И., Осколкова Т.Н., Балакиров С.Н. Модификация структуры и свойств вольфрамокобальтовых твердых сплавов. Москва; Вологда: Инфра-Инженерия; 2023:400.
3. Zimmermann M., Kirsch B., Kang Y., Herrmann T., Aurich J.C. Influence of the laser parameters on the cutting edge preparation and the performance of cemented carbide indexable inserts. *Journal of Manufacturing Processes*. 2000;58:845–856. https://doi.org/10.1016/j.jmapro.2020.09.003
4. Tabakov V.P. Formation of Wear-Resistant Ion-Plasma Coatings for Cutting Tools. Moscow: Mashinostroenie; 2008:311. (In Russ.).
Табаков В.П. Формирование износостойких ионно-плазменных покрытий режущего инструмента. Москва: Машиностроение; 2008:311.
5. Grigor'ev S.N., Volosova M.A. Coating of Tools. Moscow: ITO; 2007:64. (In Russ.).

Григорьев С.Н., Волосова М.А. Нанесение покрытий на инструмент. Москва: ИТО; 2007:64.

6. Yares'ko S.I. The effect of cobalt phase composition in hard alloys on tool wear after laser hardening. *Powder Metallurgy and Functional Coatings.* 2009;(2):54–61. (In Russ.).

   Яресько С.И. Влияние состава кобальтовой фазы твердых сплавов на изнашивание инструмента после лазерного упрочнения. *Известия вузов. Порошковая металлургия и функциональные покрытия*. 2009;(2):54–61.
7. Karatas C., Yilbas B.S., Aleem A., Ahsan M. Laser treatment of cemented carbide cutting tool. *Journal of Materials Processing Technology*. 2007;183(2-3):234–240. https://doi.org/10.1016/j.jmatprotec.2006.10.012
8. Oskolkova T.N., Glezer A.M. Current state of the scientific problem of WC–Co hard alloys surface hardening (Review). *Izvestiya. Ferrous Metallurgy*. 2017;60(12):980–991. (In Russ.). https://doi.org/10.17073/0368-0797-2017-12-980-991

   Осколкова Т.Н., Глезер А.М. Современное состояние научной проблемы поверхностного упрочнения карбидовольфрамовых твердых сплавов (обзор). *Известия вузов. Черная металлургия*. 2017;60(12):980–991. https://doi.org/10.17073/0368-0797-2017-12-980-991
9. Li T., Lou Q., Dong J., Wei Y., Liu J. Phase transformation during surface ablation of cobalt-cemented tungsten carbide with pulsed UV laser. *Applied Physics A*. 2001;73(3):391–397. https://doi.org/10.1007/s003390100745
10. Kolodziejczak P., Wilkowski J., Barlak M. Modification of the surfaces of wood cutting tools using CO_2 laser – SEM analysis. *Annals of Warsaw University of Life Sciences – SGGW. Forestry and Wood Technology*. 2017;98:48–52.
11. Yilbas B.S., Shuja S.Z., Khan S.M.A. Laser repetitive pulse heating of tool surface. *Optics & Laser Technology*. 2011;43(4):754–761. https://doi.org/10.1016/j.optlastec.2010.12.013
12. Hazzan K.E., Pacella M., See T.L. Understanding the surface integrity of laser surface engineered tungsten carbide. *The International Journal of Advanced Manufacturing Technology*. 2022;118:1141–1163. https://doi.org/10.1007/s00170-021-07885-8
13. Schwanekamp T., Gussone J., Reuber M. Impact of laser irradiation on microstructure and phase development of tungsten carbide-cobalt. *Procedia CIRP*. 2020;94:239–242. https://doi.org/10.1016/j.procir.2020.09.045
14. Yilbas B.S., Arif A.F.M., Karatas C., Ahsan M. Cemented carbide cutting tool: Laser processing and thermal stress analysis. *Applied Surface Science*. 2007;253(12):5544–5552. https://doi.org/10.1016/j.apsusc.2006.12.123
15. Yares'ko S.I. Wear and wear resistance analysis of hard alloy tools after laser treatment. *Izvestiya SamNTs RAN*. 2001;3(1):27–37. (In Russ.).

   Яресько С.И. Анализ стойкости и изнашивания твердосплавного инструмента после лазерной термообработки. *Известия СамНЦ РАН*. 2001;3(1):27–37.
16. Kresse T., Meinhard D., Bernthaler T., Schneider G. Hardness of WC–Co hard metals: Preparation, quantitative microstructure analysis, structure-property relationship and modelling. *International Journal of Refractory Metals and Hard Materials*. 2018;75:287–293. https://doi.org/10.1016/j.ijrmhm.2018.05.003
17. Kabaldin Yu.G., Seryi S.V., Kretinin O.V., Laptev I.L. Self-Organization and Nanostructural Processes in Metal Cutting. Nizhny Novgorod: Alekseev NSTU; 2014:173. (In Russ.).

   Кабалдин Ю.Г., Серый С.В., Кретинин О.В., Лаптев И.Л. Самоорганизация и наноструктурные процессы при резании металлов. Нижний Новгород: НГТУ им. Р.Е. Алексеева; 2014:173.
18. Kabaldin Yu.G., Kretinin O.V., Seryi S.V., Shatagin D.A. Nanostructuring contact surface carbide tools in cutting. *Trudy NGTU im. R.E. Alekseeva*. 2012;(4(97)):123–132. (In Russ.).

   Кабалдин Ю.Г., Кретинин О.В., Серый С.В., Шатагин Д.А. Наноструктурирование контактных поверхностей твердосплавного инструмента при резании. *Труды НГТУ им. Р.Е. Алексеева*. 2012;(4(97)):123–132.
19. Dvornik M.I., Mikhailenko E.A. Research of WC-8%Co hard alloy strength by finite elements method. *Chemical Physics and Mesoscopics*. 2009;11(4):433–440. (In Russ.).

   Дворник М.И., Михайленко Е.А. Исследование прочности твердого сплава ВК8 методом конечных элементов. *Химическая физика и мезоскопия*. 2009;11(4):433–440.
20. Brackmann L., Röttger A., Weber S., Theisen W. Subcritical crack growth in hard alloys under cyclic loading. *Fatigue & Fracture of Engineering Materials and Structures*. 2021;44(2):349–365. https://doi.org/10.1111/ffe.13363
21. Lantsev E.A., Nokhrin A.V., Chuvil'deev V.N., Boldin M.S., Blagoveshchenskiy Yu.V., Andreev P.V., Murashov A.A., Smetanina K.E., Isaeva N.V., Terentev A.V. Study of high-temperature deformation features of ceramics of binderless tungsten carbide with various particle sizes. *Inorgamic Materials: Applied Research*. 2022;13:1324–1332. https://doi.org/10.1134/S2075113322050240
22. Montik S.V. Influence of the mechanothermal formation technology of on wear resistance of a hard alloy. *Vestnik Brestskogo gosudarstvennogo tekhnicheskogo universiteta*. 2000;(4):32–35. (In Russ.).

   Монтик С.В. Влияние технологии механотермического формирования на износостойкость твердого сплава. *Вестник Брестского государственного технического университета*. 2000;(4):32–35.
23. Tumanov V.I. Properties of Alloys of the Tungsten Carbide-Cobalt System. Moscow: Metallurgiya; 1971:95. (In Russ.).

   Туманов В.И. Свойства сплавов системы карбид вольфрама-кобальт. Москва: Металлургия; 1971:95.

Information about the Authors / Сведения об авторах

Sergei I. Yaresko, *Dr. Sci. (Eng.), Head of the Laboratory of Laser-Induced Processes,* Samara Branch of the Lebedev Institute of Physics, Russian Academy of Sciences
ORCID: 0000-0001-5299-886X
E-mail: serg19541959@mail.ru

Сергей Игоревич Яресько, *д.т.н., заведующий лабораторией лазерно-индуцированных процессов,* Самарский филиал Физического института им. П.Н. Лебедева РАН
ORCID: 0000-0001-5299-886X
E-mail: serg19541959@mail.ru

Sergei N. Balakirov, *Engineer of the Laboratory of Laser-Induced Processes*, Samara Branch of the Lebedev Institute of Physics, Russian Academy of Sciences
E-mail: s.balakirov@yandex.ru

Tat'yana N. Oskolkova, *Dr. Sci. (Eng.), Prof. of the Chair of Ferrous Metallurgy and Chemical Technology*, Siberian State Industrial University
ORCID: 0000-0003-1310-1284
E-mail: oskolkova@kuz.ru

Сергей Николаевич Балакиров, *инженер лаборатории лазерно-индуцированных процессов*, Самарский филиал Физического института им. П.Н. Лебедева РАН
E-mail: s.balakirov@yandex.ru

Татьяна Николаевна Осколкова, *д.т.н., профессор кафедры металлургии черных металлов и химической технологии*, Сибирский государственный индустриальный университет
ORCID: 0000-0003-1310-1284
E-mail: oskolkova@kuz.ru

Contribution of the Authors

S. I. Yaresko – conceptualization, research planning, generalization and interpretation of results, formulation of conclusions, preparation of the manuscript, laser treatment.

S. N. Balakirov – development of the calculation methodology, calculation, interpretation of results, work with graphic material.

T. N. Oskolkova – metallophysical studies, interpretation of results.

Вклад авторов

С. И. Яресько – разработка концепции исследования, планирование исследований, обобщение и интерпретация результатов исследования, формулирование выводов, подготовка рукописи статьи, лазерная обработка.

С. Н. Балакиров – разработка методики расчета, выполнение расчета, интерпретация полученных результатов, работа с графическим материалом.

Т. Н. Осколкова – проведение металлофизических исследований и интерпретация полученных результатов.

Received 26.12.2024
Revised 03.02.2025
Accepted 10.02.2025

Поступила в редакцию 26.12.2024
После доработки 03.02.2025
Принята к публикации 10.02.2025

INNOVATION IN METALLURGICAL INDUSTRIAL AND LABORATORY EQUIPMENT, TECHNOLOGIES AND MATERIALS

ИННОВАЦИИ В МЕТАЛЛУРГИЧЕСКОМ ПРОМЫШЛЕННОМ И ЛАБОРАТОРНОМ ОБОРУДОВАНИИ, ТЕХНОЛОГИЯХ И МАТЕРИАЛАХ

UDC 621.746+621.771
DOI 10.17073/0368-0797-2025-4-366-371

Оригинальная статья
Original article

Calculation of temperature and thermoelastic stresses in strikers during production of hollow steel billets in a unit of combined casting and deformation. Part 1

O. S. Lekhov, D. Kh. Bilalov

Russian State Vocational Pedagogical University (11 Mashinostroitelei Str., Yekaterinburg 620012, Russian Federation)

MXlehov@yandex.ru

Abstract. The article solves the problem of determining the temperature of calibrated strikers in a unit of combined casting and deformation during production of hollow steel billets. The authors substantiate the relevance of determining temperature fields and thermoelastic stresses in calibrated strikers when compressing the wall of a hollow billet and at full speed when cooling the strikers with water, and describe the strength and thermophysical properties of the steel from which the strikers are made. Geometry of the striker for producing a hollow billet in one pass is shown. The paper considers the initial data and temperature boundary conditions for calculating the temperature field of the striker during production of hollow billets in a unit of combined casting and deformation. The boundary conditions are given to determine the striker temperature as well as the values of heat flow and effective heat transfer coefficient. The results of calculating the temperature fields are performed in four sections and are presented for characteristic lines and points located on the striker contact surface and in the contact layer at a depth of 5 mm from the working surface. Dimensions of the finite element grid were used in calculating the temperature field of the strikers. The temperature field of the strikers with collars was determined based on solution of the unsteady thermal conductivity equation with the corresponding initial and boundary conditions. The values and patterns of temperature distribution in a calibrated striker are presented when the wall of a hollow billet is compressed and when a hollow billet is produced in one pass in a unit of combined casting and deformation.

Keywords: installation, calibrated striker, casting, deformation, mold, hollow billet, temperature field, final element

For citation: Lekhov O.S., Bilalov D.Kh. Calculation of temperature and thermoelastic stresses in strikers during production of hollow steel billets in a unit of combined casting and deformation. Part 1. *Izvestiya. Ferrous Metallurgy*. 2025;68(4):366–371.
https://doi.org/10.17073/0368-0797-2025-4-366-371

Расчет температуры и термоупругих напряжений в бойках при получении стальных полых заготовок на установке совмещенного литья и деформации. Часть 1

О. С. Лехов, Д. Х. Билалов

Российский государственный профессионально-педагогический университет (Россия, 620012, Екатеринбург, ул. Машиностроителей, 11)

MXlehov@yandex.ru

Аннотация. В статье решается задача определения температуры калиброванных бойков установки совмещенного литья и деформации при получении стальных полых заготовок. Авторы обосновывают актуальность определения температурных полей и термоупругих напряжений в калиброванных бойках при обжатии стенки полой заготовки и на холостом ходу при охлаждении бойков водой, приводят прочностные и теплофизические свойства стали, из которой изготовлены бойки. Показана геометрия бойка для получения полой заготовки за один проход. Приводятся исходные данные для расчета температурного поля бойка установки совмещенного литья и деформации при получении полых заготовок, а также представлены температурные граничные условия для расчета температурных полей бойков. Статья описывает граничные условия для определения температуры бойка и значения теплового потока и эффективного коэффициента теплоотдачи. Результаты расчета температурных полей были выполнены в четырех сечениях для характерных линий и точек, расположенных на контактной поверхности бойка и в приконтактном слое на глубине 5 мм от рабочей поверхности. Размеры сетки конечных элементов

приведены для использования при расчете температурного поля бойков. Температурное поле бойков с буртами определялось на основе решения уравнения нестационарной теплопроводности с соответствующими начальными и граничными условиями. Представлены величины и закономерности распределения температуры в калиброванном бойке при обжатии стенки полой заготовки и на холостом ходу при получении за один проход полой заготовки на установке совмещенного литья и деформации.

Ключевые слова: установка, калиброванные бойки, литье, деформация, кристаллизатор, полая заготовка, температурное поле, конечный элемент

Для цитирования: Лехов О.С., Билалов Д.Х. Расчет температуры и термоупругих напряжений в бойках при получении стальных полых заготовок на установке совмещенного литья и деформации. Часть 1. *Известия вузов. Черная металлургия*. 2025;68(4):366–371. https://doi.org/10.17073/0368-0797-2025-4-366-371

Introduction

The technology for producing hollow steel billets at pipe plants entails high capital, energy, and operating costs, since it includes casting solid round billets on horizontal continuous casting machines, heating them in furnaces, and piercing on presses or piercing rolling mills. Note that this equipment is predominantly of foreign manufacture, and under anti-Russian sanctions its supply may be halted. Accordingly, a domestic unit of combined casting and deformation has been developed that successfully replaces foreign equipment and can produce hollow steel billets in one pass [1 – 3]. The most heavily loaded elements of the unit during hollow-billet production are calibrated strikers, which, during the working stroke, simultaneously compress the wall of the hollow billet and draw it out of the mold. In this case, calibrated strikers experience combined stresses from the compression force and the temperature load, which reduce the service life of the strikers. To select the design parameters and material of the calibrated strikers on a sound basis, it is necessary to determine their stress state during the production of hollow billets on the unit of combined casting and deformation. To this end, the temperature field and thermoelastic stresses in the strikers during compression of the wall of the hollow billet must be determined [4 – 6].

This paper presents a procedure for calculating temperature fields and thermoelastic stresses in the strikers of a unit of combined casting and deformation. The pipe billet material is steel grade 09G2S; the inner and outer diameters of the pipe billet are 60 and 100 mm, respectively. The angular speed of the eccentric shafts is 40 rpm. At this speed, the striker contact time in the working stroke is 0.375 s, and the pause time is 0.375·3 = 1.125 s. The temperature of the pipe billet at the entry to the striker is 1200 °C, and after exiting the strikers it is 1000 °C.

The striker material is forged tool steel 4Kh4VMFS. For calculations for this steel in the temperature range from 20 to 700 °C, the following were adopted: modulus of elasticity E, density ρ, thermal conductivity λ, heat capacity c, coefficient of linear expansion α, and yield strength σ_y [2].

The geometry of the striker with dimensions is shown in Fig. 1.

By symmetry, the calculation was performed for one half of the striker (Fig. 2). A part of visible lines is shown, for which calculation results will be presented below.

The results of the temperature and stress calculations are given for three sections (*1*, *2* and *3*), in each section, results are presented for five lines. The positions of the sections, the lines for each section, and the points

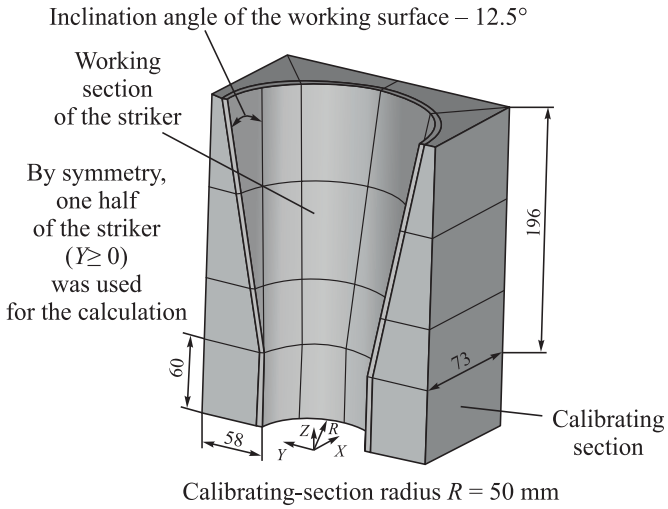

Fig. 1. Geometry of the striker with dimensions

Рис. 1. Геометрия бойка с размерами

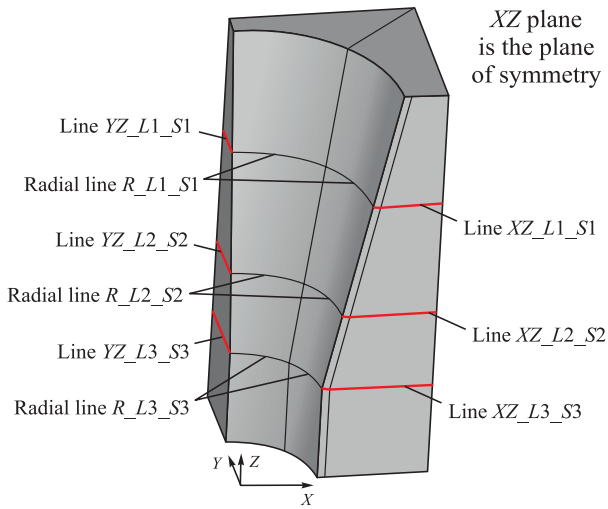

Fig. 2. Geometry of one half of the striker (part of the visible lines)

Рис. 2. Геометрия половины бойка (часть видимых линий)

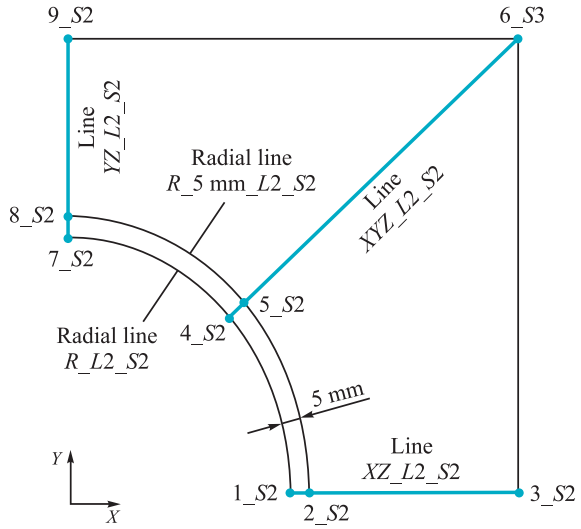

Fig. 3. Position of points and lines in section *2* (sections are shown in Fig. 2)

Рис. 3. Положение точек и линий в сечении *2* (сечения указаны на рис. 2)

through which the lines pass are shown in Fig. 3. Table 1 lists the names of all the lines and indicates the points through which these lines pass.

Calculations of the thermal and stress states of the strikers – for each thermal load (temperature boundary conditions), the specified thermo-physical and mechanical properties of the striker material, and the striker geometry – were performed as follows:

1. Using the thermal element SOLID 70, with the given temperature boundary conditions and thermophysical parameters (density, thermal conductivity, heat capacity) of the striker material, a quasi-steady-state (QSS) temperature field of the striker at the end of the working stroke and at the end of the pause [7 – 9].

2. Using the structural element SOLID 185, together with the modulus of elasticity and Poisson's ratio and the temperature field at the end of the working stroke (from step *1*), the thermal stress state of the striker at the end of the working stroke was determined along the striker length [10 – 12].

The temperature field of the strikers is found by solving the unsteady thermal conductivity equation with the corresponding initial and temperature boundary conditions in the ANSYS package [10]:

$$c\rho\frac{dT}{dt}=\sum_{i=1}^{3}\frac{\partial}{\partial x_i}\left(\lambda\frac{\partial T}{\partial x_i}\right), \quad (1)$$

All coefficients are taken as temperature-dependent for the strikers.

The initial condition for $T(\vec{X}, t)$ is:

$$T(\vec{X}, t)=T_0(\vec{X}). \quad (2)$$

The initial temperature of the strikers is 20 °C.

For the working surface of the striker, boundary conditions of the second kind have the form

$$\lambda\frac{\partial T}{\partial n}\bigg|_S(t)=q, \quad (3)$$

where q is the density of heat flow from the metal in the deformation zone.

During the pause, the boundary conditions of the third kind for the working surface have the form

$$\lambda\frac{\partial T}{\partial n}=-\alpha_1(T-T_k), \quad (4)$$

where α_1 is the effective heat transfer coefficient on the working surface during the pause; $T_k = 60$ °C is the temperature of the water supplied to the working surface of the strikers during the pause.

On the striker end face, the back wall, and the top and bottom of the striker, the boundary conditions of the third kind have the form

$$\lambda\frac{\partial T}{\partial n}=-\alpha_2(T-T_a), \quad (5)$$

where α_2 is the heat transfer coefficient for cooling the back wall and the top and bottom with water or air,

Table 1. **Names of the lines for three sections, the points through which these lines pass**

Таблица 1. **Наименования линий для трех сечений, точки, через которые проходят эти линии**

Line	Points	Line	Points	Line	Points
Section *1*		Section *2*		Section *3*	
XZ_L1_S1	1_*S*1, 2_*S*1, 3_*S*1	*XZ_L2_S2*	1_*S*2, 2_*S*2, 3_*S*2	*XZ_L3_S3*	1_*S*3, 2_*S*3, 3_*S*3
XYZ_L1_S1	4_*S*1, 5_*S*1, 6_*S*1	*XYZ_L2_S2*	4_*S*2, 5_*S*2, 6_*S*2	*XYZ_L3_S3*	4_*S*3, 5_*S*3, 6_*S*3
YZ_L1_S1	7_*S*1, 8_*S*1, 9_*S*1	*YZ_L2_S2*	7_*S*2, 8_*S*2, 9_*S*2	*YZ_L3_S3*	7_*S*3, 8_*S*3, 9_*S*3
R_L1_S1	1_*S*1, 4_*S*1, 7_*S*1	*R_L2_S2*	1_*S*2, 4_*S*2, 7_*S*2	*R_L3_S3*	3_*S*3, 4_*S*3, 7_*S*3
R_5mm_L1_S1	2_*S*1, 5_*S*1, 8_S1	*R_5mm_L2_S2*	2_*S*2, 5_*S*2, 8_*S*2	*R_5mm_L3_S3*	2_*S*3, 5_*S*3, 8_*S*3

depending on the calculation case; T_a = 60 °C is the ambient temperature at the end face, back wall, and top and bottom.

In this formulation, one assumption is that the radiative heat flow from the metal is neglected in calculating the striker temperature fields [13 – 15].

Equations (1) – (5) constitute an initial boundary-value problem for the unsteady temperature field of the strikers in the unit of combined casting and deformation [16 – 18].

This scheme for determining temperature and thermoelastic stresses in the strikers by the finite element method is implemented in one of the modules of the ANSYS package [19; 20].

Temperature values at all points along the lines are given in Table 2.

Analysis of calculation results

Under heat flow during wall reduction, the contact surface of the striker reaches 370 – 451 °C (results shown only for the portion between sections *1 – 3*; Table 1, points 7_*S*3 and 1_*S*1). The maximum temperature occurs in section 1 on the plane of symmetry of the striker. During idle operation with water cooling, the contact-surface temperature decreases to 289 – 370 °C (points 7_*S*3 and 1_*S*1) while the maximum remains in section *1* on the plane of symmetry.

At a depth of 5 mm, the temperatures at the end of contact and at the end of the pause in the QSS mode coincide and depend only on location; they lie within 295 – 392 °C (points 8_*S*3 and 2_*S*1). The maximum is again in section *1* on the plane of symmetry.

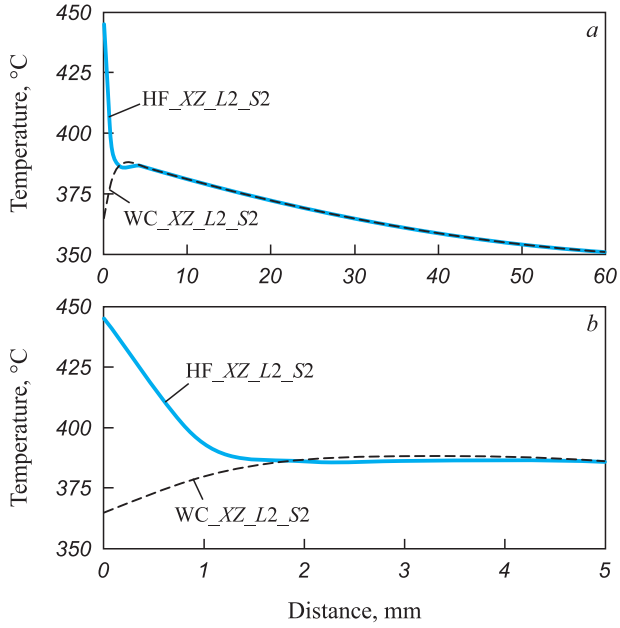

Fig. 4. Nature of temperatures along the *XZ_L2_S*2 line due to the effect of heat flow (HF) and cooling with water (WC) on the striker along its thickness (*a*) and from the contact surface to a depth of 5 mm (*b*)

Рис. 4. Характер температур вдоль линии *XZ_L2_S*2 в зависимости от воздействия на боек теплового потока (HF) и охлаждения водой (WC) по толщине бойка (*a*) и от поверхности контакта на глубине 5 мм (*b*)

Temperature variation is similar through the thickness and along the radius. The maximum temperature – at the end of contact and at the end of the pause – at the working surface of the striker and at a depth of 5 mm occurs in the part of the striker located closer to the mold; toward the calibrating section the tempera-

Table 2. **Temperature values at all points of the lines**

Таблица 2. **Значения температур во всех точках линий**

Section *1*			Section *2*			Section *3*		
Point	Temperature, °C		Point	Temperature, °C		Point	Temperature, °C	
	WC	HF		WC	HF		WC	HF
1_*S*1	370	451	1_*S*2	365	445	1_*S*3	354	435
2_*S*1	392	392	2_*S*2	386	386	2_*S*3	373	373
3_*S*1	370	370	3_*S*2	350	350	3_*S*3	310	310
4_*S*1	368	448	4_*S*2	360	441	4_*S*3	348	429
5_*S*1	389	389	5_*S*2	381	381	5_*S*3	366	366
6_*S*1	344	344	6_*S*2	330	330	6_*S*3	285	285
7_*S*1	304	385	7_*S*2	294	375	7_*S*3	289	370
8_*S*1	314	314	8_*S*2	302	302	8_*S*3	295	295
9_*S*1	286	286	9_*S*2	252	252	9_*S*3	221	221

N o t e. WC and HF denote the temperature at the end of the pause and at the end of the working stroke (end of contact), respectively.

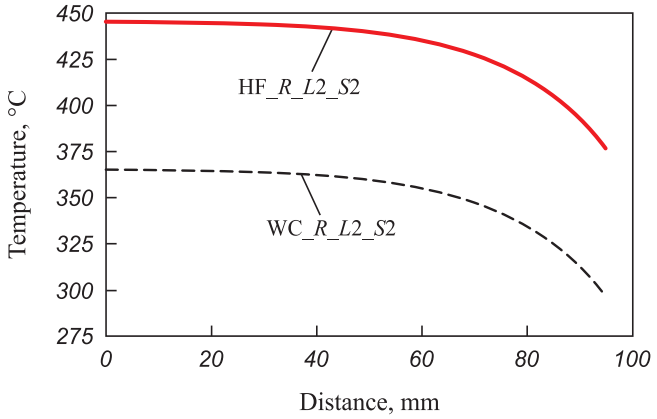

Fig. 5. Nature of temperatures along the *R_L2_S*2 line due to the effect of heat flow (HF) and cooling with water (WC) on the striker

Рис. 5. Характер температур вдоль линии *R_L2_S*2 в зависимости от воздействия на боек теплового потока (HF) и охлаждения водой (WC)

ture decreases. Radially, the temperature is highest on the plane of symmetry and decreases toward the lateral surface of the striker.

Through the thickness, the striker temperature decreases: on the support side surface it is 285 – 370 °C (points 6_*S*3 and 3_*S*1); on the lateral surface side it is 221 – 286 °C (points 9_*S*3 and 9_*S*1).

Temperature equalization occurs at a depth of 2 mm from the contact surface, both through the thickness and along the radius.

Figs. 4 and 5 show the temperature distribution along characteristic lines of the calibrated striker in section *2* during wall reduction and during idle operation with water cooling. Temperatures at characteristic points in sections *1* and *2* differ only slightly (Table 2).

Conclusions

A procedure has been developed for calculating temperature fields and thermoelastic stresses in calibrated strikers of a unit of combined casting and deformation during the production of steel pipe billets. The temperature distribution along characteristic lines has been determined for both wall reduction and idle operation with water cooling. It has been established that, under heat flow during wall reduction, the temperature of the contact surface of the striker is 370 – 451 °C.

References / Список литературы

1. Lekhov O.S., Mikhalev A.V. Unit of Combined Continuous Casting and Deformation for Production of Steel Sheets for Welded Pipes. Theory and Calculation. Yekaterinburg: UPI; 2017:151. (In Russ.).

   Лехов О.С., Михалев А.В. Установка совмещенного процесса непрерывного литья и деформации для производства листов из стали для сварных труб. Теория и расчет. Екатеринбург: изд. УМЦ УПИ; 2017:151.

2. Lekhov O.S., Mikhalev A.V., Shevelev M.M. Stresses in the Striker–Strip System during Production of Steel Sheets at a Unit of Continuous Casting and Deformation. Yekaterinburg: UPI; 2018:125. (In Russ.).

   Лехов О.С., Михалев А.В., Шевелев М.М. Напряжения в системе бойки – полоса при получении листов из стали на установке непрерывного литья и деформации. Екатеринбург: изд. УМЦ УПИ; 2018:125.

3. Lekhov O.S., Bilalov D.Kh. Technological capabilities of installations for combined continuous casting and deformation processes for the production of metal products. *Proizvodstvo prokata*. 2016;(7):24–26. (In Russ.).

   Лехов О.С., Билалов Д.Х. Технологические возможности установок совмещенных процессов непрерывного литья и деформации для производства металлопродукции. *Производство проката*. 2016;(7):24–26.

4. Khloponin V.N., Kosyreva M.V., Kosyak A.S. Influence of cooling system on thermal operating conditions of roll surface layer. In: *Proceedings of the MISIS. Issue 100*. Moscow: MISiS; 1977:90–93. (In Russ.).

   Хлопонин В.Н., Косырева М.В., Косяк А.С. Влияние системы охлаждения на тепловые условия работы поверхностного слоя валка. В кн.: *Труды МИСиС. Вып. 100*. Москва: изд. МИСиС; 1977:90–93.

5. Boley B.A., Weiner J.H. Theory of Thermal Stresses. New York: John Wiley & Sons; 1960:586.

   Боли Б., Уэйнер Дж. Теория температурных напряжений. Москва: Мир; 1976:349.

6. Lekhov O.S. Study of stress-strain state of rolls-band system at rolling of broad-flanged beam in stands of universal beam mill. Report 2. *Izvestiya. Ferrous Metallurgy*. 2014;57(12):15–19. (In Russ.).
   https://doi.org/10.17073/0368-0797-2014-12-15-19

   Лехов О.С. Исследование напряженно-деформированного состояния системы валки – полоса при прокатке широкополочной балки в клетях универсально-балочного стана. Сообщение 2. *Известия вузов. Черная металлургия*. 2014;57(12):15–19.
   https://doi.org/10.17073/0368-0797-2014-12-15-19

7. Kushner V.S., Vereshchaka A.S., Skhirtladze A.G., Negrov D.A. Technological Processes in Mechanical Engineering. Part II. Metal Forming and Welding Production. Omsk: OmSTU; 2005:200. (In Russ.).

   Кушнер В.С., Верещака А.С., Схиртладзе А.Г., Негров Д.А. Технологические процессы в машиностроении Ч. II. Обработка металлов давлением и сварочное производство. Омск: изд. ОмГТУ; 2005:200.

8. Bulanov L.V., Karlinskii S.E., Volegova V.E. Durability of casters for external and internal cooling. In: *Reliability of Large Machines. Collection of Sci. Papers. NIItyazhmash*. Sverdlovsk: NIItyazhmash; 1990:126–132. (In Russ.).

   Буланов Л.В., Карлинский С.Е., Волегова В.Е. Долговечность роликов МНЛЗ при наружном и внутреннем охлаждении. В кн.: *Надежность крупных машин. Сб. науч. тр. НИИтяжмаш*. Свердловск: изд. НИИтяжмаш; 1990:126–132.

9. Lykov A.V. Theory of Thermal Conductivity. Moscow: Vysshaya shkola; 1967:600. (In Russ.).

Лыков А.В. Теория теплопроводности. Москва: Высшая школа; 1967:600.
10. ANSYS. Structural Analysis Guide. Rel. 15.0.
11. Matsumia T., Nakamura Y. Mathematical model of slab bulging during continuous casting. In: *Applied Mathematical, and Physical Models in Iron and Steel Industry: Proceedings of the 3rd Process. Tech. Conf., Pittsburgh, Pa, 28-31 March 1982*. New York; 1982:264–270.
12. Takashima Y., Yanagimoto I. Finite element analysis of flange spread behavior in H-beam universal rolling. *Steel Research International*. 2011;82(10):1240–1247. https://doi.org/10.1002/srin.201100078
13. Kobayashi S., Oh S.-I., Altan T. Metal Forming and Finite-Element Method. New York: Oxford University Press; 1989:377.
14. Karrech A., Seibi A. Analytical model of the expansion in of tubes under tension. *Journal of Materials Processing Technology*. 2010;210:336–362.
15. Kazakov A.L., Spevak L.F. Numeral and analytical studies of nonlinear parabolic equation with boundary conditions of a special form. *Applied Mathematical Modelling*. 2013; 37(10-13):6918–6928. https://doi.org/10.1016/j.apm.2013.02.026
16. Jansson N. Optimized sparse matrix assembly in finite element solvers with one-sided communication. In: *High Performance Computing for Computational Science – VECPAR 2012*. Berlin, Heidelberg: Springer; 2013:128–139.
17. Park C.Y., Yang D.Y. A study of void crushing in large forgings II. Estimation of bonding efficiency by finite-element analysis. *Journal of Materials Processing Technology*. 1997;72(1):32-41.
18. Sorimachi K., Emi T. Elastoplastic stress analysis of bulging as a major cause of internal cracks in continuously cast slabs. *Tetsu-to-Hagane*. 1977;63(8):1297–1304. https://doi.org/10.2355/tetsutohagane1955.63.8_1297
19. Marciniak Z., Duncan J.L., Hu S.J. Mechanics of Sheet Metal Forming. Oxford: Butterworth-Heinemann Elsevier Ltd.; 2002:228.
20. Fujii H., Ohashi T., Hiromoto T. On the formation of the internal cracks in continuously cast slabs. *Tetsu-to-Hagane*. 1978; 18(8):510–518. https://doi.org/10.2355/tetsutohagane1955.62.14_1813

Information about the Authors / Сведения об авторах

Oleg S. Lekhov, *Dr. Sci. (Eng.), Prof. of the Chair of Engineering and Vocational Training in Machinery and Metallurgy,* Russian State Professional Pedagogical University
E-mail: MXLehov38@yandex.ru

Damir Kh. Bilalov, *Assist. Prof. of the Chair of Engineering and Vocational Training in Machinery and Metallurgy,* Russian State Professional Pedagogical University
ORCID: 0000-0002-4336-5339
E-mail: master_ddd@mail.ru

Олег Степанович Лехов, *д.т.н., профессор кафедры инжиниринга и профессионального обучения в машиностроении и металлургии,* Российский государственный профессионально-педагогический университет
E-mail: MXLehov38@yandex.ru

Дамир Харасович Билалов, *доцент кафедры инжиниринга и профессионального обучения в машиностроении и металлургии,* Российский государственный профессионально-педагогический университет
ORCID: 0000-0002-4336-5339
E-mail: master_ddd@mail.ru

Received 16.09.2024
Revised 27.09.2024
Accepted 25.12.2024

Поступила в редакцию 16.09.2024
После доработки 27.09.2024
Принята к публикации 25.12.2024

INNOVATION IN METALLURGICAL INDUSTRIAL AND LABORATORY EQUIPMENT, TECHNOLOGIES AND MATERIALS

ИННОВАЦИИ В МЕТАЛЛУРГИЧЕСКОМ ПРОМЫШЛЕННОМ И ЛАБОРАТОРНОМ ОБОРУДОВАНИИ, ТЕХНОЛОГИЯХ И МАТЕРИАЛАХ

UDC 539.5;621.74
DOI 10.17073/0368-0797-2025-4-372-382

Original article
Оригинальная статья

Modeling and optimization of the effect of temperature seams on stress-strain state of spherical metal casting molds

A. I. Evstigneev, D. V. Chernyshova, V. I. Odinokov, E. A. Dmitriev, A. A. Evstigneeva, Yu. B. Koloshenko, D. A. Potyanikhin

Komsomolsk-on-Amur State University (27 Lenina Ave., Komsomolsk-on-Amur, Khabarovsk Territory 681013, Russian Federation)

diss@knastu.ru

Abstract. The objective of this theoretical study is to evaluate the effect of annular temperature seams in the inner surface of a spherical metal casting mold on the level of stress-strain state (SSS) in it during crystallization of a steel casting. The specificity of this technological process consists in the geometric shape (sphere) of the casting model, when the crystallizing metal creates significant compressive stresses in the inner surface of the mold (in the first moments), which are enhanced by the mold curvature: the mold inner layer, heating up, tries to increase in volume, but this is prevented not only by the cooler outer layers, but also by curvature of the surface layer itself. Two possible applications of the casting mold are being considered: with and without seams. The problem of optimizing the design parameters of temperature seams (recesses) is formulated. It depends on the magnitude of the normal stresses occurring in the casting mold at the initial stage of the steel casting crystallization. When solving the problem, the equations of the linear theory of elasticity, the equations of thermal conductivity and the proven numerical method are used. The paper presents a numerical scheme and a developed algorithm for solving the problem. Crack resistance was estimated based on the magnitude of normal stresses in a spherical metal mold. The optimal design options (schemes) of a spherical metal casting mold found as a result of solving the test problem depend on location of the temperature seams in the shell mold, the stress values in them under conditions of the min-max objective function and the developed algorithm. The results of solving the problem are presented graphically in the form of plots of stresses and temperatures in the studied area in different sections and periods of cooling of the shell mold and the metal growing crust. The obtained results of resistance of a metal spherical casting mold were analyzed.

Keywords: metal casting mold, casting, stress-strain state, modeling, optimization

Acknowledgements: The research was supported by the Russian Science Foundation, grant No. 24-29-00214, https://rscf.ru/project/24-29-00214/.

For citation: Evstigneev A.I., Chernyshova D.V., Odinokov V.I., Dmitriev E.A., Evstigneeva A.A., Koloshenko Yu.B., Potyanikhin D.A. Modeling and optimization of the effect of temperature seams on stress-strain state of spherical metal casting molds. *Izvestiya. Ferrous Metallurgy*. 2025; 68(4):372–382. https://doi.org/10.17073/0368-0797-2025-4-372-382

Моделирование и оптимизация влияния температурных швов на напряженно-деформированное состояние сферических металлических литейных форм

А. И. Евстигнеев, Д. В. Чернышова, В. И. Одиноков, Э. А. Дмитриев, А. А. Евстигнеева, Ю. Б. Колошенко, Д. А. Потянихин

Комсомольский-на-Амуре государственный университет (Россия, 681013, Хабаровский край, Комсомольск-на-Амуре, пр. Ленина, 27)

diss@knastu.ru

Аннотация. Задачей настоящего теоретического исследования является оценка влияния кольцевых температурных швов на внутренней поверхности литейной металлической сферической формы на уровень напряженно-деформированного состояния (НДС) в ней при кристаллизации стальной отливки. Специфика данного технологического процесса состоит в геометрической форме (сфера) литейной модели, когда кристаллизующийся металл создает во внутренней поверхности литейной формы (в первые мгновения) значительные сжимающие напряжения, которые усиливаются кривизной формы: внутренний слой формы, нагреваясь, пытается увеличиться в объеме, но этому препятствуют не только более холодные внешние слои, но и кривизна самого поверхностного слоя. Рассматриваются два варианта применения литейной формы: со швами и без них. Формулируется задача оптимизации конструктивных параметров температурных швов (выточек) от величины возникающих в литейной форме нормальных напряжений в начальной стадии кристаллизации стальной отливки. При решении задачи используются уравнения линейной теории упругости, уравнения теплопроводности и апробированный численный метод. Приведена численная схема и разработанный алгоритм решения задачи. Оценка трещиностойкости проводится по величине нормальных напряжений в металлической сферической форме. Найденные в результате решения тестовой задачи оптимальные конструктивные варианты (схемы) литейной сферической металлической формы зависят от расположения температурных швов в оболочковой форме, значений напряжений в них в условиях целевой функции min-max и разработанного алгоритма. Результаты решения задачи представлены графически в виде эпюр напряжений и температур по исследуемой области в разных сечениях и временах охлаждения ОФ и нарастающей корочки металла. Дан анализ полученных результатов стойкости металлической сферической литейной формы.

Ключевые слова: металлическая литейная форма, отливка, напряженно-деформированное состояние, моделирование, оптимизация

Благодарности: Исследование выполнено за счет гранта Российского научного фонда № 24-29-00214, https://rscf.ru/project/24-29-00214/.

Для цитирования: Евстигнеев А.И., Чернышова Д.В., Одиноков В.И., Дмитриев Э.А., Евстигнеева А.А., Колошенко Ю.Б., Потянихин Д.А. Моделирование и оптимизация влияния температурных швов на напряженно-деформированное состояние сферических металлических литейных форм. *Известия вузов. Черная металлургия*. 2025;68(4):372–382. https://doi.org/10.17073/0368-0797-2025-4-372-382

Introduction

Metal casting molds are widely used in foundry production across various casting methods, including permanent mold casting, centrifugal casting, die casting, continuous casting, liquid forging, and others. A major drawback of these casting methods is the limited service life of metal molds due to the combined effects of mechanical and thermal loads. These loads lead to elevated stress–strain states (SSS) within the molds, which can result in structural fracture or deformation of the mold geometry due to thermal stresses. To mitigate these effects, various technological and design solutions are implemented in practice.

Both the analysis of the literature and practical experience indicate that the geometry of the casting produced in the mold significantly affects mold resistance. Among all geometries, the spherical (ball-shaped) casting is considered the most unpredictable in terms of mold resistance.

In industrial production of spherical castings, different types of casting molds are used, including expendable sand–clay molds, ceramic molds, and split metal molds. These molds are subjected to varying degrees of mechanical and thermal loads, which may lead to structural degradation or reduced operational life.

A theoretical concept and a fundamentally new technological solution[1] were proposed by the authors of [1] to improve the resistance of spherical ceramic shell molds (SMs) by introducing annular temperature seams on the inner surface of the mold. This idea emerged from the analysis of a well-known foundry technique used to reduce thermal stresses in castings – namely, the use of "stiffening ribs" [2]. In the context of this study, annular temperature seams (recesses) serve a similar purpose. An annular temperature seam is a ring-shaped recess located on the inner surface of the ceramic shell mold.

The evolution of the SSS in metal molds during permanent mold casting has been discussed in detail in articles [3; 4].

[1] Pat. No. 2828801. Multilayer shell mold for casting / V.I. Odinokov, A.I. Evstigneev, E.A. Dmitriev, D.V. Chernyshova, Yu.I. Tkacheva, A.N. Namokonov. Appl. 05.03.2024; publ. 21.10.2024. Bull. No. 30.

The SSS of permanent molds is evaluated using the finite element method [3] in two stages: first, solving the heat conduction problem; and second, solving the elastoplastic deformation problem using the obtained temperature fields. The simulation results enabled the design and implementation of new, more durable cast iron molds with reduced weight.

Reference [4] presents data on numerical modeling of casting formation processes in metal molds. The finite difference method was used as the computational foundation, specifically in the form of an explicit difference scheme. A rectangular spatial grid within the mold base was employed to simulate heat transfer in the system. Grid spacing in the solidifying casting, mold wall, and insulation layer was coordinated with the thermophysical properties of the base to ensure thermal uniformity. Computational stability was maintained by choosing a time step of $\overline{\Delta}\tau \leq 30$ s, under which the Fourier number did not exceed its critical value. The problem was formulated in two dimensions.

The modeling results for the SSS in a solidifying steel casting [5; 6] made it possible to predict crack formation. The development of these cracks depends not only on temperature fields and the resulting thermal stresses and strains but also on the localization of shrinkage porosity.

In [7], a general expression was derived for calculating shrinkage and thermal stresses in an elastoplastic sphere caused by a spherically symmetric heat source. The expression accommodates arbitrary nonlinear hardening laws and includes elastic unloading of the elastoplastic sphere.

Study [8] examined elastoplastic and residual stresses in a thick-walled spherical vessel subjected to external hydrostatic pressure. The findings led to the development of a process for inducing favorable compressive residual stresses in the inner regions of cylindrical and spherical vessels.

The subject of [9] was a functionally graded hollow sphere with spherical isotropy under internal pressure. The goal was to achieve a favorable stress distribution in the hollow sphere subjected to internal pressure, accounting for both ductile and brittle material behavior.

In [10], a transient thermoelastic analysis was conducted for a multilayered hollow cylinder with piecewise power-law material inhomogeneity, subjected to asymmetric surface heating. The study examined the influence of functional grading on the development of thermal stresses.

A numerical simulation was carried out in ANSYS Mechanical [11] for a two-layer thick-walled spherical shell under combined thermal and mechanical loading [11].

Reference [12] presented the solution to a problem involving stresses and displacements in a thick spherical shell subjected to internal and external pressure [12].

Based on plane elasticity theory [13] derived the displacement and stress components in thick-walled spherical pressure vessels made of inhomogeneous materials exposed to both internal and external pressure. The influence of material inhomogeneity on elastic deformations and stress distribution was evaluated.

The structural optimization of a three-layer cylinder assembled by thermal shrink-fitting from different materials and subjected to very high internal pressure was investigated in [14].

In [15], axisymmetric modeling of a multilayer shell was performed. A plane strain problem was solved for a cylinder surrounded by concentric ring layers. A numerical solution was provided to analyze how the distribution of residual stresses depends on the material properties during cooling.

Study [16] investigated the influence of the angle of contact between a spherical ceramic SM and a support filler (SF) on the mold's SSS during the casting of a steel spherical part. An optimization problem was formulated to enhance the resistance of the spherical ceramic SM by varying the angle of contact during the solidification and cooling of the steel casting, using a min–max objective function. The crack resistance of SM was evaluated based on magnitude of the normal stresses.

To model the evolution of the SSS in the mold at the initial cooling stage, equations from linear elasticity theory, heat conduction, and a validated numerical method were used [17]. This method has been widely applied to similar problems in casting mechanics.

Modeling and optimization of related processes in other domains were addressed in [18; 19].

The aim of study [18] was to develop an efficient numerical algorithm for solving axisymmetric inverse problems related to the design of thermal masking devices, specifically multilayer spherical masking shells, and to analyze the results of the corresponding computational experiments. As the numerical optimization procedure for solving these problems, the authors used the particle swarm optimization method proposed in [20].

Study [19] examined the problem of plastic instability in a thin-walled plastically orthotropic spherical pressure vessel subjected to internal impulsive loading. Using Mathematica software, the study identified how strain rate and the orthotropic plasticity parameter affect the critical deformation level at which instability occurs.

This study examines the resistance of a spherical casting mold during the crystallization of a steel casting. It develops a previously proposed technological solution originally applied to ceramic spherical SMs, which aimed to reduce the magnitude of normal stresses in the mold's cross section by introducing an ordered arrangement of recesses. The focus of the present work is to determine

the optimal structural design of a spherical metal mold capable of withstanding the thermal gradient that arises in the mold during the initial stage of cooling after the molten steel is poured. Ensuring the resistance of such mold configurations is critical for the production of spherical castings used in a wide range of engineering applications that demand high dimensional precision.

Mathematical formulation of the problem

An axisymmetric body of revolution is considered (Fig. 1), consisting in meridional section of the following domains: *I* – liquid phase (steel); *II* – solid phase (solid metal); *III* – metal casting mold with annular recesses on its inner surface; *IV* – support structure (SS). The mold is a split-type design with inner annular recesses. Molten metal is poured into the mold cavity from the top through a funnel. View *A* presents a sketch of an annular recess on the inner surface of the mold, along with the corresponding surfaces where boundary conditions are applied.

The computational scheme presented below closely reflects the actual technological process used to produce spherical steel castings in a metal mold.

Since the problem is formulated as a Cauchy problem, the physical process of heat removal during cooling may be implemented by any known technological method, such as natural or forced cooling, etc.

A configuration with two recesses on the inner surface of the mold is considered (Fig. 2). The objective is to determine an optimal arrangement of these recesses such that the maximum absolute values of the normal stresses σ_{22} are minimized.

The objective function for this condition is defined as:

$$F = \min\left|\sigma_{22}(\gamma)\right| \max\left|\sigma_{22}\left(Q\big|_{S_2}, \tau\right)\right| \quad (1)$$

with constrains

$$\begin{aligned} 0 \le \gamma_0 \le 120°; \\ 0 < \tau \le 15 \text{ s}; \end{aligned} \quad (2)$$

here, Q is the area of the meridional cross section of mold.

The constraint on τ is based on the solution to a similar problem, where, during the cooling of liquid metal in a mold without recesses, the magnitudes of the normal stresses σ_{22}, and σ_{33} in cross sections begin to decrease at $\tau > 10$ c. The constraint on the recess opening angle γ_0

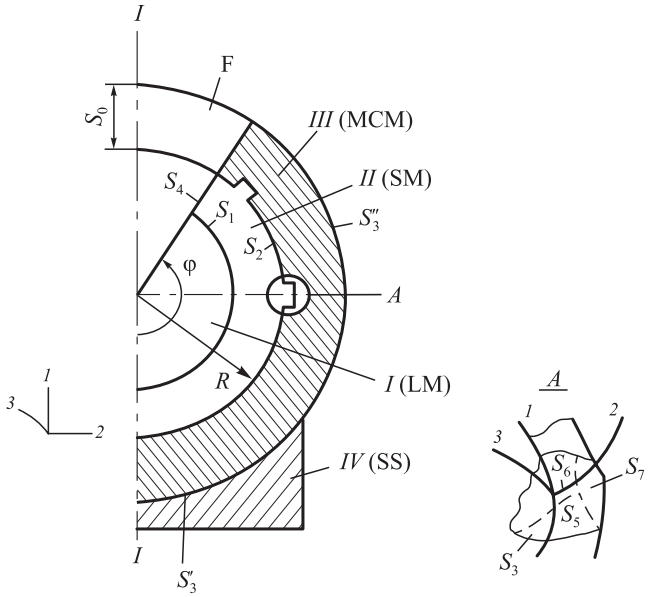

Fig. 1. Calculation scheme of the system with indication of the surface to the boundary conditions of the problem: S_1 – contact surface of the liquid and solidified metal; S_2 – inner contact surface of the solidified metal and the metal mold; S_3' – outer surface of the metal mold in contact with the support structure (SS); S_3'' – outer surface of the metal mold in contact with the environment; *I* – liquid metal (LM); *II* – solid metal (SM); *III* – metal casting mold (MCM); *IV* – support structure (SS); F – funnel

Рис. 1. Расчетная схема системы с указанием поверхности к граничным условиям задачи: S_1 – поверхность контакта жидкого и затвердевшего металла; S_2 – внутренняя поверхность контакта затвердевшего металла и металлической формы; S_3' – внешняя поверхность металлической формы контакта с опорной конструкцией (SS); S_3'' – внешняя поверхность металлической формы контакта с окружающей средой; *I* – жидкий металл (LM); *II* – твердый металл (SM); *III* – литейная металлическая форма (MCM); *IV* – опорная конструкция (SS); F – литниковая воронка

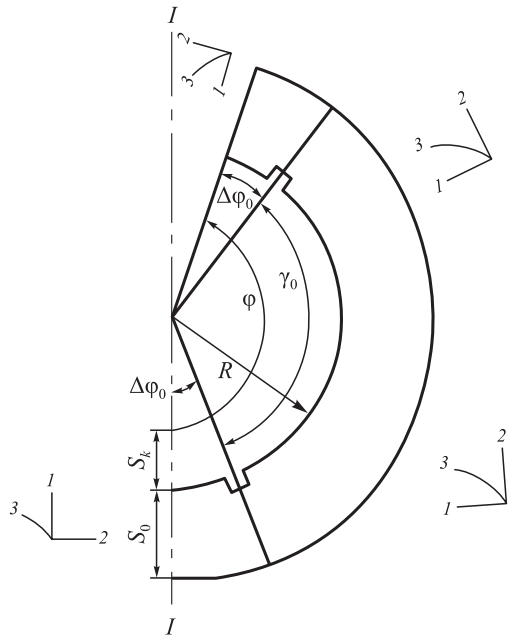

Fig. 2. Scheme of the system *I* (LM) – *II* (SM) – *III* (MCM) for optimizing the structure with two recesses on the mold inner surface

Рис. 2. Схема системы *I* (LM) – *II* (SM) – *III* (MCM) к оптимизации конструкции с двумя выточками на внутренней поверхности формы

arises from the condition that the reduction in compressive stress σ_{22} caused by the recess affects only a limited region.

The central part of the problem involves solving a system of equations from the linear theory of elasticity at a given time step $\bar{\Delta}\tau_n$.

Using the equations of linear elasticity, we formulate for each domain the corresponding system of equations in Cartesian coordinates:

– domain *I* (liquid metal):

$$\begin{gathered}\sigma_{11} = \sigma_{22} = \sigma_{33} = \sigma = -P_1; \\ \dot{\theta} = a_1 \Delta\theta;\end{gathered} \tag{3}$$

– domains *II* and *III* (solid metal and mold):

$$\begin{cases}\sigma_{ij,j} = 0,\ i; \\ \sigma_{ij} - \sigma\delta_{ij} = 2G_p\varepsilon^*_{ij};\ \varepsilon^*_{ij} = \varepsilon_{ij} - \dfrac{1}{3}\varepsilon\delta_{ij}; \\ \varepsilon = \varepsilon_{ii}; \\ \varepsilon_{ii} = 3k_p\sigma + 3\alpha_p\left(\theta - \theta^*_p\right); \\ \varepsilon_{ij} = 0{,}5\left(U_{i,j} + U_{j,i}\right); \\ \dot{\theta} = a_p\Delta\theta,\end{cases} \tag{4}$$

where U_i is displacements; ε_{ij} is strain components; σ is hydrostatic stress; $p = I, II, III$ – computational domains; $G_p(\theta)$ is shear modulus in domain p ($p = II, III$); G_p ($p = II, III$) – shear modulus for solid metal ($p = II$) and mold material ($p = III$); δ_{ij} is Kronecker delta; k_p is bulk compression coefficients; α_p is coefficients of linear thermal expansion ($p = II, III$); a_p is thermal diffusivity ($p = I, II, III$); θ is current temperature; τ is time; θ^*_p is initial temperatures in domains $p = I, II, III$; P_1 is pressure in the domain *I*; $a_p = \dfrac{\lambda_p}{c_p\gamma_p}$; λ_p is thermal conductivity; c_p is specific heat capacity; γ_p is specific weight; Δ is Laplace operator.

During the cooling of the liquid metal, provided that $\theta_m \le \theta_c$ (where θ_m is the metal temperature and θ_c is the crystallization temperature), the thickness of the solidified layer is determined from the phase transition solution:

$$\frac{d\theta_1}{dn}\lambda_1 - \frac{d\theta_2}{dn}\lambda_2 = \frac{dx}{d\tau}L\rho, \tag{5}$$

where θ_1, θ_2 are temperatures of the solid and liquid phases; λ_1, λ_2 are thermal conductivities of the solid and liquid phases; *L* is latent heat of fusion; ρ is density of the solid phase; *x* is current thickness of the solidified metal layer; *n* is normal to the phase boundary.

Assuming that the temperature in the solid phase across the thickness δx_n varies linearly, and the temperature gradient in the liquid phase is zero, the solution to equation (5) yields the following expression for determining the thickness of the solidified shell δx_n at a given time step $\bar{\Delta}\tau_n$ [21]:

$$\delta x_n = C\sqrt{\tau};\ \ C = \sqrt{\frac{2\bar{\Delta}\theta_1\lambda_1}{\rho L}}; \tag{6}$$

where $\bar{\Delta}\theta_1$ is the temperature drop in the solid phase near the crystallization front.

Initial conditions for problem (3), (4):

– $\delta x\big|_{\tau=0} = 0$ – no solid phase present in the metal;

– $\theta_1\big|_{\tau=0} = \theta_0$ – temperature of the poured liquid metal (1500 °C);

– $\theta^*_3\big|_{\tau=0} = \theta^*$ – initial temperature of the mold (20 °C).

Initial stresses are assumed to be zero.

The system of equations (3), (4) is solved in an orthogonal coordinate system. The problem is axisymmetric, with the following symmetry conditions:

$$U_3 = 0;\ \sigma_{31} = \sigma_{32} = 0;\ \varepsilon_{31} = \varepsilon_{32} = 0.$$

Boundary conditions for equations (3), (4) (see Fig. 1):

– on the axis of symmetry

$$U_2 = 0;\ \sigma_{21} = 0;\ q_{hf} = 0;$$

– on surfaces $S_1 - S_8$

$$\begin{gathered}\sigma_{11}\big|_{S_1} = -P_1;\ \ \sigma_{12}\big|_{S_i} = 0\ \ (i = 1,\ 5,\ 6); \\ \sigma_{11}\big|_{S''_3} = 0;\ \ \sigma_{11}\big|_{S_i} = 0\ \ (i = 5,\ 6); \\ \sigma_{12}\big|_{S_3} = 0;\ \ \sigma_{22}\big|_{S_i} = 0\ \ (i = 7,\ 8); \\ U_1\big|_{S'_3} = 0;\ \ U_2\big|_{S_4} = 0;\ \ \sigma_{21}\big|_{S_i} = 0\ \ (i = 4,\ 7,\ 8); \\ \theta\big|_{S_1} = \theta_0;\ \ \theta\big|_{S_3} = \theta^*,\end{gathered} \tag{7}$$

where q_{hf} is heat flux; $S_3 = S'_3 + S''_3$ – surfaces where the mold is in contact with the support structure or exposed to the surrounding environment.

To solve the system of equations (3), (4) with boundary conditions (7), a numerical method was used, as described in [17] and previously applied in studies [21; 22]. The computational domain is divided by a system of orthogonal surfaces into finite-sized elements. For each element, the system (3), (4) is written in finite-difference form using the stress and displacement values on the element faces and the arc lengths of the edges forming the element. The resulting equations are solved using the initial and boundary conditions according to the algorithm and methodology developed in. The solution outputs include: stresses and displace-

ments on the faces of each element; the average temperature of each element at the given time step. The numerical solution was implemented using a custom-developed program and the software package Odyssey[2].

The finite-difference analogue of the heat conduction equation for an orthogonal element is constructed based on the principle of thermal balance [17]. It incorporates the average temperature within the element, the temperatures of the surrounding elements, and the arc lengths that define the orthogonal elements. The resulting system of equations is solved using a tridiagonal matrix algorithm (Thomas algorithm).

Solution algorithm

The solution of problem (1) with constraints (2) is carried out according to the following algorithm.

1. The computational domain is divided into a finite number of orthogonal elements; geometric dimensions S and R are specified.

2. The total cooling time $\tau^* = 15$ s in problem (1) with constraints (2) is divided into a finite number of time steps: $\tau^* = \sum \bar{\Delta}\tau_n$, where n is the time step number.

3. The physical and mechanical properties of the materials are specified: liquid and solidifying steel, and the mold material.

4. The geometric parameters of the recesses are specified: $\bar{\Delta}\varphi_0$, φ, γ_0.

5. The increment step for the current parameter γ is specified: $\bar{\Delta}\gamma$.

6. Initial and boundary conditions are assigned to the elements that form the computational domain, including those forming the recesses.

7. Arc lengths of the elements within each domain are calculated.

8. The temperature field at the current time step $\bar{\Delta}\tau_n$ is determined by solving the heat conduction equation using the initial and boundary conditions for that step.

9. If the temperature at surface S_2 in domain I satisfies $\theta|_{S_2} \le \theta_c$, the thickness of the solidified shell is calculated using equation (6); and the computational mesh is reconstructed starting from step ***7***. If $\theta|_{S_2} > \theta_c$, proceed to step ***10***.

10. The system of equations (4) (excluding the heat conduction equations) is solved using the method described in [17]. The stress fields σ_{ij} and displacement fields U_i ($i, j = 1, 2, 3$) are determined.

11. Across domain Q on surface S_2 the maximum absolute value of the normal stress σ_{22} is identified and entered into matrix $\{\sigma_2\}'$.

12. A time step is performed. If $\sum \bar{\Delta}\tau_n < \tau^*$, return to step ***8***. If $\sum \bar{\Delta}\tau_n = \tau^*$, proceed to step ***13***.

13. From matrix $\{\sigma_2\}'$ the value $\sigma_{22} = \max\{\sigma_2\}'$ is found and recorded in matrix $\{\sigma_2\}''$.

14. The parameter is updated: $\gamma_n = \gamma_{n-1} - \bar{\Delta}\gamma$; then $\tau = 0$. If $\gamma_n = 0$, proceed to step ***15***, if $\gamma_n > 0$, return to step ***6***.

15. From matrix $\{\sigma_2\}''$ the minimum value of $\overline{\sigma_{22}} = \min\{\sigma_3\}'$ is selected along with the corresponding values of τ and γ.

16. End of the solution procedure.

Results and discussion

Geometric parameters of the mold: $S_0 = 50$ mm, $R = 20$ mm, $\varphi = 150°$.

Time intervals (s): $\bar{\Delta}\tau_n$: 0.01; 0.02; 0.03; 0.04; 0.05; 0.1; 0.2; 0.3; 0.4; 0.5; 2.0; 5.0; 6.0; 8.0; 9.0; $P_1 = 1$ kg/cm^2.

Domain discretization: $N_1 \times N_2 = 13 \times 20$.

According to the calculations, dividing the domain into 13×20 elements along the first and second coordinate axes for the mold without recesses is entirely suitable for the analysis performed. The same discretization (13×20 elements along the same coordinate axes) is equally justified for the mold with recesses.

Parameters of the poured steel for $\theta > 1000$ °C ($\theta_m^* = 1000$ °C):

$$\begin{gathered} G_2 = 10^4 \text{ MPa};\ \alpha_{1,2} = 12 \cdot 10^{-6}\ ^\circ\text{C}^{-1}; \\ \lambda = 0.0298 \text{ W/(mm}\cdot^\circ\text{C)}; \\ L_1 = 270 \cdot 10^3 \text{ J/kg (latent heat of fusion)}; \\ C_{1,2} = 444 \text{ J/(kg}\cdot^\circ\text{C)};\ \gamma_1 = 7.80 \cdot 10^{-6} \text{ kg/mm}^3; \\ \theta_c = 1450\ ^\circ\text{C}. \end{gathered} \tag{8}$$

The physical properties of the metal mold are the same as in equation (8), except that

$$G_3 = 81{,}000\left[1 - 1.2\left(\frac{Q}{1000}\right)^2\right] \text{ MPa}. \tag{9}$$

Initial values for the optimization process: $\bar{\Delta}\varphi_0 = 23°$, $\gamma_0 = 104°$; recess dimensions A_1, A_2 (7.1×2.6) mm along axes *1* and *2* (Fig. 3). The recess dimensions correspond to the dimensions of the mesh elements.

As a result of the calculations performed using the above algorithm, the following parameters were obtained:

[2] Odinokov V.I., Prokudin A.N., Sergeeva A.M., Sevastyanov G.M. Certificate of state registration of a computer program No. 2012661389, Odyssey. Registered in the Register of Computer Programs on December 13, 2012.

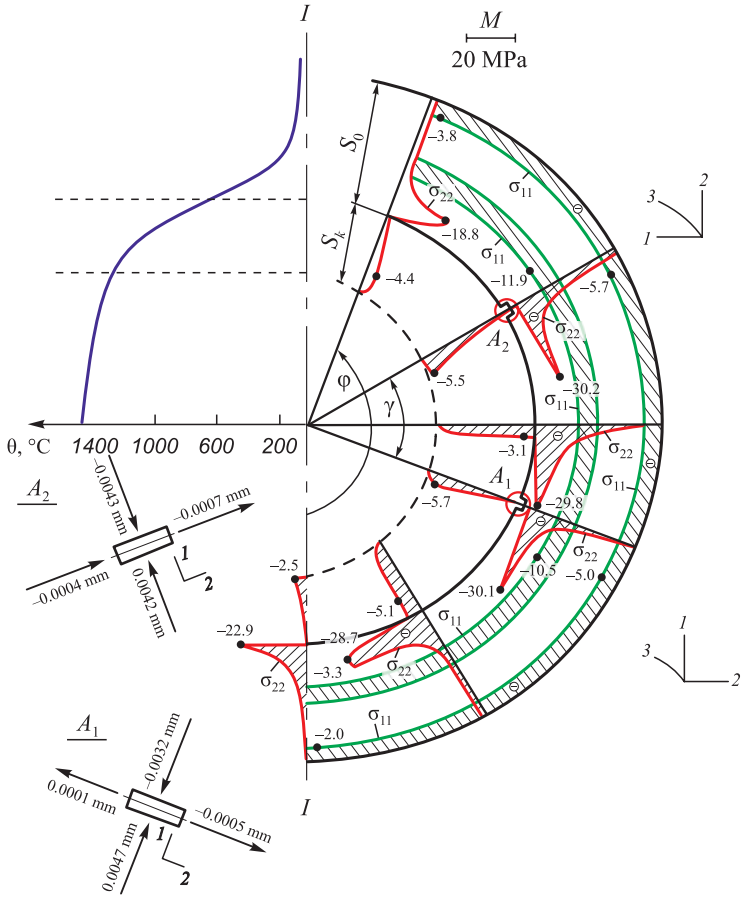

Fig. 3. Plots of normal stresses σ_{11}, σ_{22} and displacements U_1, U_2 along the edges of the recesses A_1 and A_2 in the mold at $\tau = 8.6$ s

Рис. 3. Эпюры нормальных напряжений σ_{11}, σ_{22} и перемещений U_1, U_2 по граням выточек A_1 и A_2 в форме при $\tau = 8{,}6$ с

$$F = 29.8 \text{ MPa}; \gamma = 60°; \tau = 8.6 \text{ s}. \quad (10)$$

Fig. 3 presents the distributions of σ_{11}, σ_{22} and displacements U_1, U_2 along the edges of recesses A_1 and A_2 in the mold. It can be seen that at the inner corners of recesses A_1 and A_2 there are stress concentrations for σ_{22}, with values of –30.1 MPa and –30.2 MPa, respectively. These values are slightly higher (in magnitude) than the value of F obtained above. For comparison, Fig. 4 shows the σ_{22} distribution (in MPa) across the section of a mold without recesses at the same time ($\tau = 8.6$ s). The σ_{33} distribution is not shown, as it is approximately equal to σ_{22}, differing by no more than ±1 %.

A pronounced difference in σ_{22} values is evident.

Fig. 5 shows the σ_{33} distribution for the parameters given in equation (10).

Although σ_{33} decreases (in magnitude) in many sections, a considerable portion of the mold still experiences high compressive stresses (more than 60 MPa). This indicates that optimization should be carried out for both σ_{22} and σ_{33}. The σ_{22} stress was chosen for initial optimization because the recesses in the mold effectively cut through the regions of high S_3, at the early stage of cooling (Fig. 4), without disturbing axial symmetry. However, to achieve a more global reduction in compressive stresses σ_{22} and σ_{33}, it would likely be necessary to introduce additional recesses perpendicular to the existing ones.

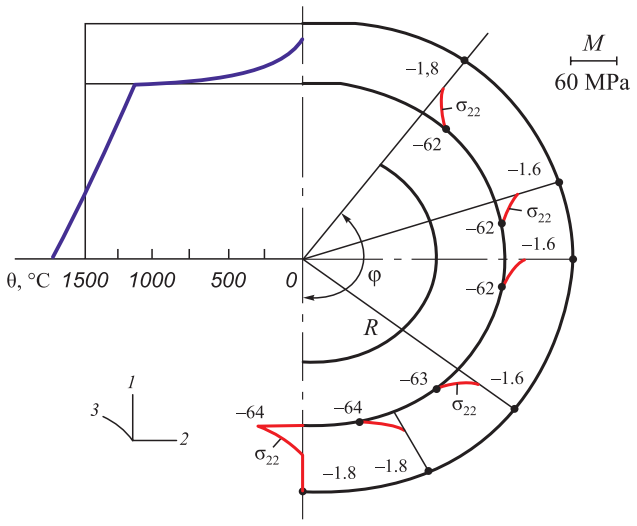

Fig. 4. Plots of normal stresses σ_{22} along the mold section without recesses at $\tau = 8.6$ s

Рис. 4. Эпюры нормальных напряжений σ_{22} по сечению формы без выточек при $\tau = 8{,}6$ с

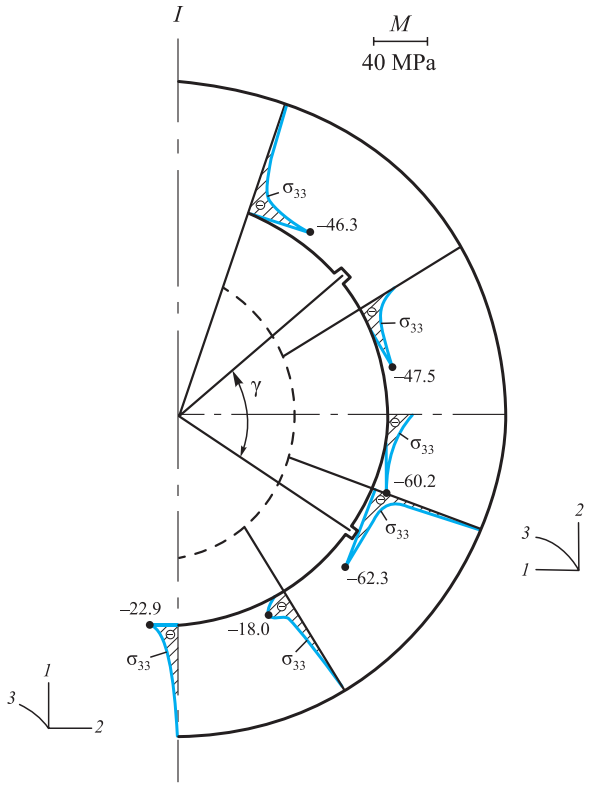

Fig. 5. Plots of normal stresses σ_{33} in the mold at optimal design parameters (10)

Рис. 5. Эпюры нормальных напряжений σ_{33} в форме при оптимальных расчетных параметрах (10)

This, however, represents a different, non-axisymmetric problem, requiring different equations and boundary conditions.

Within the present study, an attempt was made to reduce σ_{33} (in magnitude) by introducing additional recesses on surface S_2. According to equation (10), the recesses are arranged symmetrically on surface S_2 at an angle φ, with an opening angle γ (Fig. 2). The highest σ_{33} values (in magnitude) occur within this opening angle γ (Fig. 5). Therefore, two additional recesses were placed on surface S_2 within the previously determined opening angle γ. The SSS of the shell-type steel mold with four recesses on surface S_2 was then calculated using the above algorithm for $\tau = 8.6$ s. In this case, the algorithm was significantly simplified, as the recess configuration was fixed and the cooling time predetermined. Fig. 6 shows the σ_{22} and σ_{33} distributions across the mold section at the end of the time step $\tau^* = 8.6$ s. The results indicate a marked reduction (in magnitude) in both σ_{22} and σ_{33} stresses.

In summary, the novelty of this work lies in formulating a problem aimed at determining the optimal arrangement of temperature seams as technologically significant areas, along with the corresponding stress values in a spherical metal mold, within the framework of a min–max objective function, as well as in developing a solution algorithm.

The proposed methodology, modeling algorithm, and optimization approach for enhancing the crack resistance of spherical metal molds can also be applied to numerical solutions of other problems involving various functional shells.

CONCLUSIONS

The problem of optimizing the design parameters of temperature seams in a spherical metal casting mold during the pouring of molten metal has been formulated and solved. The analysis of the SSS revealed structural features of the spherical metal casting mold design.

The presence of temperature seams on the surface in contact with the molten metal in the mold's inner part sig-

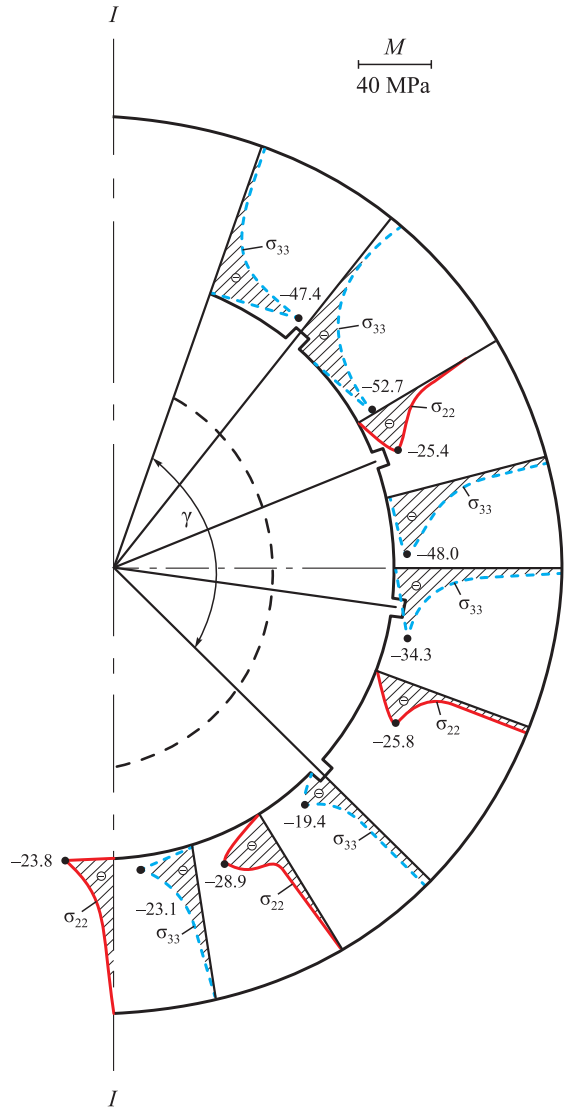

Fig. 6. Plots of calculated values of normal stresses σ_{22} and σ_{33} along the mold section at $\tau^* = 8.6$ s:
— – σ_{22}; - - - – σ_{33}

Рис. 6. Эпюры расчетных значений нормальных напряжений σ_{22} и σ_{33} по сечению формы при $\tau^* = 8{,}6$ с:
— – σ_{22}; - - - – σ_{33}

nificantly reduces the effect of thermal stresses that arise in the initial moments of casting cooling.

Rational regions for placing temperature seams in the meridional section of the mold and the corresponding stress values have been determined under the conditions of a min–max objective function, using the developed solution algorithm.

References / Список литературы

1. Evstigneev A.I., Dmitriev E.A., Odinokov V.I., Chernyshova D.V., Evstigneeva A.A., Ivankova E.P. On the crack resistance of a ceramic shell mold according to the smelted models when a spherical steel casting solidifies in it. *Foundry. Technologies and Equipment*. 2022;(9):17–21. (In Russ.).

   Евстигнеев А.И., Дмитриев Э.А., Одиноков В.И., Чернышова Д.В., Евстигнеева А.А., Иванкова Е.П. О трещиностойкости керамической оболочковой формы по выплавляемым моделям при затвердевании в ней шарообразной стальной отливки. *Литейное производство*. 2022;(9):17–21.
2. Mikhailov A.M., Bauman B.V., Blagov B.N. B.N., etc. Foundry Production: Textbook for metallurgical specialties of universities. Moscow: Mashinostroenie; 1987:256. (In Russ.).

   Литейное производство: Учебник для металлургических специальностей вузов / А.М. Михайлов, Б.В. Бауман, Б.Н. Благов и др. Москва: Машиностроение; 1987:256.
3. Golofaev A.N. Calculation of stress-strain state of coils by the finite element method. *Foundry. Technologies and Equipment*. 1983;(5):16. (In Russ.).

   Голофаев А.Н. Расчет напряженно-деформированного состояния кокилей методом конечных элементов. *Литейное производство*. 1983;(5):16.
4. Dembovskii V.V. Numerical modeling of castings forming in metal molds. *Foundry. Technologies and Equipment*. 1992;(6):31–32. (In Russ.).

   Дембовский В.В. Численное моделирование процессов формирования отливок в металлических формах. *Литейное производство*. 1992;(6):31–32.
5. Ogorodnikova O.M. Stress-strain state of metal in the effective crystallization interval. *Foundry. Technologies and Equipment*. 2012;(9):21–24. (In Russ.).

   Огородникова О.М. Напряженно-деформированное состояние металла в эффективном интервале кристаллизации. *Литейное производство*. 2012;(9):21–24.
6. Desnitskaya L.V., Desnitskii V.V., Matveev I.A. Consideration of the stress-strain state of crystallizing steel castings in their production technology. *Foundry. Technologies and Equipment*. 2019;(4):6–8. (In Russ.).

   Десницкая Л.В., Десницкий В.В., Матвеев И.А. Учет напряженно-деформированного состояния кристаллизующихся стальных отливок в технологии их производства. *Литейное производство*. 2019;(4):6–8.
7. Gamer U. On the elastic-plastic deformation of a sphere subjected to As spherically symmetrical temperature field. *Journal of Thermal Stresses*. 1988;11(3):159–173. https://doi.org/10.1080/01495738808961930
8. Kholdi M., Loghman A., Ashrafi H., Arefi M. Analysis of thick-walled spherical shells subjected to external pressure: Elastoplastic and residual stress analysis. *Proceedings of the Institution of Mechanical Engineers, Part L: Journal of Materials: Design and Applications*. 2019;234(1):146442071988295. https://doi.org/10.1177/1464420719882958
9. Güven U. On stress distributions in functionally graded isotropic spheres subjected to internal pressure. *Mechanics Research Communications*. 2001;28(3):277–281. https://doi.org/10.1016/s0093-6413(01)00174-4
10. Ootao Y., Ishihara M. Transient thermoelastic analysis for a multilayered hollow cylinder with piecewise power law nonhomogeneity due to asymmetric surface heating. *Acta Mechanica*. 2014;225(10):2903–2922. https://doi.org/10.1007/s00707-014-1204-3
11. Saiyan S.G., Paushkin A.G. Development and verification of the two-layer thick-walled spherical shell's finite element model under temperature and force exposure. *IOP Conference Series: Materials Science and Engineering*. 2020;913(3):032058. https://doi.org/10.1088/1757-899X/913/3/032058
12. Miller G.K. Stresses in a spherical pressure vessel undergoing creep and dimensional changes. *International Journal of Solids and Structures*. 1995;32(14):2077–2093. https://doi.org/10.1016/0020-7683(94)00197-5
13. Karami K., Abedi M., Zamani Nejad M., Lotfian M.H. Elastic analysis of heterogeneous thick-walled spherical pressure vessels with parabolic varying properties. *Frontiers of Mechanical Engineering*. 2012;7(4):433–438. https://doi.org/10.1007/s11465-012-0336-1
14. Abdelsalam O.R. Design optimization for a three-layers shrink-fitted pressure vessel exposed to very high pressure. *IOP Conference Series: Materials Science and Engineering*. 2019;610:012077. https://doi.org/10.1088/1757-899x/610/1/012077
15. Vitucci G., Mishuris G. Analysis of residual stresses in thermoelastic multilayer cylinders. *Journal of the European Ceramic Society*. 2016;36(9):2411–2417. https://doi.org/10.1016/j.jeurceramsoc.2015.12.003
16. Odinokov V.I., Dmitriev E.A., Evstigneev A.I., Namokonov A.N., Chernyshova D.V., Evstigneeva A.A. Modeling the stress-strain state and optimizing the angle of contact of a spherical shell mold by a support filler. *Journal of Applied Mechanics and Technical Physics*. 2025;(1):189–196. (In Russ.). https://doi.org/10.15372/PMTF202415455

    Одиноков В.И., Дмитриев Э.А., Евстигнеев А.И., Намоконов А.Н., Чернышова Д.В., Евстигнеева А.А. Моделирование напряженно-деформированного состояния и оптимизация угла охвата сферической оболочковой формы опорным наполнителем. *Прикладная механика и техническая физика*. 2025;(1):189–196. https://doi.org/10.15372/PMTF202415455
17. Odinokov V.I., Kaplunov B.G., Peskov A.V., Bakov A.V. Mathematical Modeling of Complex Technological Processes. Moscow: Nauka; 2008:178. (In Russ.).

    Математическое моделирование сложных технологических процессов / В.И. Одиноков, Б.Г. Каплунов, А.В. Песков, А.В. Баков. Москва: Наука; 2008:178.
18. Alekseev G.V., Levin V.A., Tereshko D.A. Simulation and optimization in the problems of design of spherical layered

thermal shells. *Journal of Applied Mechanics and Technical Physics*. 2019;60(2):323–331.
https://doi.org/10.15372/PMTF20190213

Алексеев Г.В., Левин В.А., Терешко Д.А. Моделирование и оптимизация в задачах проектирования сферических слоистых тепловых оболочек. *Прикладная механика и техническая физика*. 2019;60(2):158–168.
https://doi.org/10.15372/PMTF20190213

19. Zhang Y.C., Jin C.W., Pang M. Plastic instability for a plastic orthotropic spherical pressure vessel under internal impulsive loading. *Journal of Applied Mechanics and Technical Physics*. 2022;63(2):343–346. (In Russ.).
https://doi.org/10.1134/S0021894422020183

Чзан Ю., Цзинь Ч., Пан М. Пластическая неустойчивость сферического сосуда высокого давления из ортотропного материала, нагруженного внутренним импульсным давлением. *Прикладная механика и техническая физика*. 2022;63(2):192–196.
https://doi.org/10.15372/PMTF20220218

20. Alekseev G.V., Soboleva O.V., Tereshko D.A. Identification problems for a steady-state model of mass transfer. *Journal of Applied Mechanics and Technical Physics*. 2008; 49(4):537–547. https://doi.org/10.1007/s10808-008-0071-x

Алексеев Г.В., Соболева О.В., Терешко Д.А. Задачи идентификации для стационарной модели массопереноса. *Прикладная механика и техническая физика*. 2008;49(4(290)):24–35.

21. Evstigneev A.I., Dmitriev E.A., Chernyshova D.V., Odinokov V.I., Evstigneeva A.A., Ivankova E.P. Modeling of external force action on a shell mold for pouring steel. *Matematicheskoe modelirovanie*. 2022;34(5):61–72. (In Russ.). https://doi.org/10.20948/mm-2022-05-04

Евстигнеев А.И., Дмитриев Э.А., Чернышова Д.В., Одиноков В.И., Евстигнеева А.А., Иванкова Е.П. Моделирование внешнего силового воздействия на стойкость оболочковой формы при заливке в нее стали. *Математическое моделирование*. 2022;34(5):61–72.
https://doi.org/10.20948/mm-2022-05-04

22. Evstigneev A.I, Odinokov V.I., Dmitriev E.A., Sviridov A.V., Ivankova E.P. The influence of external heat exposure on the stress state of shell forms by smelting models. *Matematicheskoe modelirovanie*. 2021;33(1):63–76. (In Russ.).
https://doi.org/10.20948/mm-2021-01-05

Евстигнеев А.И., Одиноков В.И., Дмитриев Э.А., Свиридов А.В., Иванкова Е.П. Влияние внешнего теплового воздействия на напряженное состояние оболочковых форм по выплавляемым моделям. *Математическое моделирование*. 2021;33(1):63–76.
https://doi.org/10.20948/mm-2021-01-05

Information about the Authors / Сведения об авторах

Aleksei I. Evstigneev, *Dr. Sci. (Eng.), Prof., Chief Researcher of the Department of Research Activities*, Komsomolsk-on-Amur State University
ORCID: 0000-0002-9594-4068
E-mail: diss@knastu.ru

Dar'ya V. Chernyshova, *Postgraduate of the Chair of Aircraft Engineering*, Komsomolsk-on-Amur State University
ORCID: 0000-0001-5142-2455
E-mail: daracernysova744@gmail.com

Valerii I. Odinokov, *Dr. Sci. (Eng.), Prof., Chief Researcher of the Department of Research Activities*, Komsomolsk-on-Amur State University
ORCID: 0000-0003-0200-1675
E-mail: 79122718858@yandex.ru

Eduard A. Dmitriev, *Dr. Sci. (Eng.), Assist. Prof., Rector*, Komsomolsk-on-Amur State University
ORCID: 0000-0001-8023-316X
E-mail: rector@knastu.ru

Anna A. Evstigneeva, *MA Student of the Chair "Applied Mathematics"*, Komsomolsk-on-Amur State University
ORCID: 0000-0003-0667-2468
E-mail: annka.ewstic@mail.ru

Yuliya B. Koloshenko, *Senior Lecturer of the Chair of Aircraft Engineering*, Komsomolsk-on-Amur State University
ORCID: 0009-0005-4480-075X
E-mail: koloschenko2011@yandex.ru

Dmitrii A. Potyanikhin, *Cand. Sci. (Phys.-Math.), Assist. Prof. of the Chair of Aircraft Engineering*, Komsomolsk-on-Amur State University
ORCID: 0000-0001-6113-6073
E-mail: potyanikhin@mail.ru

Алексей Иванович Евстигнеев, *д.т.н., профессор, главный научный сотрудник Управления научно-исследовательской деятельностью*, Комсомольский-на-Амуре государственный университет
ORCID: 0000-0002-9594-4068
E-mail: diss@knastu.ru

Дарья Витальевна Чернышова, *аспирант кафедры «Авиастроение»*, Комсомольский-на-Амуре государственный университет
ORCID: 0000-0001-5142-2455
E-mail: daracernysova744@gmail.com

Валерий Иванович Одиноков, *д.т.н., профессор, главный научный сотрудник Управления научно-исследовательской деятельностью*, Комсомольский-на-Амуре государственный университет
ORCID: 0000-0003-0200-1675
E-mail: 79122718858@yandex.ru

Эдуард Анатольевич Дмитриев, *д.т.н., доцент, ректор*, Комсомольский-на-Амуре государственный университет
ORCID: 0000-0001-8023-316X
E-mail: rector@knastu.ru

Анна Алексеевна Евстигнеева, *магистрант кафедры «Прикладная математика»*, Комсомольский-на-Амуре государственный университет
ORCID: 0000-0003-0667-2468
E-mail: annka.ewstic@mail.ru

Юлия Борисовна Колошенко, *старший преподаватель кафедры «Авиастроение»*, Комсомольский-на-Амуре государственный университет
ORCID: 0009-0005-4480-075X
E-mail: koloschenko2011@yandex.ru

Дмитрий Андреевич Потянихин, *к.ф.-м.н., доцент кафедры «Авиастроение»*, Комсомольский-на-Амуре государственный университет
ORCID: 0000-0001-6113-6073
E-mail: potyanikhin@mail.ru

Contribution of the Authors

A. I. Evstigneev – conceptualization, setting goals and objectives of research, analysis of research results, writing the text.

D. V. Chernyshova – carrying out and processing calculations, preparing references, processing graphic material.
V. I. Odinokov – scientific guidance, analysis of research results, editing and correction of the final version of the article.

E. A. Dmitriev – carrying out calculations and their analysis, preparation and correction of the text.
A. A. Evstigneeva – carrying out calculations, preparation of the text and graphic material.
Yu. B. Koloshenko – carrying out and processing calculations, formulation of a numerical scheme and calculation algorithm.
D. A. Potyanikhin – carrying out and processing calculations.

Вклад авторов

А. И. Евстигнеев – формирование концепции статьи, определение цели и задачи исследования, анализ результатов исследования, подготовка текста.
Д. В. Чернышова – проведение и обработка расчетов, подготовка библиографического списка, обработка графического материала.
В. И. Одиноков – научное руководство, анализ результатов исследований, редактирование и корректировка финальной версии статьи.
Э. А. Дмитриев – проведение расчетов, их анализ, подготовка и корректировка текста.
А. А. Евстигнеева – проведение расчетов, подготовка текстового и графического материала.
Ю. Б. Колошенко – проведение и обработка расчетов, формулирование численной схемы и алгоритма расчетов.
Д. А. Потянихин – проведение расчетов и их обработка.

Received 06.11.2024
Revised 27.06.2025
Accepted 27.06.2025

Поступила в редакцию 06.11.2024
После доработки 27.06.2025
Принята к публикации 27.06.2025

Innovation in metallurgical industrial and laboratory equipment, technologies and materials / **Инновации в металлургическом промышленном и лабораторном оборудовании, технологиях и материалах**

UDC 621.793:621.783.24
DOI 10.17073/0368-0797-2025-4-383-394

Original article
Оригинальная статья

Metallization of ore-coal briquettes in an annular furnace heated by generator gas

B. P. Kulikov, Yu. I. Storozhev, A. S. Potapenko

Siberian Federal University (79 Svobodnyi Ave., Krasnoyarsk 660041, Russian Federation)

albin1941@mail.ru

Abstract. The paper considers the features of producing granular pig iron using an annular furnace with a rotating hearth during implementation of ITmk3 technology (*Ironmaking Technology Mark Three*). The design of a coal gasifier with a synthesized gas purification system and the cross-section of an annular furnace are shown. The article briefly describes the process of industrial production of granular high-quality pig iron. The prospects of using the technology in question on the territory of the Russian Federation were assessed. At the first stage of research on the metallization of iron-ore concentrate (IOC) with coal, the thermogravimetric method of a complete factor experiment was used to determine the optimal metallization conditions. In the experiments, the ratio of IOC was varied: coal, size of coal, lime additives as a percentage of the amount (IOC + coal). As a result of thermogravimetric analysis, the authors obtained the curves of changes in mass of the samples, composition and amount of released gas when the heating temperature changed during sintering of IOC with coal and lime. At the second stage, a laboratory chamber furnace with a portable hearth, heated by generator gas from coal, was developed to test the ITmk3 technology. Ore-coal briquettes were made with a ratio of IOC, coal, bentonite 80:20:5 and heat-treated in a chamber furnace with heating by generator gas from a coal gasifier. Iron-ore concentrate from the Korshunovsky MPP and Kasyanovsky coal from the Cheremkhovsky deposit were used as experimental raw materials. Based on laboratory studies, the authors determined the temperature-time firing mode of ore-coal briquettes, which ensures a high degree of metallization of iron-ore materials of 80 – 87 % when firing briquettes in the temperature range of 1080 – 1424 °C for 40 min. The yield of briquettes after drying and firing was determined to be 66.45 %. The mechanism of solid-phase reduction of iron-ore materials in annular furnaces with a rotating hearth and liquid-phase separation of reduction products is considered. The composition of the gases released during calcination of ore and coal briquettes was determined.

Keywords: metallization, briquettes, annular furnace, granular pig iron, generator gas, rotating hearth, heat exchange, gasifier

For citation: Kulikov B.P., Storozhev Yu.I., Potapenko A.S. Metallization of ore-coal briquettes in an annular furnace heated by generator gas. *Izvestiya. Ferrous Metallurgy*. 2025;68(4):383–394. https://doi.org/10.17073/0368-0797-2025-4-383-394

Металлизация рудно-угольных брикетов в кольцевой печи, отапливаемой генераторным газом

Б. П. Куликов, Ю. И. Сторожев, А. С. Потапенко

Сибирский федеральный университет (Россия, 660041, Красноярск, Свободный пр., 79)

albin1941@mail.ru

Аннотация. Рассмотрены особенности процесса получения гранулированного чугуна с применением кольцевой печи с вращающимся подом при реализации технологии ITmk3 (*Ironmaking Technology Mark Three*). Авторы показывают конструкцию угольного газификатора с системой очистки синтезируемого газа и поперечное сечение кольцевой печи. Статья кратко описывает процесс промышленного получения гранулированного высококачественного чугуна. Проведена оценка перспективы использования рассматриваемой технологии на территории Российской Федерации. На первом этапе исследований металлизации железорудного концентрата (ЖРК) углем применен термогравиметрический метод полного факторного эксперимента по определению оптимальных условий металлизации. В экспериментах варьировали соотношение ЖРК: уголь, крупность угля, добавки извести в процентах от суммы (ЖРК + уголь). В результате термогравиметрического анализа авторы получили кривые изменения массы образцов, состава и количества выделившегося газа при изменении температуры нагрева в процессе спекания ЖРК с углем и известью. На втором этапе для отработки технологии ITmk3 разработана лабораторная камерная печь с выдвижным подом, отапливаемая генераторным газом из каменного угля. Рудно-угольные брикеты были изготовлены с соотношением ЖРК, уголь, бентонит 80:20:5 и термообработаны в камерной печи с отоплением генераторным газом из угольного газификатора. В качестве

опытного сырья были использованы железорудный концентрат Коршуновского горно-обогатительного комбината и Касьяновский каменный уголь Черемховского месторождения. На основе лабораторных исследований был определен температурно-временной режим обжига рудно-угольных брикетов, обеспечивающий высокую степень металлизации железорудных материалов (80 – 87 %) при обжиге брикетов в диапазоне температур 1080 – 1424 °С в течение 40 мин. Выход брикетов после сушки и обжига составил 66,45 %. Авторы изучили механизмы твердофазного восстановления железорудных материалов в кольцевых печах с вращающимся подом и жидкофазного разделения продуктов восстановления, а также определили состав выделившихся газов при прокаливании рудно-угольных брикетов.

Ключевые слова: металлизация, брикеты, кольцевая печь, гранулированный чугун, генераторный газ, вращающийся под, теплообмен, угольный газификатор

Для цитирования: Куликов Б.П., Сторожев Ю.И., Потапенко А.С. Металлизация рудно-угольных брикетов в кольцевой печи, отапливаемой генераторным газом. *Известия вузов. Черная металлургия*. 2025;68(4):383–394. https://doi.org/10.17073/0368-0797-2025-4-383-394

Introduction

Over the past 10 years, the production of direct reduced iron (DRI) has increased by 18 % globally and by 66 % in Russia, indicating rapid development in this sector [1]. The widespread adoption of the direct reduction process was first observed in the 1980s, when natural gas began to be used extensively as a reductant in the mining and metallurgical industry. In addition to natural gas, the use of coal gasification products also proved feasible in the direct reduction of iron. Neither method requires the use of expensive coke [2].

According to metallurgical thermal engineers, the most advantageous option is to produce partially metallized iron-ore materials with a metallization degree of 30 – 50 %, which are used in blast furnace production. Highly metallized iron-ore products with a metallization degree of 85 – 95 % are used for remelting in steelmaking units to obtain high-quality steel [2]. The method of direct reduction of iron-ore materials is particularly suitable for regions that lack natural gas reserves but possess abundant coal deposits.

In the 2000s, more than a dozen inventions were developed in Russia related to the production of granular pig iron using annular furnaces with a rotating hearth, incorporating elements of well-known processes such as FASTMET and ITmk3. One invention [3] describes a method for producing granular pig iron by dosing the components of the iron-ore burden to achieve CaO/MgO and SiO_2/Al_2O_3 ratios within the ranges of 2 – 5 and 4 – 6, respectively, ensuring that the primary slag melting temperature does not exceed 1400 °C. Several other patents [4 – 6] focus on the design features of annular furnaces that allow for optimization of heat exchange processes. In particular, patent [6] describes air-cooled suspended screens with vertical movement capability in the briquette loading and unloading zones, and the loading zone is additionally equipped with a device for feeding protective material onto the hearth.

For Siberian conditions, developments using coal gasifiers [7; 8] are especially attractive, as they enable annular furnaces to operate on gasified fuel in the absence of natural gas. Based on these inventions, a process line was developed for producing a metallized product in an annular furnace with a rotating hearth, allowing for maximum utilization of the heat from exhaust gases [9; 10].

One example of such implementation is the construction of a plant for producing granular pig iron in Cheremkhovo, Irkutsk Region, using ITmk3 technology. The site was selected based on the following factors:

– proximity to one of the main raw material sources – coal (Cheremkhovsky coal basin);

– relatively close location of other key raw material source – iron-ore concentrate (Korshunovsky MPP, Zheleznogorsk, Irkutsk Region);

– a well-developed regional transportation network, including both rail (Trans-Siberian Railway) and road access (federal highway).

The project investor is NPO Khimiko-Metallurgicheskaya Kompaniya LLC. The plant's design capacity is 100,000 tons per year of granular pig iron. This production method, unique for Russia, is based on the reduction firing of briquetted mixture (iron-ore concentrate (IOC) + coal + dolomite) at 1350 – 1450 °C in an annular hearth furnace heated by generator gas synthesized from coal. The production complex includes the following key facilities:

– IOC unloading section with raw material silos;

– open coal yard and coal preparation section;

– coal gasification section for generator gas production;

– section for preparing the mixture (IOC + coal + dolomite), briquetting, and drying the briquettes;

– ore–coal briquette metallization section;

– section for processing and separation of metallization products;

– closed-loop water supply section;

– gas cleaning section.

The main process units of the plant under construction include:

– two SM89 coal gasifiers manufactured in China, each with an inner diameter of 3.6 m, a cross-sectional area of 10.17 m^2, and a height of 12.5 m, equipped with a generator gas purification system (Fig. 1);

– annular furnace with a rotating hearth (Fig. 2). The outer diameter of the furnace is 20.99 m, the inner diameter is 15.6 m, and the hearth width is 2.69 m. Fourteen pairs of MS568 tuyeres are installed in the inner and outer walls of the furnace, positioned directly opposite each other so that the flame jets from opposing tuyeres meet and dissipate in the center of the furnace. The hearth rotation speed is variable: the time for one full revolution of the hearth can range from 27 to 45 min.

Below is a brief description of the technological process for producing granular pig iron at the plant currently under construction. Raw materials are delivered to the ore yard by rail and truck. Coal and dolomite are transported by road, while iron-ore concentrate is delivered in open rail cars.

After crushing, the coal is screened on an inertial screen with 12 mm mesh openings. This separates it into two fractions: the oversize fraction, with particle sizes over 12 mm, is directed to the coal gasifier for the production of fuel synthesis gas. The undersize fraction, with particle sizes under 12 mm, is sent to a mill for further grinding to the particle size required for produc-

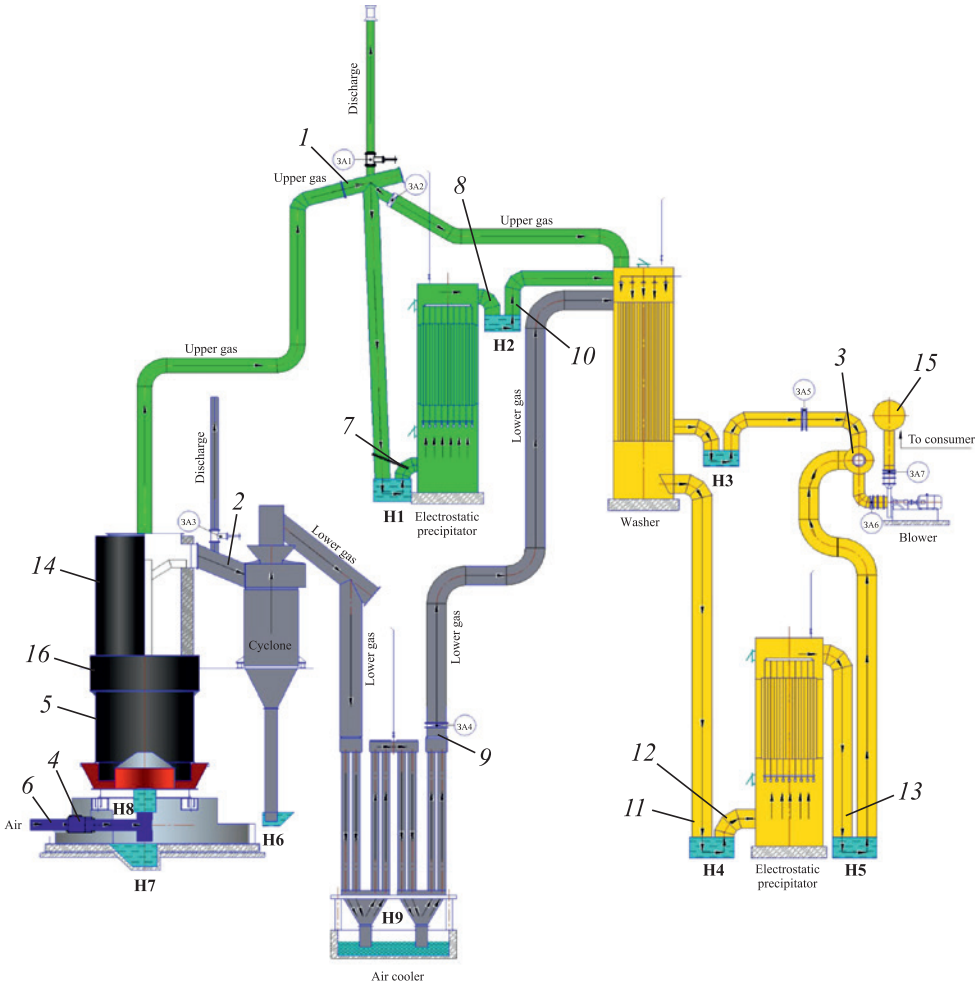

Fig. 1. Gasifier with generator synthesis gas purification system:
1 – upper gas duct; *2* – lower gas duct; *3* – low-pressure gas collector; *4* – mixing box (gasification agent production);
5 – gasifier caisson; *6* – air duct; *7* – upper gas inlet into electrostatic precipitator No. 1 from hydraulic seal 1;
8 – purified upper gas outlet from electrostatic precipitator No. 1 into hydraulic seal H2; *9* – lower gas duct from the air cooler to the washer;
10 – upper gas duct from hydraulic seal H2 to the washer; *11* – mixed upper and lower gas duct;
12 – mixed gas inlet from hydraulic seal H4 to electrostatic precipitator No. 2; *13* – mixed purified gas duct to the annular metallization furnace;
14 – valves adjustment of lower gas; *15* – collector of increased gas pressure; *16* – sizing holes of gasifier; H1 – H9 – hydraulic seals

Рис. 1. Газификатор с системой очистки генераторного синтез газа:
1 – газоход верхнего газа; *2* – газоход нижнего газа; *3* – коллектор низкого давления газа;
4 – коробка смешивания (получение агента газификации); *5* – кессон газификатора; *6* – воздуховод;
7 – ввод верхнего газа в электрофильтр *1* из гидрозатвора H1; *8* – выход очищенного верхнего газа из электрофильтра 1 в гидрозатвор H2;
9 – газоход нижнего газа из воздушного охладителя в омыватель; *10* – газоход верхнего газа из гидрозатвора H2 в омыватель;
11 – газоход смешанного верхнего и нижнего газов; *12* – ввод смешанного газа из гидрозатвора H4 в электрофильтр *2*;
13 – газоход смешанного очищенного газа к кольцевой печи металлизации; *14* – задвижки регулировки нижнего газа;
15 – коллектор повышенного давления газа; *16* – шуровочные отверстия газификатора; H1 – H9 – гидрозатворы

a

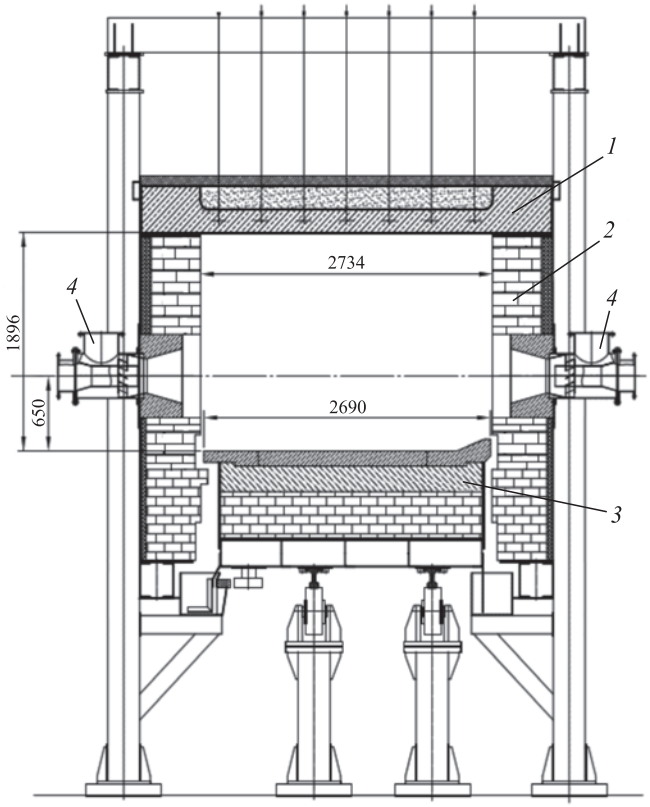

b

Fig. 2. Annular furnace for production of granular pig iron:
a – appearance of the furnace under construction;
b – cross section; *1* – suspended arch; *2* – wall lining;
3 – rotating hearth; *4* – tuyers

Рис. 2. Кольцевая печь для производства гранулированного чугуна:
a – внешний вид строящейся печи;
b – поперечный разрез; *1* – подвесной свод;
2 – футеровка стен; *3* – вращающийся под;
4 – горелочные устройства

ing ore–coal briquettes. Briquettes with the composition of 80 % IOC + 20 % coal + 5 % dolomite are produced using a roller press. The maximum throughput of the press is 14 ± 0.5 tons per hour of ore–coal briquettes. To remove excess moisture and preheat the briquettes, they are fed into a dryer, where the drying agent is air heated in a recuperator to 350 – 400 °C using exhaust gases from the annular furnace.

Metallization of the iron-ore materials within ore–coal briquettes is carried out in an annular furnace with a rotating hearth. The furnace is divided into four technological sections:

– the coal bed loading section, where the “bed” serves as a protective layer for the refractory hearth lining and as a base for laying the briquettes;

– the briquette laying section, where briquettes are placed on the hearth;

– the reduction firing section, where the briquettes are metallized;

– the product discharge section, where the metallized product is removed from the hearth.

The first step involves loading the hearth with a coal “bed” using an apron feeder. The bed is evenly distributed over the hearth in a 3 – 5 cm thick layer. After the bed is in place, pre-dried and preheated ore–coal briquettes (heated to ~250 °C on a conveyor grate) are laid evenly on top of the bed in 1 – 2 layers.

As the hearth rotates, the briquette–bed “layer” is carried into the reduction firing section. The fuel synthesis gas, produced in the gasifier and preheated to 200 – 250 °C, is automatically distributed to the tuyers through a network of thermally insulated gas ducts, ensuring the required temperature conditions in the metallization zone. To improve combustion efficiency and reduce energy consumption, the air supplied to the tuyers is preheated to 400 – 450 °C in recuperators.

From the reduction firing zone, the metallized product enters the cooling and discharge zone, where it is removed from the hearth using water-cooled screw conveyors and fed through a water-cooled chute into a drag-type cooler. The cooled product is then transferred to a rotary screen, where the coal “bed” is first separated. The remaining agglomerated metallization product undergoes mechanical treatment, resulting in its breakdown into slag and granular pig iron. Next, the mechanical mixture of slag and pig iron is transported by conveyor to a magnetic separator, where the magnetic fraction is recovered – the target product of the process: direct reduced iron in the form of granules of pig iron.

Implementation of this innovative project began with the purchase and installation of the main and auxiliary equipment, and the construction of infrastructure. Alongside the installation of the annular furnace, coal gasifiers, and other systems, laboratory-scale studies were conducted on the metallization of ore–coal briquettes. The aim of these studies was to optimize briquette composition and refine the process of producing granular pig iron using the ITmk3 technology. The results of these studies are presented in this article.

Experimental studies and discussion of the results

One of the advantages of metallizing ore–coal materials in an annular furnace using ITmk3 technology is the formation of pig iron granules coated with a slag shell. This feature facilitates the separation of pig iron granules from the main slag mass [11 – 14] and reduces the cost of subsequent processing. An important requirement of ITmk3 technology is the use of iron ore concentrates with a total Fe content exceeding 60 %, as well as achieving a carbon content in the alloy within the range of 2.5 – 4.5 % after complete iron reduction. If the residual carbon content in the alloy is below 1.5 %, the melting point of the iron does not decrease significantly, and in this case, the furnace temperature must reach a maximum of around 1450 – 1550 °C. The guaranteed specifications for the final product (granular pig iron), according to the technology, are as follows (wt. %): >96 Fe; 2.0 – 4.0 C; 0.2 Si; 0.05 P; 0.04 – 0.08 S [15 – 20]. However, the processes described in those publications are designed for high-calorific fuels, particularly natural gas.

The first stage of this study – aimed at determining the optimal conditions for metallizing IOC with coal – was carried out using thermogravimetry and the full factorial design method on a STA 449 Jupiter synchronous thermal analysis system. Samples were prepared according to the matrix of a full three-factor experimental design (Table 1), with the following control factors:

– X_1 – IOC-to-coal ratio (–1 → (70:30) % = 2.333; +1 → (80:20) % = 4).

– X_2 – coal particle size, μm (–1 → –50; +1 → –315).

– X_3 – lime additives, wt. % of the total (IOC + coal) –1 → 0; +1 → 5.

Iron recovery into the alloy was used as the optimization parameter.

The experiments were conducted using sintering-grade iron ore concentrate from the Korshunovsky MPP with the following composition (wt. %, dry basis): 62.6 Fe_2O_3; 24.0 FeO; 3.95 SiO_2; 2.654 Al_2O_3; 1.9 CaO; 4.0 MgO; 0.13 MnO; 0.255 TiO_2; 0.04 SO_2; 0.37 P_2O_5; 5.8 H_2O; and 1.65 loss on ignition (LOI). Kasyanovsky coal from the Cheremkhovsky deposit was used as the reductant. Its composition (wt. %) was as follows: 77.3 total carbon (C^t); 1.2 total sulfur (S^t); 16.5 ash (A^s); 11.5 moisture (as received); 13.7 total oxygen (O^t); 5.6 total hydrogen (H^t); 1.1 total nitrogen (N^t); and 45.6 volatile matter (V^t). The lower heating value of the coal was 23,028.5 kJ/kg. The ash fusion temperature ranged from 1310 to 1390 °C. The ash composition (wt. %) included: 67.1 SiO_2; 19.2 Al_2O_3; 2.5 Fe_2O; 2.2 CaO; 1.6 MgO; 0.7 K_2O; 0.1 TiO_2; 0.1 Na_2O; 4.4 SO_3; 0.01 MnO_2.

The prepared mixtures were pressed using a laboratory press at a pressure of 80 – 100 kg/cm^2 to form briquettes measuring 8 mm in diameter and approximately 5 mm in height. The samples were heated from 40 to 1400 °C at a rate of 30 °C/min in an argon atmosphere. Sample masses ranged from 513 to 593 mg. Tests were carried out in a corundum crucible shaped as a shallow dish. During the experiments, the qualitative and quantitative composition of the gases released during thermolysis was monitored using an Aelos quadrupole mass spectrometer with an electron impact energy of 70 eV. The degree of iron metallization was calculated based on the composition of the released gases.

Eight experiments were conducted following a full three-factor experimental design. The sintering derivatograms of the iron ore concentrate, coal, and lime – along with the corresponding gas release profiles – were recorded in 24 figures (three per sample). Due to the overall similarity of the derivatograms, Fig. 3 presents the results of gas release analysis for representative Sample *6*: $X_1 = +1$; $X_2 = -1$; $X_3 = +1$, which contained 80 % iron ore concentrate, 20 % coal, and 5 % lime (in excess of 100 %). The amounts of CO, CO_2, and H_2O were determined from the derivatograms based on the area of the gas evolution effects, by comparison with those obtained for reference samples. The degree of IOC metallization was calculated based on the following reactions:

$$Fe_3O_4 + 4C \rightarrow 3Fe + 4CO; \quad (1)$$

$$Fe_3O_4 + 2C \rightarrow 3Fe + 2CO_2; \quad (2)$$

$$Fe_3O_4 + 4H_2 \rightarrow 3Fe + 4H_2O. \quad (3)$$

The temperature range up to approximately 550 – 600 °C – corresponding to the first sharp mass

Table 1. **Levels of control factors and variation intervals**

Таблица 1. **Уровни факторов управления и интервалы варьирования**

Factor	Factor levels			Variation intervals
	– 1	0	+ 1	
X_1 – IOC-to-coal ratio	2.333	3.167	4.000	0.833
X_2 – coal particle size, μm	–50.0	–132.5	–315.0	82.5
X_3 – lime additives, wt. % of the total (IOC + coal)	0	2.5	5.0	2.5

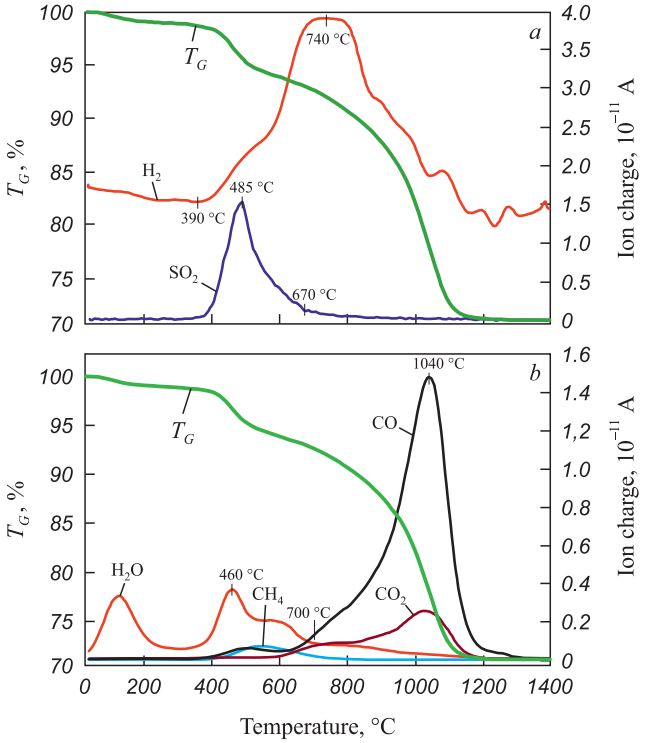

Fig. 3. Derivatogram of IOC reduction by coal with composition of gas products of thermolysis and interaction (using the example of sample *б*); T_G – curve of mass loss by the sample

Рис. 3. Дериватограмма восстановления ЖРК углем с составом газовых продуктов термолиза и взаимодействия (на примере образца *б*); T_G – кривая потери массы образцом

loss – was excluded from the metallization calculations, as this process is associated with coal decomposition without interaction with the IOC. This was confirmed by the derivatogram of a separate sample of Cheremkhovsky coal (not shown in the article). Upon heating, the samples released CO, CO_2, H_2O, and methane. The CO-to-CO_2 ratio in the gas phase is indicative of the metamorphic grade of the coal. The calculations also accounted for the amount of water formed via reaction (3) within the 800 – 1000 °C temperature range.

Thermogravimetric analysis of the eight mixtures (IOC + coal + lime) revealed that gas release from the samples occurs in three distinct temperature intervals, °C: 40 – 210; 210 – 685; and 685 – 1400. In the first zone (40 – 210 °C), the release of hygroscopic moisture is observed, resulting in a mass loss ranging from 0.61 to 1.29 %.

In the second temperature interval (210 – 685 °C), the release of volatile compounds was observed. During this stage, sulfur was released predominantly in the form of SO_2, along with most of the CH_4, H_2, and H_2O. The associated mass loss ranged from 5.46 to 8.6 %.

In the third zone (685 – 1400 °C), chemical interactions take place, leading predominantly to the formation of CO and CO_2. Mass loss in this range varies between 21.22 and 29.7 %. The mass of solid residue after firing the briquettes ranges from 60.64 to 72.48 %.

Table 2 presents the component and quantitative composition of the gas phase, calculated based on thermogravimetric data and used for computing the degree of iron metallization according to the experimental design matrix.

Table 3 presents the results of iron metallization degree calculations based on reactions (1) – (3).

Based on the obtained data, the coefficients were calculated and a linear equation was derived to describe the dependence of iron recovery from IOC (Y_1) on the IOC-to-coal ratio (X_1), coal particle size (X_2), and lime additives (X_3) expressed in coded coordinates.

$$Y_1 = 66.83 - 8.82X_1 - 4.16X_2 + \\ + 3.78X_3 + 1.77X_1X_2 + 0.84X_1X_3 + \\ + 0.0037X_2X_3 + 1.29X_1X_2X_3. \quad (4)$$

Statistical evaluation of the coefficients in the derived equation showed that, at a 95 % confidence level, the coefficients for X_1, X_2, X_3 and the interaction term X_1X_2, are statistically significant. As a result, Equation (4) is written in the reduced form as follows

$$Y_1 = 66.83 - 8.82X_1 - 4.16X_2 + 3.78X_3 + 1.77X_1X_2. \quad (5)$$

In actual (uncoded) values, Equation (5) takes the form

$$Y_1 = 6.83 - 8.82\frac{X_1 - 3.167}{0.833} - 4.16\frac{X_2 - 132.5}{82.5} + \\ + 3.73\frac{X_3 - 2.5}{2.5} + 1.77\frac{X_1 - 3.167}{0.833}\frac{X_2 - 132.5}{82.5}, \quad (6)$$

Table 2. **Composition of the gas phase released during sintering of IOC with coal and lime**

Таблица 2. **Состав газовой фазы, выделившейся при спекании ЖРК с углем и известью**

Component, mg	Sample (experiment) No.							
	1	*2*	*3*	*4*	*5*	*6*	*7*	*8*
CO	105.78	59.72	66.12	66.61	74.30	67.89	64.45	55.40
CO_2	2.60	26.86	28.89	35.89	35.78	31.70	35.69	26.00
$H_2O_{(800-1000\ °C)}$	0.61	1.75	2.38	1.28	1.91	0.39	1.44	1.40

Table 3. **Results of calculating the degree of samples metallization by reactions (1) – (3) of magnetite reduction**

Таблица 3. **Результаты расчета степени металлизации образцов по реакциям (1) – (3) восстановления магнетита**

Parameter	Sample (experiment) No.							
	1	*2*	*3*	*4*	*5*	*6*	*7*	*8*
Fe (1), mg	201.95	89.58	99.18	99.92	111.46	101.84	96.67	83.10
Fe (2), mg	4.97	51.28	55.15	68.52	68.31	60.52	68.14	49.64
Fe (3), mg	1.42	4.08	5.55	2.99	4.46	0.91	3.36	3.27
Total Fe in sample, mg	242.79	253.97	234.90	278.50	238.17	256.17	235.65	273.62
Fe recovery, %	85.81	57.07	68.06	61.55	77.35	63.73	71.36	49.70
N o t e: Fe (1) – amount of reduced iron with the formation of CO; Fe (2) – amount of reduced iron with the formation of CO_2; Fe (3) – amount of reduced iron with the formation of H_2O. The average iron content in IOC from the Korshunovsky MPP is 62.6 %.								

where the numerators represent the zero values of the factor levels, and the denominators correspond to the variation intervals of the respective factors as listed in Table 1.

Based on the conducted thermogravimetric analysis of the samples, the following conclusions were drawn.

• The most significant factor affecting the degree of IOC metallization is the IOC-to-coal ratio; the next most influential factor is coal particle size.

• An increase in coal particle size (from –50 to –315 μm) raises the final temperature of the iron reduction process from 1255 to 1367 °C.

• The addition of lime intensifies the reduction process and shifts it to a lower temperature range (from 1367 to 1300 °C).

• The obtained results indicate that the metallization reaction proceeds in two stages, as evidenced by at least two sharp changes in the rate of mass loss (DTG), each corresponding to CO release. This fact can be interpreted as the direct reduction of iron oxides (the primary stage). The second stage involves the aggregation of molten iron droplets and the expulsion of gas from capillaries and inter-droplet spaces. The first stage begins at 640 °C with an increasing rate of mass loss, reaching up to 990 °C. This is followed by a stabilization and subsequent decrease in the rate of mass loss until about 1180 – 1250 °C. The second reduction stage then begins and completes within the temperature range of 1250 – 1360 °C.

• The relatively low degree of iron metallization observed in this stage of the study (50 – 85 %) can be attributed to the following factors:

– the analysis and calculations were based solely on the gas phase;

– metallization occurred in an argon atmosphere;

– the Cheremkhovsky coal used in the experiments had a high degree of metamorphism;

– partial iron metallization may have occurred in the temperature range up to ~550 – 600 °C (corresponding to the first major mass-loss event), but this was not accounted for in the calculations;

• For effective reduction of iron oxides, it is advisable to use coal with a low volatile matter content and a high carbon content in briquette compositions.

To determine the operating conditions for the pig iron plant under construction, the next stage of the study was carried out, involving the preparation and firing of briquettes composed of iron ore concentrate, coal, and lime under laboratory conditions. A laboratory furnace with a portable hearth (Fig. 4) was designed for this purpose. The furnace is heated using gasified bituminous coal. Its internal dimensions are 500×500 mm in cross section and 650 mm in length. The furnace is equipped with a water-cooled flue gas duct and a forced gas extraction system. A platinum–platinum-rhodium thermocouple was installed to measure the furnace temperature. Before loading the briquettes, the furnace was preheated for 1.5 h to a temperature of approximately 1100 °C.

Sintering-grade iron ore concentrate from the Korshunovsky MPP and Kasyanovsky bituminous coal from the Cheremkhovsky deposit were used to produce the briquettes. The furnace was heated using steam–air generator gas with the following composition (wt. %): 5.0 CO_2; 0.2 O_2; 27.0 CO; 13.0 H_2; 2.7 CH_4; 0.3 C_2H_4; 51.8 N_2. The lower heating value of the generator gas was 5976 kJ/m^3.

The briquettes, pressed to a height and diameter of approximately 22 mm, were placed into ceramic pallets on a coke bed and fired on the portable hearth of the furnace (Fig. 5). The composition, mass before and after firing, and firing conditions are summarized in Table 4.

The briquettes were heated to a temperature of 1424 °C (Fig. 6). The initial temperature drop in the furnace to 1078 °C was due to the induction heating period after

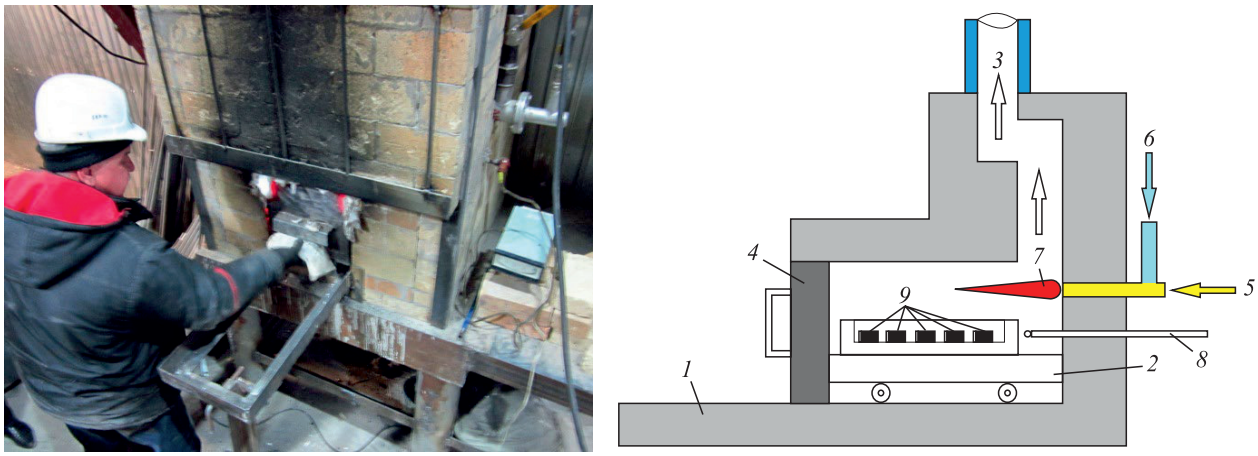

a *b*

Fig. 4. Laboratory furnace with portable hearth on generator gas:
a – general view; *b* – scheme; *1* – furnace; *2* – portable hearth; *3* – water-cooled duct; *4* – door; *5* – generator gas supply; *6* – air; *7* – torch; *8* – platinum-platinum-rhodium thermocouple; *9* – ore-coal briquettes

Рис. 4. Лабораторная печь с выдвижным подом на генераторном газе:
a – общий вид; *b* – схема; *1* – печь; *2* – выдвижной под; *3* – водоохлаждаемый газоход; *4* – дверь; *5* – подвод генераторного газа; *6* – воздух; *7* – факел; *8* – платина-платинородиевая термопара; *9* – рудно-угольные брикеты

introducing the cold briquettes. In the second stage, the briquettes were intensively heated to 1249 °C at a rate of 21.4 °C/min over 8 min. The average gas temperature in the furnace during this stage was 1163 °C.

In the third section of the temperature profile, within the 1249 – 1277 °C range, the heating rate decreased to approximately 2 °C/min. This segment effectively formed a temperature plateau, attributed to the endothermic effect of iron oxide reduction. The average gas temperature in the furnace during this stage was 1263 °C.

Further heating up to 1424 °C was required to establish the thermal conditions necessary for the liquid-phase separation of the metallic and slag phases [21]. The average heating rate over this 16 min interval was 9.2 °C/min. The average furnace gas temperature in this stage was 1350 °C. After drying and firing the briquettes for 40 min, the average yield of the final product was 69.3 ± 2.01 % (Table 4).

Fig. 7 shows the appearance of the briquettes after the completion of the metallization process. The inner part of the briquettes contains iron granules, while the outer surface is covered with an ash–slag shell, which partially protects the iron from oxidation.

Fig. 5. Ore-coal briquettes during metallization in ceramic pallets

Рис. 5. Рудно-угольные брикеты в процессе металлизации в керамических поддонах

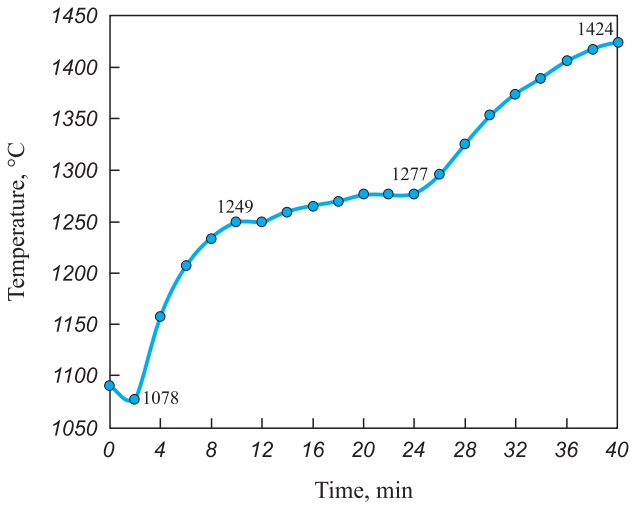

Fig. 6. Temperature-time graph of metallization of ore-coal briquettes

Рис. 6. Температурно-временной график металлизации рудно-угольных брикетов

Table 4. **Characteristics of IOC briquettes + coal + lime before and after firing**

Таблица 4. **Характеристика брикетов ЖРК + уголь + известь до и после обжига**

Parameter, unit	Batch *1*	Batch *2*	Batch *3*
Briquette composition	80 % IOC + 20 % coal + + 5 % lime (in excess of 100 %)		
Pressing pressure, atm	100		
Briquette mass, g:			
1	21.8	22.8	22.2
2	22.8	25.4	20.8
3	23.6	24.0	22.0
4	23.8	23.6	21.0
5	24.0	21.4	21.0
6	21.4	21.4	22.4
7	22.6	22.8	21.8
8	23.2	22.8	21.0
9	21.0	–	22.0
10	25.4	–	21.2
Average briquette mass, g	22.960	23.025	21.540
Average mass after drying, g	21.77	21.95	21.00
Moisture content, %	5.17	4.67	2.51
Total mass after firing, g	150.6	117.7	151.0
Average mass after firing, g	15.06	14.71	15.10
Firing temperature, °C	1090 – 1425		
Firing time, min	40		

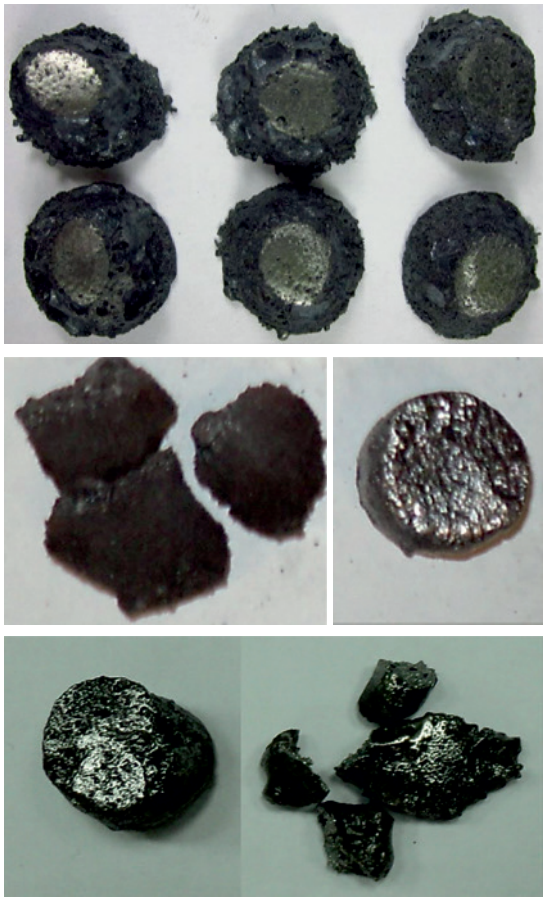

Fig. 7. Ore-coal briquettes after metallization with separation of metal and slag

Рис. 7. Рудно-угольные брикеты после металлизации с разделением металла и шлака

Briquette metallization proceeds according to the mechanism described in [22; 23]. The iron ore concentrate from the Korshunovsky MPP contains Fe_2O_3 and FeO oxides. Iron reduction from these oxides occurs in a stepwise manner, following the scheme: $Fe_2O_3 \rightarrow Fe_3O_4 \rightarrow FeO \rightarrow Fe$.

Carbon monoxide acts as the primary reducing agent, synthesized through the interaction of coal carbon with carbon dioxide:

$$C + CO_2 = 2CO. \quad (7)$$

A portion of the iron becomes carburized, forming iron carbide:

$$3Fe + C = Fe_3C. \quad (8)$$

When the carbon content in the reduced metal reaches 2 – 4 %, the melting point of the alloy decreases from 1539 °C to 1170 – 1380 °C. This reduction in melting temperature causes the carburized iron to transition into the liquid state. Due to cohesive forces, fine droplets of molten iron coalesce into larger ones, while the slag components of the charge remain solid. As the temperature of the charge increases to the ash fusion point (1310 – 1390 °C), the slag components also begin to melt. In the molten state, metal and slag do not mix due to their density difference and instead form separate phases. Upon cooling, the melt crystallizes to produce pig iron and slag.

As a result, the metallization process and formation of granulated pig iron proceed as follows: pelletized charge in the form of briquettes → reduction of iron oxides at 300 – 1200 °C → melting of iron at 1200 – 1300 °C with molten Fe_3C emerging on the surface of the porous briquettes → slag melting at 1310 – 1390 °C and formation of distinct metal and slag phases → separation of metal and slag at ~1400 °C → cooling and solidification into pig iron and slag.

Table 5 presents the average composition of the metallization products from three batches of briquettes with the following formulation: 80 wt. % IOC + 20 wt. % coal + + 5 wt. % lime (in excess of 100 wt. %), as characterized in Table 4.

It should be noted that the generator gas used – purified from tar compounds – exhibits low emissivity, approximately 0.2 – 0.3. At such low emissivity levels,

Table 5. **Composition of the products obtained as a result of metallization of IOC from Korshunovsky MPP**

Таблица 5. **Состав продуктов, полученных в результате металлизации ЖРК Коршуновского ГОК**

Batch No.	Iron alloy content in the bead, %	Metallization degree, %	Impurity content, wt. %		
			carbon	phosphorus	sulfur
1	77.9 ± 1.22	81.6 ± 1.46	1.73 ± 0.14	0.090 ± 0.02	0.117 ± 0.025
2	76.1 ± 1.65	79.9 ± 1.60	1.78 ± 0.18	0.135 ± 0.02	0.182 ± 0.033
3	86.0 ± 2.11	87.8 ± 1.89	2.59 ± 0.26	0.099 ± 0.02	0.144 ± 0.030

radiative heat transfer during the heating of ore–coal briquettes is insufficiently effective. The radiative heat flux from the tyuer flame to the surface of the heated material can be significantly increased – by approximately 20 – 25 % – by enhancing the emissivity of the gas stream through flame carburization [24]. This can be accomplished by injecting a small amount of finely ground, low-ash dry coal or off-spec calcined petroleum coke into the flame's reduction zone. As a result, the emissivity of the gas stream increases by a factor of 1.5 to 2.0, leading to higher flame luminosity, improved heat transfer to the briquettes, and a reduction in the time required to reach the target temperature.

Conclusions

Thermogravimetric analysis and laboratory-scale metallization experiments on ore–coal briquettes in a chamber furnace have demonstrated the feasibility of producing granulated pig iron on an industrial scale in a rotating hearth furnace using generator gas derived from coal gasification as the fuel.

The required metallization temperatures (1450 – 1550 °C) can be achieved by burning generator gas and recovering heat from exhaust gases to preheat the incoming air, fuel, and briquettes. If needed, heat transfer within the furnace can be further intensified by carburizing the flame using finely ground dry coal or calcined petroleum coke.

Key findings from the thermogravimetric studies are as follows:

• the IOC-to-coal ratio is the most influential factor affecting the degree of iron metallization.

• increasing the coal particle size raises the final temperature of the iron reduction process from 1255 to 1367 °C.

• the addition of lime intensifies the reduction process and shifts it to a lower temperature range (from 1367 to 1300 °C).

• to ensure effective reduction of iron oxides, the briquette composition should include coal with minimal volatile content and maximum fixed carbon content.

Based on the laboratory studies, a temperature–time mode was developed for the firing of ore–coal briquettes that ensures a high degree of iron metallization (80 – 87 %) when firing at temperatures between 1080 – 1424 °C for 40 min. The yield of metallized briquettes under these conditions was 66.45 %.

According to the design material balance, the annual production of granulated pig iron for the considered furnace setup will be 100,000 tons.

This coke-free method of producing granulated pig iron is particularly suitable for small-scale applications, especially where metallurgical and coal production facilities are located within the same regional economic area, allowing for simplified logistics and reduced transportation complexity.

References / Список литературы

1. Anikin A.E., Galevskii G.V., Rudneva V.V. Technological modes of efficient metallization of iron-oxide-containing waste from metallurgical production. *Izvestiya. Ferrous Metallurgy*. 2020;63(5):335–343. (In Russ.). https://doi.org/10.17073/0368-0797-2020-5-335-343

   Аникин А.Е., Галевский Г.В., Руднева В.В. Исследование технологических режимов эффективной металлизации оксиджелезосодержащих отходов металлургического производства. *Известия вузов. Черная металлургия*. 2020;63(5):335–343. https://doi.org/10.17073/0368-0797-2020-5-335-343

2. Yaroshenko Yu.G., Gordon Ya.M., Khodorovskaya I.Yu. Efficient and Resource-Saving Technologies of Modern Metallurgy: Manual. Yekaterinburg: LLC UIPC; 2012:670. (In Russ.).

   Ярошенко Ю.Г., Гордон Я.М., Ходоровская И.Ю. Эффективные и ресурсосберегающие технологии черной металлургии: Учебное пособие. Екатеринбург: ООО «УИПЦ»; 2012:670.

3. Rashnikov V.F., Dubrovskii B.A., Galkin V.V. Method of metallization of iron-ore raw materials to produce granulated cast iron. Patent RF no. 2490332. MPK C21B 11/06, C21B 13/08. *Bulleten' izobretenii*. 2013;(23). (In Russ.).

   Пат. 2490332 RU. Способ металлизации железорудного сырья с получением гранулированного чугуна / Рашников В.Ф., Дубровский Б.А., Галкин В.В. и др.; заявл. 12.05.2011; опубл. 20.08.2013. Бюллетень № 23.

4. Grigor'ev V.G., Patkin P.G., Tepikin S.V. Furnace for obtaining reduced metal. Patent RF no. 92522. MPK F27B 3/06, C21B 13/10. *Bulleten' izobretenii*. 2010;(8). (In Russ.).

Пат. 92522 RU. Печь для получения восстановленного металла / Григорьев В.Г., Паткин П.Г., Тепикин С.В.; заявл. 12.01.2009; опубл. 20.03.2010. Бюллетень № 8.

5. Grigor'ev V.G., Patkin P.G., Tepikin S.V. Furnace for obtaining reduced metal. Patent RF no. 94680. MPK F27B 3/06, C21B 13/10. *Bulleten' izobretenii*. 2010;(15). (In Russ.).

Пат. 94680 RU. Печь для получения восстановленного металла / Григорьев В.Г., Паткин П.Г., Тепикин С.В.; заявл. 02.02.2010; опубл. 27.05.2010. Бюллетень № 15.

6. Grinberg I.S., Grinberg A.I. Annular furnace with rotary hearth. Patent RF no. 134532. MPK C21B 13/10, F27B 3/06. *Bulleten' izobretenii*. 2013;(32). (In Russ.).

Пат. 134532 RU. Кольцевая печь с вращающимся подом / Гринберг И.С., Гринберг А.И.; заявл. 27.06.2013; опубл. 20.11.2013. Бюллетень № 32.

7. Chernykh V.E., Grigor'ev V.G., Tepikin S.V., etc. Technological line for production of metallized product. Patent RF no. 87166. MPK C22B 13/08, C21B 13/14. *Bulleten' izobretenii*. 2009;(27). (In Russ.).

Пат. 87166 RU. Технологическая линия для производства металлизированного продукта / Черных В.Е., Григорьев В.Г., Тепикин С.В. и др.; заявл. 21.05.2009; опубл. 27.09.2009. Бюллетень № 27.

8. Grigor'ev V.G., Patkin P.G., Tepikin S.V., etc. Technological line for production of metallized product. Patent RF no. 93802. MPK C21B 13/14. *Bulleten' izobretenii*. 2010;(13). (In Russ.).

Пат. 93802 RU. Технологическая линия для производства металлизированного продукта / Григорьев В.Г., Паткин П.Г., Тепикин С.В. и др.; заявл. 11.01.2010; опубл. 05.10.2010. Бюллетень № 13.

9. Storozhev Yu.I., Podborskii L.N., Khudyakov I.A. Metallization of molded ore-coal materials in circular furnace. *Izvestiya. Ferrous Metallurgy*. 2015;58(4):235–240. (In Russ.).
https://doi.org/10.17073/0368-0797-2015-4-235-240

Сторожев Ю.И., Подборский Л.Н., Худяков И.А. Металлизация формованных рудно-угольных материалов в кольцевой печи. *Известия вузов. Черная металлургия*. 2015;58(4):235–240.
https://doi.org/10.17073/0368-0797-2015-4-235-240

10. Storozhev Yu.I., Podborskii L.N., Khudyakov I.A. Cooling of metallization products in annular furnace. *Ferrous Metallurgy. Bulletin of Scientific, Technical and Economic Information*. 2015;1382(2):33–36. (In Russ.).

Сторожев Ю.И., Подборский Л.Н., Худяков И.А. Охлаждение продуктов металлизации в кольцевой печи. *Черная металлургия. Бюллетень научно-технической и экономической информации*. 2015;1382(2):33–36.

11. Gorbachev V.A., Evstyugin S.N., Kopot' N.N., Rybkin V.S., Shavrin S.V. Selecting technology for direct iron production. *Stal'*. 2006;12(6):42–46. (In Russ.).

Горбачев В.А., Евстюгин С.Н., Копоть Н.Н., Рыбкин В.С., Шаврин С.В. Принципы выбора технологии прямого получения железа. *Сталь*. 2006;12(6):42–46.

12. Yunes R., Opryshko I.A., Loboda P.I. Analysis of technologies of direct metal oxides reduction in circular furnaces. *Vestnik NTUU "KPI"*. 2011;61:184–192. (In Russ.).

Юнес Р., Опрышко И.А., Лобода П.И. Анализ технологий прямого восстановления оксидов металлов с применением печей с вращающимся подом. *Вестник Национального технического университета Украины «Киевский политехнический институт»*. 2011;61:184–192.

13. Dubrovskii B.A., Shilyaev P.V., Redin E.V., etc. Metallization of spatic iron ores of the Bakalsky deposit and production of granulated iron. In: *Proceedings of the VI Int. Conf. "Energy Saving Technologies in Industry, Combustion Equipment, Environment Protection"*. Moscow: NUST "MISIS"; 2012:178–182. (In Russ.).

Дубровский Б.А., Шиляев П.В., Редин Е.В. и др. Металлизация шпатовых железняков Бакальского месторождения с получением гранулированного чугуна. В кн.: *Сборник трудов VI Международной конференции «Энергосберегающие технологии в промышленности, печные агрегаты, экология»*. Москва: НИТУ «МИСиС»; 2012: 178–182.

14. Kikuchi S., Ito S., Kobayashi I., Tsuge O., Tokuda K. ITmk3 process. *KOBELCO Technology Review*. 2010;29:77–84.

15. Tanaka N., Miyagawa K., Harada T. FASTMET, FASTMELT, and ITmk3. Development of new coal-based ironmaking processes. *Direct from Midrex, RHF Technologies*. 2007/2008:8–13.

16. Kobayashi I., Tanigaki Y., Liagami A. A new process to produce iron directly from fine ore and coal. *Iron and Steelmaker*. 2001;28(9):19–22.

17. Sohn I., Fruehan R.J. The reduction of iron oxides by volatiles in a rotary hearth furnace process: Part I. The role and kinetics of volatile reduction. *Metallurgical and Materials Transactions B*. 2005;36:605–612.
https://doi.org/10.1007/s11663-005-0051-y

18. Gordon Y., Els J. ITmk3 technology and its application for mining and steel industry in Ukraine and Russia. In: *Int. Conf. on Ironmaking Technology (Kyiv, 21 March 2007)*. Kyiv; 2007:128–131.

19. Ishikawa H., Kopfle J., Mcclelland J., Ripke J. Rotary hearth furnace technologies for iron ore and recycling applications. *Archives of Metallurgy and Materials*. 2008;53(2):541–545.

20. Rutherford S.D., Kopfle J.T. Mesabi Nugget: World's first commercial ITmk3 Plant. *Iron and steel Technology*. 2010;7:38–43.

21. Asanov A.V., Roshchin A.V., Roshchin V.E. Liquid-phase separation of products of solid-phase reduction of ferrovanadium concentrates. *Vestnik YuUrGU. Metallurgiya*. 2010;(13(189)):37–40. (In Russ.).

Асанов А.В., Рощин А.В., Рощин В.Е. Жидкофазное разделение продуктов твердофазного восстановления железо-ванадиевых концентратов. *Вестник ЮУрГУ. Металлургия*. 2010;(13(189)):37–40.

22. Wegman E.F., Zherebin B.N., Pokhvisnev A.N., etc. Metallurgy of Cast Iron. Textbook for Universities. Moscow: Akademkniga; 2004:774. (In Russ.).

Вегман Е.Ф., Жеребин Б.Н., Похвиснев А.Н. и др. Металлургия чугуна. Учебник для вузов. Москва: Академкнига; 2004:774.

23. Patrushov A.E. Development of pyrometallurgical technology for extracting iron and zinc from electric steelmaking dust: Extended Abstract of Cand. Sci. Diss. Irkutsk; 2021:19. (In Russ.).

Патрушов А.Е. Разработка пирометаллургической технологии извлечения железа и цинка из пылей электросталеплавильного производства: Автореферат диссертации ... кандидата технических наук. Иркутск; 2021:19.

24. Gushchin S.N., Kazyaev M.D., Kryuchenkov Yu.V., etc. Theory and Practice of Heat Generation: Textbook. 2nd ed. Ekaterinburg. UGTU-UPI; 2005:379. (In Russ.).

Гущин С.Н., Казяев М.Д., Крюченков Ю.В. и др. Теория и практика теплогенерации. Учебник. Изд. 2-е. Екатеринбург: УГТУ-УПИ; 2005:379.

Information about the Authors

Boris P. Kulikov, *Dr. Sci. (Chem.), Leading Researcher of the Chair "General Metallurgy"*, Siberian Federal University
ORCID: 0009-0004-5881-8515
E-mail: Kulikov-Boris@Yandex.ru

Yurii I. Storozhev, *Cand. Sci. (Eng.), Assist. Prof.,* Siberian Federal University
ORCID: 0009-0004-6083-8777
E-mail: albin1941@mail.ru

Aleksandr S. Potapenko, *Cand. Sci. (Eng.), Assist. Prof. of the Chair of Technosphere and Environmental Safety*, Siberian Federal University
ORCID: 0009-0004-5881-8515
E-mail: komvzvodt-81@mail.ru

Сведения об авторах

Борис Петрович Куликов, *д.х.н., ведущий научный сотрудник кафедры «Общая металлургия»*, Сибирский федеральный университет
ORCID: 0009-0004-5881-8515
E-mail: Kulikov-Boris@Yandex.ru

Юрий Иванович Сторожев, *к.т.н., доцент*, Сибирский федеральный университет
ORCID: 0009-0004-6083-8777
E-mail: albin1941@mail.ru

Александр Сергеевич Потапенко, *к.т.н., доцент кафедры техносферной и экологической безопасности*, Сибирский федеральный университет
ORCID: 0009-0004-5881-8515
E-mail: komvzvodt-81@mail.ru

Contribution of the Authors

B. P. Kulikov – development of a research plan, organization of laboratory and production tests, analysis of literary sources.

Yu. I. Storozhev – participation in laboratory tests, generalization of the results of laboratory and production tests, text preparation.

A. S. Potapenko – review of information on metallization of ore-coal materials, computer processing of the article materials.

Вклад авторов

Б. П. Куликов – разработка плана исследований, организация лабораторных и производственных испытаний, анализ литературных источников.

Ю. И. Сторожев – участие в лабораторных испытаниях, обобщение результатов лабораторных и производственных испытаний, подготовка основного текста статьи.

А. С. Потапенко – обзор информации по металлизации рудно–угольных материалов, компьютерная обработка материалов статьи.

Received 27.03.2025
Revised 17.04.2025
Accepted 10.06.2025

Поступила в редакцию 27.03.2025
После доработки 17.04.2025
Принята к публикации 10.06.2025

Innovation in metallurgical industrial and laboratory equipment, technologies and materials

Инновации в металлургическом промышленном и лабораторном оборудовании, технологиях и материалах

UDC 669.013
DOI 10.17073/0368-0797-2025-4-395-401

Original article
Оригинальная статья

Improving the design and thermal operation of a rotary kiln for production of metallurgical lime from chalk

A. S. Sivkov, **S. I. Chibizova**, **A. D. Apasova**

National University of Science and Technology "MISIS" (4 Leninskii Ave., Moscow 119049, Russian Federation)

sivkovsasha777@yandex.ru

Abstract. The article is devoted to the topical issue of increasing the efficiency of rotary kilns used in the production of metallurgical lime from chalk. Methods of improving the structures and thermal operation of these units are considered, which is especially important in modern production conditions. The work begins with a description of the importance of lime in the metallurgical industry and the specifics of using rotary kilns as the main units for its production. There is a need to increase productivity and reduce energy consumption. The article provides an overview of promising technical solutions, such as: design changes, optimization of heat exchange devices, improvement of burner mechanisms, introduction of automatic control and process control systems. The results of tests confirming the expediency of using chalk of certain brands are also considered. Attention is drawn to the importance of factors such as the quality of raw materials and the qualifications of service personnel that affect the firing efficiency. The authors proposed new technical solutions to increase the efficiency of roasting process and reduce energy consumption. The article discusses the main problems associated with the production of lime from chalk. The proposed improvements are aimed at solving the mentioned problems and improving the quality of the final product. Special attention is paid to optimizing the thermal mode of the furnace; this will make it possible to use thermal energy more efficiently and reduce fuel consumption, which in turn will lead to reduction in the cost of lime production. Implementation of the proposed technical solutions will significantly increase the economic and environmental efficiency of lime production. The article emphasizes that continued research in this area is promising for improving the performance of rotary furnaces and, consequently, the quality of the resulting product.

Keywords: lime, limestone, chalk, heater, rotary kiln, roasting, steel, Oskol Electrometallurgical Combine (OEMK), Lebedinsky Mining and Processing Combine (LGOK)

For citation: Sivkov A.S., Chibizova S.I., Apasova A.D. Improving the design and thermal operation of a rotary kiln for production of metallurgical lime from chalk. *Izvestiya. Ferrous Metallurgy*. 2025;68(4):395–401. https://doi.org/10.17073/0368-0797-2025-4-395-401

Направления совершенствования конструкции и тепловой работы вращающейся печи для реализации технологии производства металлургической извести из мела

А. С. Сивков, **С. И. Чибизова**, **А. Д. Апасова**

Национальный исследовательский технологический университет «МИСИС» (Россия, 119049, Москва, Ленинский пр., 4)

sivkovsasha777@yandex.ru

Аннотация. Статья посвящена актуальной теме повышения эффективности вращающихся печей, используемых при производстве металлургической извести из мела. Рассмотрены методы усовершенствования конструкций и тепловой работы этих агрегатов, что особенно важно в условиях современного производства. Работа начинается с описания значимости извести в металлургической отрасли и особенностей применения вращающихся печей как основных агрегатов для ее производства. Отмечена необходимость повышения производительности и снижения энергозатрат. В статье представлен обзор перспективных технических решений, таких как конструктивные изменения, оптимизация теплообменных устройств, совершенствование горелочных механизмов, внедрение систем автоматического контроля и управления технологическим процессом. Также рассмотрены результаты испытаний, подтверждающих целесообразность использования мела

определенных марок. Авторы обращают внимание на важность таких факторов, как качество сырья и квалификация обслуживающего персонала, которые влияют на эффективность обжига. Предложены новые технические решения, позволяющие повышать эффективность процесса обжига и снижать энергозатраты. Изучены основные проблемы, связанные с производством извести из мела. Предлагаемые усовершенствования направлены на решение указанных в работе проблем и улучшение качества конечного продукта. Особое внимание уделено оптимизации теплового режима печи, что позволит более эффективно использовать тепловую энергию и снизить расход топлива, что в свою очередь приведет к снижению себестоимости производства извести. Реализация предложенных технических решений позволит значительно повысить экономическую и экологическую эффективность ее производства. Авторы подчеркивают, что продолжение исследований в данной области перспективно для улучшения эксплуатационных характеристик вращающихся печей и, соответственно, качества получаемого продукта.

Ключевые слова: известь, известняк, мел, подогреватель, вращающаяся печь, обжиг, сталь, ОЭМК, ЛГОК

Для цитирования: Сивков А.С., Чибизова С.И., Апасова А.Д. Направления совершенствования конструкции и тепловой работы вращающейся печи для реализации технологии производства металлургической извести из мела. *Известия вузов. Черная металлургия*. 2025;68(4):395–401. https://doi.org/10.17073/0368-0797-2025-4-395-401

Introduction

In today's world, lime is one of the key materials used in the metallurgical industry, and the rotary kiln remains one of the most efficient and widely adopted process units for its production. The need to enhance the performance of rotary kilns employed in the technology of producing metallurgical lime from chalk is a pressing challenge. Improving the design and thermal operation of these kilns will enable increased productivity, reduced energy consumption, and improved quality of the final product [1; 2].

An overview is provided of the most relevant and promising technical solutions whose implementation would enhance the efficiency of rotary kilns used for the production of metallurgical lime from chalk, reduce energy consumption, and improve the environmental performance of the process [3].

Classification and main design features of rotary kilns

The rotary kiln is one of the most widely used types of thermal units employed in metallurgy, as well as in the production of cement, lime, ceramics, refractories, and other materials [4; 5]. The design features and operating principles of rotary kilns account for their broad application in carrying out high-temperature processes such as drying, roasting, reduction, sintering, and more. The key advantages of rotary kilns over other types of thermal units include:

– continuous process operation (the material loaded into the loading device at the upper end of the kiln gradually moves along the inclined rotating drum toward the discharge device at the lower end, thereby ensuring continuity of the process and the ability to regulate the material's residence time within the working space);

– intensive heat and mass transfer (the rotation of the drum, along with internal lifting blades mounted on the inner surface, ensures thorough mixing of the material, which promotes efficient heat and mass exchange between the solid and gas phases);

– fuel flexibility (rotary kilns can operate on solid, gaseous, or liquid fuels), which enhances the adaptability of the production process);

– relative simplicity of design and operation (compared to other types of thermal units – such as shaft and chamber kilns – rotary kilns have a simpler structure, which facilitates maintenance and repair);

– high productivity (due to the continuous operation and intensive heat and mass transfer, rotary kilns can deliver production capacities reaching hundreds or even thousands of tons per day).

The specific design solutions and configuration of rotary kiln components are determined by the characteristics of the technological process, the physical and chemical properties of the raw materials, the quality requirements for the final product, and energy and environmental considerations. The rotary kiln design is shown in Fig. 1 [6; 7].

Key areas for improving rotary kiln design for lime production

Tests carried out on a laboratory-scale model at NUST "MISIS" for the production of metallurgical lime from chalk confirmed the feasibility and expediency of using chalk from Lebedinsky Mining and Processing Combine (LGOK) at Oskol Electrometallurgical Combine (OEMK). Both enterprises are part of the Metalloinvest holding company [8].

The rotary kiln is a heat exchange unit in the form of an inclined rotating tube, in which hot gases flow countercurrent to the movement of limestone. The size of the material loaded into the kiln ranges from 20 to 60 mm. The kiln has a nominal capacity of 360 tons per day.

The main component of the rotary kiln is a steel cylindrical drum, with a diameter of 3.6 m and a length of 75 m. The diameter of the drum remains constant along the entire length of the kiln.

An analysis of the operational characteristics of existing rotary kiln designs used for lime production makes

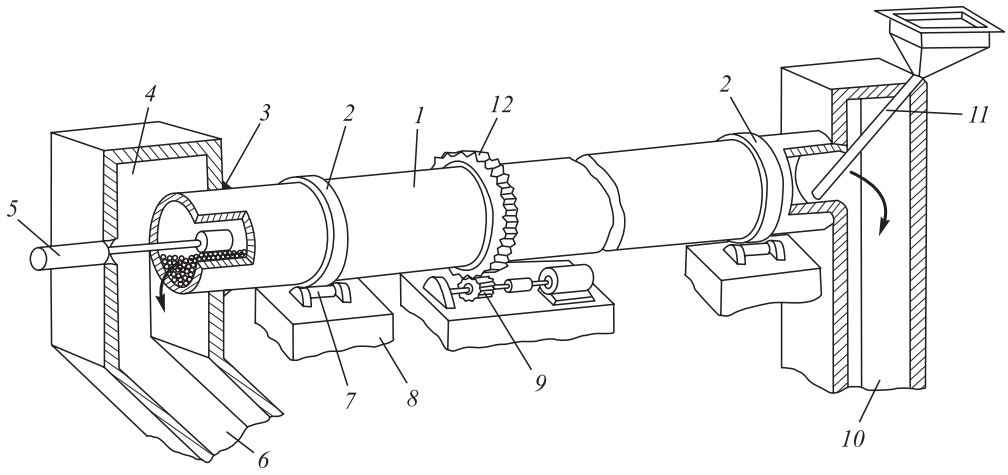

Fig. 1. Rotary kiln design:
1 – drum; *2* – bandages; *3* – seal; *4* – kiln chamber (hot head); *5* – burner; *6* – discharge flow; *7* – support rollers; *8* – foundation; *9* – drum drive; *10* – exhaust chamber; *11* – loading device; *12* – ring gear

Рис. 1. Устройство вращающейся печи:
1 – барабан; *2* – бандажи; *3* – уплотнение; *4* – топочная камера (горячая головка); *5* – горелка; *6* – разгрузочная течка; *7* – опорные ролики; *8* – фундамент; *9* – привод барабана; *10* – газоотводная камера; *11* – загрузочное устройство; *12* – венцовая шестерня

it possible to identify several key areas for improvement aimed at increasing the energy efficiency, environmental performance, and economic viability of this technological process. A number of foundational studies have been devoted to enhancing the efficiency of technological processes in lime roasting units, particularly in rotary kilns.

In the monograph *Lime Production* by A.V. Monastyriev [9], the design features and thermal operating modes of various types of firing kilns, including rotary kilns, are examined in detail. The author identifies the key factors influencing fuel efficiency in lime production: raw material quality and preparation, kiln design solutions, operation of auxiliary equipment, and qualifications of service personnel. The book presents technical solutions for improving rotary kiln design, such as the use of in-kiln heat exchange devices, optimization of raw material loading and discharge systems, and modernization of burner mechanisms.

In the monograph *Kilns for Lime Production* by A.V. Monastyriev and R.F. Galiahmetov [10], the structural features and operating modes of rotary kilns are considered in greater detail, particularly those affecting fuel efficiency. The authors analyze the influence of factors such as kiln drum length and inclination, the presence of internal heat exchangers, and loading and unloading modes of the raw materials.

Patent RF No. 2079785 *Gas Burner* [11], by L.V. Kalashnikov and G.L. Kalashnikov, proposes a design for a adjustable gas burner that allows regulation of the flame parameters and the intensity of heat exchange within the working space of the kiln. This innovation contributes to more efficient fuel combustion in firing units (Fig. 2).

In the monograph by N.P. Tabunshchikov *Lime Production*, the issues of proper kiln operation, maintaining optimal process conditions, and monitoring the composition of off-gases are discussed. These factors are noted to significantly affect fuel efficiency in lime production.

One of the main factors limiting the efficiency of rotary kilns is the uneven distribution and movement of raw materials inside the kiln drum [12]. To address this issue in the studied kiln, a promising direction is the development of advanced loading and discharge devices that ensure optimal distribution and transport of raw material along the kiln length. A key area for improving the energy efficiency of rotary kilns used for lime production is the enhancement of heat and mass transfer systems. The kiln under consideration is characterized by significant heat losses with exhaust gases, as well as insufficient utilization of the thermal potential of calcined products for preheating the raw materials [13].

The efficiency of heat exchange processes can be increased by:

– installing high-efficiency regenerative or recuperative heat exchange devices (such as rotary air preheaters and tubular heat exchangers);

– implementing multi-stage heat exchange schemes with recirculation and cascade utilization of thermal energy.

The introduction of these technical solutions will reduce fuel consumption, decrease heat losses, and increase the temperature of the air supplied to the combustion zone, ultimately leading to higher thermal efficiency of the rotary kiln.

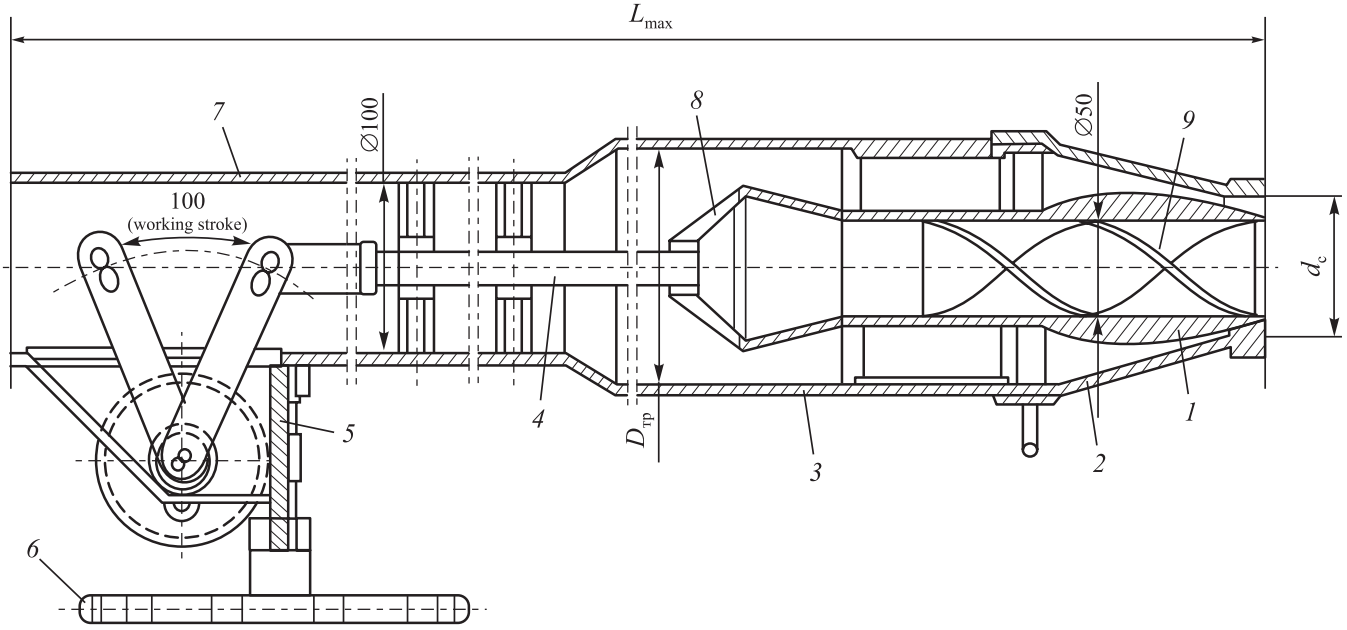

Fig. 2. Single-channel adjustable cement burner [11]:
1 – housing of the burner first stage; *2* – vortex stabilizer; *3* – mixing chamber of the first stage;
4 – mixing chamber of the second stage; *5* – housing of the second stage; *6* – burner mounting flange;
7 – fuel supply regulator of the second stage; *8* – fuel supply nozzle (or sprayer);
9 – nozzle or air supply blowpipe of the second stage

Рис. 2. Горелка одноканальная регулируемая типа ГРЦ (горелки регулируемые цементные) [11]:
1 – корпус первой ступени горелки; *2* – вихревой стабилизатор; *3* – камера смешения первой ступени;
4 – камера смешения второй ступени; *5* – корпус второй ступени; *6* – фланец крепления горелки;
7 – регулирующий орган подачи топлива второй ступени; *8* – форсунка подачи топлива (или распылитель);
9 – форсунка или сопло подачи воздуха второй ступени

Studying combustion processes and flame heat transfer in the working space of kilns used for lime production is a critical task, as it determines the size of the firing zone, the intensity of thermal impact on the material, and the condition of the lining.

A.A. Anisimov et al. [14] developed a mathematical model and a calculation algorithm for evaluating the thermal characteristics of limestone firing in a rotary kiln. The authors established an empirical relationship for determining the length of the gas burner flame, taking into account parameters such as burner diameter, inner kiln diameter, and fuel and air flow rates. A method was proposed for calculating the average effective temperature of the gas stream in the contact zone with the surface of the fired limestone.

Based on the developed model, a numerical study was conducted on the influence of various factors on flame heat transfer and the temperature state of the calcined material. It was shown that the flame heat transfer is significantly affected by the excess air ratio, preheated air temperature, lining emissivity, and the lower heating value of the fuel [14]. At the same time, the thickness of the lining has a lesser effect. To optimize the firing mode, an algorithm was proposed for calculating the resulting thermal flux of the flame into the firing zone. This algorithm allows for achieving the required calcination temperature by adjusting the fuel flow rate, excess air ratio, and air preheating temperature, thereby preventing overheating of the kiln lining.

E.E. Merker et al. [15] also addressed the issue of improving fuel combustion efficiency in rotary kilns for lime production. The authors emphasize that key factors determining heat transfer in the working space of the kiln include the flame length and temperature. Flame characteristics, in turn, depend on the design and operating modes of the burner devices.

Studies have shown that optimizing fuel combustion conditions and heat transfer in the firing zone of rotary kilns used for lime production is a relevant and important task. The developed mathematical models and calculation algorithms make it possible to determine optimal operating parameters that ensure the required quality of lime while minimizing energy consumption.

Existing kiln designs are characterized by high emissions of nitrogen and sulfur oxides, as well as significant heat losses with flue gases [16].

To address these issues, the following technical solutions can be applied:

– use of staged or two-stage fuel combustion to reduce NO_x formation;

– implementation of flue gas recirculation to limit excess air and lower the temperature in the firing zone;

– application of low-emission burner mechanisms equipped with automatic air and fuel control systems;

– introduction of catalytic or selective non-catalytic treatment systems for removing nitrogen and sulfur oxides from exhaust gases.

The integrated implementation of these measures will help reduce fuel consumption during the roasting process and significantly lower atmospheric emissions of harmful substances. A key factor affecting the operational performance of rotary kilns is the reliability and durability of their main structural components, such as the drum and lining [17].

The implementation of these technical solutions will help extend kiln service life, reduce maintenance and repair costs, and improve the overall reliability and economic efficiency of lime production [18]. An important direction for improving the performance of rotary kilns is the introduction of automatic control and process management systems. This will make it possible to maintain optimal operating conditions, ensure stable firing conditions, and thereby achieve high and consistent lime quality. In addition to improving traditional rotary kiln designs to enhance their performance characteristics, a promising direction is the development and implementation of nontraditional technical solutions [19; 20]. The main directions for improving the design of rotary kilns for lime production include:

– enhancing raw material loading and discharge systems;

– improving the efficiency of heat exchange processes;

– optimization of fuel combustion systems;

– improving the design of the drum and lining;

– automating process control;

– developing and applying nontraditional design solutions.

The implementation of these measures will improve the energy efficiency, environmental performance, and cost-effectiveness of lime production in rotary kilns, while also ensuring high and stable quality of the final product.

Conclusions

An analysis of the operational characteristics of the existing rotary kiln design with a diameter of 3.6 m and a length of 75 m, used for producing 360 tons of lime per day, revealed a number of deficiencies and issues that negatively affect the technical, economic, and environmental performance of this technological process. The main problematic aspects include: limited potential for increasing productivity, low energy efficiency, challenges in ensuring consistent quality of limestone firing, accelerated wear of main structural components, and significant emissions of carbon dioxide and other pollutants.

The main directions for improving the rotary kiln design for lime production are identified. Their implementation will enhance the energy and economic efficiency of lime production in rotary kilns, ensure high and stable product quality, and support compliance with environmental standards.

A review of the current state of lime production and existing rotary kiln designs has confirmed the relevance of improving kiln construction and thermal operation in the context of lime production from chalk. Addressing this challenge is of significant practical importance for improving both the efficiency and environmental safety of the production process.

References / Список литературы

1. Sivkov A.S., Shumakov V.V. Production of lime for metallurgical industry. In: *Scientific Community of Students of the XXI Century. Natural Sciences: Proceedings of the XLV Int. Student Sci.-Pract. Conf.* 2016;9(44). Available at: https://sibac.info/archive/nature/9(44).pdf (Accessed 07.06.2025). (In Russ.).

   Сивков А.С., Шумаков В.В. Производство извести для металлургического производства / *Научное сообщество студентов XXI столетия. Естественные науки: Сборник статей по материалам XLV Международной студенческой научно-практической конференции*. 2016;9(44). URL: https://sibac.info/archive/nature/9(44).pdf (дата обращения 07.06.2025).

2. Sivkov A.S., Shumakov V.V., Mamonov R.I. Study of properties of chalk from LGOK. In: *Scientific Community of Students of the XXI Century. Natural Sciences: Proceedings of the XLV Int. Student Sci.-Pract. Conf.* 2016;11(47). Available at: https://sibac.info/archive/technic/11(47).pdf (Accessed 07.06.2025). (In Russ.).

   Сивков А.С., Шумаков В.В., Мамонов Р.И. Исследование свойств мела АО «Лебединский ГОК» / *Научное сообщество студентов XXI столетия. Технические науки: Сборник статей по материалам XLVIII Международной студенческой научно-практической конференции*. 2016;11(47). URL: https://sibac.info/archive/technic/11(47).pdf (дата обращения 07.06.2025).

3. Sivkov A.S., Shilov A.A. Study of physical and mechanical characteristics of chalk and limestone, with the aim of using chalk as a raw material for lime production. In: *Scientific Community of Students of the XXI Century. Natural Sciences: Proceedings of the XLV Int. Student Sci.-Pract. Conf.* 2018;1(60). Available at: https://sibac.info/archive/technic/1(60).pdf (Accessed 07.06.2025). (In Russ.).

   Сивков А.С., Шилов А.А. Исследование физико-механических характеристик мела и известняка с целью использования мела как сырья для производства извести / *Научное сообщество студентов XXI столетия. Технические науки: Сборник статей по материалам LXI*

Международной студенческой научно-практической конференции. 2018;1(60). URL: https://sibac.info/archive/technic/1(60).pdf (дата обращения 07.06.2025).

4. Mikulcic H., Berg E.V., Vujanovic M., Priesching P., Perkovic L., Tatschl R., Duic N. Numerical modelling of calcination reaction mechanism for cement production. *Chemical Engineering Science*. 2012;69(1):607–615. https://doi.org/10.1016/j.ces.2011.11.024
5. Sinhal K., Ghoshdastidar P.S., Dasgupta B. Computer simulation of drying of food products with superheated steam in a rotary kiln. *ASME Journal of Thermal Science and Engineering Applications*. 2012;4(1):011009. https://doi.org/10.1115/1.4005256
6. Li S.Q., Ma L.B., Wan W., Yao Q. A mathematical model of heat transfer in a rotary kiln thermo-reactor. *Chemical Engineering Technology*. 2005;28(12):1480–1489. https://doi.org/10.1002/ceat.200500241
7. Guo Y.C., Chan C.K., Lau K.S. Numerical studies of pulverized coal combustion in a tubular coal combustor with slanted oxygen jet. *Fuel*. 2003;82(8):893–907. https://doi.org/10.1016/S0016-2361(02)00367-8
8. Sivkov A.S., Shumakov V.V., Mamonov R.I. Possibility of using chalk for the production of lime used in metallurgy. In: *Scientific Community of Students of the XXI Century. Natural Sciences: Proceedings of the XLV Int. Student Sci.-Pract. Conf.* 2016;9(45). Available at: https://sibac.info/archive/technic/9(45).pdf (Accessed 07.06.2025). (In Russ.).

   Сивков А.С., Шумаков В.В., Мамонов Р.И. Возможность использования мела для производства извести, применяемой в металлургии / *Научное сообщество студентов XXI столетия. Технические науки: Сборник статей по материалам XLVI Международной студенческой научно-практической конференции*. 2016;9(45). URL: https://sibac.info/archive/technic/9(45).pdf (дата обращения 07.06.2025).
9. Monastyrev A.V. Lime Production. Moscow: Vysshaya shkola; 1971:272. (In Russ.).

   Монастырев А.В. Производство извести. Москва: Высшая школа; 1971:272.
10. Monastyrev A.V., Galiakhmetov R.F. Kilns for Lime Production. Voronezh: Istoki; 2011:392. (In Russ.).

    Монастырев А.В., Галиахметов Р.Ф. Печи для производства извести. Воронеж: Истоки; 2011:392.
11. Kalashnikov L.V., Kalashnikov G.L. Gas burner. Patient RF no. 2079785 1997 (In Russ.).

    Пат. 2079785 RU. Газовая горелка / Калашников Л.В., Калашников Г.Л.; заявл. 13.04.1995; опубл. 20.05.1997.
12. Selivanov N.I. Technology and Equipment for Production of Building Materials. Moscow: Vysshaya shkola; 2005:366. (In Russ.).

    Селиванов Н.И. Технология и оборудование для производства строительных материалов. Москва: Высшая школа; 2005:366.
13. Alekseev A.D. Theory and Practice of Limestone Roasting in Rotary Kilns. Moscow: Metallurgiya; 1973:344. (In Russ.).

    Алексеев А.Д. Теория и практика обжига известняка во вращающихся печах. Москва: Металлургия; 1973:344.
14. Ansimov A.A., Merker E.E., Kharlamov D.A., Kochetov A.I., Kazartsev V.O. Studying the heat transfer of the torch and optimization of the regime of firing in the revolver. *Bulletin of Cherepovets State University*. 2013; (2-1(47)):5–9. (In Russ.).

    Ансимов А.А., Меркер Э.Э., Харламов Д.А., Кочетов А.И., Казарцев В.О. Исследование теплоотдачи факела и оптимизация режима обжига во вращающейся печи. *Вестник Череповецкого государственного университета*. 2013;(2-1(47)):5–9.
15. Merker E.E., Kharlamov D.A., Ansimov A.A. Increasing the efficiency of fuel combustion in rotary kilns for lime roasting. *Ferrous Metallurgy. Bulletin of Scientific, Technical and Economic Information*. 1995;(5):28–30. (In Russ.).

    Меркер Э.Э., Харламов Д.А., Ансимов А.А. Повышение эффективности сжигания топлива во вращающихся печах обжига извести. *Черная металлургия. Бюллетень научно-технической и экономической информации*. 1995;(5):28–30.
16. Sheludyak B.L. Technology of Lime Production. Moscow: Stroyizdat; 1988:272. (In Russ.).

    Шелудяк Б.Л. Технология производства извести. Москва: Стройиздат; 1988:272.
17. Alekseev A.D. Theory and Practice of Limestone Roasting in Rotary Kilns. Moscow: Metallurgiya; 2018:344. (In Russ.).

    Алексеев А.Д. Теория и практика обжига известняка во вращающихся печах. Москва: Металлургия; 2018:344.
18. Kuznetsov N.V., Baskakov A.P. Thermal Engineering. Moscow: Energoatomizdat; 2018:479. (In Russ.).

    Кузнецов Н.В., Баскаков А.П. Теплотехника. Москва: Энергоатомиздат; 2018:479.
19. Mastorakos E., Massias A., Tsakiroglou C.D., Goussis D.A., Burganos V.N. CFD predictions for cement kiln including flame modelling, heat transfer and clinker chemistry. *Applied Mathematical Modelling*. 1999;23(1):55–76. https://doi.org/10.1016/S0307-904X(98)10053-7
20. Mujumdar K.S., Ganesh K.V., Kulkarni S.V., Ranade V.V. Rotary cement kiln simulator (RoCKS): Integrated modeling of pre-heater, calciner, kiln and clinker cooler. *Chemical Engineering Science*. 2007;62(9):2590–2607. https://doi.org/10.1016/j.ces.2007.01.063

Information about the Authors / Сведения об авторах

Aleksandr S. Sivkov, *Postgraduate of the Chair "Energy-Efficient and Resource-Saving Industrial Technologies"*, National University of Science and Technology "MISIS"
E-mail: sivkovsasha777@yandex.ru

Svetlana I. Chibizova, *Cand. Sci. (Eng.), Assist. Prof. of the Chair "Energy-Efficient and Resource-Saving Industrial Technologies"*, National University of Science and Technology "MISIS"
ORCID: 0000-0002-9444-5670
E-mail: s.chibizova@misis.ru

Anna D. Apasova, *Postgraduate of the Chair "Energy-Efficient and Resource-Saving Industrial Technologies"*, National University of Science and Technology "MISIS"
E-mail: annhope@bk.ru

Александр Сергеевич Сивков, *аспирант кафедры энергоэффективных и ресурсосберегающих промышленных технологий*, Национальный исследовательский технологический университет «МИСИС»
E-mail: sivkovsasha777@yandex.ru

Светлана Игоревна Чибизова, *к.т.н., доцент кафедры энергоэффективных и ресурсосберегающих промышленных технологий*, Национальный исследовательский технологический университет «МИСИС»
ORCID: 0000-0002-9444-5670
E-mail: s.chibizova@misis.ru

Анна Дмитриевна Апасова, *аспирант кафедры энергоэффективных и ресурсосберегающих промышленных технологий*, Национальный исследовательский технологический университет «МИСИС»
E-mail: annhope@bk.ru

Contribution of the Authors / Вклад авторов

A. S. Sivkov – highlighting areas of improvement, development and application of a thermal calculation model, conducting experiments, assessment of environmental and economic effects.
S. I. Chibizov – highlighting areas of improvement, conducting experiments.
A. D. Apasov – analytical review, description of scientific novelty and practical significance.

А. С. Сивков – выделение направлений оптимизации, разработка и применение модели теплового расчета, проведение экспериментов, оценка экологических и экономических эффектов.
С. И. Чибизова – выделение направлений оптимизации, проведение экспериментов.
А. Д. Апасова – аналитический обзор, описание научной новизны и практической значимости.

Received 26.03.2025
Revised 29.04.2025
Accepted 23.06.2025

Поступила в редакцию 26.03.2025
После доработки 29.04.2025
Принята к публикации 23.06.2025

UDC 669.162.263
DOI 10.17073/0368-0797-2025-4-402-410

Original article
Оригинальная статья

Information modeling system for assessing instability of blast furnace functioning

N. A. Spirin, I. A. Gurin, V. V. Lavrov

Ural Federal University named after the first President of Russia B.N. Yeltsin (28 Mira Str., Yekaterinburg 620002, Russian Federation)

n.a.spirin@urfu.ru

Abstract. The article discusses the development of an information modeling system for assessing the instability of a blast furnace. The presented approach is based on the application of mathematical models and methods for analyzing the parameters of the blast furnace process, which makes it possible to assess the impact of technological and organizational factors on the furnace stability. The developed system is designed for automated collection, processing and analysis of data in real time, as well as forecasting technological deviations. The methodology is based on the use of integral stability indicators, including the technical and economic characteristics of smelting, the properties of raw materials, the parameters of blast, gas dynamic, thermal and slag modes. To determine the integral indicators, a set of controlled and calculated features is used, ranked according to the degree of significance. The main modules of the system include functional blocks for data collection, calculations, analysis and visualization. The system architecture is implemented on the basis of a client-server approach, which provides the possibility of integration with existing metallurgical production management systems. The practical implementation of the system makes it possible to improve the performance of blast furnace smelting, reduce fluctuations in the parameters of the technological process and improve the quality of the resulting cast iron. The above calculation examples confirm effectiveness of the developed tool. The presented results may be useful for the specialists in the field of blast furnace production automation, as well as for the researchers involved in analysis and forecasting of instability of technological processes.

Keywords: blast furnace, modeling, instability, information system, metallurgy, mathematical model

For citation: Spirin N.A., Gurin I.A., Lavrov V.V. Information modeling system for assessing instability of blast furnace functioning. *Izvestiya. Ferrous Metallurgy*. 2025;68(4):402–410. https://doi.org/10.17073/0368-0797-2025-4-402-410

Информационно-моделирующая система оценки нестабильности функционирования доменной печи

Н. А. Спирин, И. А. Гурин, В. В. Лавров

Уральский федеральный университет имени первого Президента России Б. Н. Ельцина (Россия, 620002, Екатеринбург, ул. Мира, 28)

n.a.spirin@urfu.ru

Аннотация. В статье рассматривается разработка информационно-моделирующей системы оценки нестабильности функционирования доменной печи. Представленный подход базируется на применении математических моделей и методов анализа параметров доменного процесса, что позволяет оценивать влияние технологических и организационных факторов на стабильность работы печи. Разработанная система предназначена для автоматизированного сбора, обработки и анализа данных в реальном времени, а также прогнозирования технологических отклонений. В основе методики лежит использование интегральных показателей стабильности, включая технико-экономические характеристики плавки, свойства сырья, параметры дутьевого, газодинамического, теплового и шлакового режимов. Для расчета интегральных показателей применяется совокупность контролируемых и расчетных признаков, ранжированных по степени значимости. Основные модули системы включают функциональные блоки сбора данных, расчетов, анализа и визуализации. Архитектура системы реализована на основе клиент-серверного подхода, что обеспечивает возможность интеграции с существующими системами управления металлургическим производством. Практическая реализация системы позволяет улучшить показатели производительности доменной плавки, снизить колебания параметров технологического процесса и повысить качество получаемого чугуна. Приведенные примеры расчетов подтверждают эффективность разработанного инструмента. Представленные результаты

могут быть полезны для специалистов в области автоматизации доменного производства, а также для исследователей, занимающихся анализом и прогнозированием нестабильности технологических процессов.

Ключевые слова: доменная печь, моделирование, нестабильность, информационная система, металлургия, математическая модель

Для цитирования: Спирин Н.А., Гурин И.А., Лавров В.В. Информационно-моделирующая система оценки нестабильности функционирования доменной печи. *Известия вузов. Черная металлургия*. 2025;68(4):402–410. https://doi.org/10.17073/0368-0797-2025-4-402-410

Introduction

The development of information and control systems for blast furnaces aims to create an efficient management framework that ensures stable production while minimizing costs. These systems must account for technological requirements and the specific features of the equipment. To support the advancement of an automated system for analyzing the operating parameters of individual furnaces and the blast furnace shop as a whole, an information modeling system is being developed to assess process instability in blast furnace operations [1].

Fluctuations in charge composition [2 – 4] and smelting parameters [5 – 7] can significantly impact furnace performance. These variations affect the composition and temperature of the hot metal and lead to pressure losses in the burden's gas column. As a result, key parameters may exceed the limits defined by hot metal quality requirements and the need to maintain steady furnace operation under varying counterflow conditions [8; 9]. Several factors directly influence the furnace's thermal state and the resulting temperature and composition of the hot metal. These include the iron content in the charge, moisture and ash content of the coke, blast air temperature and humidity, natural gas consumption, the ratio of iron-bearing materials to coke, and their distribution at the furnace top [10 – 12]. Variations in these parameters lead to fluctuations in the furnace's thermal balance, causing deviations in the average silicon content and temperature of the hot metal. Instability in the smelting process, especially when using iron ore feedstock with variable chemical composition, can significantly degrade the quality of the molten blast furnace products. For example, reference data [5] show that reducing fluctuations in sinter basicity (CaO/SiO_2) by ±(0.075 – 0.100) units can increase blast furnace productivity by 1.5 % and lower specific coke consumption by 0.8 %.

The total potential benefit of reducing variability in blast furnace parameters is estimated at a 5 – 6 % reduction in coke consumption and a 9 – 10 % increase in productivity. Moreover, a 0.1 % reduction in the standard deviation of iron content in the burden results in a 0.28 % decrease in coke consumption and a 0.29 % increase in productivity [2]. Organizational factors that affect the process include furnace downtime, idle running, regularities in burden charging, and tapping schedules. The impact of some of these factors remains poorly studied and is proposed to be evaluated using empirical data [13 – 15]. These include the mechanical and physicochemical properties of raw materials and coke, as well as gas distribution within the furnace. Assessing their influence requires further research and development of mathematical process models.

Existing systems often lack the precision or flexibility to fully account for all factors affecting operational stability. This highlights the need for advanced information-based modeling systems capable of handling multiple variables and providing real-time analysis of blast furnace instability.

Algorithmic support of the information modeling system

To assess the smelting process stability, the following key integral indicators (B_1) have been developed:

1. Technical, economic, and technological performance indicators of smelting (B_1).

2. Indicators of raw material properties (iron ore materials, coke, fluxes) (B_2).

3. Indicators of blast and gas dynamic modes (B_3).

4. Indicators of the thermal mode (B_4).

5. Indicators of the slag mode (B_5).

6. An integral indicator of blast furnace operating stability based on B_3, B_4, B_5, characterizing the blast, gas-dynamic, thermal, and slag modes (B_{BF}).

7. Final stability indicator of raw material properties and overall blast furnace operation (B_{final}).

The types and number of features used in the assessment depend on the specific integral indicator being calculated.

In addition to controlled (measured) parameters, the stability assessment incorporates a set of calculated parameters that describe the blast conditions, gas dynamics, thermal and slag modes, and the technological parameters of blast furnace smelting, as detailed in [16 – 18].

The approximate number of features used for evaluating each integral indicator is provided in the Table.

For a given time interval of blast furnace operation, the root mean square (RMS) deviations ΔX_i of both controlled and calculated features are used as input data for computing each integral indicator (B_1).

Under stable operating conditions, the RMS deviation ΔX_i of the i-th feature – used to characterize furnace stability during the specified period – must not exceed a predefined threshold value ΔX_i^{pre}, which is a model setting:

Number of features used to calculate the stability indicators of the furnace operation

Количество признаков, используемых для расчета показателей стабильности работы печи

Designation	Indicator	Number of features		
		Controlled	Calculated	Total
B_1	Technical, economic, and technological performance indicators	6	6	12
B_2	Raw material properties (iron ore materials, coke, fluxes)	16	0	16
Blast furnace stability indicators				
B_3	Blast and gas dynamic modes	9	10	19
B_4	Thermal mode	4	7	11
B_5	Slag mode	6	4	10
Total features		41	27	68

$$\Delta X_i \le \Delta X_i^{\text{pre}}. \quad (1)$$

If condition (1) is satisfied (“True”), the i-th feature identifier P_i is assigned a value of 1; otherwise (“False”), it is assigned a value of 0. All features are then ranked. Each feature is assigned a normalized rank value R_i, ranging from 0 to 1, determined using an expert evaluation method.

The stability of blast furnace operation for each of the integral indicators B_j is calculated using the following relationship:

$$B_j = \left(\sum_{i=1}^{n} P_i \frac{R_i}{\sum_{i=1}^{n} R_i} \right) \cdot 100\ \%, \quad (2)$$

where n is the number of features associated with the given integral indicator B_j.

If the resulting value of B_j exceeds 80 % (according to normative and reference data), the furnace operation is considered stable with respect to that indicator.

If B_j falls within the range of 60 – 80 %, the furnace operation is assessed as unstable with respect to that indicator.

If B_j is below 60 %, the blast furnace is considered to have operated in an unstable mode for the corresponding integral indicator.

To determine the overall stability criteria for furnace operation and process conditions, the following integral indicators are calculated:

– the integral indicator of blast furnace operating stability B_{BF}, based on B_3, B_4, B_5, characterizing the blast, gas-dynamic, thermal, and slag modes:

$$B_{\text{BF}} = \left(\sum_{i=3}^{5} B_i \frac{R_i}{\sum_{i=3}^{5} R_i} \right) \cdot 100\ \%, \quad (3)$$

– the final stability indicator of furnace operation:

$$B_{\text{final}} = \frac{B_1 R_1 + B_2 R_2 + B_{\text{BF}} R_{\text{BF}}}{R_1 + R_2 + R_{\text{BF}}}.$$

Key system requirements

Key system requirements are as follows:

– automated data collection: the system must automatically collect real-time data on blast furnace operating parameters;

– real-time visualization: the system must present analysis results in the form of graphs, tables, and charts that are easy for operating personnel to interpret;

– seamless integration: the system should integrate smoothly with the plant’s existing process control systems.

Functional modeling of the information modeling system

The design of the information modeling system is based on functional modeling methodology and the IDEF0 graphical notation for structured analysis and design. The IDEF0 method is founded on the SADT (*Structural Analysis and Design Technique*) [19 – 21]. The model, developed using the Ramus Educational software package [21], consists of more than 50 blocks across four levels of decomposition. These blocks define the system’s key functions, the relationships among functional units, the control inputs, and the execution mechanisms for each function.

Architecture of the information modeling system

The architecture of the developed information modeling system for assessing blast furnace operation instability is shown in Fig. 1. The system is divided into small, independent blocks – modules – each implementing a functionally complete segment of the program. This modular approach allows the functionality of individual

components to be updated without requiring changes to the entire system, enhancing its reliability and scalability. The modules are implemented using mathematical libraries and classes [22].

The information modeling system includes the following modules:

– input module for entering the permissible values of the RMS deviations and the feature ranks (ΔX_i^{pre}, R_i);

– computation module for calculating the arithmetic means and RMS deviations of parameters characterizing the technical, economic, and technological indicators of smelting; the properties of raw materials (iron ore materials, coke, and fluxes); as well as the blast, gas-dynamic, thermal, and slag modes;

– module for calculating stability scores of blast furnace operation for each integral indicator B_j, the overall stability indicator B_{BF}, and the final stability indicator B_{final};

– analysis and output module for processing and presenting the results.

The output from the calculation modules is analyzed and presented in both numerical and graphical formats. The system also provides the option to generate and export reports in Microsoft Excel format.

Software implementation of the Information modeling system

The software implementation of the information modeling system is based on a client–server architecture, designed to to enable seamless integration with existing enterprise software and facilitate data exchange via an API (*Application Programming Interface*) [23]. The client–server model follows a classic three-tier architecture consisting of the presentation layer, application layer, and data layer.

The presentation layer is implemented using high-level web technologies: JavaScript, HTML5, and CSS (*Cascading Style Sheets*). The visual design is built using the Bootstrap *framework*, and the user interface is developed with the UmiJS and React libraries. Graph plotting is handled by Ant Design Charts. This layer is supported by the users' computing resources – specifically, their web browsers.

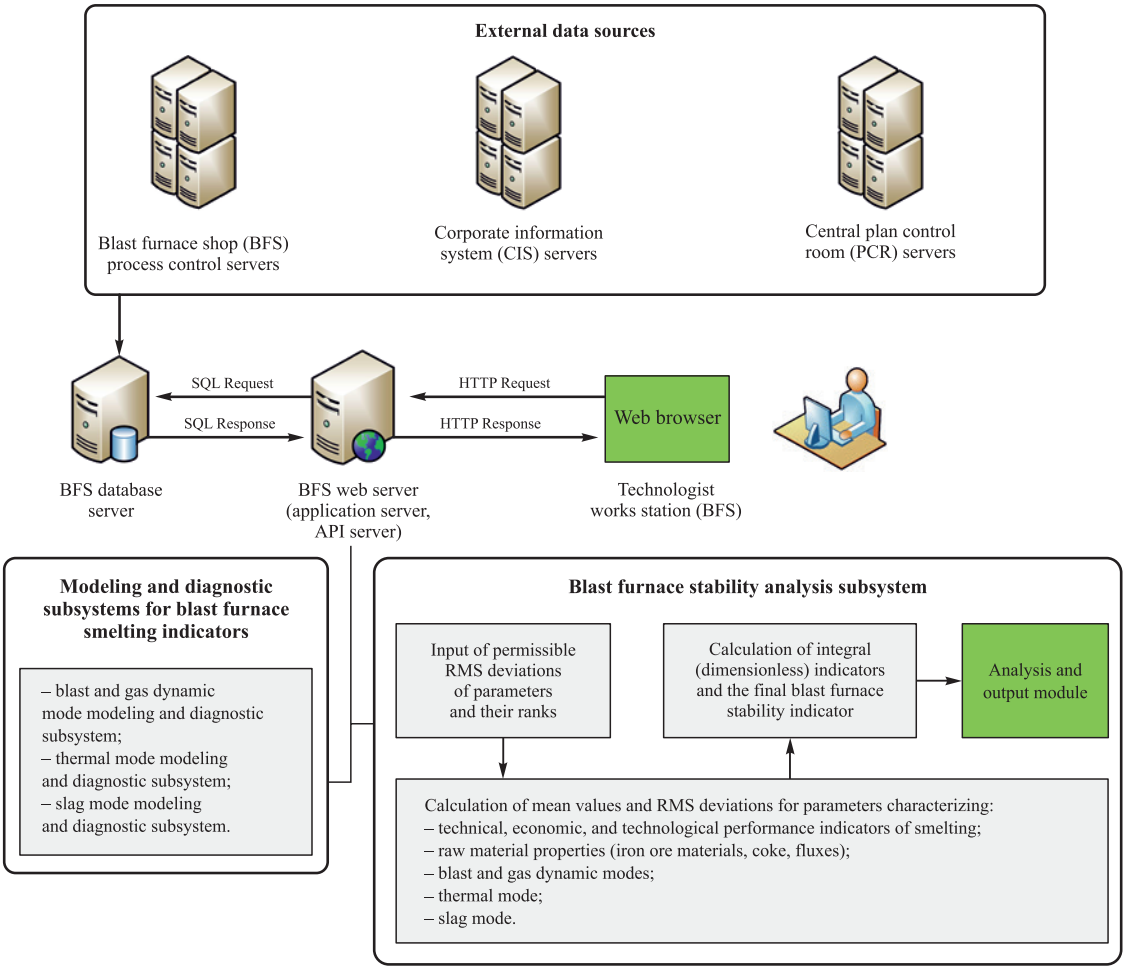

Fig. 1. Architecture of the information modeling system for assessing the instability of a blast furnace

Рис. 1. Архитектура информационно-моделирующей системы оценки нестабильности функционирования доменной печи

The application layer is developed in C# using the ASP.NET Core MVC framework and the .NET 8 platform [24]. ASP.NET Core handles user requests through a middleware pipeline, which includes the following components.

Error handling middleware, which enables the system to signal software-related issues when exceptions occur, and to continue functioning properly, including correctly displaying web pages in cases such as database connection failures, calculation algorithm errors, and other similar situations.

Authentication middleware, which integrates the standard ASP.NET Identity mechanism for authentication and authorization into the information system and manages user accounts.

Session middleware, which processes temporary user data during system usage.

Web API middleware, which incorporates the routing system, dependency injection, model binding, and data validation.

The data layer consists of a database and software components for managing read/write access. The system uses PostgreSQL as the database management system. Communication between the application and the database is handled via Entity Framework Core, which uses ORM (*Object-Relational Mapping*) technology. ORM allows developers to work with data as objects or classes in object-oriented programming languages and to build virtual database schemas. Input of initial blast furnace operation data for a given time period can be carried out either through the API and integration with the blast furnace process control systems (PCS) or manually.

Description of the information modeling system software functions

The developed software module provides the following capabilities:

1. Selection of operating periods via a calendar interface, with the option to set the data averaging interval (hour, shift, day, week, or hot metal tapping period).

2. Selection of one or more blast furnaces to be included in the analysis.

3. Calculation of average values and RMS deviations for a set of operational indicators.

4. Presentation of analysis results in an intuitive format, including tables and histograms; individual blast furnaces can be assigned distinct colors for baseline and comparison periods.

5. Notification of out-of-range values, with customizable alerts configured for all or selected blast furnaces.

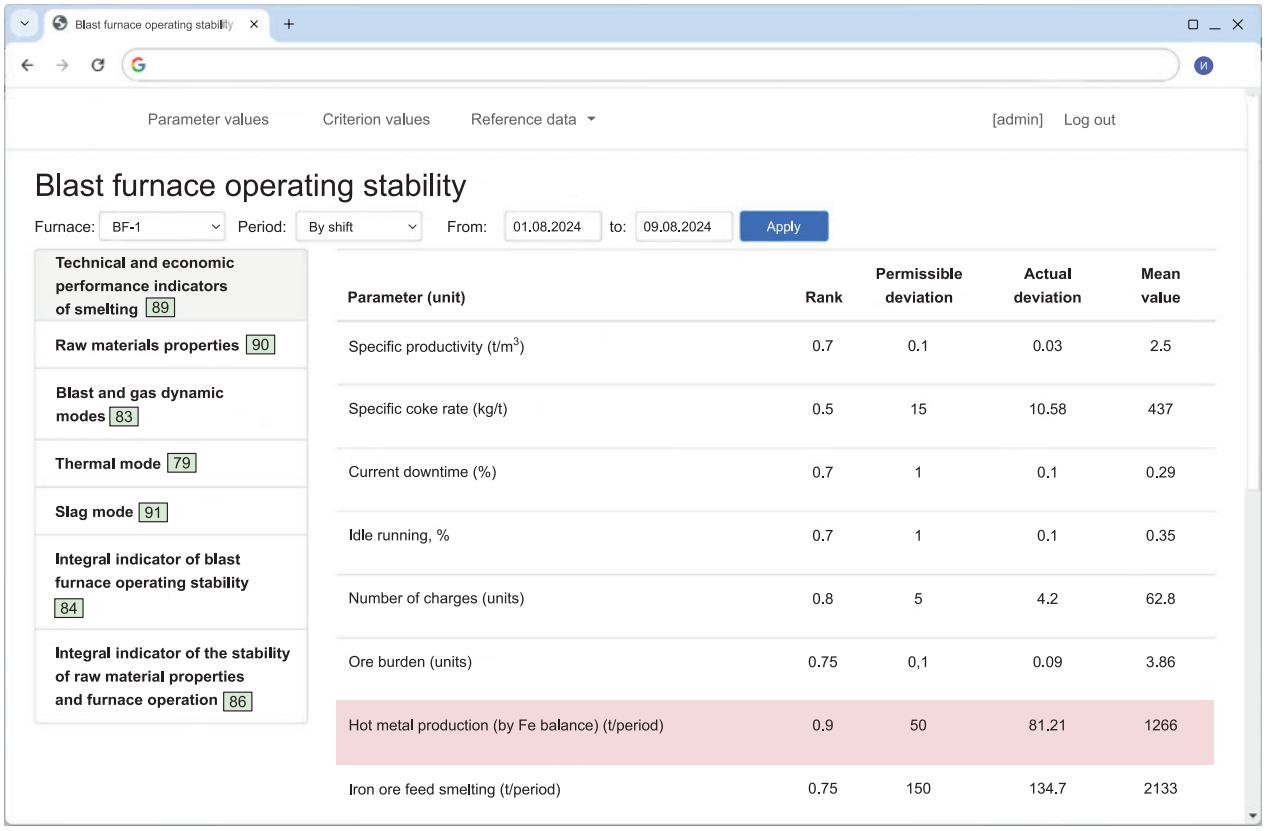

Fig. 2. Fragment of a web page for assessing the instability of technical, economic and technological indicators of a blast furnace

Рис. 2. Фрагмент веб-страницы оценки нестабильности технико-экономических и технологических показателей доменной печи

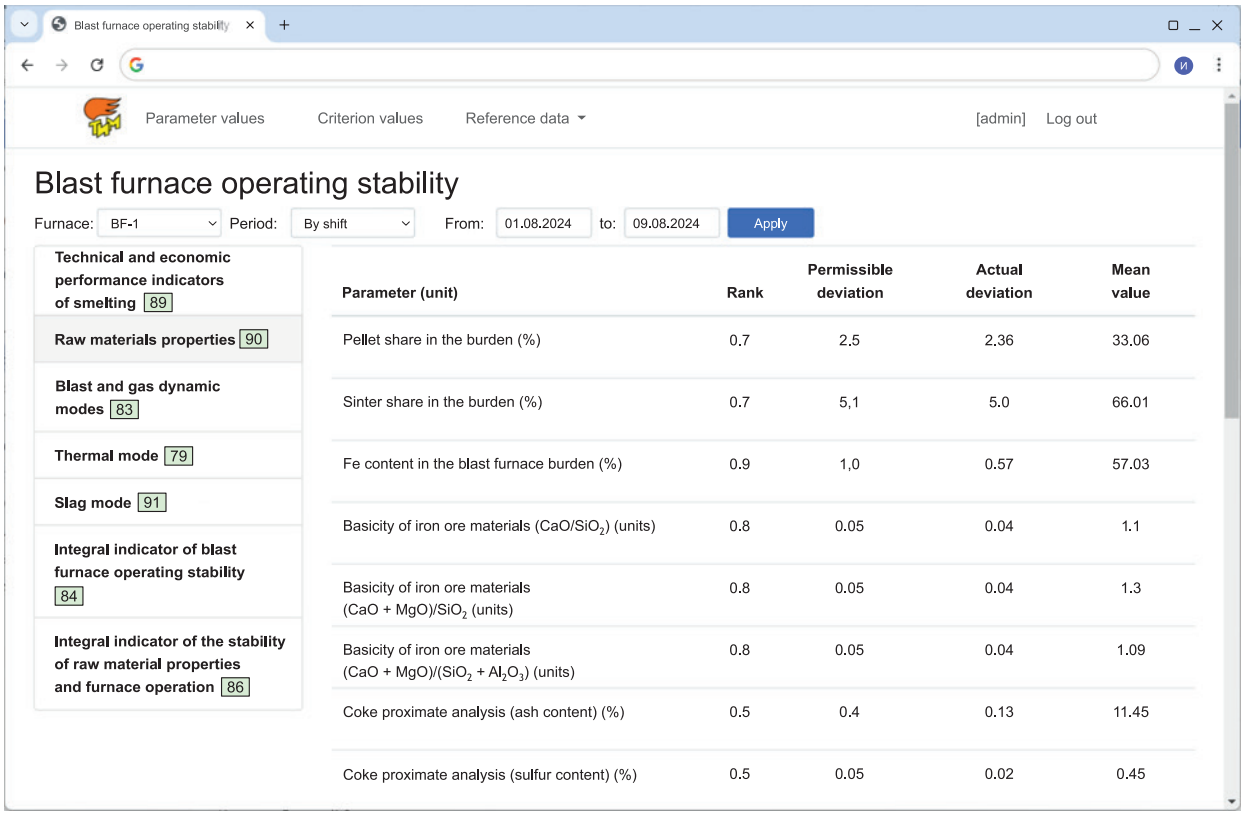

Fig. 3. Fragment of a web page for assessing the instability of raw material properties (iron ore materials, coke, fluxes)

Рис. 3. Фрагмент веб-страницы оценки нестабильности свойств сырья (железорудных материалов, кокса, флюсов)

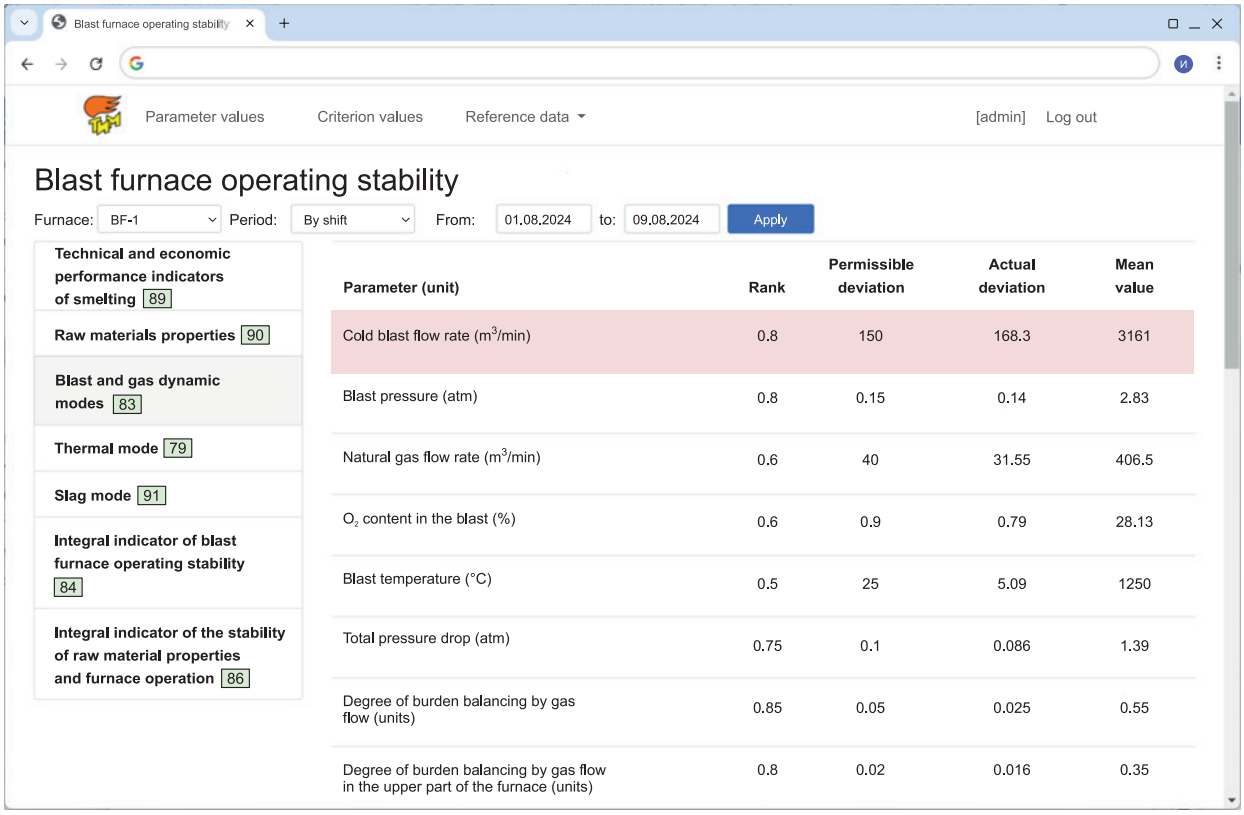

Fig. 4. Fragment of a web page for assessing the instability of indicators of blast and gas dynamic modes of a blast furnace

Рис. 4. Фрагмент веб-страницы оценки нестабильности показателей дутьевого и газодинамического режимов доменной печи

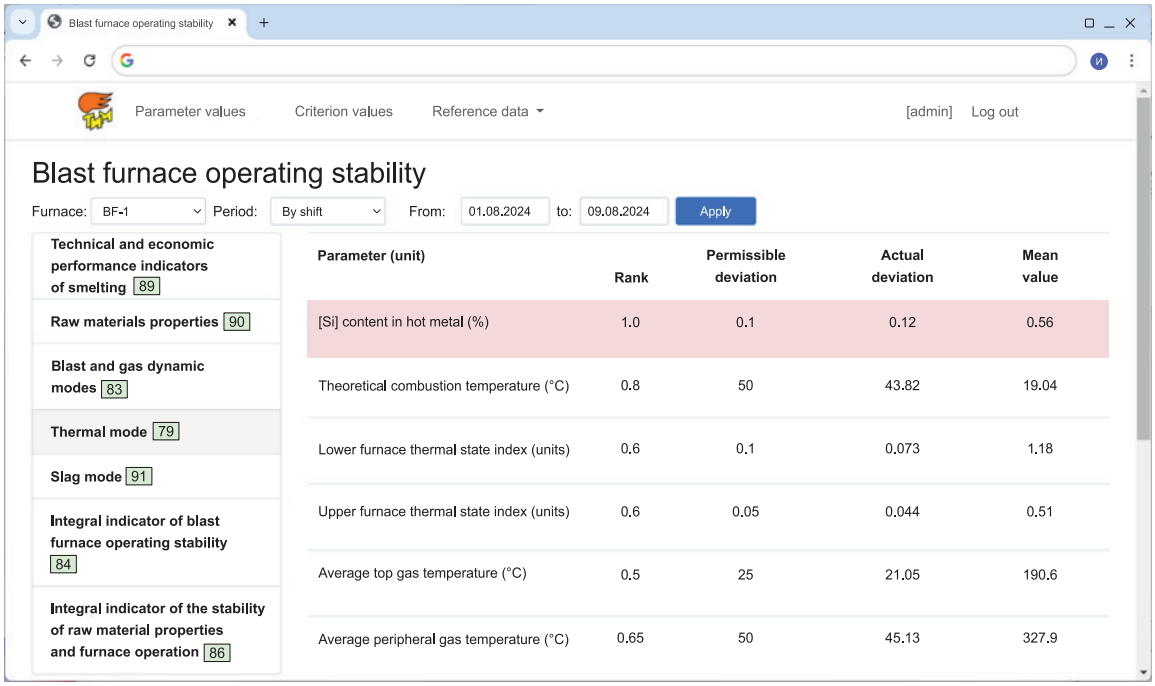

Fig. 5. Fragment of a web page for assessing the instability of thermal mode indicators

Рис. 5. Фрагмент веб-страницы оценки нестабильности показателей теплового режима

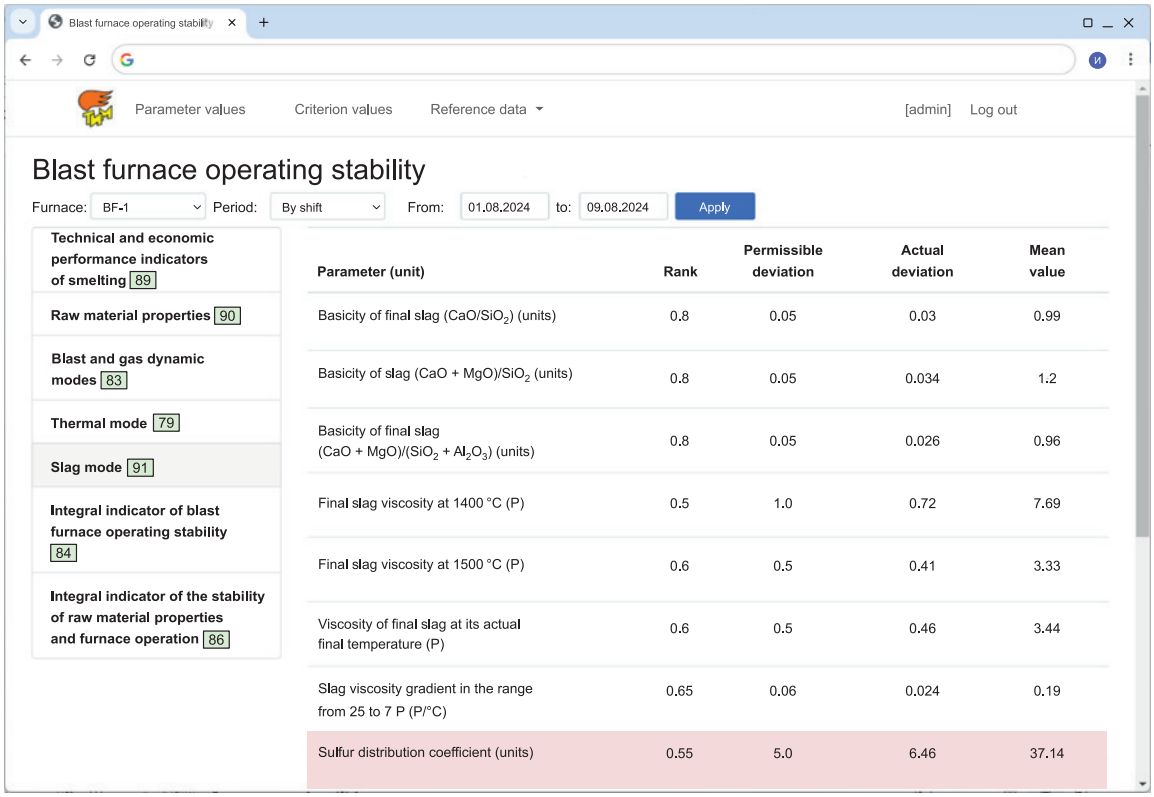

Fig. 6. Fragment of a web page for assessing the instability of slag mode indicators

Рис. 6. Фрагмент веб-страницы оценки нестабильности показателей шлакового режима

Figs. 2 – 6 show fragments of the system's web interface illustrating the modeling results of blast furnace instability assessment.

For the analyzed period, the modeling results indicated stable operation with respect to technical, economic, and technological indicators, raw material properties, blast

and gas dynamic modes, and the slag mode. However, instability was observed in the thermal mode. The values of the integral indicators exceeded 80 %, indicating overall stable operation of the blast furnace.

Conclusions

Using modern information technologies, an information modeling system has been developed for evaluating the instability of blast furnace operation. The system supports automated data collection and processing, and calculates a set of parameters that characterize the technical, economic, and technological performance of the smelting process, raw material properties, and the thermal, blast, and gas dynamic modes, as well as the processing of molten blast furnace products.

References / Список литературы

1. Spirin N.A., Lavrov V.V., Gurin I.A., Zubakov S.V. Evaluation of blast furnace instability. In: *Automation Systems (in Education, Science and Production) AS'2024. Proceedings of the All-Rus. Sci. and Pract. Conf. (with Int. Participation).* Novokuznetsk: SibSIU; 2024:167–171. (In Russ.).

   Спирин Н.А., Лавров В.В., Гурин И.А., Зубаков С.В. Оценка нестабильности функционирования доменной печи. В кн.: *Системы автоматизации (в образовании, науке и производстве) AS'2024. Труды Всероссийской научно-практической конференции (с международным участием).* Новокузнецк: ИЦ СибГИУ; 2024:167–171.
2. Tovarovskii I.G. Blast-Furnace Smelting. Dnepropetrovsk: Porogi; 2009:768. (In Russ.).

   Товаровский И.Г. Доменная плавка. Днепропетровск: Пороги; 2009:768.
3. Tovarovsky I.G., Merkulov A.E. Analytical study of blast-furnace smelting processes and modes at various iron contents in the charge. *Ferrous Metallurgy. Bulletin of Scientific, Technical and Economic Information*. 2010;(4(1324)): 19–27. (In Russ.).

   Товаровский И.Г., Меркулов А.Е. Аналитическое исследование процессов и режимов доменной плавки при различных содержаниях железа в шихте. *Черная металлургия. Бюллетень научно-технической и экономической информации*. 2010;(4(1324)):19–27.
4. Gerdes M., Chenault R., Kurunov I., Lingardi O., Ricketts D. Modern Blast Furnace Process. Moscow: Metallurgizdat; 2016:280. (In Russ.).

   Современный доменный процесс / М. Геердес, Р. Ченьо, И. Курунов, О. Лингарди, Д. Риккетс. Москва: Металлургиздат; 2016:280.
5. Ostroukhov M.Ya., Shparber L.Ya. Guide of Blast Furnace Master. Moscow: Metallurgiya; 1977:304. (In Russ.).

   Остроухов М.Я., Шпарбер Л.Я. Справочник мастера-доменщика. Москва: Металлургия; 1977:304.
6. Bolshakov V.I., Semenov Y.S., Ivancha N.G., Vishnyakov V.I., Shumelchik E.I., Podkorytov A.L., Semion I.Y., Kuznetsov A.M., Zubenko A.V. Study of the flow of burden materials and their distribution on the furnace top of a modern blast furnace. *Metallurgical and Mining Industry*. 2012;4(3):158–165.
7. Bol'shakov V.I. The Technology of High-Efficiency Energy-Saving Blast Furnace Smelting. Kyiv: Naukova dumka; 2007:411. (In Russ.).

   Большаков В.И. Технология высокоэффективной энергосберегающей доменной плавки. Киев: Наукова думка; 2007:411.
8. Bol'shakov V.I., Murav'eva I.G., Semenov Yu.S. Forecasting the thermal condition of blast furnace hearth. *Stal'*. 2009;(5):7–9. (In Russ.).

   Большаков В.И., Муравьева И.Г., Семенов Ю.С. Прогнозирование теплового состояния горна доменной печи. *Сталь*. 2009;(5):7–9.
9. Babarykin N.N. Theory and Technology of Blast Furnace Process. Magnitogorsk: MSTU; 2009:257. (In Russ.).

   Бабарыкин Н.Н. Теория и технология доменного процесса. Магнитогорск: МГТУ; 2009;257.
10. Fojtik D., Tuma J., Faruzel P. Computer modelling of burden distribution in the blast furnace equipped by a bell-less top charging system. *Ironmaking & Steelmaking*. 2021;48(10):1226–1238. https://doi.org/10.1080/03019233.2021.1952829
11. Cameron I., Sukhram M., Lefebvre K., Davenport W. Blast Furnace Ironmaking: Analysis, Control and Optimization. 1st ed. Elsevier Science; 2019:828. https://doi.org/10.1016/C2017-0-00007-1
12. Gordon Y., Izumskiy N., Matveienko G., Chaika O., Lebid V., Vyshinskya O. Diagnostics, optimization and mathematical models of coke-sinter-hot metal production process. In: *AISTech 2019 – Proceedings of the Iron & Steel Technology Conference*. 2019;2019:479–484. https://doi.org/10.33313/377/050
13. Agrawal A., Agarwal M.K., Kothari A.K., Mallick S. A mathematical model to control thermal stability of blast furnace using proactive thermal indicator. *Ironmaking & Steelmaking*. 2019;46(2):133–140. https://doi.org/10.1080/03019233.2017.1353765
14. Ueda S., Natsui S., Nogami H., Yagi J., Ariyama T. Recent progress and future perspective on mathematical modeling of blast furnace. *ISIJ International*. 2010;50(7):914–923. https://doi.org/10.2355/isijinternational.50.914
15. Taylor A.G. The application of principal component analysis for predicting blast furnace stability. *IFAC Proceedings Volumes*. 1998;31(23):223–226. https://doi.org/10.1016/S1474-6670(17)35884-6
16. Pavlov A.V., Onorin O.P., Spirin N.A., Lavrov V.V., Gurin I.A. Some Issues of Technology, Management and Diagnostics of Blast Furnace Smelting. Yekaterinburg: AMK "Den' RA"; 2023:282. (In Russ.).

   Некоторые вопросы технологии, управления и диагностики доменной плавки: монография / А.В. Павлов, О.П. Онорин, Н.А. Спирин, В.В. Лавров, И.А. Гурин. Екатеринбург: АМК «День РА»; 2023:282.
17. Spirin N.A., Lavrov V.V., Rybolovlev V.Yu., Krasnobaev A.V., Onorin O.P., Kosachenko I.E. Model Decision Support Systems in the Automated Process Control System of Blast Furnace. Yekaterinburg: UrFU; 2011:462. (In Russ.).

   Модельные системы поддержки принятия решений в АСУ ТП доменной плавки: монография / Н.А. Спирин, В.В. Лавров, В.Ю. Рыболовлев, А.В. Краснобаев, О.П. Онорин, И.Е. Косаченко. Екатеринбург: УрФУ; 2011:462.

18. Spirin N.A., Lavrov V.V., Rybolovlev V.Yu., Gileva L.Yu., Krasnobaev A.V., Shvydkii V.S., Onorin O.P., Shchipanov K.A., Burykin A.A. Mathematical Modeling of Metallurgical Processes in Automated Process Control. Yekaterinburg: UrFU; 2014:558. (In Russ.).

Математическое моделирование металлургических процессов в АСУ ТП / Н.А. Спирин, В.В. Лавров, В.Ю. Рыболовлев, Л.Ю. Гилева, А.В, Краснобаев, В.С. Швыдкий, О.П. Онорин, К.А. Щипанов, А.А. Бурыкин; под ред. Н.А. Спирина. Екатеринбург: УрФУ; 2014:558.

19. Methodology of functional modeling IDEF0. State standard of Russia. Moscow: IPK "Izdatel'stvo standartov"; 2000:75.

Методология функционального моделирования IDEF0. Госстандарт России. Москва: ИПК «Издательство стандартов»; 2000:75.

20. Waissi G.R., Demir M., Humble J.E., Lev B. Automation of strategy using IDEF0 – A proof of concept. *Operations Research Perspectives*. 2015;2:106–113. https://doi.org/10.1016/j.orp.2015.05.001

21. Popov A.I. Free Tools for Designing Information Systems. Moscow: IPK "Izdatel'stvo standartov"; 2014;78. (In Russ.).

Попов А.И. Свободные инструменты проектирования информационных систем. Москва: ИПК «Издательство стандартов»; 2014:78.

22. Gurin I.A., Lavrov V.V., Spirin N.A., Nikitin A.G. Web-technologies for construction of automated information-modeling systems of technological processes in metallurgy. *Izvestiya. Ferrous Metallurgy*. 2017;60(7):573–579. (In Russ.). https://doi.org/10.17073/0368-0797-2017-7-573-579

Гурин И.А., Лавров В.В., Спирин Н.А., Никитин А.Г. Веб-технологии построения автоматизированных информационно-моделирующих систем технологических процессов в металлургии. *Известия вузов. Черная металлургия*. 2017;60(7):573–579. https://doi.org/10.17073/0368-0797-2017-7-573-579

23. Peralta J.H. Microservice APIs in Python: Using Python, Flask, Fastapi, Openapi and More. Manning Publications; 2023:425.

Перальта Х. Микросервисы и API. Санкт-Петербург: Питер; 2024:464.

24. Price M.J. C# 10 and .NET 6 – Modern Cross-Platform Development. 6th Ed. Packt Publishing; 2021:826.

Прайс М. C# 10 и .NET 6. Современная кросс-платформенная разработка, 6-е изд.: пер. с англ. Санкт-Петербург: Питер; 2023:848.

Information about the Authors / Сведения об авторах

Nikolai A. Spirin, *Dr. Sci. (Eng.), Prof., Head of the Chair "Thermal Physics and Informatics in Metallurgy"*, Ural Federal University named after the First President of Russia B.N. Yeltsin
ORCID: 0000-0001-6582-3428
E-mail: n.a.spirin@urfu.ru

Ivan A. Gurin, *Cand. Sci. (Eng.), Assist. Prof. of the Chair "Thermal Physics and Informatics in Metallurgy"*, Ural Federal University named after the First President of Russia B.N. Yeltsin
ORCID: 0000-0002-4989-7029
E-mail: ivan.gurin@urfu.ru

Vladislav V. Lavrov, *Dr. Sci. (Eng.), Prof. of the Chair "Thermal Physics and Informatics in Metallurgy"*, Ural Federal University named after the First President of Russia B.N. Yeltsin
ORCID: 0000-0002-6953-5519
E-mail: v.v.lavrov@urfu.ru

Николай Александрович Спирин, *д.т.н., профессор, заведующий кафедрой теплофизики и информатики в металлургии*, Уральский федеральный университет имени первого Президента России Б.Н. Ельцина
ORCID: 0000-0001-6582-3428
E-mail: n.a.spirin@urfu.ru

Иван Александрович Гурин, *к.т.н., доцент кафедры теплофизики и информатики в металлургии*, Уральский федеральный университет имени первого Президента России Б.Н. Ельцина
ORCID: 0000-0002-4989-7029
E-mail: ivan.gurin@urfu.ru

Владислав Васильевич Лавров, *д.т.н., профессор кафедры теплофизики и информатики в металлургии*, Уральский федеральный университет имени первого Президента России Б.Н. Ельцина
ORCID: 0000-0002-6953-5519
E-mail: v.v.lavrov@urfu.ru

Contribution of the Authors / Вклад авторов

N. A. Spirin – creating the article idea, justifying the topic relevance, conceptualization, preparing a detailed plan and draft version of the article, preparing examples of practical implementation of modern information systems in industry, selecting references, final editing, preparing a conclusion.
I. A. Gurin – development of the sections content related to the development and software implementation of modern information systems in metallurgy, preparing abstracts and keywords, translation of the article materials into English.
V. V. Lavrov – development of the main sections content, selection and verification of references, preparing of the article materials for publication.

Н. А. Спирин – идея статьи, обоснование актуальности темы, подготовка концепции, развернутого плана и чернового варианта статьи, подготовка примеров практической реализации современных информационных систем в промышленности, подбор библиографических ссылок, окончательная правка, подготовка заключения.
И. А. Гурин – проработка содержания разделов, связанных с разработкой и программной реализацией современных информационных систем в металлургии; подготовка аннотации и ключевых слов, перевод на английский язык материалов статьи.
В. В. Лавров – проработка содержания основных разделов, подбор и проверка библиографических ссылок, подготовка материалов статьи к публикации.

Received 22.02.2025
Revised 21.03.2025
Accepted 24.03.2025

Поступила в редакцию 22.02.2025
После доработки 21.03.2025
Принята к публикации 24.03.2025

INFORMATION TECHNOLOGIES AND AUTOMATIC CONTROL IN FERROUS METALLURGY / **ИНФОРМАЦИОННЫЕ ТЕХНОЛОГИИ И АВТОМАТИЗАЦИЯ В ЧЕРНОЙ МЕТАЛЛУРГИИ**

UDC 669.162.212.9:669.162.211.1
DOI 10.17073/0368-0797-2025-4-411-416

Original article
Оригинальная статья

Mathematical model of the blast furnace main trough lining condition

A. N. Dmitriev[1], D. A. Vit'kin[2], M. O. Zolotykh[1], G. Yu. Vit'kina[1]

[1] **Institute of Metallurgy named after Academician N.A. Vatolin, Ural Branch of the Russian Academy of Sciences** (101 Amundsena Str., Yekaterinburg 620016, Russian Federation)
[2] **JSC Kalugin** (33 Mira Str., Yekaterinburg 620078, Russian Federation)

20procents@mail.ru

Abstract. The main trough of a blast furnace represents a complex technological structure that plays a critical role in the ironmaking process by draining molten cast iron and slag from the furnace hearth, thus ensuring the continuity and safety of the process. The reliable operation of the trough directly impacts the blast furnace productivity. The trough must be designed to withstand extremely high temperatures and aggressive chemical environments, and its proper functioning requires constant monitoring and maintenance. Selection of refractory materials and lining technology, as well as the potential for enhancing the resistance of refractory linings in the main mining troughs and extending their service life, are contingent on the timely acquisition of information regarding the thermal load on the refractory layers and casing, the operating conditions, design characteristics, and destruction processes of refractories in interaction with cast iron and slag. The control systems of the blast furnace main mining trough are designed to ensure its safe and efficient operation, by detecting deviations from normal mode in a timely manner and preventing emergency situations. These systems include visual, instrumental and automatic control. The monitoring system of the main mining troughs heat-up will allow the blast furnace technological personnel to control the condition of troughs, estimate their remaining life and make timely decisions on their repair. The developed mathematical model of the blast furnace main trough lining condition takes into account real-time thermocontrol of the blast furnace mining trough casings. It is aimed at obtaining operative information on the main mining troughs heat-up, and is based on the solution of the problem of stationary heat conduction of a multilayer flat wall, each layer of which is a homogeneous wall.

Keywords: blast furnace, main mining trough, mathematical modelling, thermocouple, heating, lining, temperature, control, algorithm, heat transfer

Acknowledgements: The work was performed within the framework of the State assignment of the Institute of Metallurgy named after Academician N.A. Vatolin, Ural Branch of the Russian Academy of Sciences.

For citation: Dmitriev A.N., Vit'kin D.A., Zolotykh M.O., Vit'kina G.Yu. Mathematical model of the blast furnace main trough lining condition. *Izvestiya. Ferrous Metallurgy*. 2025;68(4):411–416. https://doi.org/10.17073/0368-0797-2025-4-411-416

Математическая модель состояния футеровки главного желоба доменной печи

А. Н. Дмитриев[1], Д. А. Витькин[2], М. О. Золотых[1], Г. Ю. Витькина[1]

[1] **Институт металлургии имени академика Н.А. Ватолина Уральского отделения РАН** (Россия, 620016, Екатеринбург, ул. Амундсена, 101)
[2] **АО «Калугин»** (Россия, 620078, Екатеринбург, ул. Мира, 33)

20procents@mail.ru

Аннотация. Главный горновой желоб доменной печи – это сложная технологическая конструкция, играющая критическую роль в процессе выплавки чугуна. Он служит для отвода расплавленного чугуна и шлака из горна печи, обеспечивая непрерывность и безопасность процесса. Надежная работа желоба напрямую влияет на производительность доменной печи. Конструкция желоба должна выдерживать экстремально высокие температуры и агрессивную химическую среду, а его правильное функционирование требует постоянного контроля и обслуживания. Корректный выбор огнеупорных материалов, технологии футерования, а также выявление возможности повышения стойкости огнеупорной футеровки главных горновых желобов и продления срока их службы определены своевременным получением информации о тепловой нагрузке на слои огнеупоров и кожух, об условиях эксплуатации, конструктивных особенностях и процессах разрушения огнеупоров при их взаимодействии с чугуном и шлаком. Системы контроля работы главного горнового желоба доменной печи призваны обеспечивать безопасную и эффективную его эксплуатацию, своевременно выявляя отклонения от нормаль-

ного режима и предотвращая аварийные ситуации. Они включают в себя визуальный, инструментальный и автоматический контроль. Система мониторинга разгара главных горновых желобов позволит технологическому персоналу доменной печи контролировать состояние желобов, оценивать их остаточный ресурс и принимать своевременные решения об их ремонте. Разработанная математическая модель состояния футеровки главного желоба доменной печи учитывает термоконтроль кожухов горновых желобов в реальном времени. Она нацелена на получение оперативной информации по разгару главных горновых желобов и основана на решении задачи стационарной теплопроводности многослойной плоской стенки, каждый слой которой является однородной стенкой.

Ключевые слова: доменная печь, главный горновой желоб, математическое моделирование, термопара, разгар, футеровка, температура, контроль, алгоритм, теплопередача

Благодарности: Работа выполнена в рамках реализации государственного задания Института металлургии имени академика Н.А. Ватолина Уральского отделения РАН.

Для цитирования: Дмитриев А.Н., Витькин Д.А., Золотых М.О., Витькина Г.Ю. Математическая модель состояния футеровки главного желоба доменной печи. *Известия вузов. Черная металлургия*. 2025;68(4):411–416. https://doi.org/10.17073/0368-0797-2025-4-411-416

Introduction

The blast furnace runner system usually includes a main trough and pouring troughs, with the main trough serving as the location where molten cast iron is separated from slag. Consequently, it operates under the most severe conditions. For this reason, the improvement of its lining receives the greatest attention from both refractory manufacturers and end users.

Available research on heat transfer in the lining of the blast furnace main trough is far more limited compared to studies on the furnace's internal lining. However, in recent years, information from international publications has made it possible to assess the efforts made to study this issue.

In scientific studies addressing molten cast iron – slag separation in blast furnace main troughs, a wide range of methods has been employed, combining experimental and numerical approaches [1 – 3]. Experimental investigations, such as those reported in [4; 5], relied on physical modeling in which analog fluids (e.g., oil and water to simulate cast iron and slag) were used to examine the influence of trough geometry (inclination angle, cross sectional shape) and tapping velocity on phase separation efficiency. In [5], in particular, a 1:10 scale model was utilized to validate the results of numerical simulations.

Numerical modeling plays a central role in analyzing the complex heat and mass transfer processes in the trough [6 – 9]. Researchers have adopted different numerical approaches, including the finite volume method [7] and the finite element method [8 – 11]), solving the Navier–Stokes equations to describe flow hydrodynamics and the heat conduction equation (with allowance for radiation [11 – 13]) to simulate the temperature field. Key factors influencing separation efficiency and lining service life have been considered, such as flow turbulence [7; 9], heat transfer between the melt and the refractory [14 – 17], thermal radiation [10; 12; 13], and refractory wear [10]. For example, in [7] a k–ε turbulence model was applied, while in [10; 13] nonlocal boundary conditions were introduced to account for thermal radiation. In [8], the authors focused on identifying critical isotherms to extend lining service life, employing a two dimensional heat transfer model and comparing simulation results with experimental data. In [10], it was demonstrated that an adaptive time step regulator could be developed to improve the efficiency of long cycle blast furnace simulations.

In most cases, numerical modeling results showed good agreement with experimental data, making it possible to identify the regions of maximum temperature and stress in the lining [14 – 17] – most frequently in the sidewalls – and to predict its wear. Nevertheless, some uncertainties remain, particularly concerning the precise placement of thermocouples for temperature measurement in an operating trough [18 – 20], which necessitates the use of additional data processing techniques (e.g., the GRSA hybrid algorithm [10]) to refine the results. Overall, the combination of experimental and numerical methods has yielded a more comprehensive understanding of the complex processes occurring in blast furnace main troughs and has provided a foundation for developing recommendations to optimize their design and operation.

Input data

This study is devoted to the development of a mathematical model of the refractory lining of the blast furnace main trough, carried out at the Institute of Metallurgy of the Ural Branch of the Russian Academy of Sciences. An algorithm is presented for calculating the temperature field in the refractory lining of the trough based on thermocouple readings obtained from the outer surface of the trough's metal casing.

Fig. 1 shows a general (schematic) top view of two blast furnace main troughs.

The cross section of the refractory lining of the blast furnace main trough is shown in Fig. 2.

Calculation of heat conduction through a multilayer flat wall

The solution of this problem reduces to steady state heat conduction in a multilayer flat wall, each layer

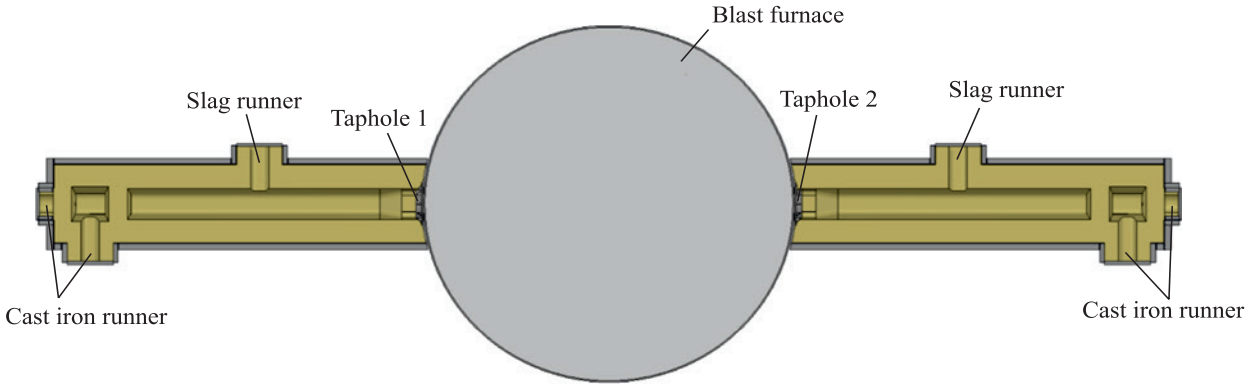

Fig. 1. Main mining troughs of the blast furnace

Рис. 1. Главные горновые желоба доменной печи

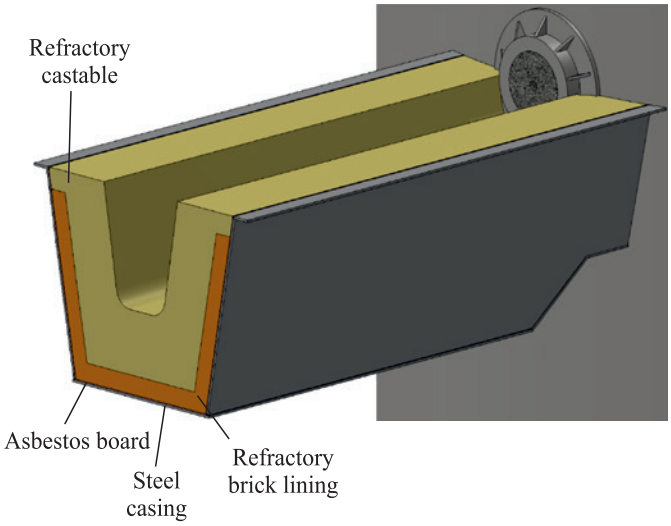

Fig. 2. Main trough lining layers in cross-section

Рис. 2. Слои футеровки главного желоба в поперечном сечении

of which is homogeneous. It is assumed that the total thickness of the multilayer wall, equal to the sum of the thicknesses of the individual layers, is much smaller than the wall's height and width. In this case, the isothermal surfaces are planes parallel to the boundary planes, including the planes of layer interfaces. The individual layers of the wall are assumed to have smooth boundary surfaces that fit tightly together, so that the temperatures of the contacting surfaces are equal (Fig. 3).

When considering heat conduction in a single layer wall, it is observed that the heat flux density does not change when moving from one isothermal surface to another along the x axis, i.e., from left to right.

The plane of the interface between the first and second layers likewise represents an isothermal surface with the same value of heat flux density as in the first layer. However, this plane serves as the "initial" surface for the second layer, in which a constant heat flux density q, equal to that in the first layer, is also established across the thickness δ_2. The same reasoning applies to all subsequent layers (δ_3, etc.).

The total heat flux, and hence its density, does not vary across the thickness of the multilayer flat wall ($Q \neq f(x)$ and $q \neq f(x)$). Therefore, for any i-th layer of the multilayer flat wall, the following relation holds

$$q_s = \frac{\Delta T_i}{\frac{\delta_i}{\lambda_i}} = \text{const}. \qquad (1)$$

This relation can be expressed sequentially for all layers, beginning with the first:

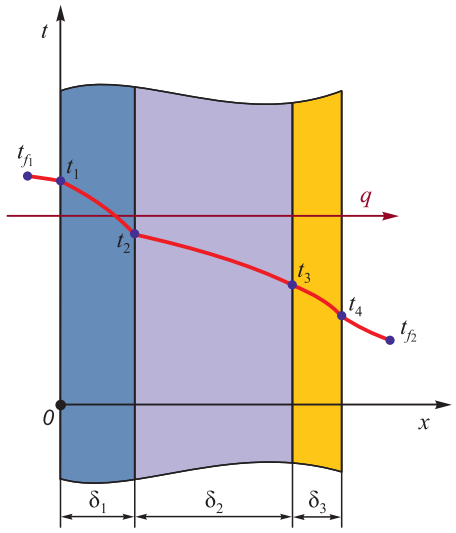

Fig. 3. Multilayer flat wall:
δ_1, δ_2, δ_3 – thickness of the first, second and third layers, respectively;
t_{f_1}, t_{f_2} – temperatures of hot and cold fluids, respectively;
t_1, t_4 – temperatures at the outer boundaries;
t_2, t_3 – temperatures at the plane of the layers interface

Рис. 3. Многослойная плоская стенка:
δ_1, δ_2, δ_3 – толщина первого, второго и третьего слоев соответственно; t_{f_1}, t_{f_2} – температуры горячего и холодного флюидов соответственно; t_1, t_4 – температуры на наружных границах; t_2, t_3 – температуры на плоскости раздела слоев

$$q_s = \frac{T_{f_1} - T_1}{\frac{1}{\alpha_1}} = \frac{T_1 - T_2}{\frac{\delta_1}{\lambda_1}} = \frac{T_2 - T_3}{\frac{\delta_2}{\lambda_2}} = \frac{T_3 - T_4}{\frac{\delta_3}{\lambda_3}} = \frac{T_4 - T_{f_2}}{\frac{1}{\alpha_2}}. \quad (2)$$

We then transform the obtained expressions into $q\frac{1}{\alpha_1} = T_{f_1} - T_2$ and sum them (combining left-hand sides with left-hand sides and right-hand sides with right-hand sides):

$$q\left(\frac{1}{\alpha_1} + \frac{\delta_1}{\lambda_1} + \frac{\delta_2}{\lambda_2} + \frac{\delta_3}{\lambda_3} + \frac{1}{\alpha_2}\right) = T_{f_1} - T_{f_2}.$$

These derivations remain valid for an arbitrary number of layers. Thus, in the general case, the expression for the surface heat flux density (q_s) is written as:

$$q_s = \frac{T_{f_1} - T_{f_2}}{\frac{1}{\alpha_1} + \sum_{i=1}^{n}\left(\frac{\delta_i}{\lambda_i} + \frac{1}{\alpha_2}\right)}, \quad (3)$$

where α_1 and α_2 are the heat transfer coefficients from the hot fluid to the wall and from the wall to the cold fluid, respectively, W/(m^2·K); λ is the thermal conductivity of the material, W/(m·K).

Fig. 4 shows a scheme of heat transfer in the blast furnace main trough.

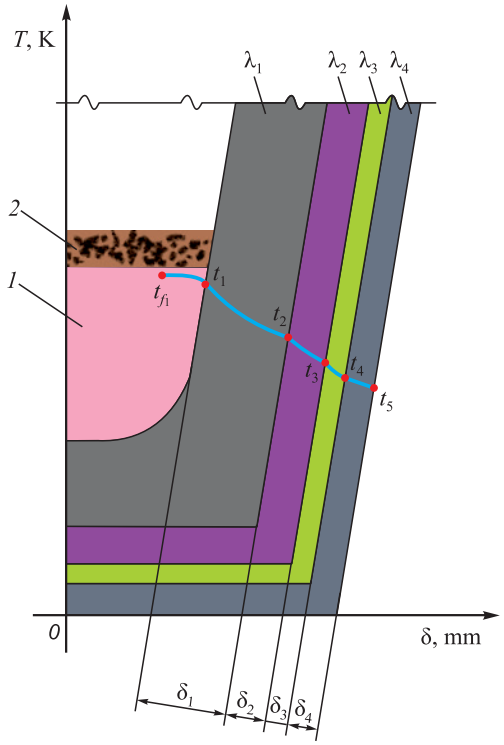

Fig. 4. Scheme of heat transfer of the main trough:
1 – cast iron; *2* – slag

Рис. 4. Схема теплопередачи главного желоба:
1 – чугун; *2* – шлак

Temperature monitoring is performed using thermocouples installed on the casing of the main trough. The lining of the main trough consists of three refractory layers and is enclosed by a steel casing; therefore, in this case, the expression for the surface heat flux density takes the form:

$$q_l = \frac{T_{f_1} - T_5}{\frac{1}{\alpha_1} + \frac{\delta_1}{\lambda_1} + \frac{\delta_2}{\lambda_2} + \frac{\delta_3}{\lambda_3} + \frac{\delta_4}{\lambda_4}}, \quad (4)$$

where T_{f_1} is the temperature of the hot fluid (cast iron, slag), K; T_5 is the casing temperature, measured by a thermocouple (heat removal can be recorded with a sampling interval from 10 s to 24 h), K; α_1 is the heat transfer coefficient from the hot fluid to the inner wall of the trough, W/(m^2·K); δ_1, δ_2, δ_3, δ_4 are the thicknesses of the refractory layers from the innermost to the outermost, m; λ_1, λ_2, λ_3, λ_4 are the thermal conductivities of the refractory materials from the innermost to the outermost, W/(m·K).

In the interfacial regions, the thermophysical properties of the materials are averaged.

Block diagram of the calculation algorithm

A block diagram of the algorithm for calculating the temperature variation across the lining layers is shown in Fig. 5.

Conclusions

The mathematical model developed for the blast furnace main trough lining, based on the solution of the steady state heat conduction problem in a multilayer wall, allows for an efficient evaluation of the thermal load on each refractory layer and the casing in real time (according to the configured heat removal sampling interval). This ensures continuous monitoring of the lining condition, enables prediction of its residual service life (specifically, the thickness of the inner layer), and supports timely decision making regarding repair or replacement. Such capabilities directly enhance the efficiency and safety of blast furnace operation, reduce the risk of emergency situations, and extend the service life of the lining. Future research will aim to further refine the model, for instance by incorporating transient thermal processes (introducing time dependence into the calculations) and by accounting for more complex geometric configurations of the trough.

References / Список литературы

1. Ranjan S., Mazumdar D., Chakraborty I.N., Sinha S., Sarkar R. Review and analysis of metallurgical processes in blast furnace main trough and trough performances. *Transactions of the Indian Institute of Metals*. 2022;75:589–611. https://doi.org/10.1007/s12666-021-02454-9

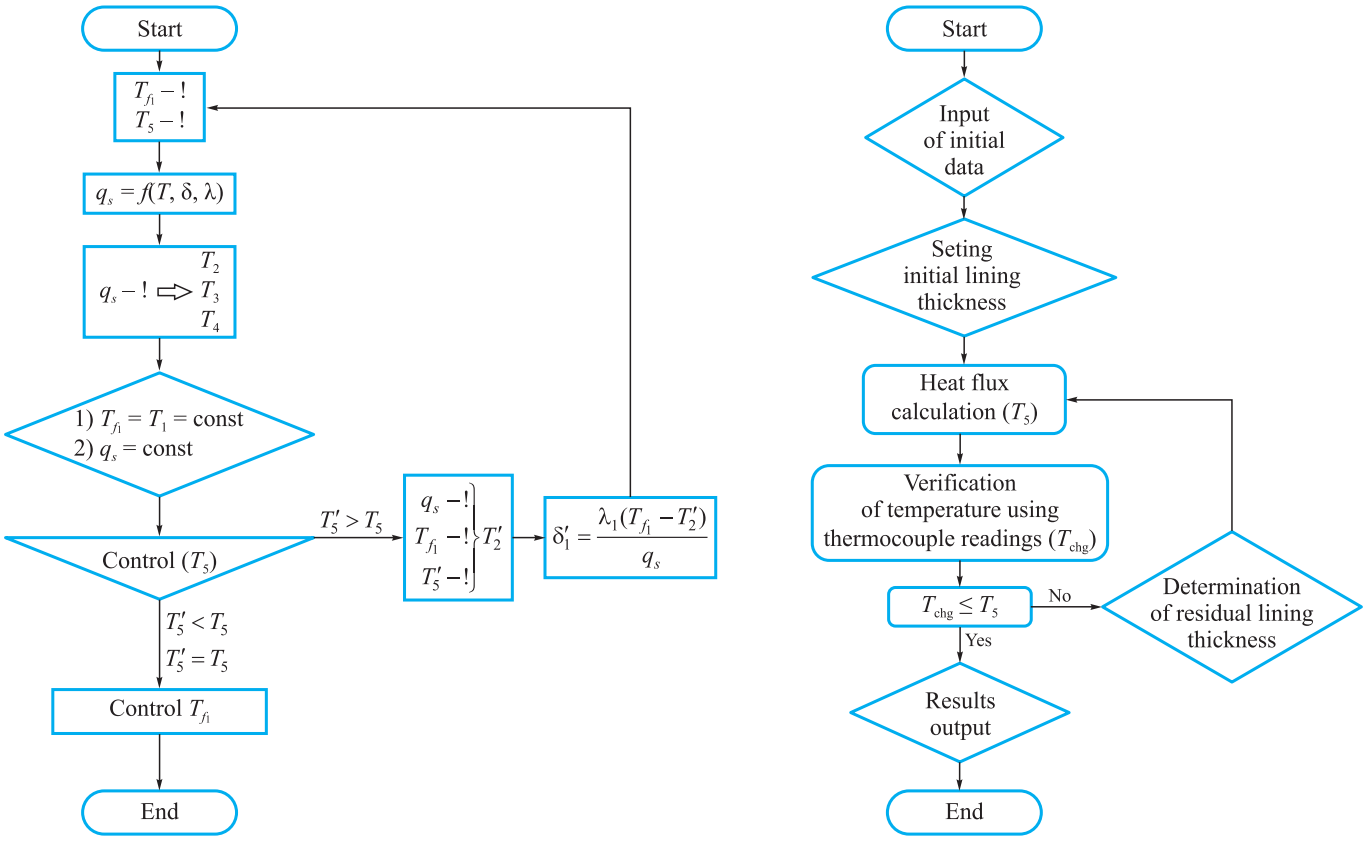

Fig. 5. Block diagram of the algorithm for calculation of temperature change by layers of the blast furnace main trough lining

Рис. 5. Блок-схема и диаграмма алгоритма расчета изменения температуры по слоям футеровки главного желоба доменной печи

2. Kostúr K. Mathematical model for optimisation of a thickness of furnace lining. In: *18th Int. Carpathian Control Conf. (ICCC)*. 2017:52–57. https://doi.org/10.1109/CarpathianCC.2017.7970370
3. Prompt N., Ouedraogo E. High temperature mechanical characterisation of an alumina refractory concrete for Blast Furnace main trough: Part I. General context. *Journal of the European Ceramic Society*. 2008;28(15):2859–2865. https://doi.org/10.1016/j.jeurceramsoc.2008.04.031
4. Kim H., Ozturk B., Fruehan R.J. Slag-metal separation in the blast furnace trough. *ISIJ International*. 1998;38(5):430–439. https://doi.org/10.2355/isijinternational.38.430
5. Monteiro de Oliveira M.J., Rodrigues G., Alves da Silva I., Peixoto J.J.M., da Silva C.A. Modeling of two-phase flow in blast furnace trough. *Steel Research International*. 2021;92(3):2000485. https://doi.org/10.1002/srin.202000485
6. Rezende R.V.P., Silva A.F.C., Maliska C.R. The blast furnace trough two-phase flow and its influence in the refractory lining wear: Mathematical modeling and numerical simulation. In: *Proceedings of the 19th Int. Congress of Mechanical Engineering*. 2007.
7. Ge Y., Li M., Wei H., Liang D. Numerical analysis on velocity and temperature of the fluid in a blast furnace main trough. *Processes*. 2020;8(2):249. https://doi.org/10.3390/pr8020249
8. Vázquez-Fernández S., Pieiga A.G.L., Lausín-González C., Quintela P. Mathematical modelling and numerical simulation of the heat transfer in a trough of a blast furnace. *International Journal of Thermal Sciences*. 2019;137:365–374. https://doi.org/10.1016/j.ijthermalsci.2018.11.025
9. Yao H., Chen H., Ge Y., Wei H. Numerical analysis on erosion and optimization of a blast furnace main trough. *Materials*. 2021;14(17):4851. https://doi.org/10.3390/ma14174851
10. Barral P., Pérez-Pérez L.J., Quintela P. Numerical simulation of the transient heat transfer in a blast furnace main trough during its complete campaign cycle. *International Journal of Thermal Sciences*. 2022;173:107349. https://doi.org/10.1016/j.ijthermalsci.2021.107349
11. Barral P., Pérez-Pérez L.J., Quintela P. Transient 3D hydrodynamic model of a blast furnace main trough. *Engineering Applications of Computational Fluid Mechanics*. 2023;17(1):2280776. https://doi.org/10.1080/19942060.2023.2280776
12. Barral P., Nicolás B., Pérez-Pérez L.J., Quintela P. Numerical simulation of wear related problems in a blast furnace runner. *Recent Advances in Differential Equations and Applications*. 2019;18:229–244. https://doi.org/10.1007/978-3-030-00341-8_14
13. Barral P., Pérez-Pérez L.J., Quintela P. Transient thermal response with nonlocal radiation of a blast furnace main trough. *Applied Mathematical Modelling*. 2022;105:197–225 https://doi.org/10.1016/j.apm.2021.12.029
14. Kou M., Yao S., Wu S., Zhou H., Xu J. Effects of blast furnace main trough geometry on the slag-metal separation based on numerical simulation. *Steel Research International*.

2019;90(2):1800383.
https://doi.org/10.1002/srin.201800383

15. Wang L., Pan C.-N., Cheng W.-T. Numerical analysis on flow behavior of molten iron and slag in main trough of blast furnace during tapping process. *Advances in Numerical Analysis*. 2017;2017(1):713160.
https://doi.org/10.1155/2017/6713160

16. Luomala M.J., Paananen T.T., Köykkä M.J., Fabritius J., Matti T., Nevala H., Härkki J.J. Modelling of fluid flows in the blast furnace trough. *Steel Research*. 2001;72(4):130–135. https://doi.org/10.1002/srin.200100096

17. He Q., Evans G., Zulli P., Tanzil F., Lee B. Flow characteristics in a blast furnace trough. *ISIJ International*. 2002;42(8):844–851.
https://doi.org/10.2355/isijinternational.42.844

18. He Q., Zulli P., Tanzil F., Lee B., Dunning J., Evans G. Flow characteristics of a blast furnace taphole stream and its effects on trough refractory wear. *ISIJ International*. 2002;42(3):235–242. https://doi.org/10.2355/isijinternational.42.235

19. Shao L., Saxén H. A simulation study of Blast furnace hearth drainage using a two-phase flow model of the taphole. *ISIJ International*. 2011;51(2):228–235.
https://doi.org/10.2355/isijinternational.51.228

20. Li Z., Wang H., Ding F., Tang H. Prolonging campaign life of blast furnace trough by water cooling. *Materials*. 2023;16(3):891. https://doi.org/10.3390/ma16030891

Information about the Authors

Andrei N. Dmitriev, *Dr. Sci. (Eng.), Prof., Chief Researcher of the Laboratory of Pyrometallurgy of Reduction Processes*, Institute of Metallurgy named after Academician N.A. Vatolin, Ural Branch of the Russian Academy of Sciences
ORCID: 0000-0001-6446-0215
E-mail: andrey.dmitriev@mail.ru

Dmitrii A. Vit'kin, *Design Engineer*, JSC Kalugin
ORCID: 0009-0004-7023-5734
E-mail: dimantg85@rambler.ru

Maksim O. Zolotykh, *Cand. Sci. (Eng.), Leading Engineer of Laboratory for Pyrometallurgy of Reduction Processes*, Institute of Metallurgy named after Academician N.A. Vatolin, Ural Branch of the Russian Academy of Sciences
ORCID: 0000-0002-8923-9872
E-mail: max@zolotyh.su

Galina Yu. Vit'kina, *Cand. Sci. (Eng.), Leading Researcher, Head of the Laboratory of Pyrometallurgy of Reduction Processes*, Institute of Metallurgy named after Academician N.A. Vatolin, Ural Branch of the Russian Academy of Sciences
ORCID: 0000-0002-1076-2709
E-mail: 20procents@mail.ru

Сведения об авторах

Андрей Николаевич Дмитриев, *д.т.н., главный научный сотрудник лаборатории пирометаллургии восстановительных процессов*, Институт металлургии имени академика Н.А. Ватолина Уральского отделения РАН
ORCID: 0000-0001-6446-0215
E-mail: andrey.dmitriev@mail.ru

Дмитрий Александрович Витькин, *инженер-конструктор*, АО «Калугин»
ORCID: 0009-0004-7023-5734
E-mail: dimantg85@rambler.ru

Максим Олегович Золотых, *к.т.н., ведущий инженер лаборатории пирометаллургии восстановительных процессов*, Институт металлургии имени академика Н.А. Ватолина Уральского отделения РАН
ORCID: 0000-0002-8923-9872
E-mail: max@zolotyh.su

Галина Юрьевна Витькина, *к.т.н., ведущий научный сотрудник, заведующий лабораторией пирометаллургии восстановительных процессов*, Институт металлургии имени академика Н.А. Ватолина Уральского отделения РАН
ORCID: 0000-0002-1076-2709
E-mail: 20procents@mail.ru

Contribution of the Authors

A. N. Dmitriev – formation of the article idea, scientific guidance, development of the research methodology, review and editing of the manuscript.
D. A. Vit'kin – performing calculations, analysis, data processing and discussion, writing the calculation algorithm, visualizing the results.

M. O. Zolotykh – writing the calculation algorithm.
G. Yu. Vit'kina – conceptualization, review preparation, text editing, data analysis and processing, writing the final manuscript.

Вклад авторов

А. Н. Дмитриев – формирование идеи статьи, научное руководство, разработка методологии исследования, рецензирование и редактирование рукописи.
Д. А. Витькин – проведение расчетов, анализ, обработка данных и их обсуждение, написание алгоритма расчета, визуализация результатов.
М. О. Золотых – написание алгоритма расчета.
Г. Ю. Витькина – концептуализация, подготовка обзора и редактирование текста, анализ и обработка данных, написание окончательного варианта рукописи.

Received 21.03.2025
Revised 27.05.2025
Accepted 11.06.2025

Поступила в редакцию 21.03.2025
После доработки 27.05.2025
Принята к публикации 11.06.2025

INFORMATION TECHNOLOGIES AND AUTOMATIC CONTROL IN FERROUS METALLURGY / **ИНФОРМАЦИОННЫЕ ТЕХНОЛОГИИ И АВТОМАТИЗАЦИЯ В ЧЕРНОЙ МЕТАЛЛУРГИИ**

UDC 621.771
DOI 10.17073/0368-0797-2025-4-417-423

Original article
Оригинальная статья

Methodology for calculating the flatness of cold-rolled steel strips

D. L. Shalaevskii

Cherepovets State University (5 Lunacharskogo Ave., Cherepovets, Vologda Region 162600, Russian Federation)

shal-dmitrij@yandex.ru

Abstract. A known cause of flat shape defects in finished cold-rolled steel strips is the inequality of the drawing ratios across the strip width. Difference in the values of these ratios is affected by the roll barrel profiling parameters, energy-power parameters of rolling, operating parameters of the automatic profile and strip shape control system. The impact of all technological factors on the strip shape is complex. The paper considers an approach that takes into account the main operating parameters of rolling equipment allowing to estimate the type and amplitude of flatness defects in finished steel strips. When implementing this approach, 6 calculation stages were performed: energy-power calculation of the cold rolling process; calculation of elastic deformations of the working roll barrel surface; assessment of wear of the working roll barrel surface; calculation of the roll thermal profile; assessment of convexity of the steel strip transverse profile; assessment of flatness indicators of the finished strip. To calculate the parameters affecting the flatness of the rolled product, known calculation methods adapted to specific process conditions were used. The results of assessing the shape indicators of the rolled strip obtained using the model were compared with the results of modeling in the Deform 3D program. The modeling results demonstrated reliability of the proposed approach to assessing the rolled product quality.

Keywords: flatness of cold-rolled steel strips, continuous rolling, rolling mode, shape defects, roll barrel profiling, elastic deformation of roll barrel, thermal profile of roll barrel, defect amplitude

For citation: Shalaevskii D.L. Methodology for calculating the flatness of cold-rolled steel strips. *Izvestiya. Ferrous Metallurgy*. 2025;68(4):417–423. https://doi.org/10.17073/0368-0797-2025-4-417-423

Методика расчета плоскостности стальных холоднокатаных полос

Д. Л. Шалаевский

Череповецкий государственный университет (Россия, 162600, Вологодская обл., Череповец, пр. Луначарского, 5)

shal-dmitrij@yandex.ru

Аннотация. Известной причиной возникновения дефектов плоской формы на готовых стальных холоднокатаных полосах является неравенство коэффициентов вытяжки по ширине полосы. На разницу значений этих коэффициентов оказывают влияние параметры профилировок бочек валков, энергосиловые параметры прокатки, параметры работы системы автоматического регулирования профиля и формы полосы. Воздействие всех технологических факторов на форму полосы будет иметь сложный характер. В работе рассмотрен подход, учитывающий основные параметры работы прокатного оборудования и позволяющий оценить вид и амплитуду дефектов плоскостности готовых стальных полос. При реализации такого подхода выполнены шесть этапов расчета: энергосиловой расчет процесса холодной прокатки; расчет упругих деформаций поверхности бочки рабочего валка; оценка износа поверхности бочки рабочего валка; расчет теплового профиля валка; оценка выпуклости поперечного профиля стальной полосы; оценка показателей планшетности готовой полосы. Для вычисления параметров, влияющих на планшетность проката, использованы известные методики расчета, адаптированные под конкретные технологические условия. Результаты оценки показателей формы катаной полосы, полученные с помощью модели, сопоставлены с результатами моделирования в программе Deform 3D. Результаты моделирования продемонстрировали достоверность предложенного подхода оценки качества проката.

Ключевые слова: плоскостность холоднокатаных стальных полос, непрерывная прокатка, режим прокатки, дефекты формы, профилировка бочки валка, упругая деформация бочки валка, тепловой профиль бочки валка, амплитуда дефекта

Для цитирования: Шалаевский Д.Л. Методика расчета плоскостности стальных холоднокатаных полос. *Известия вузов. Черная металлургия*. 2025;68(4):417–423. https://doi.org/10.17073/0368-0797-2025-4-417-423

Introduction

The primary causes of flatness defects in cold-rolled steel strips are non-uniform deformation across the strip width and low sectional stiffness. The latter is a characteristic feature of flat-rolled products.

Most established studies consider the variation in drawing ratios across the strip width as the main criterion for flatness loss. Among the influencing factors, some are viewed as more critical than others [1 – 18].

Studies [2 – 4] propose flatness criteria based solely on drawing ratio values across the strip width. The research findings reported in [5 – 8] highlight the potential to assess flatness defects through cross-sectional characteristics of the strip.

Models that incorporate multiple technological parameters for evaluating strip flatness are presented in [9 – 11].

Approaches focusing on transverse profile characteristics for identifying flat shape defects are described in [12 – 14].

Further models, found in [15 – 18], attribute flatness loss to post-rolling strip cooling processes.

The flatness evaluation method outlined in [9] enables the calculation of defect amplitudes based on rolling process parameters. This method accounts for nearly all relevant factors, including roll barrel profiling, potential work roll wear, roll axis misalignment, and several other significant influences.

The aim of this study was to develop a method for evaluating the amplitude of waviness and buckling in cold-rolled strips based on the variation in drawing ratios across the width, and to validate it by comparing calculated results with those generated using the DEFORM-3D simulation software.

Problem statement and research methods

Calculating the amplitude of *waviness* or *buckling* in cold-rolled steel strips, based on the variation in drawing ratios across the strip width, requires comprehensive input data. This includes the elastic deformations of the work and backup rolls, the wear of their barrel surfaces, and the non-uniform thermal expansion across the width of the rolled strip.

Study [19] presents a regression-based model describing the elastic deformation of a four-high (“quarto”) mill stand along the work roll barrel. This relationship was derived through numerical simulation of elastic deformations in the roll system and was previously applied to model flatness formation in hot-rolled strips produced on a continuous wide-strip mill. It is also applicable to the integrated method proposed in the present study.

Additional research [20 – 22] offers methods for evaluating barrel surface wear and non-uniform thermal expansion along the roll barrel.

The type and amplitude of flatness defects in cold-rolled strips can be assessed using the methodology described in [23].

The reliability of the calculated results can be verified by evaluating strip shape quality indicators using the DEFORM-3D simulation software.

Results and discussion

The procedure for calculating the type and amplitude of flatness defects in cold-rolled steel strips included the following stages:

– Stage 1: calculation of the energy–power parameters of the cold rolling process;

– Stage 2: analysis of elastic deformation of the work roll barrel surface;

– Stage 3: assessment of wear on the work roll barrel surface;

– Stage 4: calculation of the roll thermal profile;

– Stage 5: evaluation of the convexity of the strip’s transverse profile;

– Stage 6: assessment of flatness parameters of the finished strip.

The first stage was implemented using a model of energy–power parameters that takes into account elastic deformation zones along the deformation zone length [24 – 25].

The second stage involved modeling elastic deformations of the four-high (quarto) mill roll system using a numerical simulation tool for analyzing process mechanics.

To determine the deformation of the work roll barrel surface, taking into account elastic flattening in the contact zones with the backup roll barrel and the strip during rolling, three-dimensional computational models were developed for the work and backup roll sets of a five-stand 1700 mm continuous cold rolling mill.

The roll set was imported into the MechanicalStructure module of ANSYS R1 (Fig. 1).

In the module’s pre-processor, a mesh was generated (Fig. 1). In ANSYS Workbench, high-carbon steel with a yield strength of 900 MPa was assigned as the roll material. To simulate support conditions, boundary constraints were applied to the backup roll necks along the X, Y, and Z axes (vertical direction), and to the work roll necks along the X and Y axes. In the vertical direction, the work roll rested on the backup roll barrel.

During the creation of the solid model, a specific region was defined on the surface of the work roll barrel

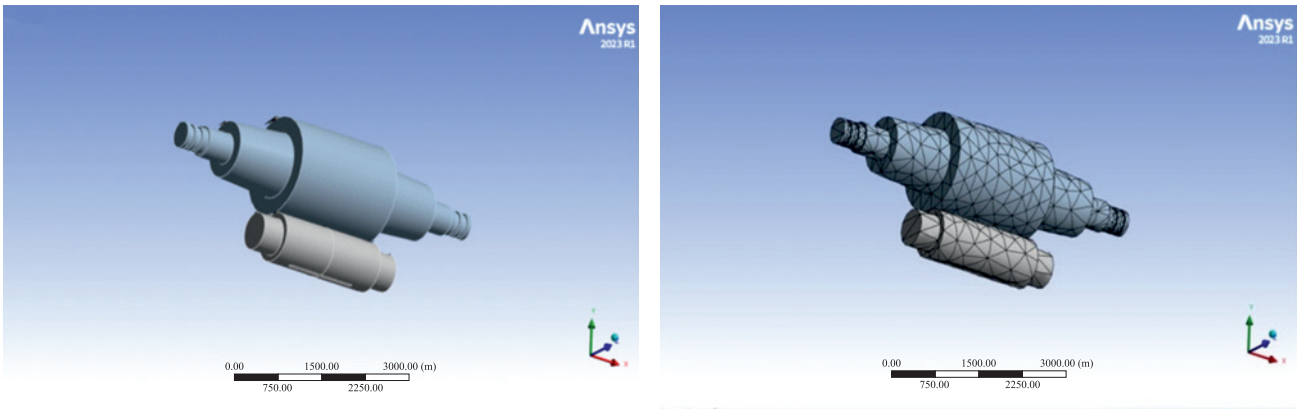

Fig. 1. Model of the roll system of "quarto" stand

Рис. 1. Модель валковой системы клети «кварто»

to represent the deformation zone, where contact pressure would be applied. In this region, a pressure load equivalent to the normal stress in the deformation zone was assigned. To enable this setup, the Static Structure solver was launched in advance.

To simulate anti-bending force, concentrated vertical loads were applied to the ends of the work roll necks along the *Y*-axis.

During the simulation, the following parameters were varied within defined ranges: the contouring of the work and backup roll barrels, contact pressure in the deformation zone, strip width, and the anti-bending force applied to the work rolls.

A contour plot illustrating the results of elastic deformation calculations is presented in Fig. 2.

The difference in elastic deformation of the work roll barrel surface between the strip edge and center (elastic deflection across the strip width) was generalized into the following regression equation

$$\Delta_{dc} - \Delta_{dedg} = 0.00001632 \cdot 10^{-5} b + 0.007703P - $$
$$- 0.00000305P_{bend} - 0.0200\Delta D_{g.c.} - 0.0169\Delta D_{g.c.b}, \quad (1)$$

where P is the rolling force in the i-th stand, MN; P_{bend} is the anti-bending force applied to the work rolls, kN; b is the strip width, mm; $\Delta D_{g.c.}$ is the ground crown of the work

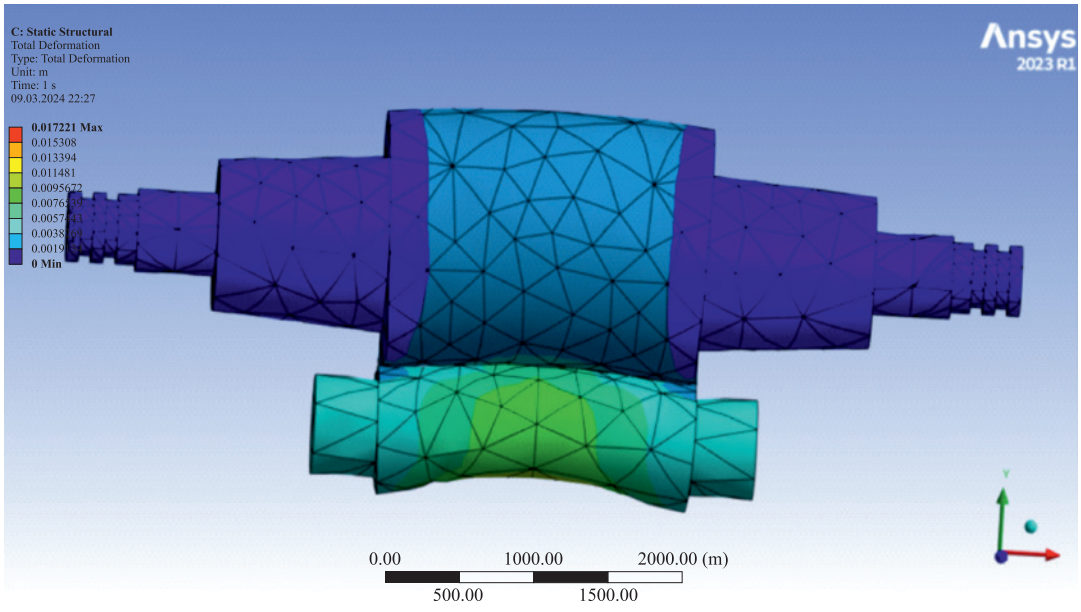

Fig. 2. Example of the result of calculating elastic deformations in vertical axial plane of the rolls of "quarto" stand in the MechanicalStructure module of the Ansys R1 program

Рис. 2. Пример результата расчета упругих деформаций в вертикальной осевой плоскости валков клети «кварто» в модуле MechanicalStructure программы Ansys R1

Table 1. **Results of checking the significance of coefficients of the equation for calculating elastic deformations**

Таблица 1. **Результаты проверки значимости коэффициентов уравнения для расчета упругих деформаций**

Parameter	Statistical significance level (p-value)
Strip width, mm	0.01
Rolling force in the i-th stand, MN	$2.07 \cdot 10^{-30}$
Anti-bending force applied to work rolls, kN	$4.31 \cdot 10^{-9}$
Ground crown of the work roll barrel at its center, mm	0.02
Ground crown of the backup roll barrel at its center, mm	$4.36 \cdot 10^{-8}$
N o t e . A parameter is considered statistically significant if the p-value is less than 0.05.	

roll barrel at its center, mm; $\Delta D_{\text{g.c.b}}$ is the ground crown of the backup roll barrel at its center, mm.

The coefficient of multiple determination R^2 was 0.86, indicating a high degree of reliability for the derived equation.

The statistical significance of the coefficients in Equation (1) was assessed using p-values, based on a dataset of forty simulation variants previously reported in [19]. The results of this evaluation are presented in Table 1.

The third stage – evaluation of wear on the work roll barrel surface – was based on experimental data that included roll operating parameters, surface hardness, and barrel contour geometry [20].

As shown in Table 2, roll wear is influenced by the rolling force, surface hardness of the roll barrel, barrel diameter, and the total length of strip rolled. Initial concavity was found to have a negligible effect.

A relationship was established to estimate roll barrel wear at both the center and strip edges, depending on the influencing parameters:

$$\Delta_c = k_w P + k_L L_{\text{m}}, \qquad (2)$$

where P is the average rolling force in the working stand since the installation of the work roll, MN; L_{m} is the total length of strip rolled on the work rolls in stand, m; k_w is the coefficient representing the influence of rolling force on the wear of the work roll barrel surface; k_L is the coefficient representing the influence of the strip length rolled on the work rolls in the stand on roll barrel wear.

The values of these coefficients, for example at the center of the roll barrel (i.e., along the strip centerline), were determined using the following regression equations

$$k_w = -0.00025HSD + 0.0000285D, \qquad (3)$$

where HSD is the Shore hardness of the roll barrel surface, D is the diameter of the work roll barrel, mm. The coefficient of determination for this equation is $R^2 = 0.89$, indicating a high degree of reliability;

$$k_L = -0.0000011HSD + 0.00000011D. \qquad (4)$$

The forth stage was the calculation of the roll thermal profile.

The thermal behavior of the continuous cold rolling mill was analyzed by formulating and solving a system of heat balance equations for the work rolls, backup rolls, and strip. The application of this model for both cold and hot continuous strip rolling has been discussed in prior studies [21; 22].

The thermal crown of the roll barrel across the strip width was calculated using the temperature distribution determined from the system of equations, with particular focus on the roll barrel center.

Table 2. **Results of assessing the Pearson correlation coefficients of the rolls parameters and technology with amount of the barrel surface wear**

Таблица 2. **Результаты оценки коэффициентов корреляции Пирсона параметров валков и технологии с величиной износа поверхности бочки**

Parameter	Rolling force, MN	Roll barrel hardness, *HSD*	Roll barrel diameter, mm	Length of strip rolled, m	Initial concavity of the roll barrel surface at its center, mm
Correlation coefficient	–0.4755	0.4277	–0.4055	0.4839	0.012

The fifth stage involved assessing the strip's profile using the components obtained in previous stages, which define the cross-sectional shape of the flat-rolled product at the roll gap exit:

– initial ground crown, adjusted for current wear, Δ_{gy};

– elastic deformation of the work roll barrel surface, Δ_{dy};

– thermal profile (thermal crown) of the roll barrel surface, Δ_{ty};

– nominal strip thickness, h_i.

The strip thickness at any point along the width (coordinate y) was calculated as:

$$\Delta_{iy} = h_i - \Delta_{gy} + \Delta_{dy} - \Delta_{ty}.$$

The six stage – evaluation of flatness parameters of the finished strip – was performed using the relationships described in [23].

By knowing the initial slab and final strip thickness profiles across the width – and thus the drawing ratios at the edges and center of the strip – it is possible to estimate the most important flatness defect parameter defined in GOST 19903–2015 – the defect amplitude:

– for "waviness" formed in the i-th stand of a continuous group of stands:

$$a_{wi} = \frac{hE\left[1-\cos\left(\frac{2\sigma_k\left(\lambda_{cr}-\lambda_c\right)}{hE}\right)\right]}{\sigma_k}, \quad (5)$$

where h is the strip thickness, E is the strip's Young's modulus, σ_k is the critical buckling stress, λ_{cr}, λ_c are the drawing ratios at the strip edge and center, respectively, based on the entry and exit cross-sections;

– "buckling" formed in the i-th stand of the continuous rolling mill:

$$a_{bi} = \frac{hE\left[1-\cos\left(\frac{2\sigma_k\left(\lambda_c-\lambda_{cr}\right)}{hE}\right)\right]}{\sigma_k}. \quad (6)$$

It has been confirmed [23] that flatness defects accumulate as the strip passes from stand to stand. Therefore, if the same type of defect occurs in subsequent stands, its amplitude increases additively.

The accuracy of the calculated amplitude and type of waviness using Equations (5) and (6) was validated by simulating the rolling process in DEFORM-3D. For this purpose, roll barrel models were created with longitudinal profiles incorporating both elastic deformation and thermal crown across the strip width. Non-uniform roll barrel wear could also be taken into account. An entry slab was modeled with a specified cross-sectional profile, and the rolling process was simulated. In the post-processor, vertical displacement differences between the strip center and edges were tracked across the width.

In Fig. 3, Line *3* represents the vertical displacement at the strip edge, while Line *1* represents displacement at the center. The difference between them was taken as the defect amplitude.

An example of amplitude evaluation using DEFORM-3D is shown in Fig. 4.

The validation results obtained from DEFORM-3D simulations confirm the sufficient accuracy of the analytical model for predicting the flatness of cold-rolled steel.

CONCLUSIONS

A well-known cause of flatness defects in finished cold-rolled steel strips is the variation in drawing ratios

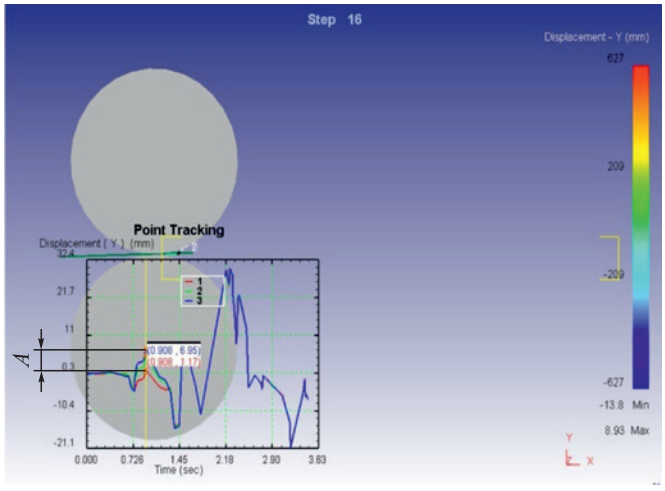

Fig. 3. Example of assessing flatness defect of the "wave" strip (A – amplitude of "wave" on the strip)

Рис. 3. Пример оценки дефекта плоскостности полосы «волна» (A – амплитуда «волны» на полосе)

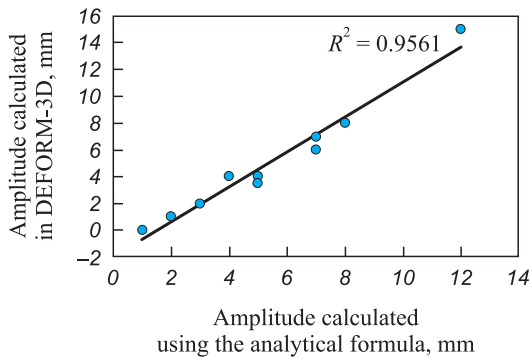

Fig. 4. Comparison of the results of calculating the non-flatness amplitude

Рис. 4. Сравнение результатов расчета амплитуды неплоскостности

across the strip width. This variation is influenced by the roll barrel contouring parameters, the energy–power parameters of the rolling process, and the operating parameters of the automatic profile and flatness control system. The combined effect of these technological factors on strip shape is complex. This paper presents an approach that incorporates the key operational parameters of rolling equipment and enables the evaluation of the type and amplitude of flatness defects in finished steel strips.

References / Список литературы

1. Shalaevskii D.L. Models for the formation of flatness defects of steel strip during its rolling and heat treatment. *Russian Metallurgy (Metally)*. 2024;2024(7):1760–1764. https://doi.org/10.1134/S0036029524703063
2. Budakva A.A., Konovalov Yu.V., Tkalich K.N. Roll Profiling for Sheet Metal Mills. Kiev: Tekhnika; 1986:190. (In Russ.).

   Будаква А.А., Коновалов Ю.В., Ткалич К.Н. Профилирование валков листовых станов. Киев: Техника; 1986:190.
3. Maksimov E.A., Shatalov R.L., Boskhamdzhiev N.Sh. Production of Flat Strips by Rolling. Moscow: Teplotekhnik; 2008:355. (In Russ.).

   Максимов Е.А., Шаталов Р.Л., Босхамджиев Н.Ш. Производство планшетных полос при прокатке. Москва: Теплотехник; 2008:355.
4. Shatalov R.L., Maksimov E.A., Verkhov E.Yu. Rational modes of control of strip flatness in thin-sheet reversible rolling. In: *Scientific and Technical Progress in Ferrous Metallurgy: Proceedings of the II Int. Sci. and Tech. Conf. (October 7–9, 2015)*. Cherepovets: Cherepovetskii gos. un-t; 2015:148–151. (In Russ.).

   Шаталов Р.Л., Максимов Е.А., Верхов Е.Ю. Рациональные режимы управления плоскостностью полос при тонколистовой реверсивной прокатке / *Научно-технический прогресс в черной металлургии: Материалы II Международной научно-технической конференции (7 – 9 октября 2015 г.)*. Череповец: Череповецкий государственный университет; 2015:148–151.
5. Shatalov R.L., Maksimov E.A. Clarification of the method for calculating critical stresses and flatness indices of strip during thin-sheet rolling. *Stal'*. 2016;(4):26–30. (In Russ.).

   Шаталов Р.Л., Максимов Е.А. Уточнение метода расчета критических напряжений и показателей плоскостности полосы при тонколистовой прокатке. *Сталь*. 2016;(4):26–30.
6. Ievlev N.G. Mathematical models of flatness of thick sheet metal applied to automated process control systems. *Matematichní mashini í sistemi*. 2018;(1):67– 77. (In Russ.).

   Иевлев Н.Г. Математические модели плоскостности толстолистового проката применительно к АСУ ТП. *Математичні машини і системи*. 2018;(1):67–77.
7. Shatalov R.L., Maksimov E.A. Analysis of asymmetric rolling efficiency for increasing accuracy of rolled strips. *Metallurg*. 2016;(7):80–84. (In Russ.).

   Шаталов Р.Л., Максимов Е.А. Анализ эффективности технологии асимметричной прокатки для повышения точности прокатываемых полос. *Металлург*. 2016;(7):80–84.
8. Bartkhol'dt Kh., Kopin F., Dzhelali M. Universal flatness model for process optimization in cold rolling mills. *Chernye metally*. 2015;(3):53–58. (In Russ.).

   Бартхольдт Х., Копин Ф., Джелали М. Универсальная модель плоскостности для оптимизации процесса холодной прокатки. *Черные металлы*. 2015;(3):53–58.
9. Shalaevskii D.L., Mitrofanov A.V., Korepina K.P. Improvement in the flatness of finished steel strips under energy saving regimes of continuous hot rolling. *Stal'*. 2022;(2): 15–17. (In Russ.).

   Шалаевский Д.Л., Митрофанов А.В., Корепина К.П. Повышение плоскостности готовых стальных полос на энергосберегающих режимах непрерывной горячей прокатки. *Сталь*. 2022;(2):15–17.
10. Garber E.A., Shalaevskii D.L., Mishnev P.A., Mikheeva I.A., Paligin R.B. Improving the flatness of high-rolled steel strips by optimizing the settings of process mode parameters. In: *Int. Sci. and Pract. Conf. "Problems of Ferrous Metallurgy – 2015*. Int. Sci. Seminar". 2016:76–82. (In Russ.).

    Гарбер Э.А., Шалаевский Д.Л., Мишнев П.А., Михеева И.А., Палигин Р.Б. Улучшение плоскостности горячекатаных стальных широких полос путем оптимизации настройки параметров технологического режима / *Всероссийская научно-практическая конференции «Проблемы черной металлургии – 2015. Международный научный семинар»*. 2016:76–82.
11. Grigoryan G.G., Zheleznov Yu.D., Chernyi V.A., etc. Adjustment, Stabilization and Control of Thin Sheet Rolling Process. Moscow: Metallurgiya; 1983:120. (In Russ.).

    Григорян Г.Г., Железнов Ю.Д., Черный В.А. и др. Настройка, стабилизация и контроль процесса тонколистовой прокатки. Москва: Металлургия; 1983:120.
12. Pimenov V.A., Bel'skii S.M., Kuznetsova E.V., Shkarin A.N. Mathematical model for identifying the shape of profile with primary cross-section of hot-rolled strips and distribution of extensions across the width of cold-rolled strips. Report 1. *Proizvodstvo prokata*. 2018;(1):11–15. (In Russ.).

    Пименов В.А., Бельский С.М., Кузнецова Е.В., Шкарин А.Н. Математическая модель идентификации формы профиля поперечного сечения горячекатаных полос и распределения вытяжек по ширине холоднокатаных полос. Сообщение 1. *Производство проката*. 2018;(1):11–15.
13. Pimenov V.A., Bel'skii S.M., Kuznetsova E.V., Shkarin A.N. Mathematical model for identifying the shape of profile with primary cross-section of hot-rolled strips and distribution of extensions across the width of cold-rolled strips. Report 2. *Proizvodstvo prokata*. 2018;(6):9–14. (In Russ.).

    Пименов В.А., Бельский С.М., Кузнецова Е.В., Шкарин А.Н. Математическая модель идентификации формы профиля поперечного сечения горячекатаных полос и распределения вытяжек по ширине холоднокатаных полос. Сообщение 2. *Производство проката*. 2018;(6):9–14.
14. Shkarin A.N. Formation of flatness of cold-rolled strips taking into account the features of cross-section profile of hot-rolled rolled products: Extended Abstract of Cand. Sci. Diss. 2021. (In Russ.).

    Шкарин А.Н. Формирование плоскостности холоднокатаных полос с учетом особенностей профиля поперечного сечения горячекатаного подката: Автореферат диссертации … кандидата технических наук. 2021.

15. Wang X., Yang Q., He A. Calculation of thermal stress affecting strip flatness change during run-out table cooling in hot steel strip rolling. *Journal of Materials Processing Technology*. 2008;207(1-3):130–146.
https://doi.org/10.1016/j.jmatprotec.2007.12.076

16. Hrabovsky J., Pohanka M., Lee P.J., Kang J.H. Experimental and numerical study of hot-steel-plate flatness. *Materials and Technology*. 2016;50(1):17–21.
https://doi.org/10.17222/mit.2014.153

17. Wu H., Sun J., Lu X., Peng W. Predicting stress and flatness in hot-rolled strips during run-out table cooling. *Journal of Manufacturing Processes*. 2022;84:815–831.
https://doi.org/10.1016/j.jmapro.2022.10.053

18. Bozhkov A.I., Kovalev D.A., Chernikov O.V., Yusupov V.S., Ivliev S.N., Degtev S.S. Influence of heat treatment on the planarity of isotropic electrical steel strip. Part 2. *Steel in Translation*. 2019;49(2):131–133.
https://doi.org//10.3103/S0967091219020049

Божков А.И., Ковалев Д.А., Черников О.В., Юсупов В.С., Ивлиев С.Н., Дегтев С.С. Влияние режимов термообработки на плоскостность полос электротехнических изотропных сталей. Сообщение 2. *Сталь*. 2019;(2):26–28.

19. Shalaevskii D.L. PPrediction of steel strip flatness based on the difference in drawing coefficients along its width during steel strip rolling. *Ferrous Metallurgy. Bulletin of Scientific, Technical and Economic Information*. 2024;80(10): 20–27. (In Russ.).

Шалаевский Д.Л. Прогнозирование плоскостности стальной полосы на основе разности коэффициентов вытяжек по ее ширине при прокатке. *Черная металлургия. Бюллетень научно-технической и экономической информации*. 2024;80(10):20–27.

20. Shalaevskiiy D.L., Sidorov A.V. Study of wear on surface of work rolls barrels of continuous stands of a wide strip hot rolling mill. *Zagotovitel'nyye proizvodstva v mashinostroenii*. 2024;22(7):315–318. (In Russ.).
https://doi.org/10.36652/1684-1107-2024-22-7-315-318

Шалаевский Д.Л., Сидоров А.В. Исследование износа поверхности бочек рабочих валков непрерывной группы клетей широкополосного стана горячей прокатки. *Заготовительные производства в машиностроении*. 2024;22(7):315–318.
https://doi.org/10.36652/1684-1107-2024-22-7-315-318

21. Garber E.A. Cold Rolling Mills: (Theory, Equipment, Technology). Moscow: Chermetinformatsiya; 2004:412. (In Russ.).

Гарбер Э.А. Станы холодной прокатки: (теория, оборудование, технология). Москва: ОАО "Черметинформация"; 2004:412.

22. Shalaevskii D.L. Investigation of thermal mode of hot-rolling mill working rolls in order to improve the accuracy of calculating the thermal profile of their barrels' surface. *Izvestiya. Ferrous Metallurgy*. 2023;66(3):283–289.
https://doi.org/10.17073/0368-0797-2023-3-283-289

Шалаевский Д.Л. Исследование теплового режима рабочих валков стана горячей прокатки с целью повышения точности расчета температур поверхностей их бочек. *Известия вузов. Черная металлургия*. 2023; 66(3):283–289.
https://doi.org/10.17073/0368-0797-2023-3-283-289

23. Shalaevskii D.L. Investigation of the influence of technological factors on continuous high-speed rolling on flatness of thin steel sheets with the aim of increasing their quality. *Metally*. 2024;(5):62–68. (In Russ.).
https://doi.org/10.31857/S0869573324056268

Шалаевский Д.Л. Исследование влияния технологических факторов при непрерывной горячей прокатке на плоскостность тонких стальных листов с целью повышения их качества. *Металлы*. 2024;(5):62–68.
https://doi.org/10.31857/S0869573324056268

24. Shalaevskiy D.L., Kozhevnikov A.V. Algorithm and design methodology for energy-efficient sheet products production technology. *IOP Conference Series: Materials Science and Engineering*. 2020;718:012015.
https://doi.org/10.1088/1757-899X/718/1/012015

25. Garber E.A., Shalaevskii D.L., Kozhevnikova I.A., Traino A.I. Procedure and algorithms for the energy-force calculation of cold rolling allowing for the number of neutral sections in the deformation zone. *Russian Metallurgy (Metally)*. 2008;2008(4):315–325.
https://doi.org/10.1134/S0036029508040083

Information about the Author / Сведения об авторе

Dmitrii L. Shalaevskii, *Cand. Sci. (Eng.), Assist. Prof. of the Chair "Metallurgy, Mechanical Engineering and Technological Equipment",* Cherepovets State University
ORCID: 0000-0002-0443-4135
E-mail: shal-dmitrij@yandex.ru

Дмитрий Леонидович Шалаевский, *к.т.н., доцент кафедры металлургии, машиностроения и технологического оборудования,* Череповецкий государственный университет
ORCID: 0000-0002-0443-4135
E-mail: shal-dmitrij@yandex.ru

Received 25.04.2025
Revised 19.06.2025
Accepted 20.06.2025

Поступила в редакцию 25.04.2025
После доработки 19.06.2025
Принята к публикации 20.06.2025

IN THE ORDER OF DISCUSSION / **В ПОРЯДКЕ ДИСКУССИИ**

UDC 669.11:669.292.34
DOI 10.17073/0368-0797-2025-4-424-433

Original article
Оригинальная статья

Electrochemistry of reduction processes and prospects for the development of reduction technologies

V. E. Roshchin ✉, **A. V. Roshchin**

South Ural State University (76 Lenina Ave., Chelyabinsk 454080, Russian Federation)

✉ roshchinve@susu.ru

Abstract. Oxidation and reduction of metals consist in the loss of valence electrons by metal atoms with the conversion of an electromagnetic metallic bond into an ionic bond during oxidation and the reverse transition of electrons from anions to metal cations with the conversion of an ionic bond into a metallic bond during reduction. The electronic reduction theory developed by the authors describes the reduction process by the sequential operation of two electrochemical cells: a fuel cell, in which the chemical energy of the oxidized reducing agent is converted into electrical energy of "free" electrons, and a solid electrolyte electrolyzer, which converts the electrical energy of these electrons into energy of the metal bond of the reduced cations in the oxide. Since the stage of the actual reduction is the formation of a metallic bond between cations due to electrons coming from outside, the shortest and therefore most effective supply of electrons to the reduced cations will be not from the fuel cell, but from the electrical network, that is, electrolysis of the oxides of the metal being reduced. Known methods for producing iron by electrolysis of molten oxides, as well as possibly alkaline solutions, are promising for extracting iron from rich ores. For the selective extraction of iron from ferromanganese, titanomagnetite, siderite, chromite and other complex ores, relatively low-temperature reduction of iron with hydrogen or solid-phase electrolysis to produce, after separation, a metallization product by melting carbon-free iron and a concentrate of active metal oxides is more promising.

Keywords: electrochemistry of reduction processes, electronic theory of reduction, electrochemical fuel cell, carbon selective reduction, hydrogen reduction, electrolysis

For citation: Roshchin V.E., Roshchin A.V. Electrochemistry of reduction processes and prospects for the development of reduction technologies. *Izvestiya. Ferrous Metallurgy*. 2025;68(4):424–433. https://doi.org/10.17073/0368-0797-2025-4-424-433

Электрохимия восстановительных процессов и перспективы развития восстановительных технологий

В. Е. Рощин ✉, **А. В. Рощин**

Южно-Уральский государственный университет (Россия, 454080, Челябинск, пр. Ленина, 76)

✉ roshchinve@susu.ru

Аннотация. Окисление и восстановление металлов заключаются в потере атомами металлов валентных электронов с преобразованием электромагнитной металлической связи в ионную при окислении и обратный переход электронов от анионов к катионам металла с превращением ионной связи в металлическую при восстановлении. Развиваемая авторами электронная теория восстановления описывает процесс восстановления последовательной работой двух электрохимических элементов: топливного, в котором химическая энергия окисляемого восстановителя превращается в электрическую энергию «свободных» электронов, и твердоэлектролитного электролизера, превращающего электрическую энергию этих электронов в энергию металлической связи восстанавливаемых катионов в оксиде. Так как стадией собственно восстановления является образование металлической связи между катионами за счет поступающих извне электронов, то самым коротким и потому самым эффективным будет подвод электронов к восстанавливаемым катионам не от топливного элемента, а из электрической сети, то есть электролиз оксидов восстанавливаемого металла. Известные способы получения железа электролизом расплавленных оксидов, а также, возможно, щелочных растворов являются перспективными при извлечении железа из богатых руд. Для селективного извлечения железа из железомарганцевых, титаномагнетитовых, сидеритовых, хромитовых и других комплексных руд более перспективным является относительно низкотемпературное восстановление железа водородом или твердофазный электролиз с получением после разделения продукта металлизации плавлением безуглеродистого железа и концентрата оксидов активных металлов.

Ключевые слова: электрохимия окислительно-восстановительных процессов, электронная теория восстановления, электрохимический топливный элемент, углеродное селективное восстановление, водородное восстановление, электролиз

Для цитирования: Рощин В.Е., Рощин А.В. Электрохимия восстановительных процессов и перспективы развития восстановительных технологий. *Известия вузов. Черная металлургия*. 2025;68(4):424–433. https://doi.org/10.17073/0368-0797-2025-4-424-433

Introduction

Contemporary methods for reducing and extracting metals from ores long predate the rise of science and took shape through the gradual refinement of the craft of metal production. In fact, the practice of turning ore into metal largely motivated the emergence of a science of material transformation – first as alchemy and later as chemistry. Only at the end of the 19th century, with the development of atomic–molecular concepts grounded in advances in the science of chemical reactions, the first scientific explanations of the mechanisms operating in metal reduction appear [1 – 3].

There is now little doubt that atoms and molecules exist only in the gas phase: condensed metals contain no discrete atoms, and ore oxides contain no molecules. In both media, metals are present as cations and the valence electrons "lost" by the atoms; these electrons, by means of the electromagnetic field, bind the metal cations into the condensed phase – metallic bonding in metals and ionic bonding in oxides. It is likewise clear that oxidation and reduction of metals amount to a redistribution of atomic valence electrons. These processes should therefore be viewed as reactions in which metal atoms lose valence electrons to oxidizer atoms, with metallic electromagnetic bonding giving way to ionic bonding during oxidation ($Me^0 = Me^{2+} + 2e$), and as the return of these electrons from oxidizer anions to the cations during reduction, restoring metallic bonding ($Me^{2+} + 2e = Me^0$). Thus, reduction and oxidation are electrochemical processes driven by the redistribution of the valence electrons of metal atoms. Nevertheless, in metallurgical science the description of ore-to-metal reduction processes is still dominated by the atomic–molecular approach [4; 5]. An obviously outdated atomistic description of reduction at the atomic–molecular level – for example, C + FeO = CO + Fe – does not, by itself, support adequate improvement of industrial technologies or their alignment with the current state of science [6 – 8].

Electronic theory of reduction

Developed in recent years by the authors and their colleagues, the electronic theory of reduction [9; 10] aims to describe the electrochemistry of electron exchange between the oxidized atoms of the reductant and the cations of the metal being reduced. The theory rests on a large number of dedicated experiments conducted by the authors and on a synthesis of published results by others. It proceeds from the electrochemical nature of reduction reactions, accounts for structural changes in solid ores (formation of anion vacancies under low oxygen partial pressure P_{O_2} and high temperature $T \approx 2000$ °C), and for composition of the gas phase corresponding to these conditions (formation of a low-temperature plasma) during heating in reduction units. It is grounded in the physics of imperfect crystals and in quantum-mechanical principles governing the distribution and motion of electrons in metals and ionic semiconductors. The theory's conclusions encompass all known reduction outcomes: metal formation on the surfaces of rich monomineralic ore lumps; metal precipitation within complex and lean ores; oxide dissociation; formation and sublimation of suboxides; and metal production by electrolysis from aqueous solutions and molten salts.

According to the theory, at high temperature and low oxygen partial pressure in the gas phase of reduction units, chemical reactions between solid ore oxides and the solid carbon of coke do not even require direct contact between the solid reagents. The plasma state of the gas phase enables ions and electrons present both in the plasma and on the surfaces of the solids in contact with it to interact over a distance under electrostatic forces, approach one another, and react in the gas phase. This, in turn, allows solid-state reduction reactions to proceed rapidly in the kinetic mode (Fig. 1, *a*).

A new and fundamentally important element of the electronic theory of reduction – derived theoretically and confirmed repeatedly by dedicated experiments with complex and lean ores – is the mechanism of electron transfer from the reductant to the cations of the metal being reduced, i.e., the mechanism of solid-state reduction. It involves the formation and migration, within the crystal lattice of each oxide lump, of anion vacancies bearing "free" electrons (not bound to any specific cation). These electrons originate in the chemical reaction between the reductant and the oxygen of the oxide in the gas phase. The low oxygen partial pressure in the gas phase, established by chemical interaction with the reductant, together with the high mobility of lattice ions at elevated temperature, causes oxygen to leave the oxide and enter the gas phase. As an oxygen atom departs the oxide lattice and accepts two electrons from the reductant in the gas phase, it leaves behind an anion vacancy accompanied by two "free" electrons previously taken by the oxygen anion from the metal cations.

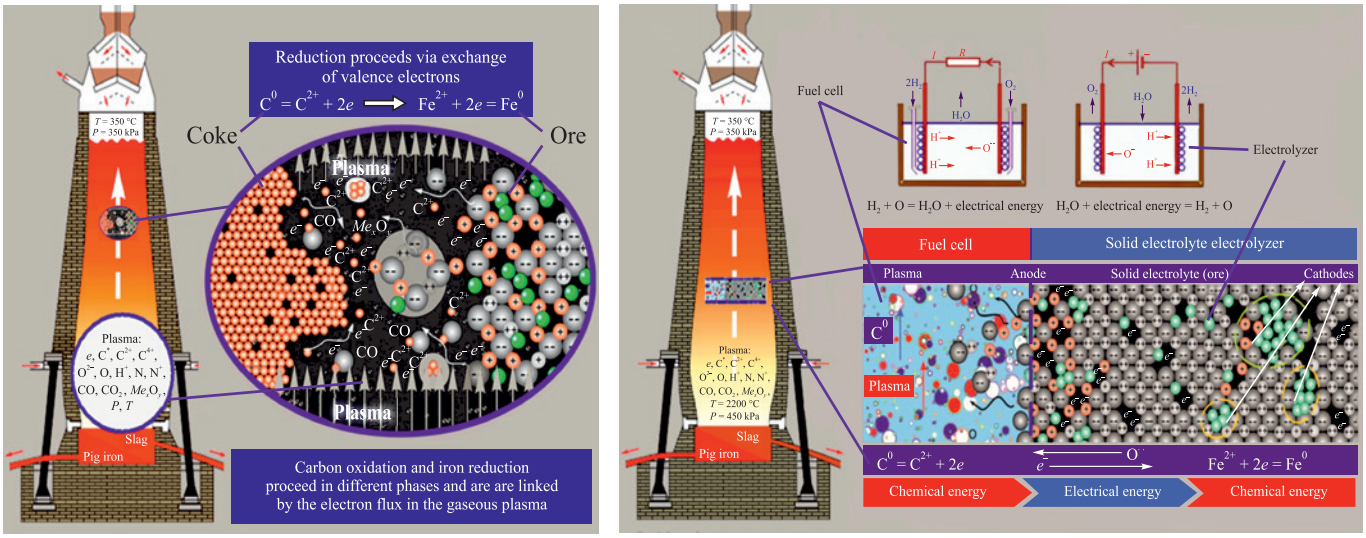

a *b*

Fig. 1. Electrochemical processes in a blast furnace:
a – plasma formation in the gas phase and appearance of anion-electron conductivity in ore oxides;
b – conversion of chemical energy into electrical energy in a fuel cell and reverse conversion of electrical energy into chemical energy in a solid electrolyte electrolyzer

Рис. 1. Электрохимические процессы в доменной печи:
a – образование плазмы в газовой фазе и появление анион-электронной проводимости в оксидах руды;
b – преобразование химической энергии в электрическую в топливном элементе и обратный переход электрической энергии в химическую в твердоэлектролитном электролизере

Owing to vigorous thermal motion of ions, these anion vacancies and their associated “free” electrons disperse through the lattices of complex oxides and migrate until they encounter cations with high electron affinity (as determined by their Fermi-level position) [11]. Owing to vigorous thermal motion of ions, these anion vacancies and their associated “free” electrons disperse through the lattices of complex oxides and migrate until they encounter cations with high electron affinity (as determined by their Fermi-level position) [11]. Where such cations accumulate, the migration of the electron-charged vacancies ceases, the vacancies coalesce, and metallic bonding forms at those sites by virtue of the “free” electrons carried with the vacancies; a metallic phase then precipitates. Thus, removal of atomic oxygen from the surface of one oxide phase can lead to selective reduction of cations with high electron affinity within the crystal lattice of a different oxide. An example is shown in Fig. 2, which presents the scheme and results of experiments on solid-state reduction by solid carbon of iron and chromium cations in crystals of chromspinelide (chromian spinel) $(Mg, Fe)[Fe, Al, Cr]_2O_4$ embedded in olivine $(Mg, Fe)_2[SiO_4]$.

The concerted migration of “free” electrons and anion vacancies under reducing conditions proceeds without an externally applied electric field because of gradients in the chemical potentials of oxygen and electrons between the surface and the bulk of the oxide phase. “Free” electrons may also move via anion vacancies of other origin (thermal or impurity-related), provided that overall and local charge neutrality is preserved.

Accordingly, the reduction process in industrial reduction units should be viewed as the combined action of two electrochemical cells operating in series: a carbon fuel cell, in which the chemical energy of the oxidized reductant is converted into the electrical energy of “free” electrons; and a solid electrolyte electrolyzer, in which the electrical energy carried by electrons that have migrated from the surface into the bulk of the oxide is taken up by cations and converted into the chemical energy of metallic bonding (Fig. 1, *b*). In reduction units, the gas phase and each individual ore lump together form such series-connected pairs of electrochemical cells (fuel cells and electrolyzers). Because the number of these cell pairs – one per ore lump – is enormous, reduction units – and blast furnaces in particular – achieve exceptionally high throughput.

Prospects for transforming carbon-based reduction technologies

The electrochemical nature of oxidation/reduction processes should no longer be a matter of debate. It follows that there must be a flow of electrons in reduction units between the reductant and the cations of the metal being reduced – that is, an electric current between them. The electronic theory describes how this current arises and is transformed as the result of two electrochemical

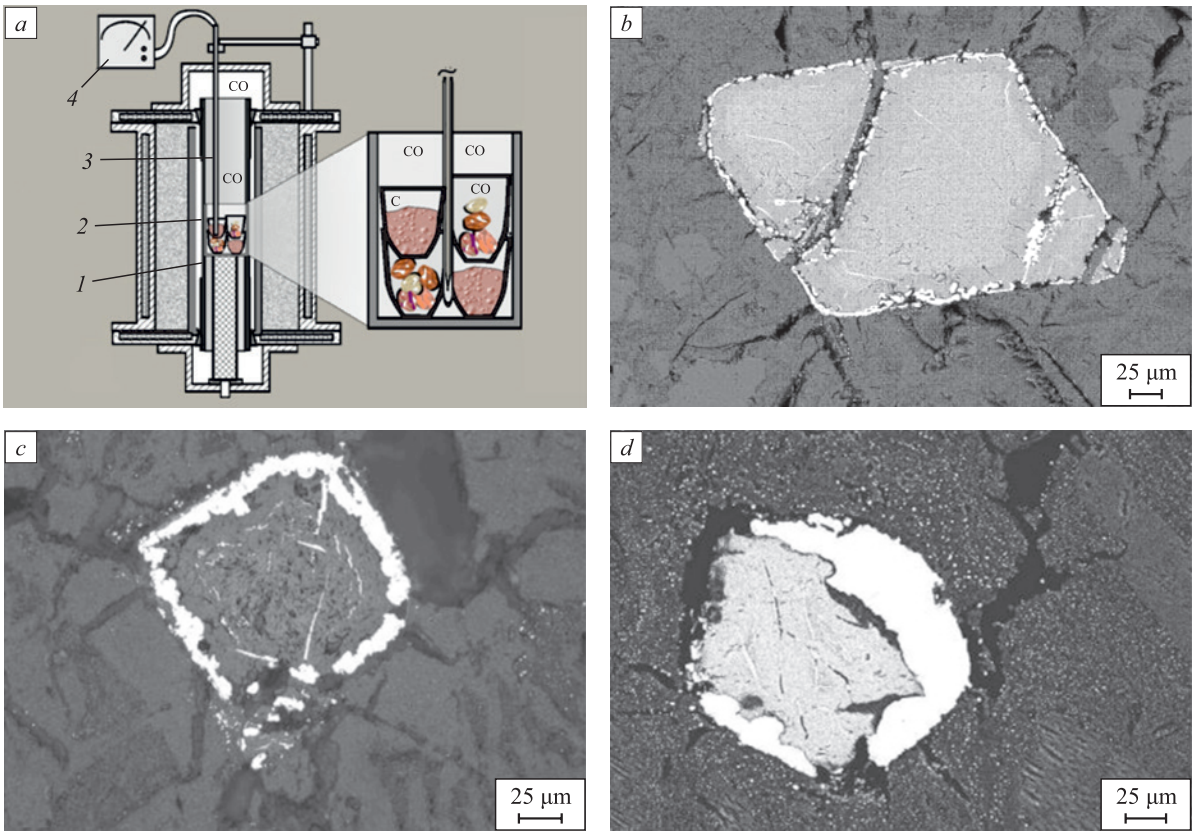

Fig. 2. Scheme of the installation based on the Tammann furnace for conducting experiments on solid-phase selective reduction of impregnated ores (*a*) and successive stages (*b – d*) of reduction of iron and chromium in a chromspinelide $(Mg, Fe)[Fe, Al, Cr]_2O_4$ crystal impregnated in olivine $(Mg, Fe)_2[SiO_4]$: *1* – graphite heater; *2* – container with crucibles; *3* – thermocouple; *4* – potentiometer

Рис. 2. Схема установки на базе печи Таммана для проведения экспериментов по твердофазному селективному восстановлению вкрапленных руд (*a*) и последовательные стадии (*b – d*) восстановления железа и хрома в кристалле хромшпинелида $(Mg, Fe)[Fe, Al, Cr]_2O_4$, вкрапленном в оливин $(Mg, Fe)_2[SiO_4]$: *1* – графитовый нагреватель; *2* – контейнер с тиглями; *3* – термопара; *4* – потенциометр

cells operating in series: an electrochemical fuel cell that converts chemical energy into electrical energy, and an electrolyzer. This mechanism is consistent with the operating practice of all types of industrial reduction units and is supported by numerous dedicated experiments using different ores and different reductants. From this, one may conclude that the final stage of today's multistage metal-reduction technologies is invariably the transfer of "free" electrons from atoms of the reductant to the cations of the metal being reduced, with atomic oxygen being released at the interfaces – on the surfaces of the oxide and of the metal within the oxide phase – i.e., solid-electrolyte electrolysis of the ore.

This raises the question of whether the many costly preliminary and intermediate stages of the reduction process are necessary, and whether it is sensible to generate "free" electrons in the fuel-cell portion of ore-reduction units at all. It is evidently far simpler and less expensive to generate electrons not by burning the reductant in metallurgical reduction units, but by modern methods at power plants, transmit them through the electrical grid, and use them directly at the final stage – the reduction of cations – in a specialized electrochemical unit (an electrolyzer). Accordingly, the existing multistage, energy-intensive process of extracting iron from ores (Fig. 3, *a – c*) should be collapsed to a single concluding stage – electrolysis (Fig. 3, *d*). In this light, extracting metals from ores by electrolysis appears to be the ultimate goal of transforming current metallurgical technologies.

Electrolysis of molten salts and oxides has long been used to reduce and produce several metals at industrial scale – for example, aluminum [12]. Work on developing units and processes for extracting iron by electrolysis from aqueous solutions of its salts has also been under way for quite some time [13]. In recent years, several companies have intensified research into units and processes for producing iron by electrolysis of molten oxides [14 – 16]. Overall, however, both practitioners – and, more importantly, the scientific community – remain not merely skeptical but largely negative about the prospects of obtaining iron by electrolysis.

Until now, the rationale for producing pig iron with subsequent conversion to steel has been the enormous throughput of blast furnaces and the availability and relatively low cost of carbonaceous materials used both as a heat source and as reductants. It is worth recalling that this technology arose and evolved historically from the need to rework "defective" product: as the temperature in the bloomery hearth increased and iron became saturated with carbon, brittle cast iron was obtained instead of low-carbon, ductile iron. Producing and then reworking this "defect" proved expedient because carbonaceous reductants were accessible and relatively inexpensive (first wood, then charcoal, and later coal). Today, however, the production of pig iron relies on the most expensive solid fuel – coke, obtained from scarce coal grades by a complex and environmentally hazardous process. As high-quality coking coals become scarce, coke prices keep rising, and meeting ever-stricter quality requirements is increasingly difficult. Moreover, because of how reduction proceeds in blast furnaces, no more than

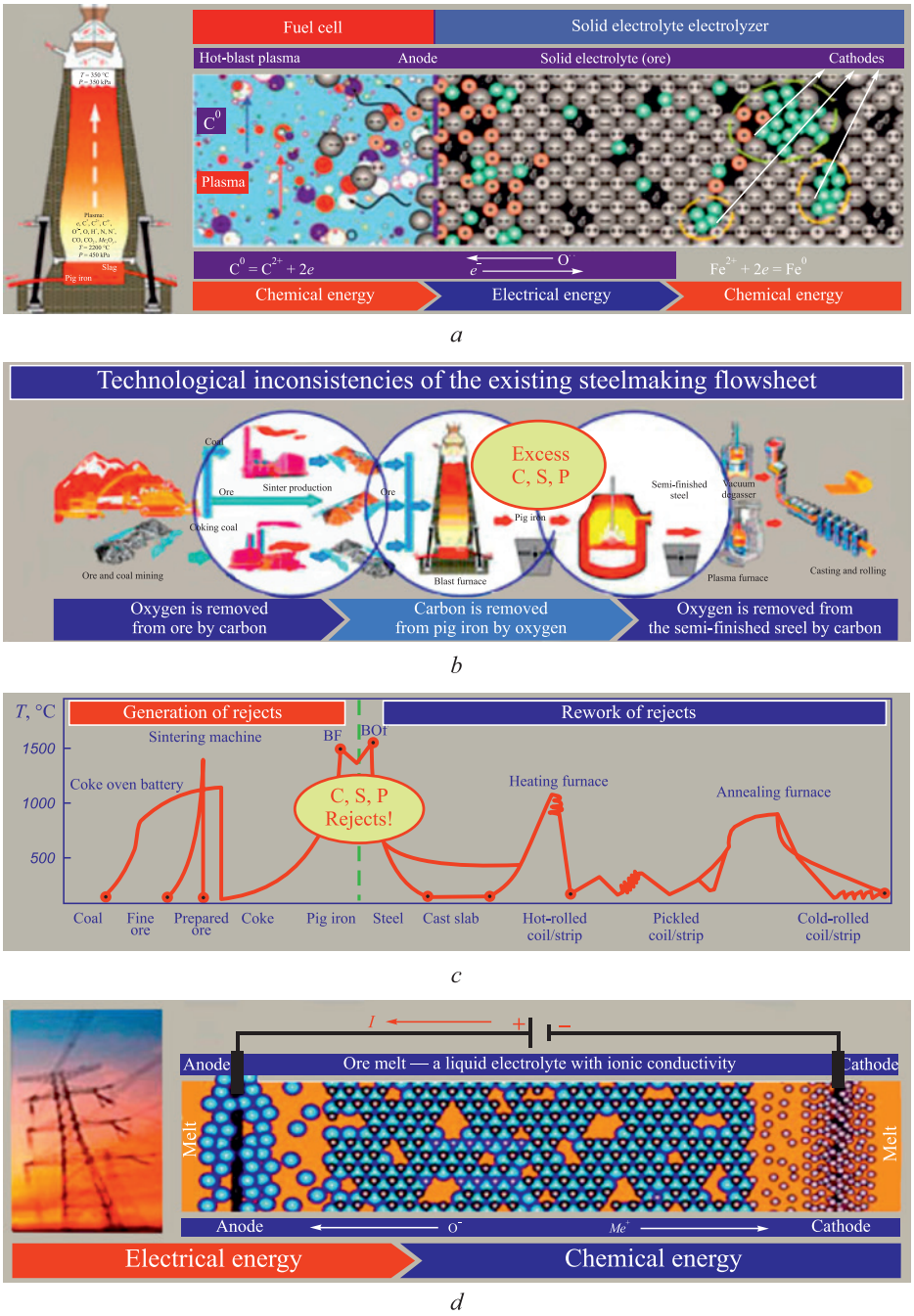

Fig. 3. Conversion and loss of energy when using a carbon fuel cell according to the existing technology (*a* – *c*) and electricity from electric network (*d*)

Рис. 3. Преобразования и потери энергии при использовании углеродного топливного элемента по существующей технологии (*a* – *c*) и электроэнергии из электрической сети (*d*)

25 % of the calorific value of this scarce and costly reductant can be used directly: during iron reduction the coke carbon is oxidized only to CO, and 75 % of the energy is released later during non-target "afterburning" of CO to CO_2 [17].

This extremely low targeted (for reduction) utilization of coke is compounded by dissolution of a portion of carbon in iron, producing pig iron. The dissolved carbon is not merely a loss – it becomes a harmful impurity that must be removed when converting pig iron to steel by oxygen blowing, which simultaneously oxidizes an appreciable amount of iron that the coke had previously reduced in the blast furnace (Fig. 3, *b*). The oxidized melt then requires deoxidation, including with carbon. Taking into account the huge heat losses across the multistage route of turning a "defect" into the final product, the pig iron → steel process must be judged extremely inefficient, fundamentally inconsistent with energy and resource conservation, and out of step with the current state of science. During steelmaking, in addition to removing the root cause of the "defect" (excess carbon), it is also necessary to remove sulfur and phosphorus, introduced mainly at the pig-iron stage by coke and flux additions. In essence, the modern scheme of producing pig iron and then converting it to steel is a process of producing and correcting a defect (Fig. 3, *b*, *c*).

Given the inconsistency of the existing production chain – alternating reduction/oxidation, contamination/refining, and heating/cooling (Fig. 3, *c*) – together with the costs of mining and transporting scarce coking coal and making coke, producing sinter and other consumables, building modern, gigantic reduction units, logistics, and environmental protection and compliance, the costs of electrolysis are likely not substantially different from those of producing and reworking pig iron. Producing iron by electrolysis of melts may already be competitive for greenfield plants (Fig. 3, *d*). As noted above, the enormous productivity of a blast furnace is achieved by the simultaneous operation within its volume of an immense number of solid electrolyte electrolyzers. A similar electroreduction principle – using grid electricity – may be applicable at the metallization stage.

Concerns about excessively high electricity costs for iron electrolysis also appear to be overstated. First, producing 1 kg of iron by electrolysis requires roughly four times less energy than producing the same mass of aluminum. Second, reserves of high-quality coking coals are rapidly declining, whereas the availability of comparatively inexpensive electric power is increasing with the expansion of nuclear energy. Tellingly, intensive research on the electrolytic production of iron is underway in the United States and France, countries with some of the highest shares of nuclear power generation [14 – 16].

Hydrogen reduction processes and technologies

The prospect of producing iron by electrolysis of ore melts appears entirely realistic for rich single-mineral ores. At the same time, there are vast reserves of complex and lean ores that are difficult or unsuitable for processing by existing methods. The advisability of preparing such ores for melt electrolysis also appears doubtful. Our studies [18] have shown that, in these ores, iron can be selectively reduced in the solid state, i.e., at relatively low temperature; after separating the products of metallization by melting, one can obtain carbon-free iron and a concentrate of oxides of metals with lower electron affinity than iron.

Accordingly, alongside producing iron by electrolysis from rich ores, it is also promising to investigate selective reduction of iron in lean and complex sideritic, iron–manganese, titanomagnetite, ilmenite, and other ores, followed – after separation of the metallization products – by obtaining iron and an oxide concentrate of reactive metals (magnesium, manganese, titanium, chromium, and others). The task is not only to maximize the reduction and recovery of iron, but also to maximize retention of valuable oxides of reactive metals in the oxide phase. Our results indicate that the most effective way to achieve this is to use hydrogen rather than carbon as the reducing agent [19].

On a large industrial scale, the only truly realistic alternative to carbon as a reducing agent for iron is hydrogen, the most abundant chemical element in the Universe. It is also among the most effective energy carriers: burning 1 kg of hydrogen releases about 140 MJ, whereas 1 kg of gasoline yields roughly 50 MJ, and 1 kg of coal 20 – 25 MJ. However, there is no free, concentrated hydrogen on Earth; to use hydrogen as an energy carrier or reducing agent, it must be produced by extracting it from abundant compounds – water or hydrocarbons. Depending on the carbon footprint of its production, hydrogen is labeled by color, from "green" (lowest footprint), obtained by electrolysis of water using renewable electricity, to "brown," obtained by coal gasification. "Green" hydrogen has the smallest carbon footprint, but it is also the most expensive. Currently, the most accessible and least costly routes of hydrogen production are processes that split fossil hydrocarbons into hydrogen and carbon – resources with which Russia is well endowed.

Because of several properties – its gaseous state; its high affinity for oxygen at low temperature that decreases as temperature rises; its negligible solubility in solid iron, among others – hydrogen can in some cases be a more effective reducing agent, particularly for selective solid-phase reduction of iron in complex ores.

Gaseous hydrogen cannot replace solid fuel in a blast furnace, but it can readily be used as a reducing agent

in existing direct-reduction units in place of natural gas (Fig. 4). As with carbon in the blast furnace, the chemical energy of hydrogen when oxidized by ore oxygen in the fuel-cell stage of the reduction unit, is converted into electrical energy, and that energy then drives metal reduction.

Analysis of the electrochemical processes based on a hydrogen solid electrolyte electrochemical fuel cell shows clear advantages of hydrogen over carbon for waste-free processing of complex ores that are difficult to treat by the blast-furnace route – ilmenite, titanomagnetite, iron–manganese, sideritic, and others – yielding new valuable products: carbon-free soft iron and valuable concentrates of oxides of titanium, manganese, magnesium, and other active metals [18; 19]. At present, for operating plants there is a commercially justified niche for using comparatively inexpensive "gray" or "brown" hydrogen to obtain carbon-free soft iron and valuable oxide concentrates from complex ores (Fig. 5).

As for the reduction of iron with "green" hydrogen, – produced by water electrolysis and often promoted as a panacea for dangerous climate change [20 – 23], – its role climate guarantor is doubtful, and its economic viability is unlikely. This is because using "green" hydrogen as a reducing agent entails sequential double electrolysis: first, electrolysis of the more stable oxide (water) using renewable electricity; second, electrolysis of the less stable iron oxide, driven by the electrical energy released in the hydrogen electrochemical fuel cell. Moreover, producing carbon-free iron via reduction with "green" hydrogen would still require subsequent carburization during melting in arc furnaces [24 – 26]. Accordingly, direct electrolysis of the less stable metal oxides remains the more rational route.

Conclusions

Metals do not contain discrete atoms, and ore oxides contain no molecules: in both media, metals are present as cations bound by the valence electrons of metal atoms – by metallic bonding in metals and by ionic bonding in ore oxides. Oxidation of metals is the loss of valence electrons by metal atoms; reduction is the return of those electrons to metal cations. In other words, oxidation and reduction are electrochemical processes.

The electronic theory of reduction describes the transfer of valence electrons from atoms of the reductant to the cations of the metal being reduced. Under the con-

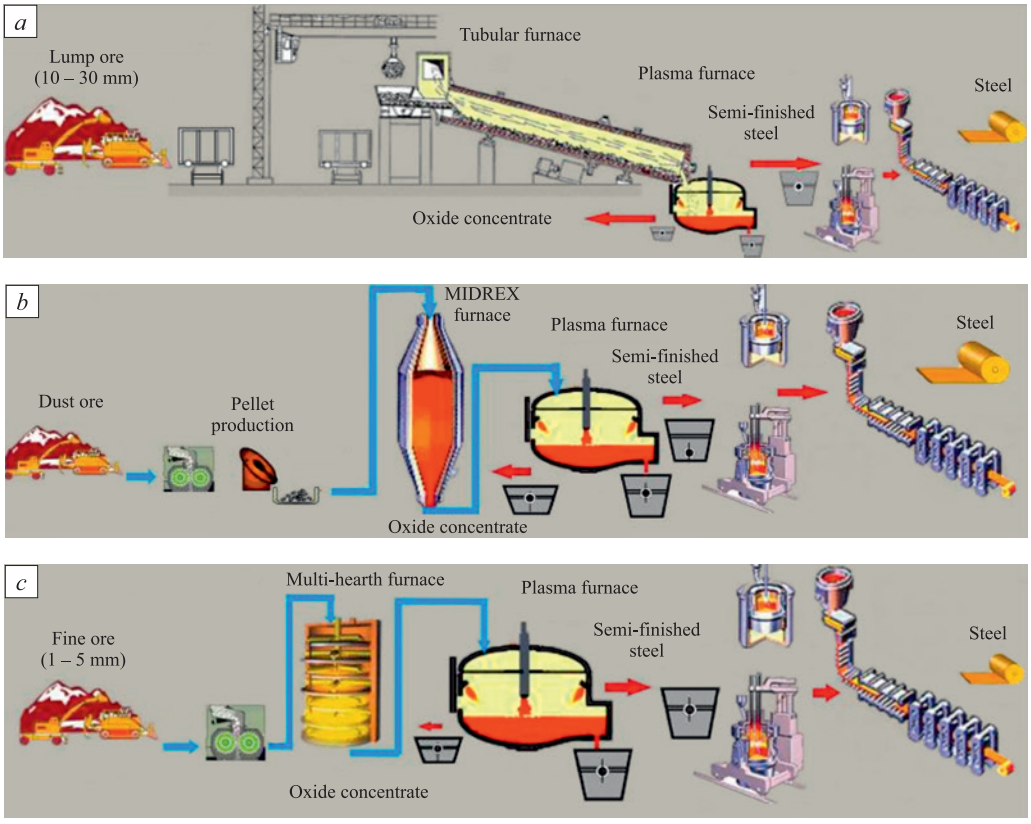

Fig. 4. Reasonable schemes for the use of hydrogen as a reducing agent for selective reduction of iron in complex ores in existing reducing units:
a – in tubular furnaces; *b* – in Midrex and Hill installations; *c* – in multi-hearth furnaces

Рис. 4. Целесообразные схемы использования водорода в качестве восстановителя для селективного восстановления железа в комплексных рудах в существующих восстановительных агрегатах:
a – в трубчатых печах; *b* – в установках Мидрекс и Хилл; *c* – в многоподовых печах

ditions of industrial reduction units, the gas phase is in a state of low-temperature plasma, while ore oxides exhibit mixed electronic–anion conductivity. As a result, electron exchange between reductants and metal cations in ores does not even require physical contact between the reductant and the ore.

The electronic theory of reduction describes the transfer of valence electrons from atoms of the reductant to the cations of the metal being reduced. Under the conditions of industrial reduction units, the gas phase is in a state of low-temperature plasma, while ore oxides exhibit mixed electronic–anion conductivity. As a result, electron exchange between reductants and metal cations in ores does not even require physical contact between the reductant and the ore.

In complex ores, the "free" electrons that form at the surface can migrate together with anion vacancies through the oxide crystal lattice until they encounter cations that, under the given conditions, have the highest electron affinity. There they become trapped; at coalesced anion-vacancy sites a metallic phase forms. In this way, oxygen departing to the gas phase from one oxide can lead to the reduction of cations within the crystal lattice of a different oxide.

By their physical operating principle, reduction units are electrochemical devices in which two familiar electrochemical cells act in series: a fuel cell, which converts the chemical energy of the reductant into the electrical energy of "free" electrons, and a solid electrolyte electrolyzer, which converts that electrical energy into the chemical energy of metallic bonding in the cations being reduced.

Since the final stage of any reduction reaction is the uptake of "free" electrons by the cations being reduced, the most direct route to reduction is to generate these electrons at modern power stations and deliver them to the cations via the electrical grid – that is, electrolysis.

Electrolysis of melts for the production of carbon-free iron constitutes a promising pathway for processing rich, single-mineral iron ores. A comparably promising avenue for processing complex and lean ores is the selective, low-temperature reduction of iron using hydrogen, with

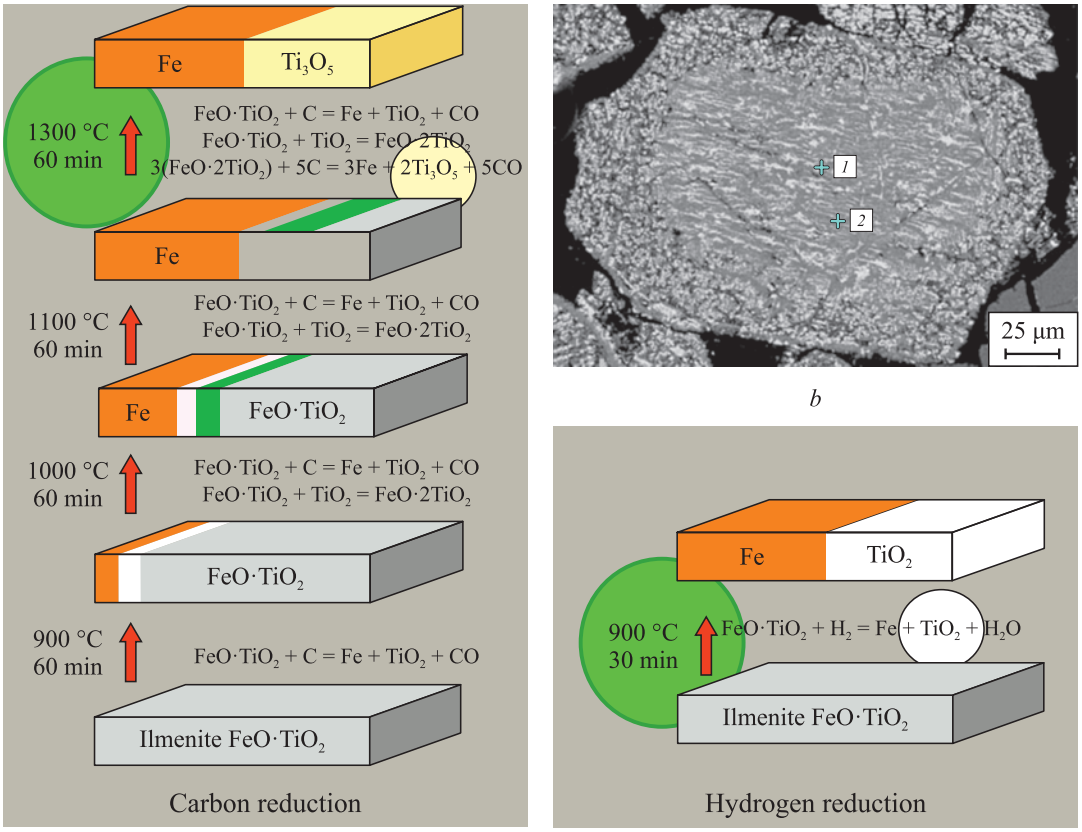

Fig. 5. Comparison of sequence and parameters (temperature (*T*) and time (*t*)) of carbon (*a*) and hydrogen (*b*, *c*) solid-phase selective reduction of iron:
1 – 100 % Fe; *2* – 100 % TiO_2

Рис. 5. Сравнение последовательности и параметров (температуры (*T*) и времени (*t*)) углеродного (*a*) и водородного (*b*, *c*) твердофазного селективного восстановления железа:
1 – 100 % Fe; *2* – 100 % TiO_2

subsequent separation to obtain carbon-free iron together with oxide concentrates of more active metals (e.g., manganese, chromium, titanium).

References / Список литературы

1. Lyuban A.P. Analysis of Blast Furnace Smelting Phenomena. Moscow: Metallurgizdat; 1962:532. (In Russ.).

   Любан А.П. Анализ явлений доменной плавки. Москва: Металлургиздат; 1962:532.
2. Bogdandy L., Engell H.-J. The Reduction of Iron Ores. Scientific Basis and Technology. Berlin; Heidelberg: Springer-Verlag; 1971:576. https://doi.org/10.1007/978-3-662-10400-2
3. Wegman E.F., Zherebin B.N., Pokhvistnev A.N., etc. Metallurgy of Cast Iron. Moscow: Metallurgiya; 1989:512. (In Russ.).

   Металлургия чугуна / Е.Ф. Вегман, Б.Н. Жеребин, А.Н. Похвистнев и др. Москва: Металлургия; 1989:512.
4. Ghosh A., Chatterjee A. Ironmaking and Steelmaking: Theory and Practice. PHI Learning Pvt. Ltd.; 2008:472.
5. Dmitriev A.N., Shumakov N.S., Leont'ev L.I., Onorin O.P. Fundamentals of the Theory and Technology of Blast Furnace Smelting. Yekaterinburg: UB RAS; 2005:545. (In Russ.).

   Основы теории и технологии доменной плавки / А.Н. Дмитриев, Н.С. Шумаков, Л.И. Леонтьев, О.П. Онорин. Екатеринбург: УрО РАН; 2005:545.
6. Korotich V.I., Naboichenko S.S., Sotnikov A.I., etc. Beginnings of Metallurgy: Textbook for Universities. Yekaterinburg: USTU; 2000:392. (In Russ.).

   Начала металлургии: учебник для вузов / В.И. Коротич, С.С. Набойченко, А.И. Сотников и др. Екатеринбург: УГТУ; 2000:392.
7. Konovalov Yu.V., Troyanskii A.A., Timoshenko S.N. Metallurgy: Textbook in three books. Book 1: Production of Cast Iron, Iron, Steel and Ferroalloys. Donetsk: DonSTU; 2011:431. (In Russ.).

   Коновалов Ю.В., Троянский А.А., Тимошенко С.Н. Металлургия: учебное пособие в трех книгах. Книга 1. Производство чугуна, железа, стали и ферросплавов. Донецк: ДонГТУ; 2011:431.
8. Yusfin Yu.S., Pashkov N.F. Metallurgy of Iron. Moscow: Akademkniga; 2007:464. (In Russ.).

   Юсфин Ю.С., Пашков Н.Ф. Металлургия железа. Москва: ИКЦ «Академкнига»; 2007: 464.
9. Roshchin V.E., Roshchin A.V. General electron theory of reduction and oxidation of metals. *Izvestiya. Ferrous Metallurgy*. 2020;63(3-4):271–285. https://doi.org/10.17073/0368-0797-2020-3-4-271-285

   Рощин В.Е., Рощин А.В. Общая электронная теория восстановления (окисления) металлов. *Известия вузов. Черная металлургия*. 2020;63(3-4):271–285. https://doi.org/10.17073/0368-0797-2020-3-4-271-285
10. Roshchin V.E., Roshchin A.V. Physics of Pyrometallurgical Processes. Textbook. Moscow; Vologda: Infra-Engineering; 2021:304. (In Russ.).

    Рощин В.Е., Рощин А.В. Физика пирометаллургических процессов. Учебник. Москва; Вологда: Инфра-Инженерия; 2021:304.
11. Ponomarenko A.G. Issues of thermodynamics of phases of variable composition having a collective electronic system. IV. The Fermi level in oxide phases. *Journal of Physical Chemistry*. 1974;XLVIII(8):1954–1958. (In Russ.).

    Пономаренко А.Г. Вопросы термодинамики фаз переменного состава, имеющих коллективную электронную систему. IV. Уровень Ферми в оксидных фазах. *Журнал физической химии*. 1974;XLVIII(8):1954–1958.
12. Galevskii G.V., Kulagin N.M., Mindis M.Ya., Sirazutdinov G.A. Metallurgy of Aluminum. Technology, Power Supply, Automation. Moscow: Flinta; Nauka; 2017:529. (In Russ.).

    Металлургия алюминия. Технология, электроснабжение, автоматизация / Г.В. Галевский, Н.М. Кулагин, М.Я. Миндис, Г.А. Сиразутдинов. Москва: Флинта: Наука; 2017:529.
13. Lopes D.V., Quina M.J., Frade J.R., Kovalevsky A.V. Prospects and challenges of the electrochemical reduction of iron oxides in alkaline media for steel production. *Frontiers in Materials*. 2022;9:1010156. https://doi.org/10.3389/fmats.2022.1010156
14. Boston Metal: electrolyzing as a pure alternative to manufacturing. Available at URL: https://econet.ru/articles/boston-metal-elektroliz-kakchistaya-alternativa-proizvodstvu-stali (Accessed 10.06.2025). (In Russ.).

    Boston Metal: электролиз как чистая альтернатива производству стали. URL: https://econet.ru/articles/boston-metal-elektroliz-kakchistaya-alternativa-proizvodstvu-stali (Дата обращения 10.06.2025).
15. Mehta A. Meet the green technologies set to transform the geopolitics of steelmaking. Available at URL: https://www.reuters.com/sustainability/decarbonizing-industries/meet-green-technologies-set-transform-geopolitics-steelmaking-2025-05-28/. (Accessed 10.06.2025).
16. Humbert M.S., Brooks G.A., Duffy A.R., etc. Economics of electrowinning iron from ore for green steel production. *Journal of Sustainable Metallurgy* 2024;10:1679–1701. https://doi.org/10.1007/s40831-024-00878-3
17. Pavlov V.V. Inconsistencies of Metallurgy. Yekaterinburg: USTU; 2013:212. (In Russ.).

    Павлов В.В. Несообразности металлургии. Екатеринбург: Изд-во УГТУ; 2013:212.
18. Roshchin V.E., Kuznetsov Yu.S., Gamov P.A., Salikhov S.P., Smirnov K.I., Suleimenov B., Kosdauletov N., Adilov G., Bil'genov A., Grigor'ev E.V. Production of active metal oxides and concentrates from complex and difficult-to-process iron-bearing ores by selective reduction of elements. Patent RF no. 2826 667C1. SEC C22B5/02; C22B1/00. *Bulleten' izobretenii*. 2024:26. (In Russ.).

    Пат. 2826667 C1 РФ МПК C22B5/02 C22B1/00. Получение оксидов активных металлов и концентратов из комплексных и трудно перерабатываемых железосодержащих руд селективным восстановлением элементов / В Е. Рощин, Ю.С. Кузнецов, П.А. Гамов, С.П. Салихов, К.И. Смирнов, Б. Сулеймен, Н. Косдаулетов, Г. Адилов, А. Бильгенов, Е.В. Григорьев. Заявл. 07.03.2024, опубл. 16.09.2024. Бюл. 26.
19. Smirnov K.I., Gamov P.A., Roshchin V.E. Justification of a rational processing scheme for ilmenite concentrate with

production of soft iron and titanium dioxide concentrate. *CIS Iron and Steel Review*. 2025;29:4–10. https://doi.org/10.17580/cisisr.2025.01.01

20. Patisson F., Mirgaux O. Hydrogen ironmaking: How it works. *Metals*. 2020;10(7):922. https://doi.org/10.3390/met10070922

21. Ma Y., Filho I.R.S., Bai Y., Schenk J., Patisson F., Beck A., van Bokhoven J.A., Willinger M.G., Li K., Xie D., Ponge D., Zaefferer S., Gault B., Mianroodi J.R., Raabe D. Hierarchical nature of hydrogen-based direct reduction of iron oxides. *Scripta Materialia*. 2022;213:114571. https://doi.org/10.1016/j.scriptamat.2022.114571

22. Cavaliere P. Hydrogen Assisted Direct Reduction of Iron Oxides. Springer Cham; 2002:399. https://doi.org/10.1007/978-3-030-98056-6

23. Lüngen H.B., Schmöle P. The way the European steel industry wants to become carbon neutral. In: *Proceedings of 9th European Coke and Ironmaking Congress (ECIC 2024). Coal, Coke, Biocoal, Biocoke, Biochar and Iron Reductions. Italy, Bardolino, 16 – 18 October 2024*. Italy: Associazione Italiana di Metallurgia (AIM); 2024:1–12.

24. West K. High-temperature molten oxide electrolysis steelmaking (ULCOLYSIS). Available at URL: https://energy.nl/data/high-temperature-molten-oxide-electrolysis-steelmaking-ulcolysis/ (Accessed 10.06.2025).

25. Electrolysis in ironmaking. Fact sheet. Available at URL: https://worldsteel.org/wp-content/uploads/Fact-sheet-Electrolysis-in-ironmaking.pdf (Accessed 10.06.2025).

26. Primary Exploration of Hydrogen Metallurgy. Zhang J., Li K., Liu Z., Yang T. eds. Springer. Springer: 2024:410.

Information about the Authors / Сведения об авторах

Vasilii E. Roshchin, *Dr. Sci. (Eng.), Prof., Chief Researcher of the Research Laboratory "Hydrogen Technologies in Metallurgy"*, South Ural State University
ORCID: 0000-0003-3648-8821
E-mail: roshchinve@susu.ru

Anton V. Roshchin, *Dr. Sci. (Eng.), Assist. Prof., Leading Researcher of the Research Laboratory "Hydrogen Technologies in Metallurgy"*, South Ural State University
ORCID: 0000-0003-4840-4410
E-mail: roshchinav@susu.ru

Василий Ефимович Рощин, *д.т.н., профессор, главный научный сотрудник научно-исследовательской лаборатории «Водородные технологии в металлургии»*, Южно-Уральский государственный университет
ORCID: 0000-0003-3648-8821
E-mail: roshchinve@susu.ru

Антон Васильевич Рощин, *д.т.н., доцент, ведущий научный сотрудник научно-исследовательской лаборатории «Водородные технологии в металлургии»*, Южно-Уральский государственный университет
ORCID: 0000-0003-4840-4410
E-mail: roshchinav@susu.ru

Received 27.03.2025
Revised 23.06.2025
Accepted 23.06.2025

Поступила в редакцию 27.03.2025
После доработки 23.06.2025
Принята к публикации 23.06.2025

Над номером работали:

Л.И. Леонтьев, *главный редактор*

Е.В. Протопопов, *заместитель главного редактора*

Е.А. Ивани, *ответственный секретарь*

Л.П. Бащенко, *заместитель ответственного секретаря*

Е.Ю. Потапова, *заместитель главного редактора по развитию*

О.А. Долицкая, *научный редактор*

В.В. Расенець, *верстка, иллюстрации*

Г.Ю. Острогорская, *менеджер по работе с клиентами*

Подписано в печать 20.08.2025. Формат 60×90 $^{1}/_{8}$. Бум. офсетная № 1.
Печать цифровая. Усл. печ. л. 13,5. Заказ 22788. Цена свободная.

Отпечатано в типографии Издательского Дома МИСИС.
119049, Москва, Ленинский пр-кт, д. 4, стр. 1.
Тел./факс: +7 (499) 236-76-17

Зарегистрирован Федеральной службой по надзору в сфере связи, информационных технологий и массовых коммуникаций. Свидетельство о регистрации ПИ № ФС77-35456.

Подписной индекс 70383.